Universiteit
Leiden
The Netherlands

The developing heartbeat: tracing and characterization of the developing cardiac conduction system

Kelder, T.P.

Citation
Kelder, T. P. (2018, January 18). *The developing heartbeat: tracing and characterization of the developing cardiac conduction system*. Retrieved from https://hdl.handle.net/1887/58994

Version:	Not Applicable (or Unknown)
License:	Licence agreement concerning inclusion of doctoral thesis in the Institutional Repository of the University of Leiden
Downloaded from:	https://hdl.handle.net/1887/58994

Note: To cite this publication please use the final published version (if applicable).

Cover Page

Universiteit Leiden

The handle http://hdl.handle.net/1887/58994 holds various files of this Leiden University dissertation.

Author: Kelder, T.P.
Title: The developing heartbeat: tracing and characterization of the developing cardiac conduction system
Issue Date: 2018-01-18

THE DEVELOPING HEARTBEAT

TRACING AND CHARACTERIZATION OF THE DEVELOPING CARDIAC CONDUCTION SYSTEM

TIM PETER KELDER

© Tim Peter Kelder, Den Haag
All rights reserved. No part of this book may be reproduced or transmitted, in any form or by any means, without written permission of the author

ISBN: 978-94-6299-751-6
Cover & chapter divider design: Tim Peter Kelder
Layout: Tim Peter Kelder & Niels van Dijk (Niels van Dijk Multimedia)
Printing: Ridderprint BV | www.ridderprint.nl

The work presented in this thesis was carried out at the Department of Anatomy and Embryology of the Leiden University Medical Center

THE DEVELOPING HEARTBEAT

TRACING AND CHARACTERIZATION OF THE DEVELOPING CARDIAC CONDUCTION SYSTEM

Proefschrift

ter verkrijging van
de graad van Doctor aan de Universiteit Leiden,
op gezag van Rector Magnificus prof.mr. C.J.J.M. Stolker,
volgens besluit van het College voor Promoties
te verdedigen op 18 januari 2018
klokke 13:45 uur

door

Tim Peter Kelder
Geboren te Leiden in 1986

Promotores:	Prof. Dr. M.C. de Ruiter
	Prof. Dr. M.J. Goumans
Co-promotor:	Dr. M.R.M. Jongbloed
Leden promotiecommissie:	Prof. Dr. N.A. Blom
	Prof. Dr. M.K. Richardson
	Prof. Dr. M.J. Schalij
	Prof. Dr. D. Sedmera (Charles University, Praag)
	Dr. W.S. Kerstjens-Frederikse (UMC Groningen)

Financial support by the Dutch Heart Foundation for the publication of this thesis is gratefully acknowledged

Ter nagedachtenis aan mijn vader

CONTENTS

1 Aim & outline of the thesis 9

2 General introduction:
Normal and abnormal development of the cardiac conduction system; implications for conduction and rhythm disorders in the child and adult 15
Modified after Differentiation, 84: 131-148 (2012)

3 Review:
The avian embryo to study development of the cardiac conduction system 51
Modified after Differentiation, 91: 90-103 (2016)

4 The sinus venosus myocardium contributes to the atrioventricular canal: potential role during atrioventricular node development? 81
Modified after Journal of Cellular and Molecular Medicine, 19: 1375-89 (2015)

5 Letter to editor:
Does the dorsal mesenchymal protrusion act as a temporary pacemaker during heart development? 111
Modified after Journal of Biological Chemistry, 290: 8013-4 (2015)

6 RHOA-ROCK signaling is necessary for lateralization and differentiation of the developing sinoatrial node 117
Modified after Cardiovascular Research, 113: 1186-97 (2017)

7 Disruption of RHOA-ROCK signaling results in atrioventricular block and disturbed development of the putative atrioventricular node 151
Submitted

8 The epicardium as modulator of the cardiac autonomic response during early development 173
Modified after Journal of Molecular and Cellular Cardiology, 89: 251-9 (2015)

9 Review:
Lessons learned from cell tracing and fate mapping experiments aimed at elucidating the developmental origin of the cardiac conduction system 197
Submitted

10 Summary & future perspectives 237

11 Nederlandse samenvatting 245

12 List of publications 255
Dankwoord 257
Curriculum vitae 259

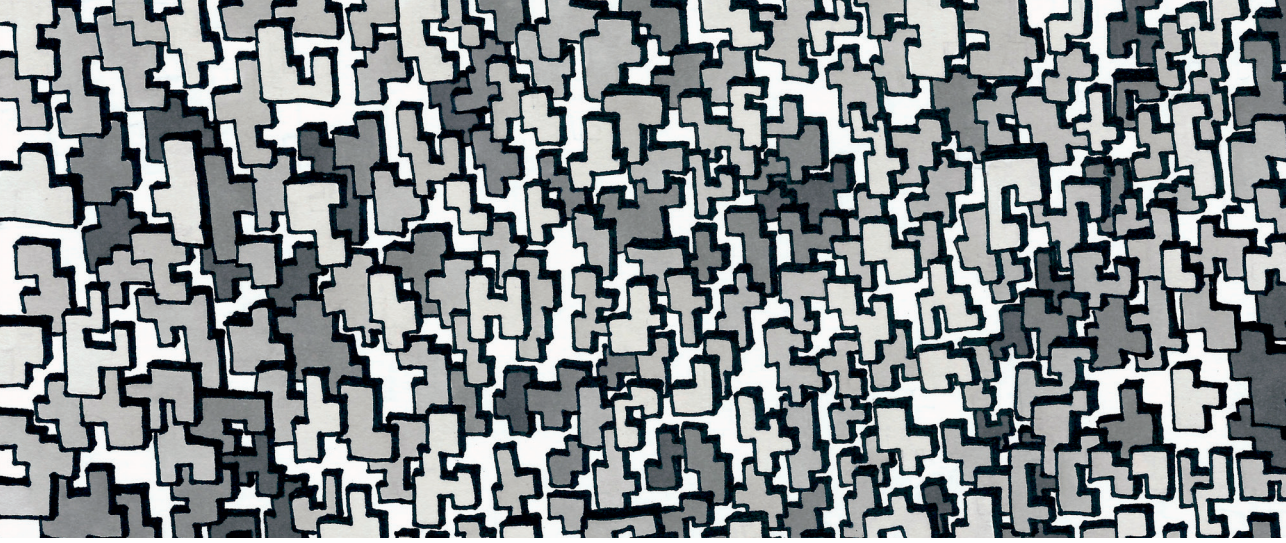

1

AIM & OUTLINE OF THE THESIS

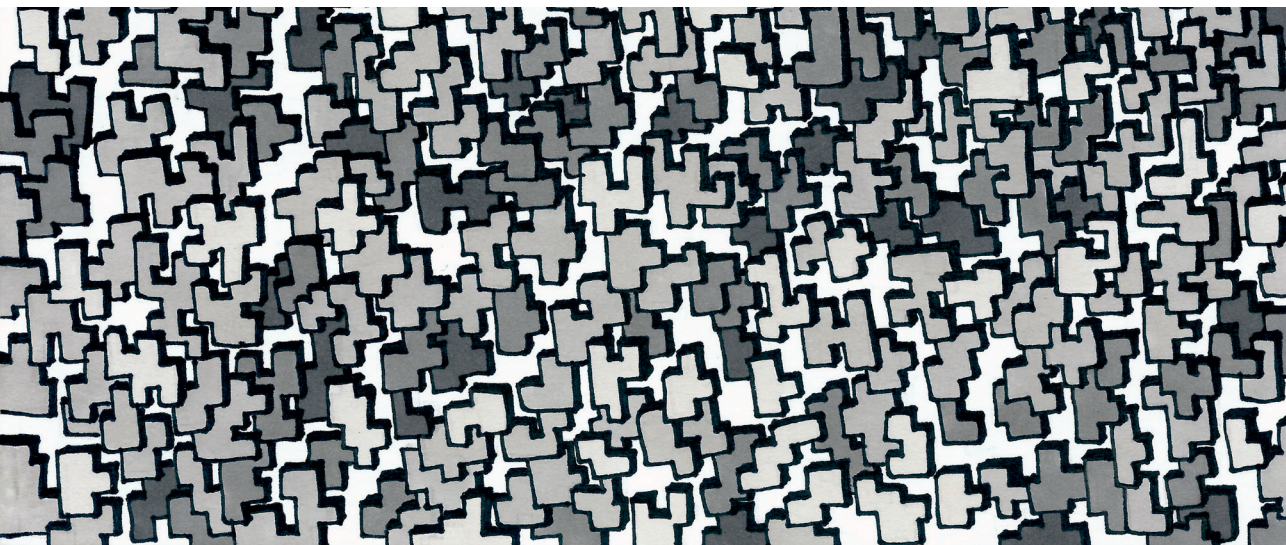

1

AIM & OUTLINE OF THE THESIS

The cardiac conduction system (CCS) ensures initiation and coordination of the electrical activation of the heart, resulting in controlled contraction of the myocardium. This process is crucial to maintain constant perfusion to the organs in the body. Failure of the CCS, clinically manifested as cardiac arrhythmias, causes serious morbidity and mortality and poses an important disease burden on the pediatric and adult population.

Understanding the developmental processes ultimately giving rise to the mature CCS can help to understand the pathophysiology of cardiac arrhythmias. This in turn can lead to new therapeutic strategies to prevent or treat this group of debilitating diseases. The main aim of the current thesis is to study the embryological origin and characteristics of key components of the developing CCS.

In **chapter 2** of this thesis, a general introduction on cardiac and CCS development is given. The development of the CCS is linked to clinical arrhythmias and arrhythmias occurring in the setting of congenital heart disease. Based on the results from the literature, a working model for the developmental background of clinical arrhythmias is provided.

The avian embryo has long been a popular and vital model system in developmental biology. A large number of the experiments described in the current thesis were performed using chick embryos. In **chapter 3** an overview of advantages and limitations of this model system is given. Furthermore, the techniques used in the avian embryo to study the developing CCS are described. The results obtained from these experiments are discussed briefly to underscribe the importance of the avian model system in understanding the development of the CCS.

The atrioventricular node (AVN) is an essential component of the CCS, responsible for delaying the electrical activation wave from the atria. This allows time for the right and left ventricular lumen to fill with blood during diastole, necessary for efficient output of the heart. The AVN itself is a complex structure that consists of multiple cell types.[1] The developmental origin of the different components of the AVN remains controversial.[1] A contribution from the myocardium of the sinus venosus to the developing AVN was suggested[2] and is investigated in **chapter 4**.

In a recent study by Sun *et al.* it was suggested that the dorsal mesenchymal protrusion (DMP) acts as a temporary pacemaker during early development.[3]

In **chapter 5** the anatomical description of the DMP that is provided by *Sun et al.*, and therefore the conclusion that this structure acts a temporary pacemaker during development, is probed.

Disturbance of the RHOA-ROCK signaling pathway results in bradycardia, atrial fibrillation and AV block in adult mice.[4,5] The developmental processes leading to these arrhythmias remain to be elucidated. In **chapter 6**, the development of the sinus venosus myocardium and sinoatrial node after inhibition of the RHOA-ROCK pathway is studied in chicken embryos. The effect of inhibition of this pathway on AV canal and AVN development is studied in **chapter 7**.

The cardiac autonomic nervous system (cANS) modulates heart rate, contraction force and conduction velocity.[6] In the adult heart, both the SAN and AVN have a rich autonomic innervation. Prior to establishment of the cANS, the early embryonic chicken heart already responds to epinephrine.[7] In **chapter 8** this early autonomic innervation is examined and a potential role for the epicardium in early modulation of the autonomic response is investigated.

In **chapter 9** the different fate mapping and cell tracing techniques aimed at elucidating the developmental origin of the CCS are discussed. Special focus will be on the specific limitations and advantages of these techniques. The data obtained from these experiments will be evaluated critically and a possible working model for the development of the CCS is generated.

Chapter 10 provides a summary of the work described in this thesis.

REFERENCE LIST

1. Jongbloed, M. R. *et al.* Normal and abnormal development of the cardiac conduction system; implications for conduction and rhythm disorders in the child and adult. *Differentiation* **84,** 131–148 (2012).

2. Vicente-Steijn, R. *et al.* Electrical activation of sinus venosus myocardium and expression patterns of RHOA and Isl-1 in the chick embryo. *J. Cardiovasc. Electrophysiol.* **21,** 1284–92 (2010).

3. Sun, C. *et al.* The short stature homeobox 2 (Shox2)-bone morphogenetic protein (BMP) pathway regulates dorsal mesenchymal protrusion development and its temporary function as a pacemaker during cardiogenesis. *J. Biol. Chem.* **290,** 2007–23 (2015).

4. Wei, L. *et al.* Disruption of Rho signaling results in progressive atrioventricular conduction defects while ventricular function remains preserved. *FASEB J.* **18,** 857–9 (2004).

5. Sah, V. P. *et al.* Cardiac-specific overexpression of RHOA results in sinus and atrioventricular nodal dysfunction and contractile failure. *J. Clin. Invest.* **103,** 1627–34 (1999).

6. Shen, M. J. & Zipes, D. P. Role of the autonomic nervous system in modulating cardiac arrhythmias. *Circ. Res.* **114,** 1004–1021 (2014).

7. Kroese, J. M., Broekhuizen, M. L. A., Poelmann, R. E., Mulder, P. G. H. & Wladimiroff, J. W. Epinephrine affects hemodynamics of noninnervated normal and all-trans retinoic acid-treated embryonic chick hearts. *Fetal Diagn. Ther.* **19,** 431–9 (2004).

2

GENERAL INTRODUCTION: NORMAL AND ABNORMAL DEVELOPMENT OF THE CARDIAC CONDUCTION SYSTEM; IMPLICATIONS FOR CONDUCTION AND RHYTHM DISORDERS IN THE CHILD AND ADULT

Monique R.M. Jongbloed, Rebecca Vicente-Steijn, Nathan D. Hahurij, Tim P. Kelder, Martin J. Schalij, Adriana C. Gittenberger-de Groot, Nico A. Blom

Modified after Differentiation, 84: 131-148 (2012)

ABSTRACT

The cardiac conduction system is a specialized network that initiates and closely coordinates the heartbeat. Cardiac conduction system development is intricately related to the development and maturation of the embryonic heart towards its four-chambered form, as is indicated by the fact that disturbed development of cardiac structures is often accompanied by a disturbed formation of the CCS. Electrophysiological studies have shown that selected conduction disturbances and cardiac arrhythmias do not take place randomly in the heart but rather at anatomical predilection sites. Knowledge on development of the CCS may facilitate understanding of the etiology of arrhythmogenic events. In this chapter we will focus on embryonic development of the CCS in relation to clinical arrhythmias, as well as on specific cardiac conduction abnormalities that are observed in patients with congenital heart disease.

1. INTRODUCTION

The cardiac conduction system (CCS, **Fig. 1**) is a specialized network that initiates and closely coordinates the heartbeat. The development of the CCS is intricately related to the development and maturation of the embryonic heart towards its four-chambered form, as is indicated by the fact that disturbed development of cardiac structures is often accompanied by a disturbed formation of the CCS.

Both in the young and in the adult population conduction disturbances and cardiac arrhythmias can occur. Electrophysiological studies have shown that these events do not take place randomly in the heart but rather at anatomical predilection sites. Specifically, ectopic foci have been reported in sinus venosus-related structures at the venous pole of the heart such as the crista terminalis[1] and the ostia of the caval veins[2], coronary sinus[3] and pulmonary veins.[4] Interestingly, during embryonic development, the area covered by the developing CCS includes structures that will not contribute to the mature CCS[5,6] like the left cardinal vein which during development goes in regression to become the ligament of Marshall, a known arrhythmogenic substrate.[7] Knowledge on development of the CCS may facilitate understanding of the etiology of arrhythmogenic events. In this chapter we will focus on embryonic development of the CCS in relation to clinical arrhythmias, as well as on specific cardiac conduction abnormalities that are observed in patients with congenital heart disease. We will first address the 'building blocks' necessary for proper cardiac development, after which development of the CCS will more specifically be discussed. The main focus of this chapter will be on the proximal part of the developing CCS, that includes the sinoatrial node (SAN), AV node (AVN) and AV junction.

2. EARLY CARDIAC DEVELOPMENT

In human, the development of the heart starts around day 19 (+/- mouse embryonic day (E)7.5, and chick Hamburger Hamilton (HH) stage 5-6) in the splanchnic part of the lateral plate mesoderm. Specific regions of the cardiac crescent will give rise to specific cardiac segments (**Fig. 2a**). The splanchnic mesoderm located at both sides of the primitive streak will fuse to form a single horseshoe-shaped heart primordium[8,9] or primary heart tube with a venous and an arterial pole, through which the blood is propulsed in a peristaltic fashion (**Fig. 2b**). This tube contains a myocardial layer on the outside, an endocardial covering on the inside, with endocardial jelly located in between (**Fig. 2b**).

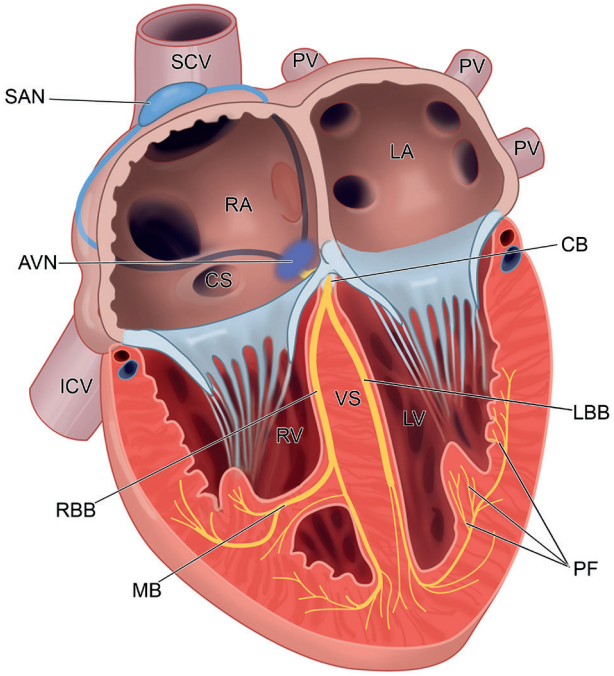

Figure 1. The adult cardiac conduction system

Schematic representation of the adult CCS. The electrical impulse is generated in the sinoatrial node (SAN), located at the entrance of the superior caval vein (SCV) into the right atrium (RA). It is conducted through the internodal atrial myocardium to the atrioventricular node (AVN) located at the right side of the base of the atrial septum in the triangle of Koch, where it is delayed. The impulse is then propagated through the common bundle or His bundle (CB), situated on the top of the ventricular septum (VS), and the left and right bundle branches (LBB and RBB, respectively) located at each side of the ventricular septum, to the Purkinje fiber network (PF) resulting in the contraction of the ventricular myocardium. CS: coronary sinus, ICV: inferior caval vein, LA: left atrium, LV: left ventricle, MB: moderator band, PV: pulmonary vein, RV: right ventricle.

3. THE "BUILDING BLOCKS" OF THE HEART

3.1. FIRST AND SECOND HEART FIELD

A widely used but controversial concept in cardiac development is the subdivision of the cardiac progenitors in a *first* and *second heart field* (FHF and SHF respectively). This concept will be introduced in this introductory chapter and the FHF and SHF nomenclature will be used. In **chapters 4, 9 and 10** the concept of dividing the cardiac progenitors into distinct and separate heart fields and the specificity of FHF and SHF markers will be discussed.

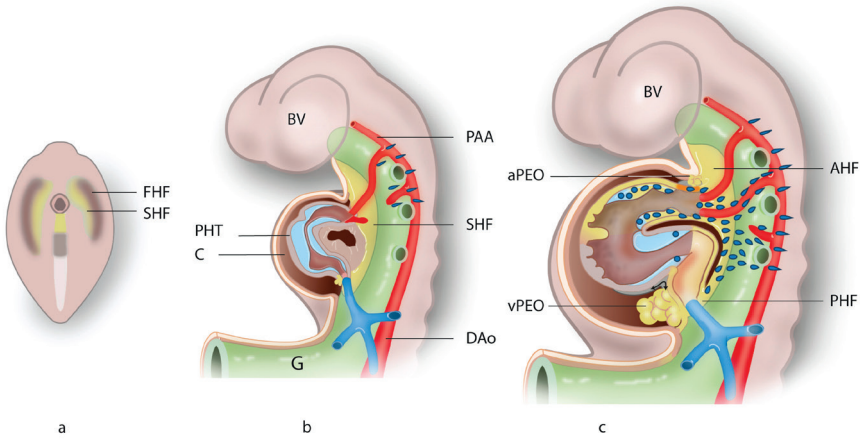

Figure 2. Development of the heart from the first (FHF) and second (SHF) heart fields
a. Early in development, bilateral fields of cardiac mesoderm are present in the primitive plate. Cells depicted in yellow will contribute to the second heart field (SHF) parts of the heart, whereas cells depicted in grey depict the first heart field (FHF) that will contribute to the primary myocardial heart tube (PHT). **b.** Schematic representation of the primitive heart tube (grey) after fusion of the bilateral plates of mesoderm. The tube is lined on the inside by cardiac jelly (blue). The mesoderm of the SHF is depicted by the yellow area behind the PHT. This region will contribute myocardium to both the arterial and venous poles of the heart (depicted by the yellow myocardium in **b**) during development. **c.** At further developmental stages, segments of the heart will develop by contribution of myocardium to the venous pole from the posterior heart field (PHF, yellow) and to the arterial pole from the anterior heart field (AHF, yellow). The yellow lobulated structure that protrudes into the pericardial cavity at the venous pole of the heart is the proepicardial organ (vPEO). At the arterial pole, also a small PEO (aPEO) can be recognized. Cardiac neural crest cells (depicted by blue dots) migrate from the neural crest along the arterial and venous pole into the heart. BV: brain ventricles, C: coelomic cavity, DAo: dorsal aorta, G: gut, PAA: pharyngeal arch arteries.

Initially, the primary heart tube will mainly consist of a left ventricle, an atrioventricular canal and part of the atria.[10] The myocardial progenitor population that will contribute to this primary heart tube has been designated the FHF. Additionally, contribution from a second progenitor pool of myocardial precursors, the so-called SHF, located in the mesoderm dorsal to the primary heart tube, is necessary (**Fig. 2b,c**). As from E8.5 in mouse[11] and stage HH14 in chick[12,13] additional cardiomyocytes are incorporated at the arterial and venous pole of the primary heart tube. Both heart field populations (FHF and SHF) can already be distinguished in the early stages of the cardiac crescent (FHF), the SHF lying medial to the first heart field (**Fig. 2a**).[10,14,15]

The cellular addition from the SHF at the arterial pole will contribute to the formation of the outflow tract and the right ventricle, also referred to as derived from the anterior or secondary heart field.[11,13,16,17] In this chapter we refer to

this population as the *anterior heart field* (AHF). Complementary to the arterial contribution, the SHF contribution to the venous pole of the primary heart tube has been referred to by our lab as the *posterior heart field* (PHF, **Fig. 2**). The PHF can be subdivided into a *myocardial* component and a *mesenchymal* component. The myocardial component will contribute to the myocardium that surrounds the cardinal (embryonic) or caval (adult) veins and the pulmonary veins. This region also includes the definitive right-sided, as well as a transient left-sided sinoatrial node.[18,19] Whether there is also a contribution to the atrioventricular node, is still controversial.[20,21] The mesenchymal component will contribute to the development of the dorsal mesenchymal protrusion (DMP), important for atrial septation, as well as to the proepicardial organ (PEO) with its derivatives, the epicardium and epicardium-derived cells (EPDCs) (described later on). Several genes are expressed throughout the SHF and have an important role in the development of both the arterial and venous pole, like the LIM homeodomain transcription factor Islet1(Isl1). Mice lacking this transcription factor do not develop an outflow tract, right ventricle and part of the atria.[10] Just like its counterpart at the arterial pole (AHF), a subset of genes and transcription factors have been found necessary for proper PHF-derived cardiac development. In contrast to the AHF derived myocardium at the arterial pole of the heart, the PHF derived myocardium is characterised by lack of expression of Nkx2.5, as well as by positive expression patterns of several markers including podoplanin[18], its downstream receptor RHOA[19,22], Tbx18[23], Tbx5[24,25], Shox2[26], HCN4[27,28] and pdgf-receptor alpha.[29] The developmental aspects of the sinus venosus myocardium, SAN and AVN will be discussed later on.

3.2. EPICARDIUM AND EPICARDIUM-DERIVED CELLS (EPDCS)

The primary heart tube is initially not covered by epicardial cells. Epicardial cells derive during development from a villous structure at the venous pole of the heart, the proepicardial organ (PEO, **Fig. 2c**), with a possible exception of the epicardium covering the arterial pole of the heart[30], that is most likely derived from the AHF. As the PEO and its derivatives are derived from the PHF, one could argue that this structure, that is in close relation to the developing heart, should not be regarded as an extracardiac structure.[31–33] In mouse embryos of E9.5-10.5, epicardial cells start to migrate from the PEO over the complete outer layer of the developing heart[32,34], and subsequently migrate to the subepicardial layer where EPDCs are generated by a process of epithelial-to-mesenchymal transition (EMT). EPDCs invade the myocardium, the subendocardial space and AV cushion tissue, where they contribute in formation of smooth muscle cells, the adventitial layer of the coronary vasculature, the AV valves and to formation of the compact myocardium.[32,34]

Of interest for the CCS is the role of EPDCs in development of the annulus fibrosus, as mechanical inhibition of proper outgrowth of the epicardium results in broad accessory AV connections and pre-excitation (described in more detail below).[35,36] Previous studies also indicate a role of the EPDCs in development of the peripheral conduction system (Purkinje fibers), as epicardial inhibition results in a significant reduction in numbers of Purkinje fiber cells as compared to normal embryos.[34,37]

3.3. NEURAL CREST CELLS (NCCS)

Neural crest cells (NCCs, **Fig. 2c**) contribute to many organs and tissues during embryonic development. At the arterial pole NCCs are involved in formation of the pharyngeal arch arteries and remodeling of the outflow tract i.e. formation and myocardialisation of the aorticopulmonary septum[38–40] and formation of the semilunar valves.[41] Furthermore, NCCs contribute in the formation of the neurons and ganglia of the cardiac autonomous nerve system, which is important for the regulation of cardiac function.[42,43] At the venous pole of the heart NCCs are involved in development of the base of the atrial septum and an important role of NCCs has been postulated in induction of the anlage of the CCS.[44–46] Although the exact role of NCCs in CCS development remains uncertain, the fact that almost all NCCs located near the developing CCS become apoptotic at a certain time point suggests an inductive role.[45,46] It was demonstrated that neural crest ablation in chick results in lack of differentiation of the compact lamellar organization of the His bundle, that separates it from the working myocardium.[47]

4. THE ORIGIN AND DEVELOPMENT OF THE CCS

It is now generally accepted that the *myocardium* is the main source from which the CCS develops.[48] Initial histological studies on CCS development demonstrated that cardiomyocytes of the CCS are characterized by reduced numbers of myofibrils and a high accumulation of glycogen as compared to the working myocardium in both human and animal species.[49,50] In the past years increasing numbers of molecular CCS markers have become available, which enabled detailed morphological analysis of the developing CCS at subsequent stages of development (reviewed in[51]). It should be noted however, that none of the markers solely stains the CCS, and in many cases also neuronal tissues are labeled.[52] Based on the histological characteristics and expression patterns during embryonic development of the different markers known to date, the embryonic CCS covers a broader area as compared to the mature CCS.[51]

In general two different approaches have been used to explain the origin of the cardiomyocytes that contribute to CCS formation: (1) "*the recruitment model*" puts forward that the CCS derives from a pool of multipotent undifferentiated

cardiomyogenic cells[53–55], whereas (2) "*the specification and ballooning model*" suggests that a population of differentiated pre-specified conduction cells located in the embryonic primary heart tube will develop into the CCS.[56] In the latter model the expression of specific genes/transcription factors in the primary heart tube myocardium prevents the differentiation of pre-specified cardiomyocytes to a working myocardium phenotype. The individual heart chambers subsequently balloon-out of the primary heart tube[57,58], after which the myocardium of the primary heart tube is restricted to specific areas (i.e. the SAN region, the AV region, the primary fold and the outflow tract area) in between the working myocardium of the cardiac chambers. These areas will, under the control of several transcription factors, including the T box transcription factors Tbx2 and Tbx3 that repress formation of the working myocardium, contribute to the developing CCS.[59,60]

The above mentioned specific areas that persist after ballooning, are highly comparable to the myocardium mentioned in the so-called "*ring theory of CCS development*" (that suggests that precursors of the CCS can be identified by several "rings" of tissue that, after looping of the heart has been initiated, can be distinguished from the surrounding working myocardium by specific cellular characteristics).[61] Although the "*ring theory*" is nowadays highly controversial, it is interesting to note that after looping of the heart has occurred, several zones of tissue (so-called transitional zones) that overlap with the areas mentioned under "*the specification and ballooning model*" can be distinguished based on expression patterns of several markers involved in CCS development.[6,62–64] These transitional zones largely correspond to the areas described in the *"ring theory"* including the sinoatrial transition, the AV transition, the primary fold area and the ventriculo-arterial transitional zone.[51]

5. NORMAL AND ABNORMAL DEVELOPMENT OF THE SINUS VENOSUS MYOCARDIUM AND SAN

5.1. NORMAL DEVELOPMENT

The SAN is located at the entrance of the superior caval vein into the right atrium (**Fig. 1**). In human and mouse the SAN is comma-shaped with a "head" at the border of the superior caval vein and the right atrium and a "tail" along the terminal crest.[49,65,66] The terminal crest is the adult derivative of the embryonic right venous valve that is an anatomical boundary between the right atrial appendage and the smooth walled sinus venosus part of the right atrium. The anatomical "mature shape" of the SAN differs between several species.[65,67,68]

The SAN can be recognized in human from the fifth week of development.[69] In mouse the first signs of the SAN primordium can be observed around E10.5-11.5, which was suggested to derive from an area of loose mesenchymal cells near

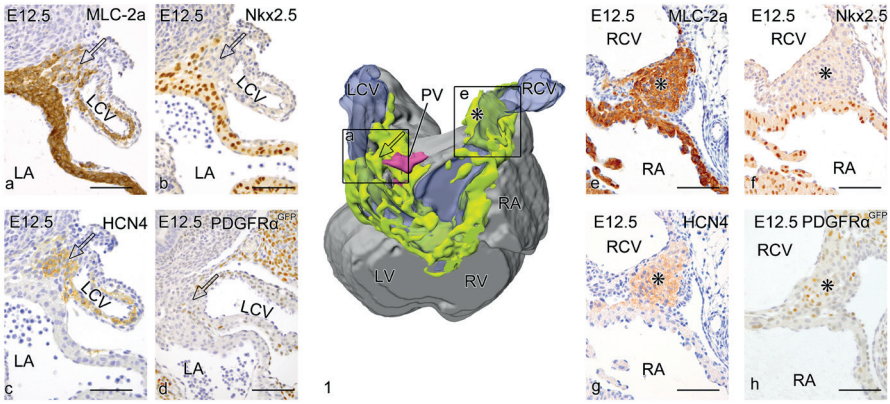

Figure 3. Molecular characteristics of the sinus venosus myocardium

1. 3D reconstruction, dorso-inferior view of E12.5 mouse heart. Sinus venosus myocardium: lime green, encompasses area of definitive right-sided SAN and transient left-sided SAN. Reconstruction of sinus venosus myocardium based on lack of Nkx2.5 expression. Nkx2.5 is markedly expressed in working myocardium (grey). Pulmonary vein (PV): pink. **a-d, e-h.** Expression patterns of MLC-2a, Nkx2.5, HCN4 and pdgf-r alpha in left/right sided SAN. Right/left-sided SAN share same expression pattern, with staining of MLC-2a (**a,e**), HCN4 (**c,g**) and pdgf-r alpha (**d,h**), Nkx2.5 staining is absent (**b,f**). LA/RA: left/right atrium, LCV/RCV: left/right cardinal vein, LV/RV: left/right ventricle. Scale bars 100μm.

the right atrium.[50] Interestingly, also a left SAN has been described at the medial border of the entrance of the left cardinal vein in the right atrium in mouse and chick.[19,22,50,70] Development of the head and tail region of the SAN is established independently in a functional order.[71]

Of interest for a possible relation to clinical arrhythmias is the fact that embryological development of the SAN is narrowly related to development of the myocardium surrounding the cardinal veins (sinus venosus myocardium) and pulmonary veins. The sinus venosus myocardium differentiates from the mesodermal precursor population of the posterior SHF and forms a "U-shaped" myocardial structure that comprises the area of the definitive right-sided SAN area as well as the transient left-sided SAN area (**Fig. 3**).[18,19,22,70] During early developmental stages the sinus venosus myocardium expresses Tbx18 and is negative for Nkx2.5.[18,23] Other genes expressed in this myocardium include podoplanin[18], Shox2[26], HCN4[27,28], Isl1[10], pdgf-receptor alpha[29], RHOA[19], and Tbx3.[72,73] The expression patterns are distinct from the non-PHF derived myocardium of the primary heart tube and working myocardium of the chambers. During further development, upregulation of Nkx2.5 and downregulation of other genes occurs in the sinus venosus myocardium including the transient left-sided SAN, so that this myocardium gains a phenotype resembling the working myocardium. An exception is the definitive right-sided SAN, which can be distinguished also in late developmental stages from the working myocardium by distinct expression patterns. Data based on expression of the hyperpolarization-

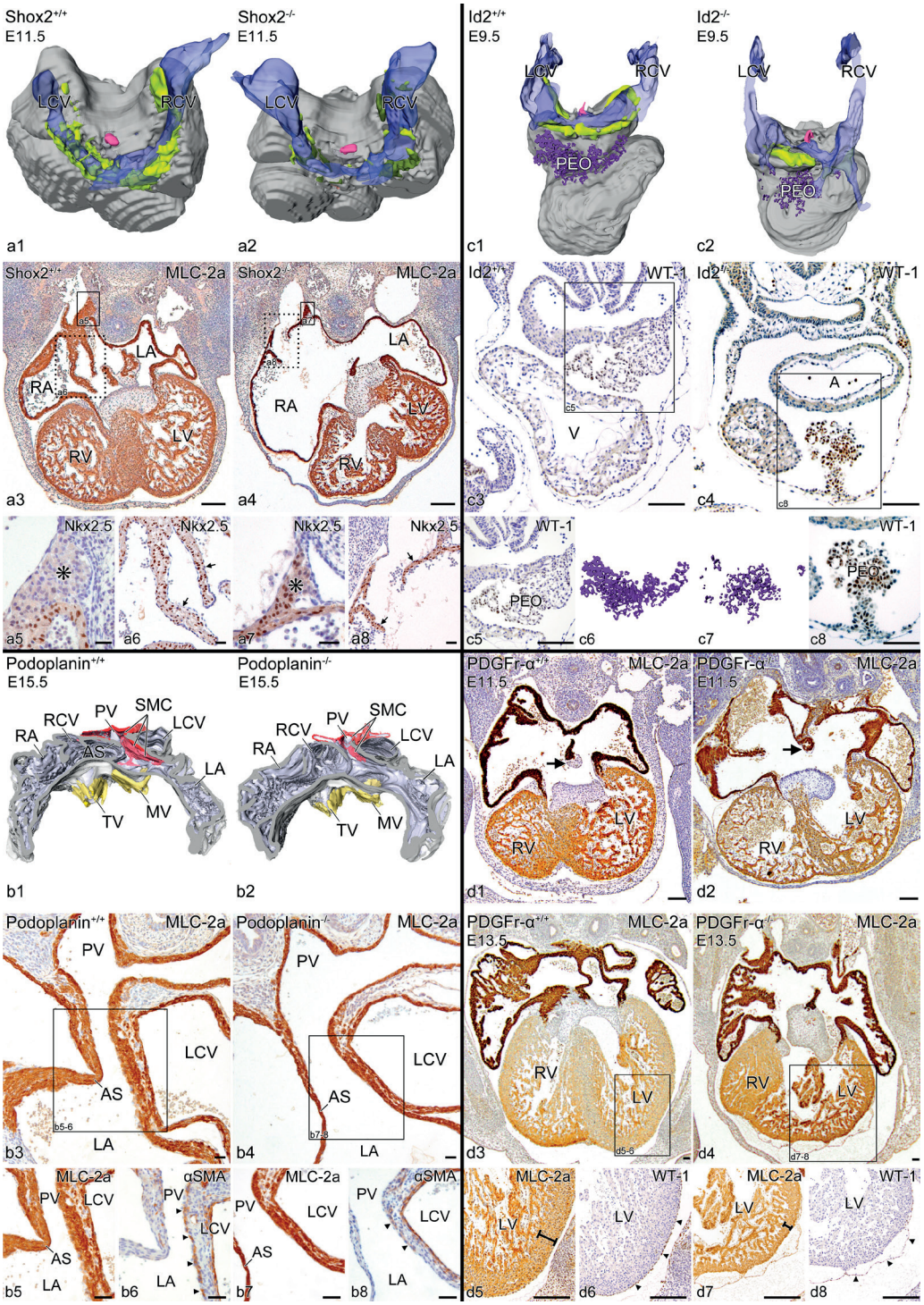

Figure 4. The posterior heart field phenotype (legend on page 25)

Figure 4. The posterior heart field phenotype (figure on page 24)
Figure demonstrates features of phenotypes observed in animal models with deficient PHF contribution. **a1-8.** Shox+/+ and -/- mouse embryos, E11.5. **a1-2.** Dorsal views 3D reconstructions Shox+/+ (**a1**) and Shox -/- (**a2**) mouse embryos. Color coding: lime green: Nkx2.5- sinus venosus myocardium, dark green: sinus venosus myocardium with aberrant upregulation Nkx2.5, grey: atrial/ventricular working myocardium, pink: primitive pulmonary vein. **a3-a4.** Overview sections Shox+/+ (**a3**) and Shox -/- (**a4**) embryonic hearts, MLC-2a staining. **a5**. Normal SAN. **a6**. Venous valves (arrows, VV), control. In knockout embryos, a hypoplastic SAN (**a7**) was observed, expressing MLC-2a (**a4**), with pathological upregulation of Nkx2.5 (**a7**) and hypoplastic VVs (arrows, **a8**). **b1-b8**. Podoplanin +/+ and -/- mouse embryos, E15.5. **b1-b2.** 3D reconstructions, atrial level. Color coding: yellow: fibrous heart skeleton, including mitral valve (MV) and tricuspid valve (TV), grey: atrial myocardium, pink: primitive pulmonary vein, red: smooth muscle cells (SMCs) of the vascular wall. **b3-b4**. Myocardium of atrial septum (AS), left cardinal vein (LCV) and pulmonary vein (PV) is hypoplastic in knockout (**b4**) as compared to wildtype (**b3**). **b5-b6, b7-b8.** Enlargements boxed areas in **b3** and **b4**, respectively. +/+ animals: SMCs (arrowheads, **b6**) cover inner wall left atrium, -/- animals: SMCs almost absent (arrowheads, **b8**). **c1-c8**. Id2 +/+ and -/- mouse embryos, E9.5. **c1-2.** 3D reconstructions, dorsal view, Id2 +/+ (**c1**), -/- (**c2**). Color coding: grey: myocardium, blue: lumen cardinal veins, lime green: MLC-2a+/Nkx2.5- sinus venosus myocardium, pink: pulmonary pit, PEO: purple. **c3-c4**. Overview WT-1 expression in wildtype (**c3**) and knockout (**c4**). **c5, c8.** Enlargements boxed areas in **c3** and **c4**, respectively. **c6-c7.** 3D reconstructions PEO in +/+ (**c6**) and -/- (**c7**) embryos. Note smaller volume PEO in -/- embryo. Also reduced amount sinus venosus myocardium in -/- (lime green, **c1**), as compared to +/+ (lime green, **c2**). **d1-d8**. Pdgf receptor alpha +/+ and -/- embryos. **d1-d2**. E11.5 overview of +/+ (**d1**) and -/- (**d2**) hearts, MLC-2a staining. Atrioventricular septal defect in -/- heart. Mesenchymal cap is lacking (compare arrow mesenchymal cap in **d1** with arrow in **d2** where mesenchymal cap is lacking). **d3-d4**. E13.5, overview of +/+ (**d3**) and -/- (**d4**) heart, MLC-2a staining. Boxed area in **d3** and **d4** enlarged in **d5-d6** and **d7-d8**, respectively. Indicate formation left ventricular (LV) compact myocardium and epicardial layer. Note pronounced myocardial blebbing in -/- (**d7-d8**) as compared to +/+ (**d5-d6**). Thin compact myocardial layer in -/- embryos (compare bars in **d7** with **d8**). A: common atrium, LA/RA: left/right atrium, LCV/RCV: left/right cardinal vein, LV/RV: left/right ventricle, PEO: proepicardial organ, V: ventricle. Scale bars: **a3-a4**: 300µm, **a5-a8**: 60µm, **b3-b8**: 30µm, all others: 100µm.
Figures in panel A (Shox2) modified after: Blaschke et al. Circulation. 2007;115(14):1830-1838
Figures in panel B (Podoplanin) modified after: Douglas et al. Pediatr. Res. 2009 Jan;65(1):27-32
Figures in panel C (Id2) modified after: Jongbloed et al. Dev. Dyn. 2011 Nov;240(11):2561-77
Figures in panel D (Pdgfr-alpha) modified after: Bax et al. Dev. Dyn. 2010;239;2307-17

activated cyclic nucleotide-gated channel HCN4 suggest that the SAN keeps a "primitive" phenotype, whereas the remainder of the sinus venosus myocardium will differentiate into a working myocardium phenotype.[28] This corresponds to other studies suggesting a primitive phenotype of the CCS as compared to the working myocardium.[74]

5.2. ABNORMAL DEVELOPMENT: MOUSE MODELS

In recent years several mutant mouse models have been described that are associated with what we refer to as a "*posterior heart field phenotype*"[18], that

can be attributed to either a deficiency of the myocardial or of the mesenchymal contributions from the PHF. These mutant mouse models present with distinct and largely overlapping phenotypes that indicate a disturbed development of the heart during recruitment of myocardial and mesenchymal structures to the venous pole of the heart from the PHF (examples are shown in **Fig. 4**). During development, the homeodomain transcription factor Shox2 is expressed in the sinus venosus myocardium, including the SAN and venous valves. Shox2 mutant mouse embryos demonstrate hypoplasia of the entire sinus venosus myocardium, including the SAN.[26] In addition, expression of Nkx2.5, which is normally lacking in the sinus venosus myocardium at early stages, is upregulated in the Shox2 mutant (**Fig. 4a**). A similar phenotype is observed in the podoplanin knockout mouse, which shows hypoplasia of the myocardium surrounding the cardinal veins, including the SAN, and of the myocardium of the pulmonary veins and deficiency of the pulmonary venous vascular smooth muscle layer (**Fig. 4b**). In addition, atrial and atrioventricular septal defects were observed. Furthermore, the PEO is small and development of the ventricular myocardial compact layer is

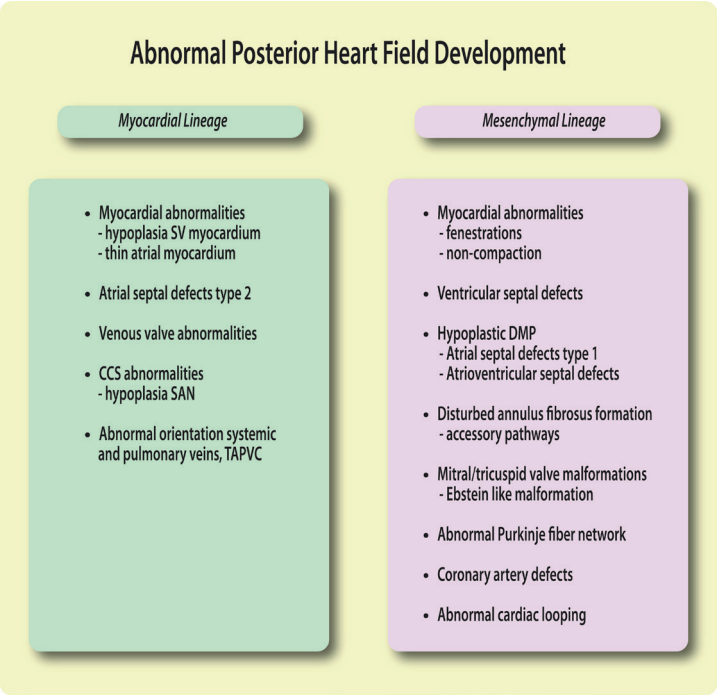

Figure 5. Schematic overview of the posterior heart field phenotype

Schematic summary of the phenotype observed in animal models with a deficiency of the contributions to the myocardial part (left) and mesenchymal part (right) of the posterior heart field. For description of the phenotypes and references: see text. Abbreviations: CCS: cardiac conduction system, DMP: dorsal mesenchymal protrusion, SAN: sinoatrial node, SV: sinus venosus, TAPVC: total anomalous pulmonary venous connections.

deficient in the podoplanin mutant embryos.[18,33,75] The phenotype of Id2 knockout embryos also includes a small PEO (**Fig. 4c**), thin sinus venosus myocardium and SAN hypoplasia, as well as large interatrial and interventricular communications and abnormal venous drainage patterns. The latter finding was also observed in Tbx3 knockout embryos[52], in which also the SAN volume is diminished.[73] Pdgfr-alpha mutant mouse embryos show a phenotype with thin sinus venosus myocardium, upregulation of Nkx2.5 in the SAN, atrial and atrioventricular septal defects, and a small PEO with pronounced epicardial blebbing and deficient numbers of EPDCs at later stages (**Fig. 4d**).[29] Furthermore, the pdgfr-alpha knockout is associated with anomalous drainage patterns of the systemic and pulmonary veins.[76] A schematic overview of abnormalities observed in animal models with a deficient myocardial and mesenchymal contribution from the posterior heart field, is provided in **Fig. 5**.

5.3. CLINICAL IMPLICATIONS: RHYTHM AND CONDUCTION DISTURBANCES

The functional importance of some of the genes expressed in the sinus venosus myocardium is further substantiated by the fact that mutations in these genes result in cardiac conduction abnormalities or rhythm disturbances, some of which have been related to rhythm and/or conduction abnormalities in human. For instance mutations in the human *HCN4* (responsible for I_f or funny-current) gene result in SAN bradycardia.[77] Of interest, the funny current inhibitor Ivabradine is increasingly being applied in clinical practice for heart rate reduction, targeting the spontaneous diastolic depolarization of the SAN. Adult mice with an over- or underexpression of the small GTPase RhoA that is downstream of podoplanin[19,22] present phenotypes with atrial fibrillation and AV-block, indicating a possible role for RhoA in the function of specific ion channels in the CCS.[78,79] Shox2 mutants show pronounced sinus bradycardia.[26] Ectopic expression of Tbx3 has been shown to result in ectopic atrial pacemaker activity[73,80] and SAN dysfunction.[80]

With regard to the occurrence of clinical arrhythmias, the sinus venosus wide expression pattern of genes is interesting in the light of the electrophysiological development of this area. In human, clinical arrhythmias are often related to sinus venosus related structures in the atria, such as the crista terminalis (embryonic right venous valve), the myocardium of the caval veins and coronary sinus (embryonic left and right cardinal veins), the ligament of Marshall (embryonic left cardinal vein) and the myocardium surrounding the pulmonary veins, that have all been described as sources from which arrhythmias can originate.[1–4,7] As described above, during development the entire sinus venosus myocardium, that includes the myocardium surrounding the cardinal veins (putative caval veins) demonstrates an expression pattern that is similar to that of the SAN, i.e. a nodal

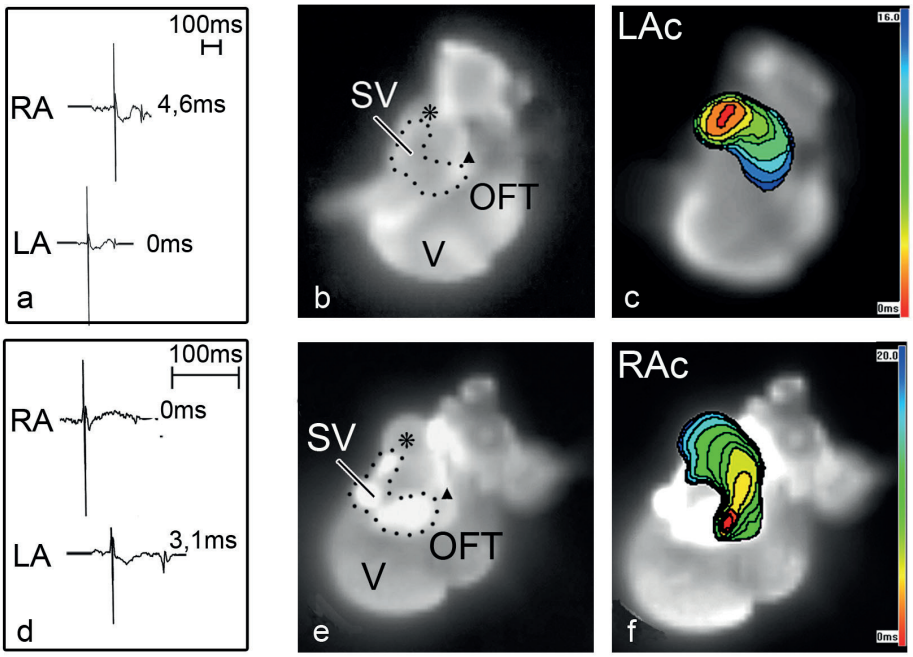

Figure 6. Electrophysiological changes during development

During development, initially the entire sinus venosus myocardium is capable of generating the first electrical activation. During development the right-sided SAN will become the definitive pacemaker. **a.** Representative example of an *ex ovo* electrophysiological recording of an embryonic chick heart (HH21), demonstrating left atrial activation (LAc) preceding right atrial activation (RAc) with 4,6ms. **b-c.** Electrical activation pattern as obtained with optical mapping, dorsal view, showing initiation of the electrical signal (red) in the LA. **d.** Representative example of an *ex ovo* electrophysiological recording of an embryonic chick heart (HH29), demonstrating RA activation preceding LA activation with 3,1ms. **e-f**. Electrical activation pattern as obtained with optical mapping, dorsal view, showing initiation of the electrical signal (red) in the RA. OFT: outflow tract, SV: sinus venosus, V: ventricle. Modified after: Vicente-Steijn et al. J. Cardiovasc. Elect. 2010;21(11):1284-1292.

phenotype. Results of electrophysiological recordings and optical mapping in chick embryonic hearts show that initially both atria have the potential to generate the first electrical activity, whereas later in development the activity becomes restricted to the right side, where the definitive SAN is located.[19] Previous studies have demonstrated electrical activation originating at the left inflow portion.[81] Interestingly the capacity of both sides of the sinus venosus myocardium to generate the first electrical activity was observed until approximately HH28 in chick, which correlated with the disappearance of markers like RHOA and Isl1 positive cells.[19] Using electrophysiology and optical mapping techniques in mouse and chick the potential of the left SAN to generate the first electrical activity of the heart was demonstrated in early developmental stages (**Fig. 6**).[19,82,83] The left-sided SAN appears earlier in development and is initially larger

in size than the right-sided SAN.[18] The myocardium of the pulmonary veins, that is well known for its arrhythmogenic capacities[4] may play a distinct role in this area, as expression patterns are not entirely similar to that of the cardinal veins. For instance, Tbx18, that is markedly present in the cardinal vein myocardium, is lacking in the pulmonary vein myocardium. However, several other markers expressed in the sinus venosus myocardium during development including the SAN, have similar expression patterns in the myocardium surrounding the pulmonary veins, such as HNK-1[62], CCS-lacZ[6], podoplanin[18], and HCN4.[28] Of particular interest in this light is the expression pattern of the latter, which is as described above responsible for the funny current in the SAN of human. HCN4 is expressed in the myocardium surrounding both the cardinal (putative caval) veins, as well as in the pulmonary vein myocardium during human[84], mouse[22] and chick[28] development. Interestingly, we have been able to follow cells from the left SAN region section-by-section towards the pulmonary vein myocardium in both chick and mouse (**Fig. 7**; Vicente Steijn *et al.*, unpublished observations). The presence of a functional pacemaker gene in the pulmonary vein myocardium during development provides an interesting link to the observed arrhythmogenic potential of this myocardium.[4] Elevated levels of HCN4 have been reported during heart failure, suggesting that the embryonic program can be reactivated during pathophysiological remodeling.[85]

Shox2 may play an important role in regulation of HCN4 expression, as Shox2

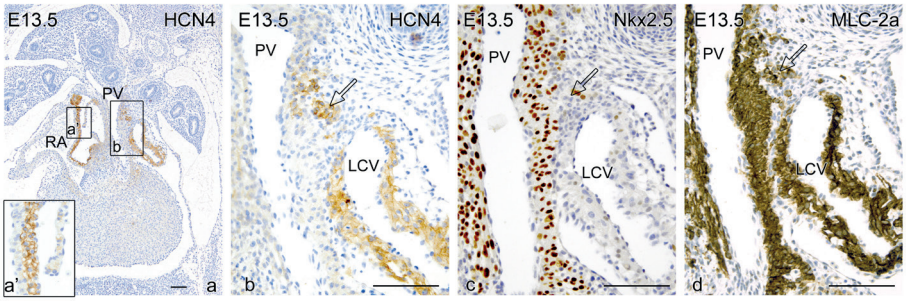

Figure 7. Left SAN and pulmonary veins

Cells from the region of the left-sided SAN can be traced section-to-section towards the myocardium surrounding the pulmonary veins (PV). **a.** Overview section, showing HCN4 expression at the level of the sinus venosus. **b-d.** Enlargements of the boxed area in **a**. Note marked expression of HCN4 in the inner layer of the right venous valve (see inset **a'**), that appears as a bilayered structure with an inner HCN4 positive, and an outer HCN4 negative layer. Expression of HCN4 (**b**) is observed in the cluster of cells (open arrows in **b-d**) that could be followed section-to-section from the left SAN region toward the PV myocardium. These cells were also characterised by expression of MLC-2a (**d**) and mostly lacking expression of Nkx2.5 (**c**). LCV: left cardinal vein, RA: right atrium. Scale bars 100μm.

knockout embryos showed absence of HCN4 expression (in situ hybridization).[86] In our own studies, we have not been able to demonstrate a reduced amount of HCN4 in the Shox2 mutant, which can possibly be attributed to different methods used (results based on protein expression data, Hahurij *et al.*, unpublished data).

Pitx2c, essential in the embryonic control of left/right asymmetry, has recently been shown to be associated with atrial fibrillation and regulation of the SAN genetic program by suppressing Shox2.[87] During development Pitx2 defines the left sinus venosus myocardium and is expressed in the left pulmonary ridge. It is needed to repress left-sided pacemaker activity[88], and Pitx2 mouse mutants show right atrial isomerism with bilateral SANs.[72,88] Both in mouse models as well as in human, Pitx mutations have been associated with atrial arrhythmias.[87,89–91] These results provide a plausible explanation for selected arrhythmias originating from ectopic pacemaker foci originating from e.g. the myocardium surrounding the caval and pulmonary veins and from the ligament of Marshall (remnant of the left cardinal vein).[4,6,7] Failure to differentiate into a chamber phenotype in these areas, or re-expression of the embryonic program may potentially lead to arrhythmogenic substrates in the adult.

5.4. CLINICAL IMPLICATIONS: ASSOCIATION CONGENITAL HEART DISEASE AND CONDUCTION SYSTEM DISEASE

The association of CCS disease with structural cardiac abnormalities, related to deficient contributions from the PHF, such as atrioventricular septal defects and abnormal venous drainage patterns, as observed in the mouse models described above (**Fig. 4** and **5**), would suggest a relation in the human situation. An interesting association between congenital heart disease and conduction disorders is observed in the human Holt Oram syndrome, based on a mutation in the Tbx5 gene. The majority of patients with conduction disease have AV conduction disorders, although sinus bradycardia and sick sinus syndrome have been reported.[92,93] Although sick sinus syndrome can be observed in non-syndromal patients with an atrial septal defect, this is usually attributed to previous surgery, such as the SAN disease observed after closure of atrial septal defects.[94] Some suggestions in literature are present though, indicating pre-existent sinus node disease in patients with atrial and atrioventricular septal defects[95–99] including prolonged sinus node recovery times on electrophysiology study. Also results in patients with anomalous pulmonary vein connections have shown a propensity to sick sinus syndrome.[100–102] Although the SAN disease is apparently asymptomatic in the majority of these patients, clinically this might imply that the SAN disease observed after surgery may be more pronounced due to pre-existent propensity to sick sinus syndrome that is developmentally associated with the occurrence of the septal/pulmonary drainage defects.

6. DEVELOPMENT OF THE VENOUS VALVES AND SEPTUM SPURIUM: INTERNODAL PATHWAYS WITH DEBATED FUNCTION

During early embryonic stages a left and right venous valve will develop in the right atrium, encompassing the entrance of the cardinal veins. The first sign of these valves is visible around E10.5 in mouse, and they are fully developed around E11.5. The right and left venous valves are dorsal structures that run in between the SAN and AVN, and will connect to the dorsal AVN during development.[62] Anteriorly, both valves fuse to form the septum spurium, that will initially connect to a transient anterior AVN.[62] In the developing embryo the 3 internodal tracts thus correspond to the right and left venous valves and the septum spurium, connecting to Bachmann's bundle (situated retro-aortically in between the right and left atrium).

Whether or not the internodal tracts are functional is still a matter of debate. The initial assumed role of the internodal tracts in fast conduction mainly derives from histological observations like the arrangements of the cardiomyocytes[103,104] and the suggested presence of Purkinje fibers.[105] The pathways were histologically described already several decades ago.[104–106] More recent marker gene expression studies in embryonic and fetal hearts have also shown distinct expression patterns in these tracts in both human[62] and animal models.[5,6,107,108] These sinus venosus related structures may represent the predilection sites of adult atrial arrhythmogenic areas. For instance, the adult counterpart of the right venous valve is the crista terminalis, a common site for atrial tachycardia and key player in the reentry path of common atrial flutter.[1] The right venous valve is a bilaminar structure with distinct expression patterns of the layers bordering the sinus venosus part of the atrium, that express a.o. HCN4, versus the appendage site of the atrium, that expresses atrial working myocardial markers (see **Fig. 7a, inset**). The left venous valve will become part of the atrial septum in human, whereas in mouse, and chick it will remain visible as a separate structure throughout development.

Most agree that preferential conduction occurs over the crista terminalis, however this has been attributed to cardiac tissue alignment[109] and not to specialized tracts. On the other hand, in the late seventies several studies showed preferential conduction of the cardiac impulse via pathways resembling to the internodal tracts as described by James.[104–106] In these studies, the administration of high doses of potassium in dog led to deprived electrical conduction in the atria except in sites corresponding with the internodal pathways and Bachman´s bundle.[110,111] Another recent study based on experiments with sodium channel blockers also indicates the presence of a preferential internodal conduction pathway in the right atrium.[83] These observations are further substantiated by studies in atrial preparations of canine hearts in which exposure to elevated

potassium levels also resulted in preferential conduction via the internodal pathway[112], as well as by results of optical mapping of atrial conduction patterns.[113] The implications of these findings for conduction pattern in the human situation however, remains to be determined.

2

7. NORMAL AND ABNORMAL DEVELOPMENT OF THE AVN

7.1. NORMAL DEVELOPMENT

The AVN is located in the posterior wall of the right atrium (**Fig. 1**), against the central fibrous body in the triangle of Koch, that is bordered by the ostium of the coronary sinus, the tendon of Todaro and the attachment of the septal leaflet of the tricuspid valve.[114] In human and lower mammals the AVN consists of a compact nodal part, that is covered by transitional cells, believed to be an atrial contribution to the AVN.[115] Nodal extensions originating from the AVN run towards the vestibules of the tricuspid and mitral valves.[116–121] During development the AVN can be identified from approximately the fifth week in human (+/- E11.5 in mouse).[122] During early developmental stages, the AVN myocardium cannot be distinguished from the AV canal myocardium, a circumferential band of myocardium between the atria and ventricles. A dual anlage of the AVN has been described, with both an anterior and posterior node present during early development, which will fuse to form the AVN primordium.[62,123,124] The posterior node connects to the His bundle and will eventually form the major part of the definitive AVN. The cellular origin of the AVN is still controversial. Among several hypotheses proposed over the past decades are (1) an origin from the AV canal myocardium[122,125–127]; (2) a confluence of the sinoatrial ring, AV ring and possibly the primary fold[38,61], or from the primary fold alone[128]; (3) an origin from the atrial dorsal wall[129], or (4) from the lower part of the interatrial septum[130] and (5) an embryonic left-sided counterpart of the SAN, that by remodeling of the left cardinal vein will be positioned at its mature location near the ostium of the coronary sinus in the right atrium.[49] The presence of morphologically and electrophysiologically distinct cells in the AVN may indicate that cells from multiple sources contribute to its formation.[49,131,132]

Whereas an origin of the SAN from the PHF is nowadays well established, whether or not there is a SHF contribution to the AVN, is still unresolved. Lineage tracing studies indicate that at least the compact part is derived from the AV ring myocardium (itself first heart field-derived).[20] However, other studies have also indicated a contribution from the second heart field.[21] The lower part of the AVN was found to be derived from ventricular myocardium, whereas the origin and function of an eventual atrial septal component of the conduction axis remains unclear.[20] During development, the murine AVN is molecularly characterized by expression of HCN4, Tbx3, Tbx5 and Cx45 and lacks Cx40 and Cx43.[20,24] Whether

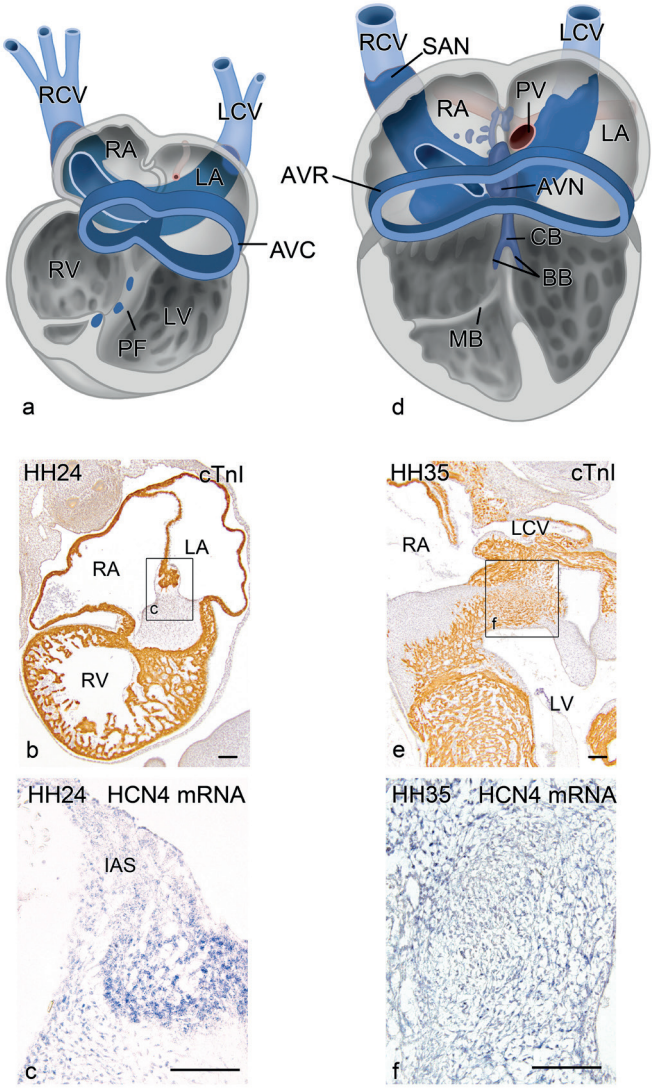

Figure 8. AVN development in chicken

a,d. Schematic representation of *HCN4* expression in the heart at an early (**a**) and later (**d**) developmental stage, after looping has progressed. Next to *HCN4* expression in the sinus venosus myocardium, *HCN4* is expressed in the entire AV canal (AVC), including the putative AVN. **b,e**. Histological sections, level: base interatrial septum (AVN region) in HH24 (**b**) and HH35 (**e**) heart. cTNI staining. AVN region is characterized by the presence of loose cells with large intercellular spaces as compared to the working myocardium. **c,f.** Histological sections demonstrating expression of *HCN4* mRNA at the same regions in HH24 (**c**) and HH35 (**f**) heart. AVR: AV ring, BB: bundle branches, CB: common bundle/His bundle, IAS: interatrial septum, LA: left atrium, LCV: left cardinal vein, LV: left ventricle, MB: moderator band, PF: primary fold, PV: pulmonary vein, RA: right atrium, RCV: right cardinal vein, RV: right ventricle, SAN: sinoatrial node. Scale bars: 150μm.

the avian system has a circumscript AVN is still a matter of debate. In contrast to mouse, we were not able to distinguish a compact and transitional nodal part in chicken. However, a distinct expression pattern of *HCN4* throughout the AV canal and lower part of the atrial septum, as well as Cx43 and PAS staining patterns could be observed (**Fig. 8**; Vicente Steijn *et al.*, unpublished data). The maturation of the AVN seems not to be completed at the time of birth, as a number of structural changes with regard to rearrangement of myocardium as well as fibrous tissue occurs in the first year of life.[133,134]

With regard to electrophysiology, an AV delay can be recorded already at early developmental stages in the AV canal, that possesses a slow-conducting phenotype.[135] Later in development, the AVN becomes responsible for the AV delay.[130] Eventually the AV myocardial continuity will disappear as a result of annulus fibrosus formation[136], with the common bundle remaining as the only myocardial continuity that will propagate the electrical impulse to the ventricles. The common bundle and bundle branches will conduct the impulse rapidly to the ventricular working myocardium, and the immature base-to-apex activation pattern of the heart will shift to the mature apex-to-base activation pattern.[136]

7.2. ABNORMAL DEVELOPMENT: MOUSE MODELS

As described above, several genes are currently recognized in the AVN during development, and mouse models that display a disturbed AVN phenotype are available. Tbx3 disruption results in AV block, pre-excitation, and an increased risk for sudden cardiac death.[80] Mutations in Tbx5, the pivotal gene disrupted in the human Holt-Oram syndrome[137], result in deficient maturation of the AVN.[24] HCN4, which as described above is responsible for the sinoatrial "funny current" is also expressed in the AV canal and AVN during development[27,28], and next to profound bradycardia, disruption results in AV block.[138] Nkx2.5 knockout animals show conduction defects that include AV block.[139] Mutations in the Nkx2.5 gene have been described in human patients with congenital AV block.[140,141]

7.3. CLINICAL IMPLICATIONS: RHYTHM AND CONDUCTION DISORDERS FROM THE AVN AND AV JUNCTION

The presence of histologically, and perhaps electrophysiologically distinct cells within the AVN is of relevance for arrhythmias originating in the AVN, the so called AV nodal reentry tachycardia (AVNRT), as a prerequisite for the occurrence of reentry is the presence of 2 pathways with distinct electrophysiological characteristics.[142] Extensions from the AVN, mostly referred to as inferior nodal extensions[120,143] are considered the substrate for the "slow pathway" that underlies the occurrence of AVNRT and are the target for radiofrequency catheter ablation.[144] The origin and cellular composition of the inferior nodal

extension has been described as a continuation of the compact AVN.[20] However, as mentioned above, it may also consist of transitional cells extending into the AVN from the atrial or sinus venosus myocardium[143] or be a combination of both. Interestingly, the gene expression profile of the inferior nodal extension was found to be similar to that of the SAN[145], indicating a possible contribution of the sinus venosus myocardium. In this respect it is interesting to note that pacemaker activity of the AV junction has been attributed to the inferior nodal extension.[146] Other arrhythmias originating from the AV junction include clinical arrhythmias originating from the tricuspid and mitral junction.[147,148]

Persistence of a fetal phenotype of the AVN, so-called fetal dispersion[134], has been related to the appearance of sudden cardiac death in the young.[149,150]

7.4. CLINICAL IMPLICATIONS: ASSOCIATION CONGENITAL HEART DISEASE AND CONDUCTION SYSTEM DISEASE

The dual developmental origin of the AVN[62] is interesting in the light of congenitally corrected transposition of the great arteries (ccTGA), which is characterized by both a atrioventricular as well as a ventriculo-arterial discordance. Due to a malalignment of the atrial and ventricular septum, leaving a "gap" preventing the dorsal AVN to reach the ventricular CCS, an antero-superior position of the AVN can be found.[151,152] In case of normal alignment a more normally situated postero-inferiorly position (between the annulus of the right-sided mitral valve and the ostium of the right atrial appendage) of the AVN is encountered, although a "sling of tissue" to an additional anterior AVN can also be observed.[151,152] There seems to be a correlation between the diameter of the pulmonary trunk and septal malalignment.[153] These findings indicate that normal development of the AVN depends on normal alignment of the atrial and ventricular septa[152], whereas an anterior AVN will be dominant in cases with septal malalignment. In case of ccTGA the bundle of His penetrates the AV junction at the area of fibrous continuity between the pulmonary and mitral valves, and there is an inversion of the bundle branches.

As mentioned previously, human mutations in the Tbx5 gene are observed in the Holt-Oram syndrome, characterized by hand-limb disorders, atrial septal defects and (predominantly) AV conduction disorders.[92]

In patients with atrioventricular septal defects (AVSD), AV conduction disorders are also common.[154–156] This is usually attributed to an abnormally positioned AVN, with a postero-inferior displacement of the AVN, and a long nonbranching bundle of His.[157] Recent studies suggest an abnormal development of the CCS in AVSD[158], rather than a downward displacement of the AVN, and lack of apposition of the two primordia of the AVN, resulting in a dorso-inferior persisting position of the inferior part of the AVN seems to be underlying the

abnormal location of the AVN in AVSD.[158] The relatively long route of the His bundle probably predisposes to the damage and/or degeneration, resulting in AV block. Alternatively, a deficient contribution of the second heart field to the CCS might underlie the occurrence of conduction abnormalities in AVSD, as is suggested by results indicating a deficiency of the dorsal mesenchymal protrusion (vestibular spine) as the underlying cause of AVSD.[158,159] The dorsal mesenchymal protrusion is derived form the PHF.[160] However, a contribution of this mesenchymal structure to the AVN has thus far not been established[20] although a SHF contribution to the AVN has been suggested.[21] Additional lineage tracing studies are needed in order to determine the exact origin of cells contributing to the AVN.

8. NORMAL AND ABNORMAL DEVELOPMENT OF THE ANNULUS FIBROSUS

8.1. NORMAL DEVELOPMENT

In a mature heart the AV conduction axis comprises the only myocardial continuity between the atria and ventricles, the remainder being separated by a layer of fibrous tissue at the AV junction i.e. the annulus fibrosus (**Fig. 1**). Development of the AV junction involves the fusion of the AV sulcus tissue from the epicardial side with the endocardially located cushion tissue of the developing heart.[161–164] Formation of the annulus fibrosus in mouse as well as in human already starts at pre-septation stages of development (around 7 weeks of human development) by formation of fibrous tissue near the primitive AV canal.[165] Around the twelfth week of human development the complete atrial and ventricular myocardium are largely separated by the annulus fibrosus.[164,165] Full formation of the annulus fibrosus is a gradual event and studies in chicken, mouse and human show persistence of accessory pathways (APs) until late developmental stages.[136,165,166] Electrophysiological recordings in embryonic and fetal quail hearts showed presence of antegrade conducting APs in otherwise normal developing hearts.[35,136] These APs decreased in number and size at subsequent stages of development. Between species, differences exist in the preferential location of APs at the annulus fibrosus. At late stages of human heart development most APs were observed subendocardially at the lateral aspect of the tricuspid valve orifice.[165]

Epicardium-derived cells (EPDCs) are important for proper development of the annulus fibrosus. During development, EPDCs will migrate into the AV annulus and play a role in fibrosation of the annulus and fusion of the epicardial sulcus tissue with the endocardial cushion tissue.[35,36] Another factor involved in formation of the annulus fibrosus is bone-morphogenetic protein (BMP) signaling.[167,168] The extracellular matrix molecule periostin was postulated to have an important role in annulus fibrosus formation because of its ability to directly

regulate collagen-I fibrillogenesis.[169] A study by the group of Zhou confirmed that EPDCs differentiate into fibroblasts contributing to the annulus fibrosus, and showed colocalization of EPDCs with periostin in the annulus fibrosus in mouse. The EPDCs in the annulus fibrosus were highly enriched for markers for fibroblasts as well as for markers for EMT and cellular migration.[170] Recent studies indicate that distinct subpopulations of EPDCs can be found, suggesting that this might also be the case in the region of the annulus fibrosus.[171] Periostin expression data in mouse showed that in the developing AV junction periostin is never co-expressed in cardiomyocytes.[166] Whether periostin is the key factor in AV isolation remains doubtful, since recent studies in periostin mutant mice showed that periostin null mutants are largely normal and do not show an abnormal cardiac phenotype.[172]

8.2. ABNORMAL DEVELOPMENT: ACCESSORY PATHWAYS IN ANIMAL MODELS AND HUMAN

APs are defined as accessory bundles of cardiomyocytes, which interconnect the atrial and ventricular myocardium next to the AV conduction axis. These APs may either conduct the action potential in an antegrade (atrium-to-ventricle) or a retrograde (ventricle-to-atrium) manner. Furthermore, APs may form the substrate for supraventricular arrhythmias such as WPW syndrome and Mahaim tachycardia. Studies in both human and animals have shown that APs can be located anywhere at the AV junction and can be positioned endocardially or epicardially. Although it has been well established that abnormal development of the AV junction, as observed in patients with Ebstein's anomaly, coincides with high numbers of APs,[173,174] there is still debate on the exact origin of APs. Electrophysiological studies in human[175,176] and animal models[177] demonstrated that not all APs share the same electrophysiological conducting properties, some APs even have decremental properties resembling to those of specialized CCS tissue[175], whereas others demonstrate a working myocardium phenotype. Moreover, morphological analysis of APs indicated that not all APs show the same cellular morphology.[178–180] In clinical practice not all APs in patients suffering from AV reentry tachycardia (AVRT) react similarly to anti-arrhythmic drugs.[181] All these arguments may indicate that not all APs share a common developmental origin.

Incomplete (pathological) maturation of the annulus fibrosus has developmentally been related to deficient contributions of EPDCs. Epicardial inhibition in chick and quail results in broad accessory AV connections, pre-excitation on the electrogram, and, in contrast to the accessory AV connections observed during normal heart development, negative staining patterns for periostin.[35,36] Furthermore, lack of expression of periostin in the AV endocardial

cushions was observed, as well as lack of delamination of mural valve leaflets, resulting in Ebstein-like valvular anomalies. The relation between EPDCs and periostin was further studied *in vitro* and *in vivo*, and indicated that during development, EPDCs are local producers of periostin.[36] Alk3 is also required for periostin expression in the developing AV valves. Targeted deletion of Alk3 results in abnormalities of the cardiac inflow tract/AV valves, as well as in disruption of the annulus fibrosus resulting in ventricular pre-excitation.[167] These data are interesting in the light of the co-occurence of accessory pathways and tricuspid valve anomalies in Ebstein's anomaly and ccTGA.[182]

A special group of accessory pathways is formed by the so-called atrio-fascicular tracts underlying Mahaim tachycardia. These tracts might be narrowly related to right ventricular inflow tract development as functional APs were observed at the right AV junction, connecting to the right bundle branch via the moderator band.[183] In Mahaim tachycardia the APs have decremental properties resembling that of the AVN[175,184], which might indicate that some APs are composed of specialized conducting tissue. Furthermore, it is well known that APs involved in Mahaim tachycardia have a morphological relation with the specialized CCS and interconnect the AVN or His bundle to the fascicles or ventricular muscle.[132] Nevertheless, the question remains whether the presence of APs with decremental properties can also be related to the normal process of cardiac development.

Several genetic mutations have been identified that coincide with high percentages of APs. Mutations in the gene encoding the gamma2 regulatory subunit of AMP-activated kinase (PRKAG-2) have been found in families with WPW syndrome. Patients carrying this mutation suffer from ventricular pre-excitation, atrial fibrillation, conduction defects and cardiac hypertrophy.[185,186] Mouse models with this specific mutation demonstrated postnatal development of APs responsible for ventricular pre-excitation.[187] Another mutation recently related to AP etiology is in the BMP receptor Alk3 described above.[167] Furthermore, the conditional knockout of Tbx2 results in disturbed development of the AV myocardium and pre-excitation.[188]

8.3. CLINICAL IMPLICATIONS: PRE-EXCITATION SYNDROMES

AVRTs represent the largest group of tachy-arrhythmias pre- and postnatally and can be potentially life-threatening.[189,190] APs underlying AVRT can present at the tricuspid as well as the mitral valve orifice. The incidence of APs tends to be higher at the left/mitral valve orifice.[191–193] The etiology of the APs underlying this specific type of arrhythmia is largely unknown. In a minority of cases genetic mutations are involved, like PRKAG-2 (in familiar WPW syndrome)[185,186] and Alk3 and Tbx2 (in mice).[167,188] Furthermore, high numbers of APs are found

in combination with other forms of congenital heart disease i.e. Ebstein's anomaly[173,174] and ccTGA.[182]

In human, two-thirds of newborns diagnosed with AVRT based on the presence of APs remain free of symptoms before the age of one year without additional anti-arrhythmic therapy or invasive treatment strategies.[190,194,195] This might suggest that annulus fibrosus formation and maturation is not finished by the time of birth and extends into the first year of life. Prolonged cardiac maturation during the first year of life might cause APs to spontaneously disappear, so that AVRT automatically resolves. This is supported by the observation that especially the development of the fibrous structures of the heart that includes the annulus fibrosus, extends into postnatal life.[196,197] The ongoing maturation of the annulus fibrosus offers a good explanation for spontaneous AVRT disappearance. However, it remains uncertain why approximately one-third of patients have a recurrent episode of AVRT later in life.[198]

8.4. CLINICAL IMPLICATIONS: CONGENITAL HEART DISEASE AND ACCESSORY PATHWAYS

The co-occurrence of right-sided AV valve anomalies and APs in Ebstein's anomaly and ccTGA might indicate a common developmental pathway. We propose a disturbed function or contribution of EPDCs during development that could account for both the valve anomalies as well as the APs that were observed in animal models, as indicated above.[36,167] In this respect it is also interesting to note the common occurrence of Mahaim tachycardia in patients with Ebstein's anomaly of the tricuspid valve[199], which has also been related to the deficient development of the right ventricular inflow tract.[183]

ccTGA is associated with accessory AV connections, indicating a deficient formation of the annulus fibrosus. Furthermore, Ebstein-like malformations of the tricuspid valve are frequently observed[200], as well as ventricular non-compaction.[201] Interestingly, a deficient formation of the annulus fibrosus, abnormalities of the AV valves as well as ventricular non-compaction have all been observed in animals models with deficient contributions of the epicardium[32,167], indicating a possible deficient contribution of the mesenchymal part of the posterior heart field, from the PEO and its derived cells. Also looping defects have been described in this phenotype.[32]

9. WORKING MODEL FOR DEVELOPMENTALLY BASED CLINICAL ARRHYTHMIAS (FIG. 9)

In children and adult patients with structurally normal hearts various arrhythmias can be observed. Electrophysiological studies have indicated predilection sites in the heart from which these arrhythmias may originate, that include the myocardium surrounding the caval veins, coronary sinus and pulmonary veins, the ligament of Marshall, accessory pathways at the AV junction, and the right ventricular outflow tract. In **Fig. 9** a working model for a developmental background of selected arrhythmias in patients with structurally normal hearts is proposed. As described in this review, the embryonic CCS is much broader than the definitive adult CCS. This means that larger areas of tissue that show CCS characteristics during development will later on differentiate to a working myocardium phenotype. In the working model it is proposed that these embryonic sites still relate to predilection sites for arrhythmias as observed in the adult. In general, remnants of tissues with an embryonic phenotype may underlie the occurrence of arrhythmias in the young, whereas the occurrence of arrhythmias in the adult might relate to the re-expression of an embryonic phenotype. The spontaneous disappearance of arrhythmias in the young is according to this model related to postnatal cardiac maturation, whereas in the adult a pathophysiological state might contribute to the re-expression of the embryonic program, as is supported by the observation of increased expression of HCN4 in patients with heart failure and atrial fibrillation.[85]

Figure 9. Working model for the developmental background of clinical arrhythmias in the child/adult (figure on page 41)

Selected clinical arrhythmias in human patients are frequently observed in anatomical predilection sites which may be related to the embryonic development of the CCS. Here a working model is presented relating embryonic structures to the adult counterparts, and the arrhythmias that have been observed to originate in these areas. For further explanation, see text.

A: common atrium, Ao: aorta, AoS: aortic sac, AV: atrioventricular, AVC: atrioventricular canal, AVN: atrioventricular node, AVRT: AV reentry tachycardia, AV-TZ: atrioventricular transitional zone, CS: coronary sinus, GCV: great cardiac vein, ICV: inferior caval vein, LA: left atrium, LBB: left bundle branch, LCV: left cardinal vein, LV: (putative) left ventricle, LVOT: left ventricular outflow tract, LVV: left venous valve, MB: moderator band, OFT: outflow tract, OFT-TZ: outflow tract transitional zone, PF: primary fold, PT: pulmonary trunk, PV: pulmonary vein(s), RA: right atrium, RBB: right bundle branch, RCV: right cardinal vein, RV: (putative) right ventricle, RVOT: right ventricular outflow tract, RVV: right venous valve, SAN: sinoatrial node, SA-TZ: sinoatrial transitional zone, SCV: superior caval vein, SP: septum primum, V: common ventricle, VM: vein of Marshall/Marshall ligament, VS: ventricular septum, VT: ventricular tachycardia, WPW: Wolff-Parkinson-White syndrome.

Figure 9. Working model for the developmental background of clinical arrhythmias in the child/ adult (legend on page 40)

REFERENCE LIST

1. Kalman, J. M. *et al.* 'Cristal tachycardias': origin of right atrial tachycardias from the crista terminalis identified by intracardiac echocardiography. *J. Am. Coll. Cardiol.* **31,** 451–9 (1998).

2. Tsai, C.-F. *et al.* Initiation of atrial fibrillation by ectopic beats originating from the superior vena cava: electrophysiological characteristics and results of radiofrequency ablation. *Circulation.* **102,** 67–74 (2000).

3. Katritsis, D. *et al.* Conduction delay within the coronary sinus in humans: implications for atrial arrhythmias. *J. Cardiovasc. Electrophysiol.* **13,** 859–62 (2002).

4. Haïssaguerre, M. *et al.* Spontaneous initiation of atrial fibrillation by ectopic beats originating in the pulmonary veins. *N. Engl. J. Med.* **339,** 659–66 (1998).

5. Hoogaars, W. M. H. *et al.* The transcriptional repressor Tbx3 delineates the developing central conduction system of the heart. *Cardiovasc. Res.* **62,** 489–99 (2004).

6. Jongbloed, M. R. M. *et al.* Embryonic conduction tissue: a spatial correlation with adult arrhythmogenic areas. *J. Cardiovasc. Electrophysiol.* **15,** 349–55 (2004).

7. Kurotobi, T. *et al.* Marshall vein as arrhythmogenic source in patients with atrial fibrillation: correlation between its anatomy and electrophysiological findings. *J. Cardiovasc. Electrophysiol.* **17,** 1062–7 (2006).

8. DeRuiter, M. C., Poelmann, R. E., van der Plas-de Vries, I., Mentink, M. M. & Gittenberger-de Groot, A. C. The development of the myocardium and endocardium in mouse embryos. Fusion of two heart tubes? *Anat. Embryol.* **185,** 461–473 (1992).

9. Lough, J. & Sugi, Y. Endoderm and heart development. *Dev. Dyn.* **217,** 327–42 (2000).

10. Cai, C.-L. *et al.* Isl1 identifies a cardiac progenitor population that proliferates prior to differentiation and contributes a majority of cells to the heart. *Dev. Cell.* **5,** 877–89 (2003).

11. Kelly, R. G., Brown, N. A. & Buckingham, M. E. The arterial pole of the mouse heart forms from Fgf10-expressing cells in pharyngeal mesoderm. *Dev. Cell.* **1,** 435–440 (2001).

12. de la Cruz, M. V, Sánchez Gómez, C., Arteaga, M. M. & Argüello, C. Experimental study of the development of the truncus and the conus in the chick embryo. *J. Anat.* **123,** 661–86 (1977).

13. Waldo, K. L. *et al.* Conotruncal myocardium arises from a secondary heart field. *Development.* **128,** 3179–3188 (2001).

14. Buckingham, M., Meilhac, S. & Zaffran, S. Building the mammalian heart from two sources of myocardial cells. *Nat. Rev. Genet.* **6,** 826–835 (2005).

15. Abu-Issa, R. & Kirby, M. L. Heart field: from mesoderm to heart tube. *Annu. Rev. Cell. Dev. Biol.* **23,** 45–68 (2007).

16. Mjaatvedt, C. H. *et al.* The outflow tract of the heart is recruited from a novel heart-forming field. *Dev. Biol.* **238,** 97–109 (2001).

17. Zaffran, S., Kelly, R. G., Meilhac, S. M., Buckingham, M. E. & Brown, N. A. Right ventricular myocardium derives from the anterior heart field. *Circ. Res.* **95,** 261–8 (2004).

18. Gittenberger-de Groot, A. C. *et al.* Nkx2.5-negative myocardium of the posterior heart field and its correlation with podoplanin expression in cells from the developing cardiac pacemaking and conduction system. *Anat. Rec.* **290,** 115–22 (2007).

19. Vicente-Steijn, R. *et al.* Electrical activation of sinus venosus myocardium and expression patterns of RHOA and Isl-1 in the chick embryo. *J. Cardiovasc. Electrophysiol.* **21,** 1284–92 (2010).

20. Aanhaanen, W. T. J. *et al.* Developmental origin, growth, and three-dimensional architecture of the atrioventricular conduction axis of the mouse heart. *Circ. Res.* **107,** 728–36 (2010).

21. Sun, Y. *et al.* Islet 1 is expressed in distinct cardiovascular lineages, including pacemaker and coronary vascular cells. *Dev. Biol.* **304,** 286–96 (2007).

22. Mahtab, E. A. F. *et al.* Podoplanin deficient mice show a RHOA-related hypoplasia of the sinus venosus myocardium including the sinoatrial node. *Dev. Dyn.* **238,** 183–93 (2009).

23. Christoffels, V. M. *et al.* Formation of the venous pole of the heart from an Nkx2-5-negative precursor population requires Tbx18. *Circ. Res.* **98,** 1555–63 (2006).

24. Moskowitz, I. P. G. *et al.* The T-Box transcription factor Tbx5 is required for the patterning and maturation of the murine cardiac conduction system. *Development.* **131,** 4107–16 (2004).

25. Puskaric, S. *et al.* Shox2 mediates Tbx5 activity by regulating Bmp4 in the pacemaker region of the developing heart. *Hum. Mol. Genet.* **19,** 4625–33 (2010).

26. Blaschke, R. J. *et al.* Targeted mutation reveals essential functions of the homeodomain transcription factor Shox2 in sinoatrial and pacemaking development. *Circulation.* **115,** 1830–8 (2007).

27. Garcia-Frigola, C., Shi, Y. & Evans, S. M. Expression of the hyperpolarization-activated cyclic nucleotide-gated cation channel HCN4 during mouse heart development. *Gene Expr. Patterns.* **3,** 777–783 (2003).

28. Vicente-Steijn, R. *et al.* Funny current channel HCN4 delineates the developing cardiac conduction system in chicken heart. *Heart Rhythm.* **8,** 1254–63 (2011).

29. Bax, N. A. M. *et al.* Cardiac malformations in Pdgfralpha mutant embryos are associated with increased expression of WT1 and Nkx2.5 in the second heart field. *Dev. Dyn.* **239,** 2307–17 (2010).

30. Pérez-Pomares, J. M., Phelps, A., Sedmerova, M. & Wessels, A. Epicardial-like cells on the distal arterial end of the cardiac outflow tract do not derive from the proepicardium but are derivatives of the cephalic pericardium. *Dev. Dyn.* **227,** 56–68 (2003).

31. Kruithof, B. P. T. *et al.* BMP and FGF regulate the differentiation of multipotential pericardial mesoderm into the myocardial or epicardial lineage. *Dev. Biol.* **295,** 507–22 (2006).

32. Lie-Venema, H. *et al.* Origin, fate, and function of epicardium-derived cells (EPDCs) in normal and abnormal cardiac development. *ScientificWorldJournal.* **7,** 1777–98 (2007).

33. Mahtab, E. A. F. *et al.* Cardiac malformations and myocardial abnormalities in podoplanin knockout mouse embryos: Correlation with abnormal epicardial development. *Dev. Dyn.* **237,** 847–57 (2008).

34. Gittenberger-de Groot, A. C., Vrancken Peeters, M.-P. F. M., Mentink, M. M. T., Gourdie, R. G. & Poelmann, R. E. Epicardium-Derived Cells contribute a novel population to the myocardial wall and the atrioventricular cushions. *Circ. Res.* **82,** 1043–1052 (1998).

35. Kolditz, D. P. *et al.* Epicardium-derived cells in development of annulus fibrosus and persistence of accessory pathways. *Circulation.* **117,** 1508–17 (2008).

36. Lie-Venema, H. *et al.* Periostin expression by epicardium-derived cells is involved in the development of the atrioventricular valves and fibrous heart skeleton. *Differentiation.* **76,** 809–19 (2008).

37. Eralp, I. *et al.* Epicardium-Derived Cells (EPDCS) are important for correct development of the Purkinje fibers in the avian heart. *Anat. Rec. A. Discov. Mol. Cell. Evol. Biol.* **288,** 1272-80 (2006).

38. Gittenberger-de Groot, A. C., Bartelings, M. M., DeRuiter, M. C. & Poelmann, R. E. Basics of cardiac development for the understanding of congenital heart malformations. *Pediatr. Res.* **57,** 169–76 (2005).

39. Poelmann, R. E., Mikawa, T. & Gittenberger-de Groot, A. C. Neural crest cells in outflow tract septation of the embryonic chicken heart: differentiation and apoptosis. *Dev. Dyn.* **212,** 373–84 (1998).

40. Waldo, K., Miyagawa-Tomita, S., Kumiski, D. & Kirby, M. L. Cardiac neural crest cells provide new insight into septation of the cardiac outflow tract: aortic sac to ventricular septal closure. *Dev. Biol.* **196,** 129–44 (1998).

41. Nakamura, T., Colbert, M. C. & Robbins, J. Neural crest cells retain multipotential characteristics in the developing valves and label the cardiac conduction system. *Circ. Res.* **98,** 1547–54 (2006).

42. Hildreth, V., Anderson, R. H. & Henderson, D. J. Autonomic innervation of the developing heart: origins and function. *Clin. Anat.* **22,** 36–46 (2009).

43. Verberne, M. E., Gittenberger-De Groot, A. C., Van Iperen, L. & Poelmann, R. E. Contribution of the cervical sympathetic ganglia to the innervation of the pharyngeal arch arteries and the heart in the chick embryo. *Anat. Rec.* **255,** 407–19 (1999).

44. Gorza, L., Schiaffino, S. & Vitadello, M. Heart conduction system: a neural crest derivative? *Brain Res.* **457,** 360–6 (1988).

45. Poelmann, R. E. *et al.* The neural crest is contiguous with the cardiac conduction system in the mouse embryo: a role in induction? *Anat. Embryol.* **208,** 389–93 (2004).

46. Poelmann, R. E. & Gittenberger-de Groot, A. C. A subpopulation of apoptosis-prone cardiac neural crest cells targets to the venous pole: multiple functions in heart development? *Dev. Biol.* **207,** 271–86 (1999).

47. Gurjarpadhye, A. *et al.* Cardiac neural crest ablation inhibits compaction and electrical function of conduction system bundles. *Am. J. Physiol. Heart Circ. Physiol.* **292,** H1291-300 (2007).

48. Gourdie, R. G., Mima, T., Thompson, R. P. & Mikawa, T. Terminal diversification of the myocyte lineage generates Purkinje fibers of the cardiac conduction system. *Development.* **121,** 1423–31 (1995).

49. James, T. N. Structure and function of the sinus node, AV node and His bundle of the human heart: part I-structure. *Prog. Cardiovasc. Dis.* **45,** 235–67

50. Viragh, S. & Challice, C. E. The development of the conduction system in the mouse embryo heart. III. The development of sinus muscle and sinoatrial node. *Dev. Biol.* **80,** 28–45 (1980).

51. Jongbloed, M. R., Mahtab, E. A., Blom, N. A., Schalij, M. J. & Gittenberger-de Groot, A. C. Development of the cardiac conduction system and the possible relation to predilection sites of arrhythmogenesis. *ScientificWorldJournal.* **8,** 239–269 (2008).

52. Mesbah, K., Harrelson, Z., Théveniau-Ruissy, M., Papaioannou, V. E. & Kelly, R. G. Tbx3 is required for outflow tract development. *Circ. Res.* **103,** 743–50 (2008).

53. Cheng, G. *et al.* Development of the cardiac conduction system involves recruitment within a multipotent cardiomyogenic lineage. *Development.* **126,** 5041–9 (1999).

54. Gourdie, R. G. *et al.* Development of the cardiac pacemaking and conduction system. *Birth Defects Res. C. Embryo Today.* **69,** 46–57 (2003).

55. Pennisi, D. J., Rentschler, S., Gourdie, R. G., Fishman, G. I. & Mikawa, T. Induction and patterning of the cardiac conduction system. *Int. J. Dev. Biol.* **46,** 765–75 (2002).

56. Moorman, A. F. M. & Christoffels, V. M. Cardiac chamber formation: development, genes, and evolution. *Physiol. Rev.* **83,** 1223–67 (2003).

57. Christoffels, V. M. *et al.* Chamber formation and morphogenesis in the developing mammalian heart. *Dev. Biol.* **223,** 266–78 (2000).

58. Christoffels, V. M., Burch, J. B. E. & Moorman, A. F. M. Architectural plan for the heart: early patterning and delineation of the chambers and the nodes. *Trends Cardiovasc. Med.* **14,** 301–7 (2004).

59. Christoffels, V. M. & Moorman, A. F. M. Development of the cardiac conduction system: why are some regions of the heart more arrhythmogenic than others? *Circ. Arrhythm. Electrophysiol.* **2,** 195–207 (2009).

60. Hoogaars, W. M. H., Barnett, P., Moorman, A. F. M. & Christoffels, V. M. T-box factors determine cardiac design. *Cell. Mol. Life Sci.* **64,** 646–60 (2007).

61. Wenink, A. C. Development of the human cardiac conducting system. *J. Anat.* **121,** 617–31 (1976).

62. Blom, N. A. *et al.* Development of the cardiac conduction tissue in human embryos using HNK-1 antigen expression: possible relevance for understanding of abnormal atrial automaticity. *Circulation.* **99,** 800–6 (1999).

63. Kondo, R. P., Anderson, R. H., Kupershmidt, S., Roden, D. M. & Evans, S. M. Development of the cardiac conduction system as delineated by minK-lacZ. *J. Cardiovasc. Electrophysiol.* **14,** 383–91 (2003).

64. Rentschler, S. *et al.* Visualization and functional characterization of the developing murine cardiac conduction system. *Development* **128,** 1785–92 (2001).

65. Liu, J., Dobrzynski, H., Yanni, J., Boyett, M. R. & Lei, M. Organisation of the mouse sinoatrial node: structure and expression of HCN channels. *Cardiovasc. Res.* **73,** 729–38 (2007).

66. Dobrzynski, H., Boyett, M. R. & Anderson, R. H. New insights into pacemaker activity: promoting understanding of sick sinus syndrome. *Circulation.* **115,** 1921–32 (2007).

67. Boyett, M. R., Honjo, H. & Kodama, I. The sinoatrial node, a heterogeneous pacemaker structure. *Cardiovasc. Res.* **47,** 658–87 (2000).

68. Opthof, T. The mammalian sinoatrial node. *Cardiovasc. Drugs Ther.* **1,** 573–97 (1988).

69. Moorman, A. F. M., de Jong, F., Denyn, M. M. F. J. & Lamers, W. H. Development of the cardiac conduction system. *Circ. Res.* **82,** 629–644 (1998).

70. Jongbloed, M. R. M. *et al.* Expression of Id2 in the second heart field and cardiac defects in Id2 knock-out mice. *Dev. Dyn.* **240,** 2561–77 (2011).

71. Wiese, C. *et al.* Formation of the sinus node head and differentiation of sinus node myocardium are independently regulated by Tbx18 and Tbx3. *Circ. Res.* **104,** 388–97 (2009).

72. Mommersteeg, M. T. M. *et al.* Molecular pathway for the localized formation of the sinoatrial node. *Circ. Res.* **100,** 354–62 (2007).

73. Hoogaars, W. M. H. *et al.* Tbx3 controls the sinoatrial node gene program and imposes pacemaker function on the atria. *Genes Dev.* **21,** 1098–112 (2007).

74. Bakker, M. L., Christoffels, V. M. & Moorman, A. F. M. The cardiac pacemaker and conduction system develops from embryonic myocardium that retains its primitive phenotype. *J. Cardiovasc. Pharmacol.* **56,** 6–15 (2010).

75. Douglas, Y. L. *et al.* Pulmonary vein, dorsal atrial wall and atrial septum abnormalities in podoplanin knockout mice with disturbed posterior heart field contribution. *Pediatr. Res.* **65,** 27–32 (2009).

76. Bleyl, S. B. *et al.* Dysregulation of the PDGFRA gene causes inflow tract anomalies including TAPVR: integrating evidence from human genetics and model organisms. *Hum. Mol. Genet.* **19,** 1286–301 (2010).

77. Nof, E. *et al.* Point mutation in the HCN4 cardiac ion channel pore affecting synthesis, trafficking, and functional expression is associated with familial asymptomatic sinus bradycardia. *Circulation.* **116,** 463–70 (2007).

78. Sah, V. P. *et al.* Cardiac-specific overexpression of RHOA results in sinus and atrioventricular nodal dysfunction and contractile failure. *J. Clin. Invest.* **103,** 1627–34 (1999).

79. Wei, L. *et al.* Disruption of Rho signaling results in progressive atrioventricular conduction defects while ventricular function remains preserved. *FASEB J.* **18,** 857–9 (2004).

80. Frank, D. U. *et al.* Lethal arrhythmias in Tbx3-deficient mice reveal extreme dosage sensitivity of cardiac conduction system function and homeostasis. *Proc. Natl. Acad. Sci. USA.* **109,** E154-63 (2012).

81. Kamino, K., Hirota, A. & Fujii, S. Localization of pacemaking activity in early embryonic heart monitored using voltage-sensitive dye. *Nature.* **290,** 595–7 (1981).

82. Sedmera, D. *et al.* Changes in activation sequence of embryonic chick atria correlate with developing myocardial architecture. *Am. J. Physiol. Heart Circ. Physiol.* **291,** H1646-52 (2006).

83. Yi, T. *et al.* Electrophysiological mapping of embryonic mouse hearts: mechanisms for developmental pacemaker switch and internodal conduction pathway. *J. Cardiovasc. Electrophysiol.* **23,** 309–18 (2012).

84. Sizarov, A. *et al.* Molecular analysis of patterning of conduction tissues in the developing human heart. *Circ. Arrhythm. Electrophysiol.* **4,** 532–42 (2011).

85. Stillitano, F. *et al.* Molecular basis of funny current (If) in normal and failing human heart. *J. Mol. Cell. Cardiol.* **45,** 289–99 (2008).

86. Espinoza-Lewis, R. A. *et al.* Shox2 is essential for the differentiation of cardiac pacemaker cells by repressing Nkx2-5. *Dev. Biol.* **327,** 376–85 (2009).

87. Wang, J. *et al.* Pitx2 prevents susceptibility to atrial arrhythmias by inhibiting left-sided pacemaker specification. *Proc. Natl. Acad. Sci. USA.* **107,** 9753–8 (2010).

88. Ammirabile, G. *et al.* Pitx2 confers left morphological, molecular, and functional identity to the sinus venosus myocardium. *Cardiovasc. Res.* **93,** 291–301 (2012).

89. Chinchilla, A. *et al.* PITX2 insufficiency leads to atrial electrical and structural remodeling linked to arrhythmogenesis. *Circ. Cardiovasc. Genet.* **4,** 269–79 (2011).

90. Gudbjartsson, D. F. *et al.* Variants conferring risk of atrial fibrillation on chromosome 4q25. *Nature.* **448,** 353–7 (2007).

91. Kirchhof, P. *et al.* PITX2c is expressed in the adult left atrium, and reducing Pitx2c expression promotes atrial fibrillation inducibility and complex changes in gene expression. *Circ. Cardiovasc. Genet.* **4,** 123–33 (2011).

92. Bossert, T. *et al.* Cardiac malformations associated with the Holt-Oram syndrome--report on a family and review of the literature. *Thorac. Cardiovasc. Surg.* **50,** 312–4 (2002).

93. Patel, C., Silcock, L., McMullan, D., Brueton, L. & Cox, H. TBX5 intragenic duplication: a family with an atypical Holt-Oram syndrome phenotype. *Eur. J. Hum. Genet.* **20,** 863–9 (2012).

94. Greenwood, R. D., Rosenthal, A., Sloss, L. J., LaCorte, M. & Nadas, A. S. Sick sinus syndrome after surgery for congenital heart disease. *Circulation.* **52,** 208–213 (1975).

95. Benedini, G. *et al.* Pre-operative sinus node function in adult patients with atrial septal defect (ostium secundum type). *Eur. Heart J.* **6,** 261–5 (1985).

96. Bink-Boelkens, M. T., Bergstra, A. & Landsman, M. L. Functional abnormalities of the conduction system in children with an atrial septal defect. *Int. J. Cardiol.* **20,** 263–72 (1988).

97. Clark, E. B. & Kugler, J. D. Preoperative secundum atrial septal defect with coexisting sinus node and atrioventricular node dysfunction. *Circulation.* **65,** 976–980 (1982).

98. Portman, M. A., Beder, S. D., Cohen, M. H. & Riemenschneider, T. A. Conduction abnormalities detected by electrophysiologic testing following repair of ostium primum atrioventricular septal defect. *Int. J. Cardiol.* **11,** 111–9 (1986).

99. Ruschhaupt, D. G., Khoury, L., Thilenius, O. G., Replogle, R. L. & Arcilla, R. A. Electrophysiologic abnormalities of children with ostium secundum atrial septal defect. *Am. J. Cardiol.* **53,** 1643–7 (1984).

100. Korbmacher, B. *et al.* Long-term results after repair of total anomalous pulmonary venous connection. *Thorac. Cardiovasc. Surg.* **49,** 101–6 (2001).

101. Saxena, A. *et al.* Cardiac arrhythmias after surgical correction of total anomalous pulmonary venous connection: late follow-up. *Pediatr. Cardiol.* **12,** 89–91 (1991).

102. Tanel, R. E. *et al.* Long-term noninvasive arrhythmia assessment after total anomalous pulmonary venous connection repair. *Am. Heart J.* **153,** 267–74 (2007).

103. Ho, S. Y., Anderson, R. H. & Sánchez-Quintana, D. Atrial structure and fibres: morphologic bases of atrial conduction. *Cardiovasc. Res.* **54,** 325–36 (2002).

104. Sherf, L. & James, T. N. Fine structure of cells and their histologic organization within internodal pathways of the heart: clinical and electrocardiographic implications. *Am. J. Cardiol.* **44,** 345–69 (1979).

105. James, T. N. The internodal pathways of the human heart. *Prog. Cardiovasc. Dis.* **43,** 495–535 (2001).

106. James, T. N. The connecting pathways between the sinus node and AV node and between the right and left atrium of the human heart. *Am. Heart J.* **66,** 498–508 (1963).

107. Chuck, E. T. & Watanabe, M. Differential expression of PSA-NCAM and HNK-1 epitopes in the developing cardiac conduction system of the chick. *Dev. Dyn.* **209,** 182–95 (1997).

108. Ikeda, T. *et al.* Leu-7 immunoreactivity in human and rat embryonic hearts, with special reference to the development of the conduction tissue. *Anat. Embryol.* **182,** 553–562 (1990).

109. Chung, C.-Y., Bien, H. & Entcheva, E. The role of cardiac tissue alignment in modulating electrical function. *J. Cardiovasc. Electrophysiol.* **18,** 1323–9 (2007).

110. Vassalle, M. & Hoffman, B. F. The spread of sinus activation during potassium administration. *Circ. Res.* **17,** 285–295 (1965).

111. Wagner, M. L., Lazzara, R., Weiss, R. M. & Hoffman, B. F. Specialized conducting fibers in the interatrial band. *Circ. Res.* **18,** 502–518 (1966).

112. Racker, D. K. Sinoventricular transmission in 10 mM K+ by canine atrioventricular nodal inputs. Superior atrionodal bundle and proximal atrioventricular bundle. *Circulation.* **83,** 1738–1753 (1991).

113. Sakai, T., Hirota, A., Momose-Sato, Y., Sato, K. & Kamino, K. Optical mapping of conduction patterns of normal and tachycardia-like excitations in the rat atrium. *Jpn. J. Physiol.* **47,** 179–88 (1997).

114. Kozlowski, D. *et al.* Histological examination of the topography of the atrioventricular nodal artery within the triangle of Koch. *Pacing Clin. Electrophysiol.* **21,** 163–7 (1998).

115. Mazgalev, T. N., Ho, S. Y. & Anderson, R. H. Anatomic-electrophysiological correlations concerning the pathways for atrioventricular conduction. *Circulation.* **103,** 2660–2667 (2001).

116. Billette, J. What is the atrioventricular node? Some clues in sorting out its structure-function relationship. *J. Cardiovasc. Electrophysiol.* **13,** 515–8 (2002).

117. Cosio, F. G. *et al.* Living anatomy of the atrioventricular junctions. A guide to electrophysiologic mapping : A consensus statement from the cardiac nomenclature study group, working group of arrhythmias, European Society of Cardiology, and the task force on cardiac nomenclature. *Circulation.* **100,** e31–e37 (1999).

118. Dobrzynski, H. *et al.* Site of origin and molecular substrate of atrioventricular junctional rhythm in the rabbit heart. *Circ. Res.* **93,** 1102–10 (2003).

119. Hucker, W. J., McCain, M. L., Laughner, J. I., Iaizzo, P. A. & Efimov, I. R. Connexin 43 expression delineates two discrete pathways in the human atrioventricular junction. *Anat. Rec.* **291,** 204–15 (2008).

120. Inoue, S. & Becker, A. E. Posterior extensions of the human compact atrioventricular node: A neglected anatomic feature of potential clinical significance. *Circulation.* **97,** 188–193 (1998).

121. Yanni, J., Boyett, M. R., Anderson, R. H. & Dobrzynski, H. The extent of the specialized atrioventricular ring tissues. *Heart Rhythm.* **6,** 672–80 (2009).

122. Virágh, S. & Challice, C. E. The development of the conduction system in the mouse embryo heart. II. Histogenesis of the atrioventricular node and bundle. *Dev. Biol.* **56,** 397–411 (1977).

123. Truex, R. C., Marino, T. A. & Marino, D. R. Observations on the development of the human atrioventricular node and bundle. *Anat. Rec.* **192,** 337–50 (1978).

124. Marino, T. A. & Severdia, J. The early development of the AV node and bundle in the ferret heart. *Am. J. Anat.* **167,** 299–312 (1983).

125. Kim, Y. & Yasuda, M. The cardiac conducting system of the fowl. *Anat. Histol. Embryol.* **8,** 138–50 (1979).

126. Virágh, S. & Challice, C. E. The development of the conduction system in the mouse embryo heart. I. The first embryonic A-V conduction pathway. *Dev. Biol.* **56,** 382–96 (1977).

127. Wessels, A. *et al.* Spatial distribution of 'tissue-specific' antigens in the developing human heart and skeletal muscle. III. An immunohistochemical analysis of the distribution of the neural tissue antigen G1N2 in the embryonic heart; implications for the development of the atrioventricular conduction system. *Anat. Rec.* **232,** 97–111 (1992).

128. Lamers, W. H. *et al.* New findings concerning ventricular septation in the human heart. Implications for maldevelopment. *Circulation.* **86,** 1194–1205 (1992).

129. Marino, T. A. The atrioventricular node and bundle in the ferret heart: a light and quantitative electron microscopic study. *Am. J. Anat.* **154,** 365–92 (1979).

130. Argüello, C., Alanis, J. & Valenzuela, B. The early development of the atrioventricular node and bundle of His in the embryonic chick heart. An electrophysiological and morphological study. *Development.* **102,** 623–37 (1988).

131. Patten, B. M. The development of the sinoventricular conduction system. *Med. Bull. (Ann Arbor).* **22,** 1–21 (1956).

132. Scheinman, M. M. & Yang, Y. The history of AV nodal reentry. *Pacing Clin. Electrophysiol.* **28,** 1232–7 (2005).

133. James, T. N. Cardiac conduction system: fetal and postnatal development. *Am. J. Cardiol.* **25,** 213–26 (1970).

134. James, T. N. & Marshall, T. K. XVIII. Persistent fetal dispersion of the atrioventricular node and His bundle within the central fibrous body. *Circulation.* **53,** 1026–1034 (1976).

135. de Jong, F. *et al.* Persisting zones of slow impulse conduction in developing chicken hearts. *Circ. Res.* **71,** 240–50 (1992).

136. Kolditz, D. P. *et al.* Persistence of functional atrioventricular accessory pathways in postseptated embryonic avian hearts: implications for morphogenesis and functional maturation of the cardiac conduction system. *Circulation.* **115,** 17–26 (2007).

137. Mori, A. D. & Bruneau, B. G. TBX5 mutations and congenital heart disease: Holt-Oram syndrome revealed. *Curr. Opin. Cardiol.* **19,** 211–5 (2004).

138. Baruscotti, M. *et al.* Deep bradycardia and heart block caused by inducible cardiac-specific knockout of the pacemaker channel gene Hcn4. *Proc. Natl. Acad. Sci. USA.* **108,** 1705–10 (2011).

139. Kasahara, H. & Wakimoto, H. Progressive atrioventricular conduction defects and heart failure in mice expressing a mutant Csx/Nkx2. 5 homeoprotein. *J. Clin. Invest.* **108,** 189–201 (2001).

140. Jay, P. Y. *et al.* Function follows form: cardiac conduction system defects in Nkx2-5 mutation. *Anat. Rec. A. Discov. Mol. Cell. Evol. Biol.* **280,** 966–72 (2004).

141. König, K., Will, J. C., Berger, F., Müller, D. & Benson, D. W. Familial congenital heart disease, progressive atrioventricular block and the cardiac homeobox transcription factor gene NKX2.5: identification of a novel mutation. *Clin. Res. Cardiol.* **95,** 499–503 (2006).

142. Lee, P.-C., Chen, S.-A. & Hwang, B. Atrioventricular node anatomy and physiology: implications for ablation of atrioventricular nodal reentrant tachycardia. *Curr. Opin. Cardiol.* **24,** 105–12 (2009).

143. Anderson, R. H. & Ho, S. Y. The morphology of the cardiac conduction system. *Novartis Found. Symp.* **250,** 6–17 (2003).

144. Inoue, S., Becker, A. E., Riccardi, R. & Gaita, F. Interruption of the inferior extension of the compact atrioventricular node underlies successful radio frequency ablation of atrioventricular nodal reentrant tachycardia. *J. Interv. Card. Electrophysiol.* **3,** 273–7 (1999).

145. Greener, I. D. *et al.* Ion channel transcript expression at the rabbit atrioventricular conduction axis. *Circ. Arrhythm. Electrophysiol.* **2,** 305–15 (2009).

146. Li, J. *et al.* Computer three-dimensional reconstruction of the atrioventricular node. *Circ. Res.* **102,** 975–85 (2008).

147. Kistler, P. M. *et al.* Focal atrial tachycardia arising from the mitral annulus. *J. Am. Coll. Cardiol.* **41,** 2212–2219 (2003).

148. Morton, J. B. *et al.* Focal atrial tachycardia arising from the tricuspid annulus: electrophysiologic and electrocardiographic characteristics. *J. Cardiovasc. Electrophysiol.* **12,** 653–9 (2001).

149. James, T. N. Sudden death in babies: new observations in the heart. *Am. J. Cardiol.* **22,** 479–506 (1968).

150. Suarez-Mier, M. P. & Gamallo, C. Atrioventricular node fetal dispersion and His bundle fragmentation of the cardiac conduction system in sudden cardiac death. *J. Am. Coll. Cardiol.* **32,** 1885–90 (1998).

151. Anderson, R. H., Arnold, R. & Wilkinson, J. L. The conducting system in congenitally corrected transposition. *Lancet.* **1,** 1286–8 (1973).

152. Anderson, R. H., Becker, A. E., Arnold, R. & Wilkinson, J. L. The conducting tissues in congenitally corrected transposition. *Circulation.* **50,** 911–23 (1974).

153. Hosseinpour, A.-R., McCarthy, K. P., Griselli, M., Sethia, B. & Ho, S. Y. Congenitally corrected transposition: size of the pulmonary trunk and septal malalignment. *Ann. Thorac. Surg.* **77,** 2163–6 (2004).

154. Ho, S. Y. *et al.* Heart block and atrioventricular septal defect. *Thorac. Cardiovasc. Surg.* **33,** 362–5 (1985).

155. Kugler, J. & Gillette, P. Nonsurgically-acquired complete atrioventricular block in endocardial cushion defect. *Cardiovasc. Dis.* **8,** 205–209 (1981).

156. Mehta, A. V, O'Riordan, A. C., Sanchez, G. R. & Black, I. F. Acquired nonsurgical complete atrioventricular block in a child with endocardial cushion defect. *Clin. Cardiol.* **5,** 603–5 (1982).

157. Thiene, G. *et al.* Surgical anatomy and pathology of the conduction tissues in atrioventricular defects. *J. Thorac. Cardiovasc. Surg.* **82,** 928–37 (1981).

158. Blom, N. A., Ottenkamp, J., DeRuiter, M. C., Wenink, A. C. G. & Gittenberger-de Groot, A. C. Development of the cardiac conduction system in atrioventricular septal defect in human trisomy 21. *Pediatr. Res.* **58,** 516–20 (2005).

159. Blom, N. A., Ottenkamp, J., Wenink, A. C. G. & Gittenberger-de Groot, A. C. Deficiency of the vestibular spine in atrioventricular septal defects in human fetuses with down syndrome. *Am. J. Cardiol.* **91,** 180–4 (2003).

160. Snarr, B. S., Wirrig, E. E., Phelps, A. L., Trusk, T. C. & Wessels, A. A spatiotemporal evaluation of the contribution of the dorsal mesenchymal protrusion to cardiac development. *Dev. Dyn.* **236,** 1287–94 (2007).

161. Odgers, P. N. The development of the atrio-ventricular valves in man. *J. Anat.* **73,** 643–57 (1939).

162. Van Mierop, L. H., Alley, R. D., Kausel, H. W. & Stranahan, A. The anatomy and embryology of endocardial cushion defects. *J. Thorac. Cardiovasc. Surg.* **43,** 71–83 (1962).

163. Oosthoek, P. W. *et al.* Development of the atrioventricular valve tension apparatus in the human heart. *Anat. Embryol.* **198,** 317–29 (1998).

164. Wessels, A. *et al.* The development of the atrioventricular junction in the human heart. *Circ. Res.* **78,** 110–117 (1996).

165. Hahurij, N. D. *et al.* Accessory atrioventricular myocardial connections in the developing human heart: relevance for perinatal supraventricular tachycardias. *Circulation.* **117,** 2850–8 (2008).

166. Hahurij, N. D. *et al.* Accessory atrioventricular myocardial pathways in mouse heart development: substrate for supraventricular tachycardias. *Pediatr. Res.* **70,** 37–43 (2011).

167. Gaussin, V. *et al.* Alk3/Bmpr1a receptor is required for development of the atrioventricular canal into valves and annulus fibrosus. *Circ. Res.* **97,** 219–26 (2005).

168. Okagawa, H., Markwald, R. R. & Sugi, Y. Functional BMP receptor in endocardial cells is required in atrioventricular cushion mesenchymal cell formation in chick. *Dev. Biol.* **306,** 179–92 (2007).

169. Norris, R. A. *et al.* Periostin regulates collagen fibrillogenesis and the biomechanical properties of connective tissues. *J. Cell. Biochem.* **101,** 695–711 (2007).

170. Zhou, B., von Gise, A., Ma, Q., Hu, Y. W. & Pu, W. T. Genetic fate mapping demonstrates contribution of epicardium-derived cells to the annulus fibrosus of the mammalian heart. *Dev. Biol.* **338,** 251–61 (2010).

171. Smith, C. L., Baek, S. T., Sung, C. Y. & Tallquist, M. D. Epicardial-derived cell epithelial-to-mesenchymal transition and fate specification require PDGF receptor signaling. *Circ. Res.* **108,** e15-26 (2011).

172. Rios, H. *et al.* periostin null mice exhibit dwarfism, incisor enamel defects, and an early-onset periodontal disease-like phenotype. *Mol. Cell. Biol.* **25,** 11131–44 (2005).

173. Kiernan, T. J. & Fahy, G. Multiple accessory pathways, dual AV nodal physiology, non-compacted myocardium and patent foramen ovale in a patient with Ebstein's anomaly: report of a case. *Int. J. Cardiol.* **114,** 412–3 (2007).

174. Oh, J. K., Holmes, D. R., Hayes, D. L., Porter, C.-B. J. & Danielson, G. K. Cardiac arrhythmias in patients with surgical repair of Ebstein's anomaly. *J. Am. Coll. Cardiol.* **6,** 1351–1357 (1985).

175. Bohora, S., Dora, S. K., Namboodiri, N., Valaparambil, A. & Tharakan, J. Electrophysiology study and radiofrequency catheter ablation of atriofascicular tracts with decremental properties (Mahaim fibre) at the tricuspid annulus. *Europace.* **10,** 1428–33 (2008).

176. Haghjoo, M. *et al.* Electrocardiographic and electrophysiologic characteristics of anteroseptal, midseptal, and posteroseptal accessory pathways. *Heart Rhythm.* **4,** 1411–9 (2007).

177. Santilli, R. A. *et al.* Anatomic distribution and electrophysiologic properties of accessory atrioventricular pathways in dogs. *J. Am. Vet. Med. Assoc.* **231,** 393–8 (2007).

178. Becker, A. E., Anderson, R. H., Durrer, D. & Wellens, H. J. The anatomical substrates of wolff-parkinson-white syndrome. A clinicopathologic correlation in seven patients. *Circulation.* **57,** 870–9 (1978).

179. Klein, G. J., Hackel, D. B. & Gallagher, J. J. Anatomic substrate of impaired antegrade conduction over an accessory atrioventricular pathway in the Wolff-Parkinson-White syndrome. *Circulation.* **61,** 1249–1256 (1980).

180. Peters, N. S. *et al.* The Wolff-Parkinson-White syndrome: the cellular substrate for conduction in the accessory atrioventricular pathway. *Eur. Heart J.* **15,** 981–7 (1994).

181. Chen, S. A. *et al.* Electrophysiologic characteristics and anatomical complexities of accessory atrioventricular pathways with successful ablation of anterograde and retrograde conduction at different sites. *J. Cardiovasc. Electrophysiol.* **7,** 907–15 (1996).

182. Hornung, T. S. & Calder, L. Congenitally corrected transposition of the great arteries. *Heart.* **96,** 1154–61 (2010).

183. Jongbloed, M. R. M. *et al.* Development of the right ventricular inflow tract and moderator band: a possible morphological and functional explanation for Mahaim tachycardia. *Circ. Res.* **96,** 776–83 (2005).

184. Sternick, E. B. *et al.* Automaticity in Mahaim fibers. *J. Cardiovasc. Electrophysiol.* **15,** 738–44 (2004).

185. Gollob, M. H. *et al.* Novel PRKAG2 mutation responsible for the genetic syndrome of ventricular preexcitation and conduction system disease with childhood onset and absence of cardiac hypertrophy. *Circulation.* **104,** 3030–3033 (2001).

186. Gollob, M. H. *et al.* Identification of a gene responsible for familial Wolff-Parkinson-White syndrome. *N. Engl. J. Med.* **344,** 1823–31 (2001).

187. Patel, V. V *et al.* Electrophysiologic characterization and postnatal development of ventricular pre-excitation in a mouse model of cardiac hypertrophy and Wolff-Parkinson-White syndrome. *J. Am. Coll. Cardiol.* **42,** 942–951 (2003).

188. Aanhaanen, W. T. J. *et al.* Defective Tbx2-dependent patterning of the atrioventricular canal myocardium causes accessory pathway formation in mice. *J. Clin. Invest.* **121,** 534–44 (2011).

189. Bauersfeld, U., Pfammatter, J. P. & Jaeggi, E. Treatment of supraventricular tachycardias in the new millennium--drugs or radiofrequency catheter ablation? *Eur. J. Pediatr.* **160,** 1–9 (2001).

190. Ko, J. K., Deal, B. J., Strasburger, J. F. & Benson, D. W. Supraventricular tachycardia mechanisms and their age distribution in pediatric patients. *Am. J. Cardiol.* **69,** 1028–32 (1992).

191. Goldstein, M., Dunnigan, A., Milstein, S. & Benson, D. W. Bundle branch block during orthodromic reciprocating tachycardia onset in infants. *Am. J. Cardiol.* **63,** 301–6 (1989).

192. Kannankeril, P. J., Gotteiner, N. L., Deal, B. J., Johnsrude, C. L. & Strasburger, J. F. Location of accessory connection in infants presenting with supraventricular tachycardia in utero: clinical correlations. *Am. J. Perinatol.* **20,** 115–9 (2003).

193. Kugler, J. D. *et al.* Radiofrequency catheter ablation for tachyarrhythmias in children and adolescents. The Pediatric Electrophysiology Society. *N. Engl. J. Med.* **330,** 1481–7 (1994).

194. Hahurij, N. D. *et al.* Perinatal management and long-term cardiac outcome in fetal arrhythmia. *Early Hum. Dev.* **87,** 83–7 (2011).

195. Naheed, Z. J., Strasburger, J. F., Deal, B. J., Benson, D. W. & Gidding, S. S. Fetal tachycardia: mechanisms and predictors of hydrops fetalis. *J. Am. Coll. Cardiol.* **27,** 1736–40 (1996).

196. Kruithof, B. P. T., Krawitz, S. A. & Gaussin, V. Atrioventricular valve development during late embryonic and postnatal stages involves condensation and extracellular matrix remodeling. *Dev. Biol.* **302,** 208–17 (2007).

197. Visconti, R. P. & Markwald, R. R. Recruitment of new cells into the postnatal heart: potential modification of phenotype by periostin. *Ann. N. Y. Acad. Sci.* **1080,** 19–33 (2006).

198. Perry, J. C. & Garson, A. Supraventricular tachycardia due to Wolff-Parkinson-White syndrome in children: early disappearance and late recurrence. *J. Am. Coll. Cardiol.* **16,** 1215–20 (1990).

199. Aliot, E., de Chillou, C., Revault d'Allones, G., Mabo, P. & Sadoul, N. Mahaim tachycardias. *Eur. Heart J.* **19,** E25-31, E52-3 (1998).

200. Chavan, C., Rao, H. B., Badani, R. S., Raju, P. R. & Narasimhan, C. Ablation of incessant orthodromic reciprocating tachycardia in a child with congenitally corrected transposition of great arteries and ebsteinoid malformation of left atrioventricular valve. *J. Interv. Card. Electrophysiol.* **23,** 149–52 (2008).

201. Purvis, J. & Barr, S. An appearance of 'non-compaction' of the right systemic ventricle is common in congenitally corrected transposition of the great arteries. *Int. J. Cardiovasc. Imaging.* **25,** 751–2 (2009).

3

THE AVIAN EMBRYO TO STUDY DEVELOPMENT OF THE CARDIAC CONDUCTION SYSTEM

Tim P. Kelder, Rebecca Vicente-Steijn, Robert E. Poelmann, Christine L. Mummery, Marco C. DeRuiter, Monique R.M. Jongbloed

Modified after Differentiation, 91: 90-103 (2016)

ABSTRACT

The avian embryo has long been a popular model system in developmental biology. The easy accessibility of the embryo makes it particularly suitable for *in ovo* microsurgery and manipulation. Reincubation of the embryo allows long-term follow-up of these procedures. The current review focuses on the variety of techniques available to study development of the cardiac conduction system in avian embryos. Based on the large amount of relevant data arising from experiments in avian embryos, we conclude that the avian embryo has and will continue to be a powerful model system to study development in general and the developing cardiac conduction system in particular.

1. INTRODUCTION

The avian embryo has long been a popular model system in developmental biology. More than 300 years B.C., even Aristotle appreciated the value of the chick to study embryonic development.[1] Since then, numerous elegant experimental techniques have been developed, utilizing the specific advantages of avian embryos. This chapter provides an overview of the different methods used in avian embryos, specifically to elucidate the development of the cardiac conduction system (CCS). We first provide an overview of cardiac and CCS development in general and then discuss the particular advantages and disadvantages of the avian embryo to study CCS development. Finally, the techniques most effective for exposing the embryo in the egg and studying the electrophysiology and molecular differentiation of the developing CCS are described, with a short discussion of results obtained from these experiments.

2. GENERAL CARDIAC AND CCS DEVELOPMENT AND FUNCTIONING

During gastrulation, mesodermal cells arise from the primitive streak and subsequently migrate cranially and laterally to form the cardiogenic plates. The first sign of cardiomyocyte differentiation is evident in this region at approximately Hamburger and Hamilton (HH)[2] stage 8-9 in chick, when cardiac troponin-I (CTNI) and sarcomeric myosin (MF20) are first detectable. Fusion of bilateral plates of splanchnic mesoderm establishes the primary heart tube (PHT).[3,4] Subsequently, cells are added to the PHT from undifferentiated mesoderm, which is situated at the arterial and venous pole of the heart. Complex migration, proliferation and differentiation of different cardiac cell types (cardiomyocytes, endothelial cells, epicardial cells, (myo)fibroblasts and smooth muscle cells) finally establishes the mature 4-chambered heart, with its own (coronary) vasculature, specialized conduction system and valvular apparatus.[5] In addition, neural crest cells migrate into the heart from the dorsal region of the rhombencephalon and take part in processes that include induction of aortopulmonary septum formation.[6]

The CCS initiates and coordinates electrical activation of the myocardium, which is essential for normal functioning of the heart. Rhythmic contraction of the PHT starts around HH10 and differences in conduction velocity are already evident by HH13.[7] The cells contributing to the CCS are derived from precursors within the myocardial cell lineage.[8] The adult CCS has several components (**Fig. 1**): the sinoatrial node (SAN) consists of pacemaker cells responsible for initiating atrial electrical activation. Myocardial cells contributing to the SAN originate from the sinus venosus myocardium, an initially U-shaped region of myocardium with pacemaking capacity[9] encompassing the bilateral cardinal veins (putative caval veins, that will remodel in favour of the right side during

subsequent development). The SAN will eventually become the primary pacemaker of the heart. After depolarization of the atria, the electrical current is delayed in the atrioventricular node (AVN), thereby ensuring adequate filling of the ventricles. A significant part of the AVN most likely originates from the AV canal, a component of the primary heart tube, although recent data indicate an additional sinus venosus contribution to the superior part of the node.[10,11] After a short delay, the AV bundle, the bundle branches and Purkinje fibres propagate the electrical current at high velocity to the ventricular myocardium.

An important structure for proper CCS function is the annulus fibrosus, a layer of dense fibrous cells, which electrically isolates the atria and ventricles, with the

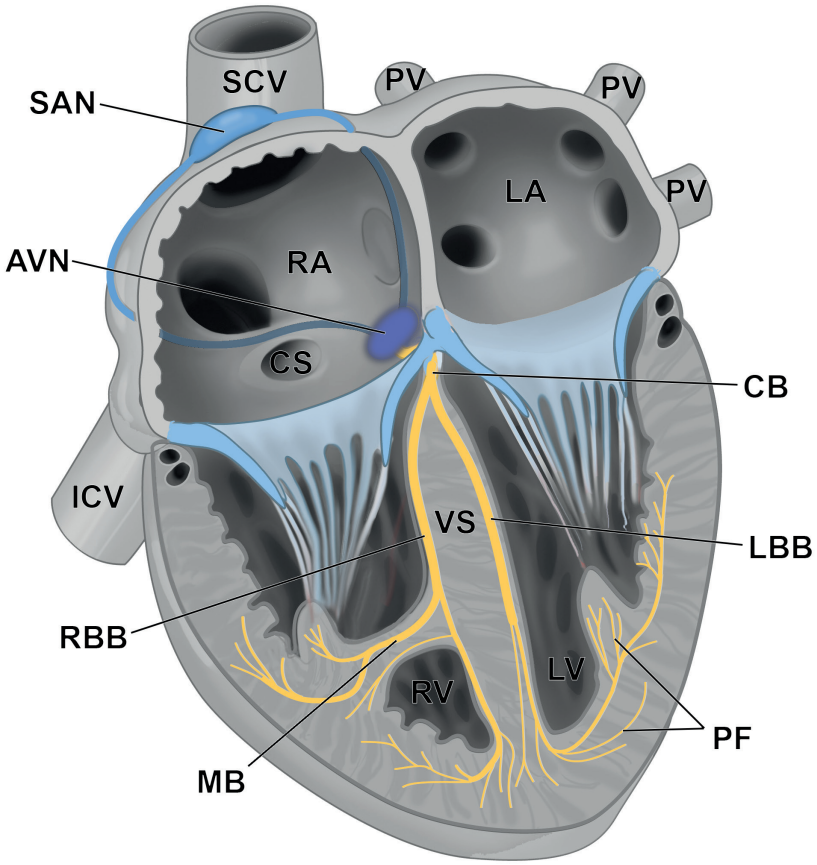

Figure 1. The components of the cardiac conduction system
Schematic drawing of the components of the adult CCS. AVN: atrioventricular node, CB: common bundle, CS: coronary sinus, ICV: inferior caval vein, LA: left atrium, LBB: left bundle branch, LV: left ventricle, MB: moderator band, PF: Purkinje fiber network, PV: pulmonary vein, RA: right atrium, RBB: right bundle branch, RV: right ventricle, SAN: sinoatrial node, SCV: superior caval vein, VS: ventricular septum.

exception of the region where the AV bundle (also referred to as His or common bundle) penetrates this layer. This electrical isolation is essential for correct timing of atrial and ventricular activation. The fibrous cells contributing to the annulus fibrosus originate from the monolayer of epithelial cells lining the heart, the epicardium. The epicardial layer in turn is derived from the proepicardial organ (PEO), a cauliflower-like structure, which protrudes from the sinus venosus surface at the venous pole of the heart into the pericardial cavity. Cells derived from the PEO attach to the myocardium of the heart and then migrate over its entire surface. Through epithelial-to-mesenchymal transformation (EMT), epicardium-derived cells (EPDCs) are formed, which migrate into the myocardium and undergo further differentiation to several cell types including fibroblasts of the annulus fibrosus. Furthermore, the EPDCs play a role during development of the Purkinje fiber network, as discussed below.[12]

3.1. ADVANTAGES OF THE AVIAN EMBRYO AS A DEVELOPMENTAL MODEL

The wide use of the avian embryo as a model system in developmental biology is because it has a number of specific advantages, which are described below.

The avian embryo is easily accessible. The avian embryo develops *ex utero* in an extracorporal egg. It is fairly easy to create a window in the eggshell without damaging the embryo (see **Section 4**). The embryo can thus be exposed and it is then possible to manipulate it directly *in situ,* essentially intact in its native environment. After micromanipulation of the embryo at room temperature, the egg can be re-sealed and incubated once more to allow development to proceed, thereby creating the opportunity to study long-term effects of the micromanipulation.

Timing of developmental stages is very precise. In 1951, Hamburger and Hamilton proposed staging criteria for avian embryos.[2] Their HH-staging is still widely used among researchers working with avian embryos. This has greatly enhanced the reproducibility and precision of experiments between different laboratories, since through careful staging, comparable groups of embryos can be created simultaneously.

The avian embryo is more widely ethically accepted than mammals and is cost-effective. Advances in science still require the use of laboratory animals for many important research questions to be investigated. In contrast to developmental studies in placental mammals like rodents, sacrifice of the pregnant mother is not required. Furthermore, fertilized eggs are inexpensive and the only specialist equipment required is a humidified incubator. In addition, large numbers of biological repeats are easily carried out on avian embryos whilst this is more limited with rodents, where litter sizes are between 8 and 10 embryos.

In addition, the administrative burden of using fertilized chicken eggs is minimal, since they do not fall under laboratory animal regulations in most countries, at least during the first part of embryonic development.

Finally, the chicken genome has now been sequenced providing the possibility for comparing molecular data with other major laboratory species and human. This solved one major drawback of the chicken model.

3.2. DISADVANTAGES OF THE AVIAN EMBRYO AS A DEVELOPMENTAL MODEL

The major disadvantage of the chick as a model is the paucity of genetic tools. Transgenic mice have become one of the most important tools for studying gene function and cell fate. Many transgenic mouse lines are now available and this has been invaluable for understanding development and disease in higher vertebrates. Transgenic chicken embryos have not been available until very recently although recent advances in biotechnological methods have now enabled the creation of transgenic chickens[13], which opens up a wide variety of possibilities for the chicken as a model system in developmental biology.

Another disadvantage is that many antibodies required for immunohistochemistry, Western blotting etc. are targeted against human or mammalian (predominantly rat and mouse) epitopes. Even though a large number of antibodies show specific cross-reactivity with avian tissue, the number of commercially available antibodies is less than for mammalian tissue. A possible method to (partially) overcome this problem is non-radioactive *in situ* hybridization. This method is used to visualize mRNA expression and was for example used to detect the expression of the hyperpolarization-activated cyclic nucleotide-gated channel 4 (HCN4), which is the ion channel responsible for the funny current.[14]

4. OPENING THE EGG

The first step to study the developing chick embryo is to open the eggshell without damaging the embryo. Our technique has proven particularly useful for accessing the embryo with minimal risk of damage and/or dehydration. Eggs of the White Leghorn chicken are incubated at 37°C and 80% humidity. Although earlier stages have been studied extensively[15–17], we will use HH stage 15 (embryonic day 2.5) as an example.

1. "Candling" the egg as a first and shown in **Fig. 2a,** ensures that the embryo is properly located before cutting a window in the shell. 2. The egg is then disinfected with 70% ethanol. 3. Three indentations are then sawn with a small handsaw in the eggshell (a "U" shape) until the eggshell membrane is reached

(**Fig. 2b**). 4. A drop of physiological saline is used to wash away eggshell debris and another drop is placed on the "U" shape. 5. Using blunt tweezers, a small hole is made in the eggshell membrane (**Fig. 2c**) to allow the saline solution to enter the egg, thereby creating space between the embryo and the eggshell; this facilitates opening the egg without damaging the embryo. 6. Blunt tweezers are then used to remove the "U" shaped window in the egg and remove the eggshell membrane and expose the embryo (**Fig. 2d**). 7. To gain access to the embryo it might be necessary to open the vitelline membrane. 8. After manipulation, imaging, microinjection etc. of the embryo as required, the window in the egg is covered with surgical or transparent tape. This prevents dehydration. 9. Finally, the egg is placed in the incubator to allow further development to the stage required.

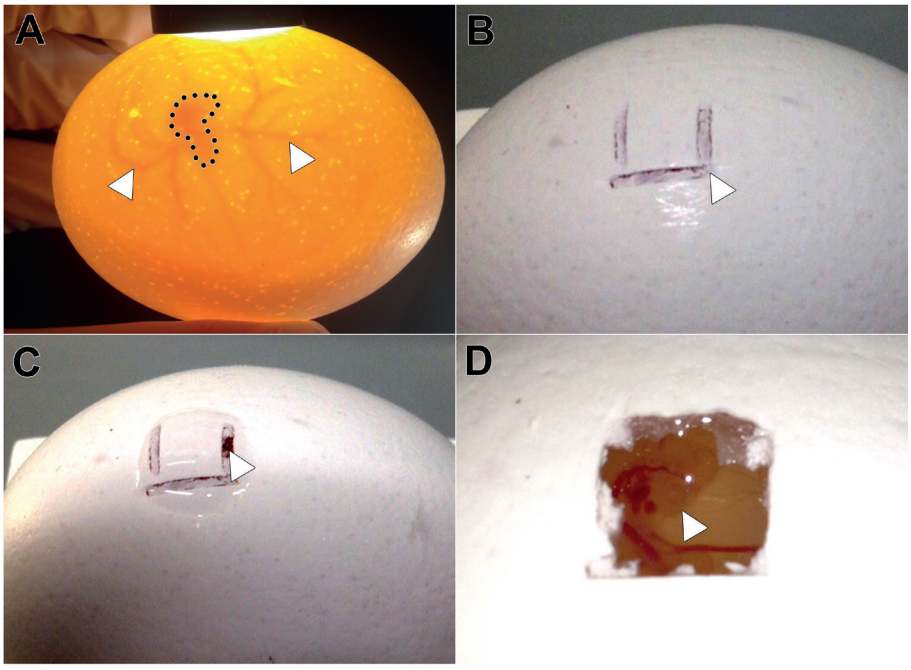

Figure 2. Procedure to safely open the egg

a. Start with "candling" the egg to locate the embryo (dotted line represents the embryo, arrowheads depict the embryonic vasculature) **b.** Saw a "U" shape in the eggshell (arrowhead) **c.** Place a drop of saline solution over the "U" shape and make a small opening (arrowhead) in the eggshell membrane to allow the saline solution to enter the egg. This creates room between the eggshell and the embryo, thereby preventing damage when opening the egg. **d.** Remove the egg shell to expose the embryo (arrowhead).

5. TECHNIQUES FOR STUDYING DEVELOPMENT OF THE CARDIAC CONDUCTION SYSTEM

The following section provides an overview of the different techniques that have been used to investigate the development of the CCS. For every technique, a short description is given, followed by discussion of relevant results obtained for CCS development.

5.1. INHIBITING OUTGROWTH OF THE EPICARDIAL LAYER

In 1993, Manner described a method for inhibiting outgrowth of the epicardial lining of the heart.[18] This was used to study the role of the epicardium during cardiac development. A recent review by Manner focuses on the different experimental techniques available to inhibit outgrowth of the epicardium from the PEO.[19] Since these techniques have been described in detail, only a summary will be given here. The focus of the current report is the use of this model for studying CCS development.

The epicardial inhibition technique is carried out at HH stage 15-17 (day 3 of development). After opening the egg (see **section 4**), the vitelline and chorionic membranes are opened to reach the pericardial cavity. A small piece of eggshell membrane is placed between the PEO and the heart tube (**Fig. 3**). The attachment and outgrowth of the epicardium over the heart tube is thus delayed or even inhibited entirely which retards development of the epicardium. Subsequently, the egg is closed with transparent tape and reincubated at 37 ^{0}C. The extent of epicardial inhibition is variable, and depends on the exact location of the eggshell membrane. In some hearts, only a small decrease in the number of subepicardial EPDCs is observed, while other hearts are (almost) entirely devoid of an epicardial layer, with severe reduction in myocardial wall thickness, abnormal shape of the heart and defects in coronary vasculogenesis and valvular development.[20–22]

5.1.1. INHIBITING OUTGROWTH OF THE EPICARDIAL LAYER TO STUDY DEVELOPMENT OF THE ANNULUS FIBROSUS

In the normal adult heart, the atria do not share myocardial continuity with the ventricles, apart from the AV bundle. The annulus fibrosus forms the insulation between the atria and ventricles, which is essential for proper function of the CCS and the coordinated mechanical activity of the heart. Development of the annulus fibrosus starts with formation of fibrous tissue in the AV sulcus at the epicardial side of the developing AV canal. Subsequent fusion with the mesenchymal tissue of the endocardial cushions in the AV canal insulates the atrial from the ventricular myocardium. During normal development and in early postnatal stages, accessory pathways connecting atrial and ventricular myocardium are still

present. Further differentiation and maturation of the fibrous tissue ultimately ensures electrical separation of the atrial and ventricular myocardium, apart from the penetrating AV bundle.[23,24]

Failure to form a complete mature annulus fibrosus underlies one of the most common cardiac arrhythmias, atrioventricular reentrant tachycardia (AVRT). Here, the myocardium of the atria and ventricles are connected through accessory pathways, which form the substrate for the reentrant circuit found in AVRT, bypassing the normal conduction axis. The treatment of choice for this debilitating arrhythmia in patients is catheter ablation of the accessory pathway.

It has been shown that inhibition of epicardial outgrowth in quail embryos resulted in the presence of large accessory pathways with prevalence within specific regions of the annulus fibrosus. Accessory pathways were observed at late stages of development, after they had disappeared in normal hearts, suggesting that they are retained and demonstrating the importance of EPDCs in proper development of the annulus fibrosus. Electrophysiological examination after epicardial inhibition showed that the ventricular base was activated prior to activation of the ventricular apex. This is characteristic of accessory pathways and underlies AVRT.

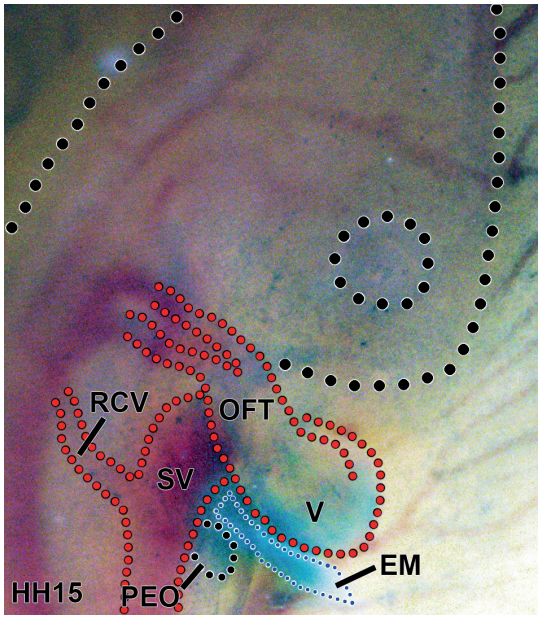

Figure 3. Inhibiting outgrowth of the epicardial layer

A chick embryo of HH15 is shown after epicardial inhibition. The red dotted line depicts the primary heart tube. A small piece of eggshell membrane (EM, blue dotted line) is placed between the proepicardial organ (PEO) and the ventricle (V), thereby inhibiting attachment and outgrowth of the epicardial layer. OFT: outflow tract, RCV: right cardinal vein, SV: sinus venosus.

5.1.2. INHIBITING OUTGROWTH OF THE EPICARDIAL LAYER TO STUDY DEVELOPMENT OF THE PURKINJE FIBER NETWORK

The Purkinje fiber network forms the distal part of the CCS, which conducts the electrical impulse at high velocity to the ventricular cardiomyocytes, followed by contraction of the ventricles. The Purkinje fibers are specialized cardiomyocytes that are clonally related to the ventricular myocardium.[25]

Eralp *et al.* performed mechanical and genetic inhibition of the epicardium to study the development of the Purkinje fiber network.[26] Mechanical inhibition was achieved by the method described above, while antisense retroviral vectors disturbing *Ets* transcription were used for genetic inhibition. *Ets* transcription factors play numerous roles in normal physiology and their disruption resulted in impaired EMT, which retards EPDC formation.[27] The developing Purkinje fiber network was studied using immunohistochemical techniques. In both models of epicardial inhibition, the Purkinje fiber network was affected as shown by a reduction in periarterially located Purkinje fibers. Furthermore, the subendocardially located Purkinje fibers displayed abnormal cellular morphology and did not form a continuous network.[26]

5.1.3. INHIBITING OUTGROWTH OF THE EPICARDIAL LAYER TO STUDY THE ROLE OF THE EPICARDIUM IN AUTONOMIC MODULATION OF THE DEVELOPING CHICK HEART

The cardiac autonomic nervous system (cANS) is essential in regulating heart rhythm, contractility and conduction velocity. The heart responds to adrenergic stimulation prior to development of the neuronal components of the cANS.[28] Recent work has shown evidence for a role of the epicardium in the autonomic response during early chicken heart development.[29] The effect of epinephrine administration was investigated in microelectrode experiments *ex vivo* in control hearts and after inhibition of epicardial outgrowth. In control hearts, a rapid and marked increase in heart rate was seen directly after administration of epinephrine. Interestingly, the response was significantly decreased after epicardial inhibition. Furthermore, in control HH15 hearts, prior to development of the epicardial layer of the heart, no response was seen after administration of epinephrine.[29] The elegant technique specifically limiting epicardial outgrowth was essential for establishing this previously unknown function of the epicardial layer.

5.2. MICROINJECTION EXPERIMENTS TO STUDY CCS DEVELOPMENT

The accessibility of the avian embryo makes targeted microinjection experiments with signaling factors, teratogens, vital dyes, viruses, small hairpin RNA and cells fairly straightforward. Microinjection can be performed at very early stages of

development with long-term follow-up.

Physical cell labeling experiments start with loading dyes, viral vectors etc. in a pulled glass needle. Injection is achieved with a programmable microinjector (IM-300 Narishige, Japan) and micromanipulator. After opening the egg (see **Section 4**), the vitelline and chorionic membranes are opened to gain access to the embryonic heart. Using a dissection microscope, the needle is positioned directly on the structure of interest and the solution is applied with the microinjector (**Fig. 4**), after which the egg is closed and reincubated at 37^{0}C. The embryos can be extracted from the egg at the required time points to analyze the fate of labeled cells, investigate the effect of reagents introduced into the embryo etc. It is also possible to perform *in* and *ex ovo* live imaging of labeled cells, thereby creating a live fate map of the cluster of labeled cells.[30]

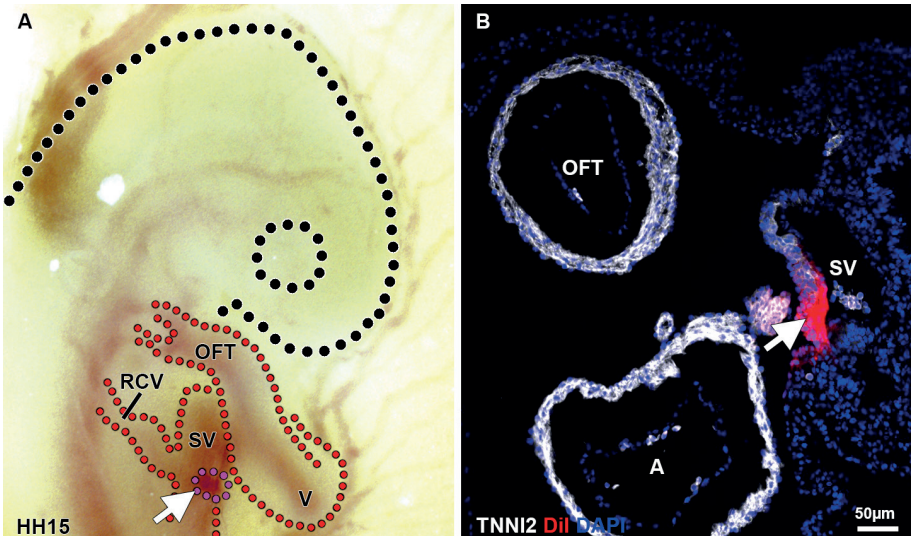

Figure 4. Performing vital dye labeling experiments

a. A chick embryo of HH15 is shown after vital dye labeling with DiI (pink dotted line/arrow). Here, the myocardium of the sinus venosus (SV) is labeled. **b.** The result of labeling is shown on a microscopic section. In pink, the DiI label is shown, located in the TNNI2+ myocardium (white) of the SV. Blue: DAPI (nuclear stain). A: atrium, OFT: outflow tract, RCV: right cardinal vein, V: ventricle.

5.2.1. IN OVO VIRAL MICROINJECTION EXPERIMENTS TO STUDY THE ORIGIN OF THE CCS

Labeling and subsequent follow-up of the fate of these cells can also be achieved by microinjection with viral vectors driving expression of a reporter construct. By choosing a lineage-specific promoter, it is possible to trace the subset of cells in the infected region expressing the gene of interest specifically. This has advantages over genetic tracing in conditional *Cre* mice since infection is of a small

subset of cells only. Apart from expression of reporter constructs, this technique also allows expression of specific genes thereby creating opportunities for site-specific overexpression or knockdown of genes. A disadvantage of this technique is the difficulty in achieving stable transfection of quantitatively reproducible numbers of cells in different embryos. Furthermore, it is difficult to target one region only, since dissolved virus may also infect cells at a larger distance, unless injection takes place in a confined space such as the lumen of the neural tube. Finally, to reach a detectable threshold takes approximately 24 hours. Therefore, this technique is less suitable to trace cells directly after labeling.

Viral labeling in chicken embryos has been essential to understand the cellular origin of the CCS. Gourdie *et al.* induced β-gal expression in functioning cardiomyocytes by retroviral infection at embryonic day 3. Subsequent lineage analysis showed that the specialized, fast-conducting ventricular Purkinje fiber network was of myocardial origin. Later retro- and adenoviral lineage tracing studies showed that also central components of the CCS, such as the AV ring tissue, His bundle and bundle branches have a myocardial origin. In these experiments, no evidence was found that the components of the CCS derive from a neurogenic progenitor, as was previously assumed.[8,31]

5.2.2. IN OVO VITAL DYE MICROINJECTION EXPERIMENTS TO STUDY THE ORIGIN OF THE CCS

Physical labeling of clusters of cells can be achieved by vital dye labeling. These dyes are incorporated in the cell membrane or cytoplasm and can be followed during development.[30] A large number of dyes are available for this purpose, ranging from Indian ink to long-chain carbocyanines, such as DiI. The latter category is fluorescent and available in different colours (DiI, DiO, DiD, and DiR are, respectively, orange, green, red and infrared in fluorescence). This allows tracing of several cell populations simultaneously. Different fluorescent markers can mark different subcellular compartments. For instance, DiI will stain the cell membrane, whereas CFSE will stain the cytoplasm of the cell.[30] Combining dyes will allow visualization of different cell compartments within the same cell simultaneously.[11] Disadvantages of this technique are the dilution of dye over a longer period of time, since dye is diluted with each new cell division and its rate of disappearance thus depends on the cell division rate in the area labeled and the amount of label used. Another disadvantage is the potential cellular toxicity of dyes (or the solvents used to dissolve the dyes, such as DMSO. The latter can be used *in ovo* if 1% solvent is not exceeded).

Bressan *et al.* performed vital dye labeling experiments to investigate the origin of the cardiac pacemaker cells during early development at HH5, HH8 and HH10.[32] They found that pacemaker precursors were situated in the *ISL1-/NKX2-5-* right lateral plate mesoderm. ISL1 is a transcription factor, which

plays an important role in cell proliferation, differentiation, and migration and is expressed in precardiac mesoderm. NKX2-5 is expressed in cardiomyocytes. Interestingly, cells from this *ISL1-/NKX2-5-* region also contributed to the atrial and atrioventricular myocardium and the PEO. These microinjection experiments identified a new region of cardiac progenitors. Furthermore, the results showed that during early development, an important portion of precardiac mesoderm does not (yet) express *ISL1* and *NKX2-5*, at least at high enough levels to be detected with *in situ* hybridization.

Another series of labeling experiments indicated a possible role for the myocardium of the sinus venosus in development of the posterior AV canal.[11] Vital dyes were injected in the ISL1+/TNNI2+ myocardium of the sinus venosus at HH15. At this stage, ISL1-/TNNI2+ myocardium is present between the ISL1+/TNNI2+ sinus venosus myocardium and ISL1-/TNNI2+ AV canal myocardium. Embryos were reincubated at 37^0C for 24 or 48 hours after which the dye distribution was analyzed. Interestingly, incorporation of ISL1+/TNNI2+ sinus venosus myocardium in the posterior region of the AV canal was found. Electrophysiological characterization and analysis of gene expression of this region indicated a role in CCS functioning (these experiments are described in further detail in **section 6** and **7**). It was hypothesized that the myocardium of the sinus venosus plays a role during normal development of the AVN.[11]

5.3. HETEROSPECIFIC TRANSPLANTATION AND NEURAL CREST ABLATION STUDIES TO INVESTIGATE THE DEVELOPING CARDIAC AUTONOMOUS NERVE SYSTEM AND CCS

The chick cardiac autonomic nerve system (cANS) is partially neural crest derived. Neural crest cells (NCCs) have their origin in the closing region of the neural tube after which they migrate throughout the body. Development of cardiac autonomic innervation has been extensively studied in chick. Next to studies based on protein expression patterns[29,33], several microsurgical techniques have been used to study the developing cANS. Inhibition of epicardial outgrowth is described above.[29] Other techniques used are neural crest ablation and heterospecific transplantation studies (in which quail-derived tissue is transplanted to chick embryos), which will be described here.

5.3.1. HETEROSPECIFIC TRANSPLANTATION OF NEURAL CREST CELLS (QUAIL-CHICK CHIMERAS)

Heterospecific transplantation of NCCs (quail-chick heterospecific chimeras)[34] is a cell lineage tracing technique used to study cardiac neural crest development in which the chick neural crest is replaced by quail neural crest. More specifically,

the dorsal part of the neural tube containing the cardiac neural crest is removed, and replaced by quail cardiac neural crest from a comparable embryonic stage (**Fig. 5**).[35] Quail cells can be distinguished from chick cells by differences in nuclear morphology and quail-specific antibodies. This allows the transplanted quail NCCs that contribute to cardiac neurons, to be traced in the chick. However, as the typical nuclear heterochromatin pattern used to distinguish the quail cells from chick cells is lost when the quail NCCs enter the heart, anti-quail nuclear antibody (anti-QCPN) can be used to visualize quail cells in the neural crest derived neuronal cells, that also express the markers HNK-1 or RMO-270.[33,35,36]

Heterospecific transplantation studies have shown that cardiac autonomic ganglia at the arterial pole are neural crest derived.[34] In addition, studies by Verberne *et al.*, using heterotopic transplantation in combination with retroviral *lacZ* transfer have shown a contribution of NCCs to parasympathetic neurons in the entire cardiac plexus, including at the venous pole of the heart.[35]

Although the technique has been used to clarify the origin of cells contributing to the cardiac sympathetic and parasympathetic innervation successfully,

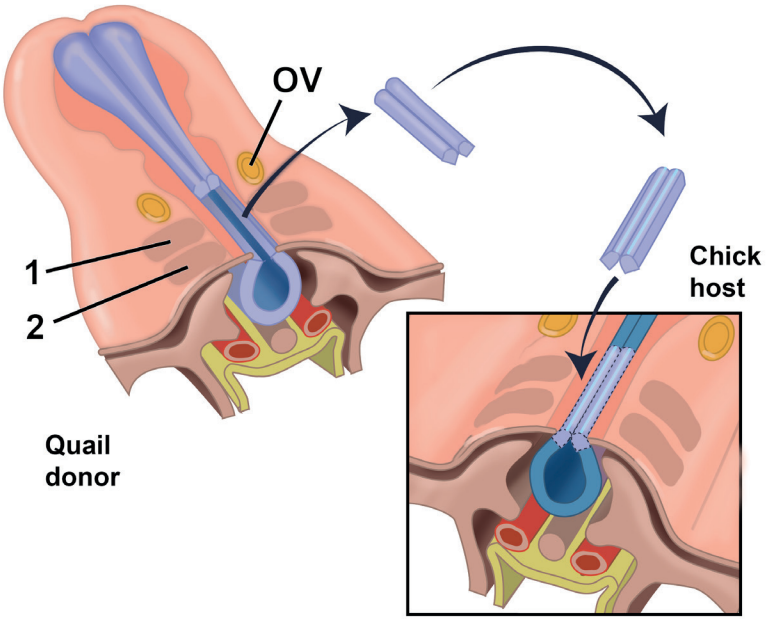

Figure 5. Heterospecific transplantation of the neural crest

Schematic representation of the technique used to perform heterospecific transplantation of the neural crest. The dorsal part of the neural tube of the quail, containing the neural crest, is excised. In the chick, of comparable embryonic stage, the same region is removed and the quail neural crest is placed in the position of the removed neural crest. 1: somite 1, 2: somite 2, OV: otic vesicle.

heterospecific transplantation reduces survival rates of treated embryos and causes surgical damage in the chimeras, confounding interpretation of results.

5.3.2. NEURAL CREST ABLATION TO INVESTIGATE THE DEVELOPING CANS

Neural crest ablation[37,38] involves the surgical removal of regions of the neural crest in the developing chick embryo using for instance a microcautery needle or laser ablation. This technique has been used to study cardiac innervation and revealed disruption of parasympathetic innervation after bilateral ablation of the neural crest over occipital somites at early developmental stages.[39] However, the technique is limited by the potential recruitment of neural derivatives from adjacent non-ablated regions compensating for the ablated cells.[40] In addition ,partial regeneration of the neural crest following surgical removal, or an alteration in the contribution of incoming sympathetic or preganglionic parasympathetic elements may account for a limited extent or impact of the applied lesions.[39]

More recently, cardiac neural crest ablation was used in chick to study ventricular activation patterns. Laser ablation of cardiac neural crest in chick embryos, followed by optical mapping techniques, resulted in immature (base-to-apex) activation patterns. Histological analysis of the laser-ablated embryos revealed a lack of differentiation and separation from the surrounding myocardium of the His bundle. This indicates a significant function of the cardiac neural crest in electrical isolation of components of the CCS from the surrounding myocardium.[41]

5.4. EFFECTS OF DRUGS AND EXPERIMENTAL COMPOUNDS

The easy accessibility of the chicken embryo makes it possible to directly administer test compounds of interest directly onto the embryo.[42,43] Furthermore, long-term follow-up (even into adulthood) of the effects of the compound is achievable, since the embryos can continue normal development to hatching.

Our technique is as follows. After opening the egg and the extraembryonic membranes, the compound can be delivered directly on the embryo. Another option is to inject compounds in the pericardial cavity, or into the vitelline veins/arteries. To perform functional inhibition, loaded heparin beads can be placed in the developing area of interest, after which the bead-bound compound is slowly released over time. We have carried this out using the ROCK inhibitor Y-27632 (Kelder and Vicente-Steijn, unpublished data) as have others.[44] The measured outcome depends on the aim of the study (e.g. assessing the effects on electrophysiological function, cell migration, proliferation, or apoptosis). Timing of administration is important and again depends on the aim of the study. We were successful in administering the ROCK inhibitor Y-27632 *in ovo* at HH10-

12 to study the effect on components of the developing CCS. Previous studies showed that the RHOA-ROCK signaling pathway is important in the developing CCS,[45–47] which we recently confirmed (Kelder and Vicente-Steijn, unpublished data).

A standardized approach to investigate the potential toxicity of compounds is called the Chick Embryotoxicity Screening Test (CHEST) as developed by Jelínek and colleagues.[48] This method has two phases. In the first phase (CHEST I) the compound is administered at HH10-11 at increasing doses and shortening of the embryonic trunk is used as outcome parameter (indicating interference with function of the caudal morphogenetic system). In the second phase (CHEST II) the last ineffective (no significant shortening of trunk length) and first two effective (significant shortening of trunk length) are used. These doses are administered at E2-4 and the embryos are analyzed at E8. The method includes analysis of mortality, gross morphological abnormalities and analysis of cardiac defects such as ventricular septal defects or outflow tract abnormalities.[48] This method was used to investigate the toxicity of bilirubin[49], mirtazapine[50], urban air particulate matter[51], ibuprofen[52], a selection of psychotropic drugs such as haloperidol[48], and mycotoxins.[53] The CHEST method can be used to study all known and newly developed compounds as a screen to identify potentially toxic substances. When a compound is identified as potentially harmful, additional experiments are carried out to assess human relevance.

5.5. GENETIC CHARACTERIZATION OF THE CCS IN THE CHICK

Quantitative gene expression can be determined using qPCR. Determining the type of input material is crucial to answer the question of interest. Expression can be studied in the entire heart or in specific regions, for example *Pitx2c*[54] in the left side of the heart (providing left-sided identity) or only in the atria and not in the ventricles, like *Nppa*[55] (exclusively found in the adult atrial tissue). Methods of tissue collection are described in the next sections.

5.5.1. QPCR OF MACROSCOPICALLY COLLECTED TISSUE IN THE CHICK

Microdissection of the region of interest within the heart can be performed under a microscope and validated with a known panel of genes expressed in that region.[56] Standard commercially available isolation kits (Qiagen RNEasy MicroKit) work well in chick and allow isolation of minute quantities of RNA from individual regions of the heart. qPCR analysis showed little sample-to-sample variation, a distinct advantage when comparing individual hearts of control and treated or manipulated hearts since the variability within and between the groups can be assessed fairly precisely. Furthermore, this high reproducibility allows dose dependency to be studied. We have been able to study gene expression at

the inflow tract including the developing SAN of ED3 chicken hearts (HH17-19) quite reproducibly and robustly. At later stages, the right and left portion of the sinus venosus can be studied separately. This is relevant since several structures of the developing CCS are bilateral or dual in origin such as the SAN[9,14] and possibly also the AVN.[57] Using this technique, it is possible to study the effects on RNA expression of a specific treatment or chemical compound on the right-left asymmetry axis of the heart[58], including the effects on lateralization of the CCS.

5.5.2. QPCR ANALYSIS AFTER LASER CAPTURE MICRODISSECTION OF SPECIFIC ELEMENTS OF THE CCS

In carrying out gene or protein characterization in conduction system tissues, an important drawback is the difficulty in dissecting subsets of cells within an organ. An elegant method to overcome this problem is laser capture microdissection (LCM).[59,60] This technique enables the user to extract a specific region of tissue from a section at very high resolution. Combining high-resolution microscopy with, for example, fluorescent staining or fluorescent reporter gene expression, allows specific isolation of clusters of cells and their further characterization. The following section describes the LCM procedure we have used.

The procedure starts with (cryo)sectioning tissue and mounting the tissue on membrane-coated slides (Carl Zeiss Microscopy). After drying (and when working with paraffin-embedded tissue, treatment with xylene to remove the paraffin) the slides are placed in the LCM microscope (PALM microbeam, Carl Zeiss Microscopy). The region of interest is excised with the laser beam (**Fig. 6**), after which it is catapulted into an adhesive cap (Carl Zeiss Microscopy). The tissue is stored at -80°C until further characterization.

We have used this approach to study the CCS in the region of the AV junction, exploring the myocardial continuity between the myocardium of the sinus venosus and AV canal.[11] LCM was performed at HH21 to dissect tissue specifically from this continuity and compare gene expression with tissue obtained from the more caudal portion of the posterior AV canal. Expression of the myocardial markers *TNNT2* and *NKX2-5* was examined as well as *HCN4,* responsible for the “funny current", which enables cardiomyocytes to depolarize spontaneously, which is used as CCS marker. Finally, *ISL1* expression was measured. *ISL1* is expressed in precardiac mesoderm and relatively undifferentiated cardiomyocytes and was recently shown to act as an important transcriptional regulator of HCN4.[61] Results showed that *ISL1* and *HCN4* expression was high in the myocardial continuity. This shows that the myocardial continuity expresses genes known to be essential for normal functioning of the CCS. Furthermore, it indicates that even during early development, different cell populations can be distinguished within the region of the putative AVN. LCM was essential to isolate the different regions of tissue and make this point.

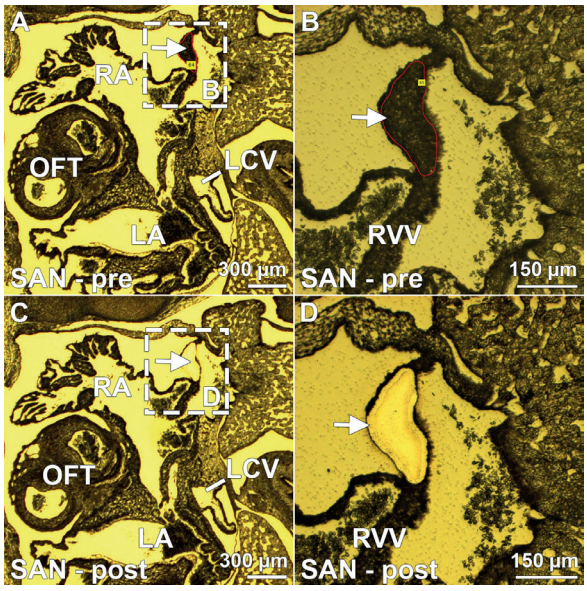

Figure 6. Laser capture microdissection of the SAN in chick

a-b. Microscopic section of the region of the SAN (arrow in **a-b**) prior to microdissection, shown at a higher magnification in **b.** The thin red line demarcates the dissection line, which in this case demarcates the SAN **c-d.** Section of the SAN (arrow in **c-d**) after LCM, shown at a higher magnification in **d.** The tissue containing the SAN is dissected and catapulted in the adhesive cap. LA/RA: left/right atrium, LCV: left cardinal vein, OFT: outflow tract, RVV: right venous valve.

5.6. ELECTROPHYSIOLOGICAL CHARACTERIZATION OF THE CCS IN THE CHICK

The main function of the CCS is coordinated electrical activation of the myocardium, resulting in synchronized contraction of the heart. Electrophysiological characteristics of the developing CCS indicate whether its function is normal or abnormal. In **Fig. 7**, an example is given of different electrophysiological techniques used to investigate the development of the early CCS. These are described in more detail below.

5.6.1. ELECTROCARDIOGRAPHY IN CHICK EMBRYOS

One of the most commonly used diagnostic tools in cardiology, the electrocardiogram (ECG), is also frequently used in the research setting. The ECG depicts the electrical activation of the myocardium. Most cardiac diseases (such as arrhythmias, channelopathies, cardiac hypertrophy and myocardial ischemia) cause abnormalities on the ECG. An important advantage of the chicken embryo is the ability to perform *in ovo* electrocardiography, enabling study of the developmental ECG changes without interfering with normal development. Furthermore the effect of different interventions like drug administration and microsurgery can be evaluated.

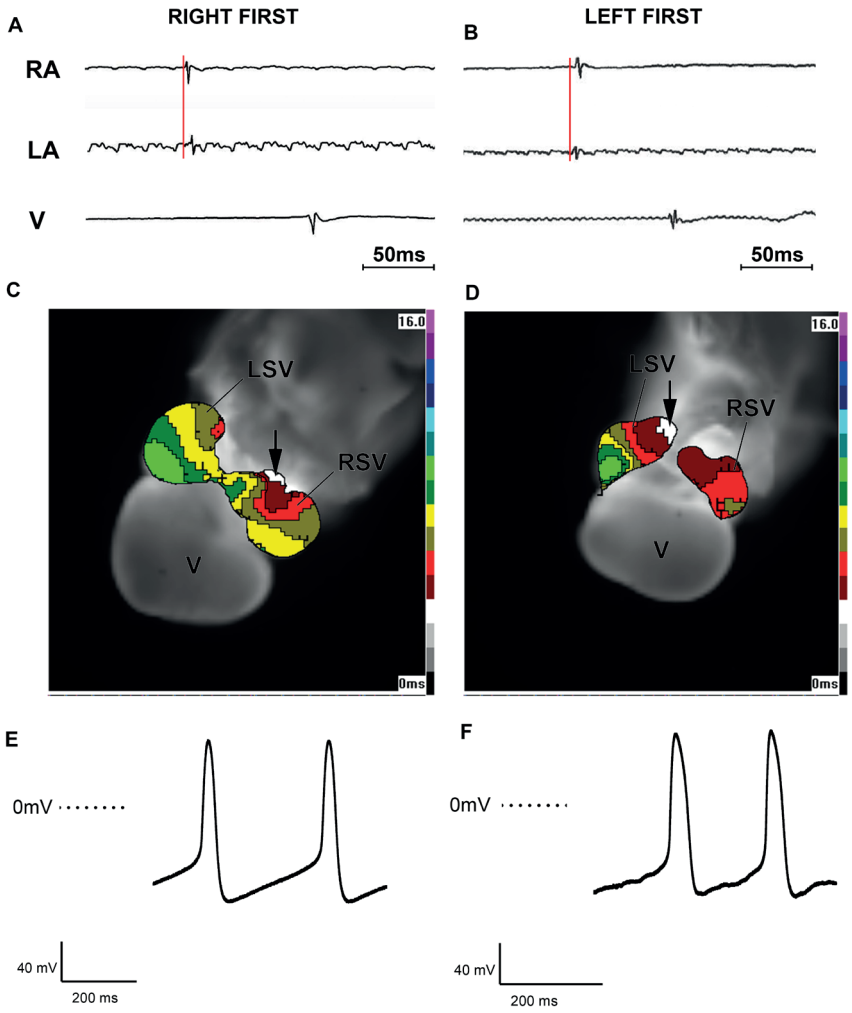

Figure 7. Examples of electrophysiological measurements to study the pacemaking potential of the sinus venosus myocardium

During early development, the left and right side of the sinus venosus myocardium have the potential to start electrical activation of the heart. **a-b.** Microelectrode recordings showing activation starting from the right (**a**) or left (**b**) side of the sinus venosus at HH20. The red line corresponds to the first electrical signal. **c-d.** Optical mapping recordings of the dorsal portion of the heart at HH24, showing first activation (arrow, color code white) from the right (**c**) or left (**d**) side of the sinus venosus (and atria). Each color respresents 1ms of propagation. **e-f.** Single-cell patch clamp trace of cells dissociated from the right (**e**) or left (**f**) part of the sinus venosus, both showing a pacemaker-like phenotype. LA: left atrium, LSV: left side sinus venosus, RA: right atrium, RSV: right side sinus venosus, V: ventricle.

Performing *in ovo* ECG recordings has been described in detail by Kolditz *et al*.[62] Briefly, the egg is candled (**Fig. 2**) to locate the embryo and to determine exactly the location on which to place the three silver chloride electrodes through the eggshell. The bipolar ECG can be recorded using a digital recording device[62] e.g. to investigate the effect of inhibition of epicardial outgrowth on the electrophysiological properties of the heart. Interestingly, after epicardial inhibition shortened PR intervals were found, which is one of the characteristics of AVRT. This arrhythmia is caused by strands of myocardium bypassing the insulating annulus fibrosus of the heart, resulting in pre-excitation of the ventricular myocardium. *In ovo* ECG recording provided important evidence that the epicardium plays a key role during normal annulus fibrosus development. Defects in epicardial development may result in AVRT.[62]

In addition to *in ovo* ECG recordings it is also possible to record an ECG *in vitro* after extraction of the heart interrupting all connections between the central nervous system and the heart, specifically to investigate the CCS independent of autonomic innervation. Furthermore, dissection of different cardiac structures makes it possible to analyze electrophysiological functioning of the right atrium separately from the left atrium, for example. In general, the technique is comparable with *in ovo* ECG recording, with the exception that the *in vitro* electrode is placed in the direct vicinity of the heart, in the tissue dish. *In vitro* ECG recordings were for example used to study the effects of *in ovo* pacing on postanoxic recovery.[63] ECG recordings showed a lower incidence of arrhythmias in hearts that were paced *in ovo*.[63]

5.6.2. FETAL ULTRASOUND FOR DETECTION OF HEART RATE

In humans, detection of fetal arrhythmias and conduction disorders is usually by fetal ultrasound. In severe cases, the rhythm disorders may cause fetal hydrops, which is also detected by ultrasound.[64–66] High frequency ultrasound has also been used to assess avian cardiovascular development.[67] In chick, fetal ultrasound was used to study haemodynamics before and after administration of epinephrine. Dorsal aortic flow velocity baseline waveform recordings were used to calculate heart rate, by measuring the cycle length between pulse waves and converting these into beats per minute.[28] The application of this technique in avian models for study of the fetal conduction system is to date limited.

5.6.3. EX OVO MICROELECTRODE MEASUREMENTS

Many electrophysiological measurements in embryonic chicken hearts have been conducted.[7,9,29,63,68–71] *Ex vivo* electrophysiology of whole embryonic chicken hearts provides useful information on heart function in the absence of external whole body influences like sympathetic or parasympathetic stimuli, which alter cardiac parameters such as heart rate, conduction velocity, and force of

contraction. For this purpose, whole heart electrophysiology of embryonic stage hearts is a useful tool to study cardiac function throughout development.

Whole heart *ex ovo* electrophysiology can be used to analyze intracardiac conduction i.e. in the presence of myocardial accessory pathways[62,72,73] or to characterize the cardiac pacemaking signal.[9,29] Briefly, hearts from chicken embryos are isolated under a dissection microscope and placed in a temperature-controlled tissue bath at 37°C, in a Petri dish containing 3% agarose gel. The heart is immobilized by placing a holding pin through non-cardiac tissue around the outflow tract of the heart. Tungsten electrodes are placed on the cardiac surface where the electrophysiological measurements are to be taken. The measuring resolution between electrodes is in milliseconds. For smaller conduction differences, optical mapping is used (see **section 5.6.4.**).

With *ex ovo* microelectrode measurements several cardiac parameters can be calculated, such as heart rate in beats per minute (bpm) or atrioventricular (AV) conduction time in milliseconds (ms), measuring the total time the signal takes to travel from the atrium to the ventricle.[9,29,62,72,73] These parameters are interesting in light of abnormal models resulting in pacemaker defects like bradycardia, tachycardia or atrial fibrillation or in models with abnormal AV conduction such as different degrees of AV block or shortened AV time as in cases with pre-excitation.[62,72,73]

Furthermore, electrical activity between two points determined by the observer can be measured, allowing for instance location of the site of first atrial activity (i.e. the pacemaking site) and ectopic activation patterns.[9] Likewise, AV conduction patterns can be recorded to study the pattern of ventricular activation. This has been used to determine the maturity of ventricular activation i.e. distinction of an immature base-to-apex from mature apex-to-base activation patterns, and the presence and location of accessory myocardial pathways causing pre-excitation.[62,73] These recordings are very stable and spontaneous arrhythmias hardly occur making this an excellent method to measure electrical signals *in toto* without the necessity of adding chemical compounds to visualize the signal as required when performing optical mapping. The disadvantage is limitation to fixed number of electrodes. If any abnormalities occur outside of the studied region e.g. when measuring pre-excitation, the initial pacemaker site cannot be traced because only one electrode can be placed at the atrial level. Optical mapping measurements provide useful complementary data as a detailed conduction map of the area studied can be obtained.

5.6.4. OPTICAL MAPPING STUDIES

Optical mapping is an electrophysiological technique that allows the depolarization wave of the cardiac electrical impulse to be followed using voltage sensitive dyes. This technique has been broadly used in both adult and fetal stages. This has been reviewed elsewhere for various stages of development.[74]

Optical mapping is accomplished by loading the cardiac tissue with a voltage sensitive dye (such as di-4-ANEPPS). Current developments allow monitoring of a wide range of parameters[74], such as ion propagation signals of calcium and sodium[75], which provide new insights into the mechanisms of specific arrhythmias. Other parameters commonly measured are conduction time and conduction velocity. Parameters like heart rate or AV delay can also be measured. The combination of voltage and calcium mapping reveals arrhythmogenic sites within the developing heart and information on the changes of ionic concentrations within regions of the developing heart. This has recently provided new insights into the pacemaking potential of the outflow tract of the heart.[74]

It is necessary to induce electromechanical dissociation for example with blebbistatin to avoid motion artifacts. These compounds have no obvious effect on cardiac parameters such as heart rate and AV delay.[76] However, inclusion of proper controls is advisable to allow conclusions from optical mapping experiments.

The main use for optical mapping is to study activation conduction patterns throughout development[9,32,71,77–79] and compare them with disease models.[41,80–82] For example, experiments have been performed showing that mechanical loading during early development is imperative for proper development of the CCS.[81] Furthermore, it was shown that exposure to prolonged hypoxia during development affects maturation of the CCS.[82]

5.6.5. MICROELECTRODE ARRAY STUDIES

Microelectrode arrays (MEA) are commonly used as a straightforward measure of electrical activity in monolayers of spontaneously beating cultured cardiomyocytes. Chicken cardiomyocytes are well-suited for this purpose and reliable measurements have already been conducted[83,84] providing a model to study toxicity for example.[85] A major advantage of MEAs is that the measurements can be conducted on a selected cardiomyocyte population, like sinoatrial, atrial or ventricular cardiomyocytes, avoiding interference from other regions of the heart, but still within a tissue monolayer, as opposed to single-cell patch clamp electrophysiology (see next section). This allows cell-cell interactions influencing the electrophysiological parameters as expected in the whole heart, but without the main pacemaker present.

Another advantage is the study of effects of a specific drug.[85] Long-term effects after *in ovo* drug or chemical compound administration can result in permanent modifications or alterations to normal heart development including altered gene expression.[58] Short-term effects of drugs on the action potential of a specific cardiomyocyte cell population can also be studied using MEA. Compounds can be administered directly onto the cell culture and the effects on electrophysiology can be studied during chosen time intervals.[86] From the recorded field potential it is possible to derive information on the action potential[86] allowing study of the effects of, for example, *in ovo* micromanipulation or drugs on specific populations of cardiomyocytes. This provides an excellent experimental model to study drug toxicity or responses in cardiomyocytes.[85] After proper comparison and validation to human cardiomyocytes, chick cardiomyocytes could provide a good model for high throughput drug testing.

5.6.6. SINGLE-CELL PATCH CLAMP RECORDINGS IN CHICK EMBRYONIC CARDIOMYOCYTES.

Single-cell patch clamping is used to study ion channel function and currents in cardiomyocytes combined with electrophysiological characteristics of the different types of cardiomyocytes in the developing heart.

To perform single-cell patch clamp the cells have to be dissociated first. Briefly (see[11] for more details) the region of cardiac conduction tissue is collected and trypsinized. After dissociation cells are plated on glass coverslips to attach. Patch clamp options include perforated patch clamp, whole-cell patch, and inside-out patch. Description of the different methods[87] is beyond the scope of the technical comment here. The acquired data can be further analyzed to quantify various electrophysiological parameters including maximal upstroke velocity, action potential duration, and action potential amplitude.

Patch clamp experiments in chick embryonic cardiomyocytes have been of great importance in understanding normal and abnormal cardiac electrophysiological functioning. First, the presence and function of ion channels and currents was investigated in a large number of studies.[88–108] Detailed description is beyond the scope here but one example is the description of the pacemaker current in chick embryonic ventricular and atrial cells, which demonstrated that not only pacemaker cells display this current.[96] Second, recent work characterized the electrical phenotype of cells derived from specific regions.[11] In **section 5.2.2.** and **5.5.2.**, the continuity between the sinus venosus myocardium and the AV canal is described. Genetic characterization of this region showed that the myocardial continuity has a pacemaker-like phenotype (expression of *HCN4/ISL1*). Electrophysiological characterization with single-cell patch clamp confirmed the pacemaker-like phenotype of the myocardial continuity.[11] The functional electrophysiological characterization using patch

clamp was paramount to attributing a role in CCS function to this specific cardiac region. Third, the single-cell patch clamp technique is also useful in studying the effects of different compounds on electrophysiological characteristics.[109–116] For instance, several studies have analyzed the effects of Bay K8644, a calcium channel antagonist, on electrophysiological properties.[110,111] This also opens the possibility of testing the therapeutic potential of drugs. Alternatively, the patch clamp technique is also useful in studying potential arrhythmogenic properties of new pharmaceutical compounds. Fourth, the effects of hormones, growth factors and neurotransmitters normally present in the body, on cardiac electrical functioning and maturation can be studied.[117–125] Several studies were aimed at elucidating the role of taurine in cardiac electrophysiology.[122–125] It was for example shown that taurine, an organic acid with a wide variety of functions in normal physiology, plays a role during spontaneous electrical activity of cardiomyocytes.[124] Fifth, patch clamp recordings can be used to study electrophysiological characteristics of cardiomyocytes in experimental disease models[126,127], such as after ablation of the neural crest during chick development.[127] Patch clamp experiments showed evidence that neural crest cells are necessary for normal development of myocardial calcium channels.[127]

In summary, cardiac patch clamp experiments performed in chicken embryos have increased our knowledge of normal cardiac electrophysiology at the single cellular level. The technique can be used to characterize cells on the basis of their electrophysiological profile and to test the effects of (pharmaceutical) compounds.

6. CONCLUSIONS

We have provided here an overview of different techniques used in the avian model system to understand normal and abnormal development and functioning of the CCS. The avian embryo has and will continue to be a powerful model system to study development in general and the developing CCS in particular. Since the avian embryo is considered an animal friendly alternative, is easy to use and is inexpensive, we hope to have encouraged readers to incorporate this model system in their own laboratory.

REFERENCE LIST

1. Stern, C. D. The chick: A great model system becomes even greater. *Dev. Cell.* **8,** 9–17 (2005).

2. Hamburger, V. & Hamilton, H. L. A series of normal stages in the development of the chick embryo. *J. Morphol.* **88,** 49–92 (1951).

3. Buckingham, M., Meilhac, S. & Zaffran, S. Building the mammalian heart from two sources of myocardial cells. *Nat. Rev. Genet.* **6,** 826–835 (2005).

4. Abu-Issa, R. & Kirby, M. L. Heart field: from mesoderm to heart tube. *Annu. Rev. Cell Dev. Biol.* **23,** 45–68 (2007).

5. Jongbloed, M. R. *et al.* Normal and abnormal development of the cardiac conduction system; implications for conduction and rhythm disorders in the child and adult. *Differentiation.* **84,** 131–148 (2012).

6. Poelmann, R. E. & Gittenberger-de Groot, A. C. A subpopulation of apoptosis-prone cardiac neural crest cells targets to the venous pole: multiple functions in heart development? *Dev. Biol.* **207,** 271–86 (1999).

7. de Jong, F. *et al.* Persisting zones of slow impulse conduction in developing chicken hearts. *Circ. Res.* **71,** 240–50 (1992).

8. Gourdie, R. G., Mima, T., Thompson, R. P. & Mikawa, T. Terminal diversification of the myocyte lineage generates Purkinje fibers of the cardiac conduction system. *Development.* **121,** 1423–31 (1995).

9. Vicente-Steijn, R. *et al.* Electrical activation of sinus venosus myocardium and expression patterns of RHOA and Isl-1 in the chick embryo. *J. Cardiovasc. Electrophysiol.* **21,** 1284–92 (2010).

10. Aanhaanen, W. T. J. *et al.* Developmental origin, growth, and three-dimensional architecture of the atrioventricular conduction axis of the mouse heart. *Circ. Res.* **107,** 728–36 (2010).

11. Kelder, T. P. *et al.* The sinus venosus myocardium contributes to the atrioventricular canal: potential role during atrioventricular node development? *J. Cell. Mol. Med.* **19,** 1375–89 (2015).

12. Gittenberger-de Groot, A. C. *et al.* The arterial and cardiac epicardium in development, disease and repair. *Differentiation.* **84,** 41–53 (2012).

13. Nishijima, K. I. & Iijima, S. Transgenic chickens. *Dev. Growth Differ.* **55,** 207–216 (2013).

14. Vicente-Steijn, R. *et al.* Funny current channel HCN4 delineates the developing cardiac conduction system in chicken heart. *Heart Rhythm.* **8,** 1254–63 (2011).

15. Le Lièvre, C. S. & Le Douarin, N. M. Mesenchymal derivatives of the neural crest: analysis of chimaeric quail and chick embryos. *J. Embryol. Exp. Morphol.* **34,** 125–54 (1975).

16. Eyal-Giladi, H. The gradual establishment of cell commitments during the early stages of chick development. *Cell Differ.* **14,** 245–55 (1984).

17. Boot, M. J., Gittenberger-de Groot, A. C., Van Iperen, L., Hierck, B. P. & Poelmann, R. E. Spatiotemporally separated cardiac neural crest subpopulations that target the outflow tract septum and pharyngeal arch arteries. *Anat. Rec. A. Discov. Mol. Cell. Evol. Biol.* **275,** 1009–18 (2003).

18. Männer, J. Experimental study on the formation of the epicardium in chick embryos. *Anat. Embryol.* **187,** 281–289 (1993).

19. Männer, J. Microsurgical procedures for studying the developmental significance of the proepicardium and epicardium in avian embryos: PE-Blocking, PE-Photoablation, and PE-Grafting. *J. Dev. Biol.* **1,** 47–63 (2013).

20. Gittenberger-de Groot, A. C., Vrancken Peeters, M.-P. F. M., Mentink, M. M. T., Gourdie, R. G. & Poelmann, R. E. Epicardium-Derived Cells contribute a novel population to the myocardial wall and the atrioventricular cushions. *Circ. Res.* **82,** 1043–1052 (1998).

21. Vrancken Peeters, M. P. F. M., Gittenberger-de Groot, A. C., Mentink, M. M. T. & Poelmann, R. E. Smooth muscle cells and fibroblasts of the coronary arteries derive from epithelial-mesenchymal transformation of the epicardium. *Anat. Embryol.* **199,** 367–378 (1999).

22. Gittenberger-de Groot, A. C., Vrancken Peeters, M. P. F. M., Bergwerff, M., Mentink, M. M. T. & Poelmann, R. E. Epicardial outgrowth inhibition leads to compensatory mesothelial outflow tract collar and abnormal cardiac septation and coronary formation. *Circ. Res.* **87,** 969–971 (2000).

23. Hahurij, N. D. *et al.* Accessory atrioventricular myocardial connections in the developing human heart: relevance for perinatal supraventricular tachycardias. *Circulation.* **117,** 2850–8 (2008).

24. Wessels, A. *et al.* The development of the atrioventricular junction in the human heart. *Circ. Res.* **78,** 110–117 (1996).

25. Sedmera, D. & Gourdie, R. G. Why do we have Purkinje fibers deep in our heart? *Physiol. Res.* **63,** S9–S18 (2014).

26. Eralp, I. *et al.* Epicardium-Derived Cells (EPDCS) are important for correct development of the Purkinje fibers in the avian heart. *Anat. Rec. A. Discov. Mol. Cell. Evol. Biol.* **288,** 1272-80 (2006).

27. Lie-Venema, H. *et al.* Ets-1 and Ets-2 transcription factors are essential for normal coronary and myocardial development in chicken embryos. *Circ. Res.* **92,** 749–56 (2003).

28. Kroese, J. M., Broekhuizen, M. L. A., Poelmann, R. E., Mulder, P. G. H. & Wladimiroff, J. W. Epinephrine affects hemodynamics of noninnervated normal and all-trans retinoic acid-treated embryonic chick hearts. *Fetal Diagn. Ther.* **19,** 431–9 (2004).

29. Kelder, T. P. *et al.* The epicardium as modulator of the cardiac autonomic response during early development. *J. Mol. Cell. Cardiol.* **89,** 251–9 (2015).

30. Darnell, D. K., Garcia-Martinez, V., Lopez-Sanches, C., Yuan, S. & Schoenwolf, G. C. in *Methods in Molecular Biology* (eds. Tuan, R. S. & Lo, C. W.) 305–321 (Humana Press Inc.).

31. Cheng, G. *et al.* Development of the cardiac conduction system involves recruitment within a multipotent cardiomyogenic lineage. *Development.* **126,** 5041–9 (1999).

32. Bressan, M., Liu, G. & Mikawa, T. Early mesodermal cues assign avian cardiac pacemaker fate potential in a tertiary heart field. *Science.* **340,** 744–748 (2013).

33. Verberne, M. E., Gittenberger-de Groot, A. C. & Poelmann, R. E. Distribution of antigen epitopes shared by nerves and the myocardium of the embryonic chick heart using different neuronal markers. *Anat. Rec.* **260,** 335–50 (2000).

34. Kirby, M. L. & Stewart, D. E. Neural crest origin of cardiac ganglion cells in the chick embryo: identification and extirpation. *Dev. Biol.* **97,** 433–43 (1983).

35. Verberne, M. E., Gittenberger-de Groot, A. C. & Poelmann, R. E. Lineage and development of the parasympathetic nervous system of the embryonic chick heart. *Anat. Embryol.* **198,** 171–84 (1998).

36. Verberne, M. E., Gittenberger-de Groot, A. C., Van Iperen, L. & Poelmann, R. E. Contribution of the cervical sympathetic ganglia to the innervation of the pharyngeal arch arteries and the heart in the chick embryo. *Anat. Rec.* **255,** 407–19 (1999).

37. Kirby, M. & Stewart, D. Adrenergic innervation of the developing chick heart: neural crest ablations to produce sympathetically aneural hearts. *Am. J. Anat.* **171,** 295–305 (1984).

38. Kirby, M. L. & Waldo, K. L. Neural crest and cardiovascular patterning. *Circ. Res.* **77,** 211–5 (1995).

39. Kirby, M. L., Aronstam, R. S. & Buccafusco, J. J. Changes in cholinergic parameters associated with failure of conotruncal septation in embryonic chick hearts after neural crest ablation. *Circ. Res.* **56,** 392–401 (1985).

40. Kirby, M. L. Nodose placode provides ectomesenchyme to the developing chick heart in the absence of cardiac neural crest. *Cell Tissue Res.* **252,** 17–22 (1988).

41. Gurjarpadhye, A. *et al.* Cardiac neural crest ablation inhibits compaction and electrical function of conduction system bundles. *Am. J. Physiol. Heart Circ. Physiol.* **292,** H1291-300 (2007).

42. Verrett, M. J., Scott, W. F., Reynaldo, E. F., Alterman, E. K. & Thomas, C. A. Toxicity and teratogenicity of food additive chemicals in the developing chicken embryo. *Toxicol. Appl. Pharmacol.* **56,** 265–73 (1980).

43. Mclaughlin, J., Marliac, J. P., Verrett, M. J., Mutchler, M. K. & Fitzhugh, O. G. The injection of chemicals into the yolk sac of fertile eggs prior to incubation as a toxicity test. *Toxicol. Appl. Pharmacol.* **5,** 760–71 (1963).

44. Schlange, T., Andrée, B., Arnold, H. H. & Brand, T. BMP2 is required for early heart development during a distinct time period. *Mech. Dev.* **91,** 259–70 (2000).

45. Sah, V. P. *et al.* Cardiac-specific overexpression of RHOA results in sinus and atrioventricular nodal dysfunction and contractile failure. *J. Clin. Invest.* **103,** 1627–34 (1999).

46. Wei, L. *et al.* Disruption of Rho signaling results in progressive atrioventricular conduction defects while ventricular function remains preserved. *FASEB J.* **18,** 857–9 (2004).

47. Wang, L., Liu, S., Zhang, H., Hu, S. & Wei, Y. RHOA activity increased in myocardium of arrhythmogenic cardiomyopathy patients and affected connexin 43 protein expression in HL-1 cells. *Int. J. Clin. Exp. Med.* **8,** 12906–13 (2015).

48. Peterka, M., Jelínek, R. & Pavlík, A. Embryotoxicity of 25 psychotropic drugs: a study using CHEST. *Reprod. Toxicol.* **6,** 367–74 (1992).

49. Peterka, M., Miler, I. & Jelínek, R. Teratogenic effects of bilirubin--a study using chick embryotoxicity screening test (CHEST). *Funct. Dev. Morphol.* **4,** 29–32 (1994).

50. Manakova, E., Hubickova, L., Kostalova, J. & Zemanova, Z. Embryotoxicity of mirtazapine: a study using Chick Embryotoxicity Screening Test. *Neuro. Endocrinol. Lett.* **31,** 8–10 (2010).

51. Binková, B., Veselý, D., Veselá, D., Jelínek, R. & Srám, R. J. Genotoxicity and embryotoxicity of urban air particulate matter collected during winter and summer period in two different districts of the Czech Republic. *Mutat. Res.* **440,** 45–58 (1999).

52. Kosar, K. Interaction of ibuprofen with early chick embryogenesis. *Pharmazie.* **48,** 207–9 (1993).

53. Veselý, D., Veselá, D. & Jelínek, R. Nineteen mycotoxins tested on chicken embryos. *Toxicol. Lett.* **13,** 239–45 (1982).

54. Yu, X. *et al.* Differential expression and functional analysis of Pitx2 isoforms in regulation of heart looping in the chick. *Development.* **128,** 1005–13 (2001).

55. Christoffels, V. M. *et al.* Formation of the venous pole of the heart from an Nkx2-5-negative precursor population requires Tbx18. *Circ. Res.* **98,** 1555–63 (2006).

56. Zhou, J. *et al.* Cadherin-11 expression patterns in heart valves associate with key functions during embryonic cushion formation, valve maturation and calcification. *Cells Tissues Organs.* **198,** 300–10 (2013).

57. Blom, N. A. *et al.* Development of the cardiac conduction tissue in human embryos using HNK-1 antigen expression: possible relevance for understanding of abnormal atrial automaticity. *Circulation.* **99,** 800–6 (1999).

58. Wei, L. *et al.* Rho kinases play an obligatory role in vertebrate embryonic organogenesis. *Development.* **128,** 2953–62 (2001).

59. Espina, V. *et al.* Laser-capture microdissection. *Nat. Protoc.* **1,** 586–603 (2006).

60. Emmert-Buck, M. R. *et al.* Laser capture microdissection. *Science.* **274,** 998–1001 (1996).

61. Vedantham, V., Galang, G., Evangelista, M., Deo, R. C. & Srivastava, D. RNA sequencing of mouse sinoatrial node reveals an upstream regulatory role for Islet-1 in cardiac pacemaker cells. *Circ. Res.* **116,** 797–803 (2015).

62. Kolditz, D. P. *et al.* Epicardium-derived cells in development of annulus fibrosus and persistence of accessory pathways. *Circulation.* **117,** 1508–17 (2008).

63. Rosa, A. *et al.* Ectopic pacing at physiological rate improves postanoxic recovery of the developing heart. *Am. J. Physiol. Heart Circ. Physiol.* **284,** H2384-92 (2003).

64. Caserta, L. *et al.* Two-dimensional fetal echocardiography: where we are. *J. Prenat. Med.* **2,** 31–5 (2008).

65. Simpson, J. M. & Sharland, G. K. Fetal tachycardias: management and outcome of 127 consecutive cases. *Heart.* **79,** 576–81 (1998).

66. Hahurij, N. D. *et al.* Perinatal management and long-term cardiac outcome in fetal arrhythmia. *Early Hum. Dev.* **87,** 83–7 (2011).

67. McQuinn, T. C. *et al.* High-frequency ultrasonographic imaging of avian cardiovascular development. *Dev. Dyn.* **236,** 3503–13 (2007).

68. Argüello, C., Alanis, J. & Valenzuela, B. The early development of the atrioventricular node and bundle of His in the embryonic chick heart. An electrophysiological and morphological study. *Development.* **102,** 623–37 (1988).

69. Kamino, K., Hirota, A. & Komuro, H. Optical indications of electrical activity and excitation-contraction coupling in the early embryonic heart. *Adv. Biophys.* **25,** 45–93 (1989).

70. Chuck, E. T., Freeman, D. M., Watanabe, M. & Rosenbaum, D. S. Changing activation sequence in the embryonic chick heart. Implications for the development of the His-Purkinje system. *Circ. Res.* **81,** 470–6 (1997).

71. Sedmera, D. *et al.* Developmental transitions in electrical activation patterns in chick embryonic heart. *Anat. Rec. A. Discov. Mol. Cell. Evol. Biol.* **280,** 1001–9 (2004).

72. Hahurij, N. D. *et al.* Accessory atrioventricular myocardial pathways in mouse heart development: substrate for supraventricular tachycardias. *Pediatr. Res.* **70,** 37–43 (2011).

73. Kolditz, D. P. *et al.* Persistence of functional atrioventricular accessory pathways in postseptated embryonic avian hearts: implications for morphogenesis and functional maturation of the cardiac conduction system. *Circulation.* **115,** 17–26 (2007).

74. Vostarek, F., Sankova, B. & Sedmera, D. Studying dynamic events in the developing myocardium. *Prog. Biophys. Mol. Biol.* **115,** 261–9 (2014).

75. Herron, T. J., Lee, P. & Jalife, J. Optical imaging of voltage and calcium in cardiac cells & tissues. *Circ. Res.* **110,** 609–23 (2012).

76. Fedorov, V. V. *et al.* Application of blebbistatin as an excitation-contraction uncoupler for electrophysiologic study of rat and rabbit hearts. *Heart Rhythm.* **4,** 619–626 (2007).

77. Sedmera, D. *et al.* Changes in activation sequence of embryonic chick atria correlate with developing myocardial architecture. *Am. J. Physiol. Heart Circ. Physiol.* **291,** H1646-52 (2006).

78. Chuck, E. T., Meyers, K., France, D., Creazzo, T. L. & Morley, G. E. Transitions in ventricular activation revealed by two-dimensional optical mapping. *Anat. Rec. A. Discov. Mol. Cell. Evol. Biol.* **280,** 990–1000 (2004).

79. Hirota, A., Kamino, K., Komuro, H. & Sakai, T. Mapping of early development of electrical activity in the embryonic chick heart using multiple-site optical recording. *J. Physiol.* **383,** 711–728 (1987).

80. Calkoen, E. E. *et al.* Abnormal sinoatrial node development resulting from disturbed vascular endothelial growth factor signaling. *Int. J. Cardiol.* **183,** 249–57 (2015).

81. Sankova, B., Machalek, J. & Sedmera, D. Effects of mechanical loading on early conduction system differentiation in the chick. *Am. J. Physiol. Heart Circ. Physiol.* **298,** H1571–H1576 (2010).

82. Nanka, O. *et al.* Abnormal myocardial and coronary vasculature development in experimental hypoxia. *Anat. Rec.* **291,** 1187–99 (2008).

83. Kienast, R., Stöger, M., Handler, M., Hanser, F. & Baumgartner, C. Alterations of field potentials in isotropic cardiomyocyte cell layers induced by multiple endogenous pacemakers under normal and hypothermal conditions. *Am. J. Physiol. Heart Circ. Physiol.* **307,** H1013-23 (2014).

84. Daus, A. W., Goldhammer, M., Layer, P. G. & Thielemann, C. Electromagnetic exposure of scaffold-free three-dimensional cell culture systems. *Bioelectromagnetics.* **32,** 351–9 (2011).

85. Natarajan, A., Molnar, P., Sieverdes, K., Jamshidi, A. & Hickman, J. J. Microelectrode array recordings of cardiac action potentials as a high throughput method to evaluate pesticide toxicity. *Toxicol. In Vitro.* **20,** 375–81 (2006).

86. Braam, S. R. *et al.* Prediction of drug-induced cardiotoxicity using human embryonic stem cell-derived cardiomyocytes. *Stem Cell Res.* **4,** 107–16 (2010).

87. Liem, L. K., Simard, J. M., Song, Y. & Tewari, K. The patch clamp technique. *Neurosurgery.* **36,** 382–92 (1995).

88. Clapham, D. E. & Logothetis, D. E. Delayed rectifier K+ current in embryonic chick heart ventricle. *Am. J. Physiol.* **254,** H192-7 (1988).

89. Veenstra, R. D. & DeHaan, R. L. Cardiac gap junction channel activity in embryonic chick ventricle cells. *Am. J. Physiol.* **254,** H170-80 (1988).

90. Clay, J. R., Hill, C. E., Roitman, D. & Shrier, A. Repolarization current in embryonic chick atrial heart cells. *J. Physiol.* **403,** 525–37 (1988).

91. Josephson, I. R. & Sperelakis, N. Two types of outward K+ channel currents in early embryonic chick ventricular myocytes. *J. Dev. Physiol.* **12,** 201–7 (1989).

92. Mazzanti, M. & DeFelice, L. J. Ca channel gating during cardiac action potentials. *Biophys. J.* **58,** 1059–65 (1990).

93. Veenstra, R. D. Developmental changes in regulation of embryonic chick heart gap junctions. *J. Membr. Biol.* **119,** 253–65 (1991).

94. Kawano, S. & DeHaan, R. L. Developmental changes in the calcium currents in embryonic chick ventricular myocytes. *J. Membr. Biol.* **120,** 17–28 (1991).

95. Gold, M. R. & Strichartz, G. R. Acute effects of repetitive depolarization on sodium current in chick myocytes. *Am. J. Physiol.* **260,** H1810-8 (1991).

96. Brochu, R. M., Clay, J. R. & Shrier, A. Pacemaker current in single cells and in aggregates of cells dissociated from the embryonic chick heart. *J. Physiol.* **454,** 503–15 (1992).

97. Aiba, S. & Creazzo, T. L. Comparison of the number of dihydropyridine receptors with the number of functional L-type calcium channels in embryonic heart. *Circ. Res.* **72,** 396–402 (1993).

98. Ruknudin, A., Sachs, F. & Bustamante, J. O. Stretch-activated ion channels in tissue-cultured chick heart. *Am. J. Physiol.* **264,** H960-72 (1993).

99. Chen, Y. H. & DeHaan, R. L. Temperature dependence of embryonic cardiac gap junction conductance and channel kinetics. *J. Membr. Biol.* **136,** 125–34 (1993).

100. Liu, S., Stimers, J. R. & Lieberman, M. A novel Cl-conductance in cultured chick cardiac myocytes: role of intracellular Ca2+ and cAMP. *J. Membr. Biol.* **141,** 59–68 (1994).

101. Sui, J. L., Chan, K. W. & Logothetis, D. E. Na+ activation of the muscarinic K+ channel by a G-protein-independent mechanism. *J. Gen. Physiol.* **108,** 381–91 (1996).

102. Hu, H. & Sachs, F. Mechanically activated currents in chick heart cells. *J. Membr. Biol.* **154,** 205–16 (1996).

103. Hall, S. K., Zhang, J. & Lieberman, M. An early transient current is associated with hyposmotic swelling and volume regulation in embryonic chick cardiac myocytes. *Exp. Physiol.* **82,** 43–54 (1997).

104. Liu, S. J. & Stimers, J. R. Calcium-inhibitable current in cultured embryonic chick cardiac myocytes: possibly via a novel chloride channel. *Exp. Physiol.* **83,** 323–36 (1998).

105. Satoh, H. Possible involvement of [Ca2+]i level in the modulation of the current-voltage relationship for the fast Na+ current in late embryonic chick cardiomyocytes. *Gen. Pharmacol.* **32,** 335–9 (1999).

106. Kawakubo, T., Naruse, K., Matsubara, T., Hotta, N. & Sokabe, M. Characterization of a newly found stretch-activated KCa,ATP channel in cultured chick ventricular myocytes. *Am. J. Physiol.* **276,** H1827-38 (1999).

107. Petit-Jacques, J., Sui, J. L. & Logothetis, D. E. Synergistic activation of G protein-gated inwardly rectifying potassium channels by the betagamma subunits of G proteins and Na(+) and Mg(2+) ions. *J. Gen. Physiol.* **114,** 673–84 (1999).

108. Bett, G. C. & Sachs, F. Activation and inactivation of mechanosensitive currents in the chick heart. *J. Membr. Biol.* **173,** 237–54 (2000).

109. Tsuji, Y., Inoue, D. & Pappano, A. J. beta-adrenoceptor agonist accelerates recovery from inactivation of calcium-dependent action potentials. *J. Mol. Cell. Cardiol.* **17,** 517–21 (1985).

110. Renaud, J. F., Bkaily, G., Benabderrazik, M., Jacques, D. & Sperelakis, N. Bay K 8644 induce enhancement of K+ current in both single heart cell and smooth muscle cell. *Mol. Cell. Biochem.* **80,** 73–8

111. Josephson, I. R. & Sperelakis, N. Fast activation of cardiac Ca++ channel gating charge by the dihydropyridine agonist, BAY K 8644. *Biophys. J.* **58,** 1307–11 (1990).

112. Gold, M. R. & Strichartz, G. R. Use-dependent block of atrial sodium current by ethylisopropylamiloride. *J. Cardiovasc. Pharmacol.* **17,** 792–9 (1991).

113. Bkaily, G. *et al.* Blockade of insulin sensitive steady-state R-type Ca2+ channel by PN 200-110 in heart and vascular smooth muscle. *Mol. Cell. Biochem.* **117,** 93–106 (1992).

114. Clay, J. R., Kristof, A. S., Shenasa, J., Brochu, R. M. & Shrier, A. A review of the effects of three cardioactive agents on the electrical activity from embryonic chick heart cell aggregates: TTX, ACh, and E-4031. *Prog. Biophys. Mol. Biol.* **62,** 185–202 (1994).

115. Conforti, L., Sumii, K. & Sperelakis, N. Dioctanoylglycerol inhibits L-type calcium current in embryonic chick cardiomyocytes independent of protein kinase C activation. *J. Mol. Cell. Cardiol.* **27,** 1219–24 (1995).

116. Mei, Y. A., Lee, P. P., Wei, H., Zhang, Z. H. & Pang, S. F. Melatonin and its analogs potentiate the nifedipine-sensitive high-voltage-activated calcium current in the chick embryonic heart cells. *J. Pineal Res.* **30,** 13–21 (2001).

117. Shimizu, T. *et al.* Platelet-derived growth factor induces cellular growth in cultured chick ventricular myocytes. *Cardiovasc. Res.* **41,** 641–53 (1999).

118. Wahler, G. M. & Sperelakis, N. Use of the cell-attached patch clamp technique to examine regulation of single cardiac K channels by cyclic GMP. *Mol. Cell. Biochem.* **80,** 27–35

119. McDonagh, J. C. & Nathan, R. D. Sialic acid and the surface charge of delayed rectifier potassium channels. *J. Mol. Cell. Cardiol.* **22,** 1305–16 (1990).

120. Haddad, G. E., Sperelakis, N. & Bkaily, G. Regulation of the calcium slow channel by cyclic GMP dependent protein kinase in chick heart cells. *Mol. Cell. Biochem.* **148,** 89–94 (1995).

121. Hall, S. K., Zhang, J. & Lieberman, M. Cyclic AMP prevents activation of a swelling-induced chloride-sensitive conductance in chick heart cells. *J. Physiol.* **488,** 359–69 (1995).

122. Bkaily, G. *et al.* Modulation of Ca2+ and Na+ transport by taurine in heart and vascular smooth muscle. *Adv. Exp. Med. Biol.* **403,** 263–73 (1996).

123. Satoh, H. & Sperelakis, N. Taurine inhibition of fast Na+ current in embryonic chick ventricular myocytes. *Eur. J. Pharmacol.* **218,** 83–9 (1992).

124. Satoh, H. Regulation by taurine of the spontaneous activity in young embryonic chick cardiomyocytes. *J. Cardiovasc. Pharmacol.* **25,** 3–8 (1995).

125. Satoh, H. Taurine-induced hyperpolarizing shift of the reversal potential of the fast Na+ current in embryonic chick cardiomyocytes. *Gen. Pharmacol.* **26,** 517–21 (1995).

126. Ujhelyi, M. R. & Creazzo, T. L. Action potentials that mimic fibrillation activate sodium current. *J. Mol. Cell. Cardiol.* **31,** 1673–84 (1999).

127. Nichols, C. A. & Creazzo, T. L. L-type Ca2+ channel function in the avian embryonic heart after cardiac neural crest ablation. *Am. J. Physiol. Heart Circ. Physiol.* **288,** H1173-8 (2005).

4

THE SINUS VENOSUS MYOCARDIUM CONTRIBUTES TO THE ATRIOVENTRICULAR CANAL: POTENTIAL ROLE DURING ATRIOVENTRICULAR NODE DEVELOPMENT?

Tim P. Kelder, Rebecca Vicente-Steijn, Tom J. Harryvan, Georgios Kosmidis, Adriana C. Gittenberger-de Groot, Rob E. Poelmann, Martin J. Schalij, Marco C. DeRuiter, Monique R.M. Jongbloed.
Modified after Journal of Cellular and Molecular Medicine, 19: 1375-89 (2015)

ABSTRACT

BACKGROUND:

The presence of distinct electrophysiological pathways within the atrioventricular node is a prerequisite for atrioventricular nodal reentrant tachycardia to occur. In this study, the different cell contributions that may account for the anatomical and functional heterogeneity of the atrioventricular node were investigated.

RESULTS:

To study the temporal development of the atrioventricular node, the expression pattern of ISL1, expressed in cardiac progenitor cells, was studied in sequential stages performing co-staining with myocardial markers (TNNI2 and NKX2-5) and HCN4 (cardiac conduction system marker). An ISL1+/TNNI2+/HCN4+ continuity between the myocardium of the sinus venosus and atrioventricular canal was identified in the region of the putative atrioventricular node, which showed a pacemaker-like phenotype based on single-cell patch clamp experiments. Furthermore, qPCR analysis showed that even during early development, different cell populations can be identified in the region of the putative atrioventricular node. Fate mapping was performed by *in ovo* vital dye microinjection. Embryos were harvested and analyzed 24 and 48 hours post-injection. These experiments showed incorporation of sinus venosus myocardium in the posterior region of the atrioventricular canal.

CONCLUSION:

The myocardium of the sinus venosus contributes to the atrioventricular canal. It is postulated that the myocardium of the sinus venosus contributes to nodal extensions or transitional cells of the atrioventricular node, since these cells are located in the posterior region of the atrioventricular node. This finding may help to understand the origin of atrioventricular nodal reentrant tachycardia.

1. INTRODUCTION

The cardiac conduction system (CCS) initiates electrical activation of the heart and ensures proper electrical propagation resulting in coordinated mechanical activation of the myocardium. Disturbances in the normal electrical activation pattern of the heart resulting in cardiac arrhythmias are an important cause of mortality and morbidity in the general population.[1]

During early cardiac development fusion of the bilateral cardiogenic plates establishes the primary heart tube (PHT). During further development a subpopulation of cells from the splanchnic mesoderm continues to differentiate towards a cardiac fate and is recruited to the PHT at the venous and arterial poles. The splanchnic mesoderm at the venous pole gives rise to the myocardium of the sinus venosus. This myocardium surrounds the cardinal and pulmonary veins and shows distinct expression patterns as compared with the atrial working myocardium.[2] In contrast to the atrial myocardium, the sinus venosus myocardium expresses *Tbx18*[3], ISL1[2,4], *Shox2*[5], *Pdgf-receptor alpha*[6], *Tbx3*[7,8] and RHOA[2], while it is negative for NKX2-5 during early stages of development.[3,9] The sinus venosus myocardium includes the definitive right-sided sinoatrial node (SAN) as well as a transient left-sided SAN, and will differentiate into a working myocardial phenotype during further development, with exception of the future right-sided SAN. The SAN will retain a primitive phenotype as characterized by relatively high automaticity, slow conduction and poor coupling of cells and becomes the dominant pacemaker of the heart.[10] The right and left venous valves are also components of the sinus venosus myocardium and are known substrates for atrial fibrillation and tachycardia in the fully developed heart.[1] They extend along the posterior wall of the right atrium towards another important structure of the CCS, the atrioventricular node (AVN).

The AVN delays conduction of the electrical impulse generated by the SAN, thereby ensuring adequate filling of the ventricles. The AVN is part of the myocardium of the atrioventricular (AV) canal and consists of a compact node, situated in the posterior part of the AV canal, covered by transitional cells as well as nodal extensions running towards the vestibules of the mitral and tricuspid valves.[11] The exact origin of the individual components of the AVN is still unclear. Studies indicate that at least the compact node derives from the myocardium of the AV canal[12,13], suggesting that the majority of cells of the AVN is formed from one source of cells. However, the presence of electrophysiologically and morphologically distinct cells (i.e. compact nodal cells, transitional cells and nodal extensions) in the region of the AVN indicates contributions from different sources, and/or with different transcriptional programs. A dual contribution would be a possible explanation for the occurrence of these different cell types and may help to understand the occurrence of atrioventricular nodal reentrant

tachycardia (AVNRT). A prerequisite for AVNRT to occur is the presence of electrophysiologically distinct pathways within the AVN[14], resulting in slow conduction in the so-called slow pathway, unidirectional conduction in the fast pathway and a central area of block. The slow pathway is a common target for catheter ablation of AVNRT, and has been described anatomically as the inferior nodal extension.[15] It has been postulated that the transitional cells and nodal extensions are an atrial contribution to the AVN[16] or are derived from the myocardium of the sinus venosus.[2] Interestingly, the inferior nodal extension has a similar gene expression profile as the SAN[17], and pacemaker activity from the AV junction has been attributed to the inferior nodal extension[18], thereby suggesting a developmental relation between the AVN and the sinus venosus myocardium.

Islet1 (Isl1), a LIM homeodomain transcription factor that plays an important role during cell proliferation, differentiation and survival[19], is expressed in the sinus venosus myocardium during early stages of development. Genetic lineage tracing with an inducible *Isl1-Cre* revealed important differences in timing of addition of cells to the developing heart and AVN. When *Cre*-recombinase was induced with tamoxifen at embryonic day (E)7, a large number of *Isl1*-positive cells was found in the heart at E9. Induction of *Cre* at E9 and analysis at E11 revealed far less *Isl1*-positive cells, with a cluster of cells in the region of the developing AVN.[20] This could indicate that the AVN develops from multiple sources, with contributions at different time points during development. Immunohistochemical analysis of ISL1 expression in chick embryos revealed a region of ISL1-positive cells in the dorsal atrial wall, just cranial to the AV junction, which is known to be the location of the future AVN, leading to the hypothesis of a contribution of the sinus venosus myocardium to the AVN.[2] However, no cell lineage tracing studies independent of gene expression to prove a contribution from the sinus venosus myocardium have been performed.

In the current study, vital dye labeling experiments aimed at studying different contributions to the developing AVN were performed, to determine the origin of cells contributing to the AVN. First, expression patterns marked by double or triple staining with ISL1 (expressed in cardiac progenitor cells), the myocardial markers TNNI2 and NKX2-5 and the CCS marker HCN4 were studied in sequential stages of chick and mouse development. These results were used as a roadmap for targeted vital dye labeling experiments.

2. MATERIALS AND METHODS

2.1. IMMUNOHISTOCHEMISTRY

To obtain a developmental series of chicken heart development, fertilized eggs of the White Leghorn chicken were incubated at 37°C and 80% humidity. Embryos (HH7-31) were excised, staged according to Hamburger and Hamilton criteria[21], and fixed in 4% paraformaldehyde for 24 hours. Subsequently, they were embedded in paraffin and sectioned serially (5µm) for immunohistochemical analysis.

To confirm the results obtained in chick embryos, immunohistochemical analysis was extended to wildtype mouse embryos with a mixed genetic background of E10.5, E11.5 and E12.5 (mouse line has been described previously[22]). The morning of the vaginal plug was considered E0.5. Pregnant dams were euthanized with CO_2 exposure followed by cervical dislocation. Processing of embryos after excision was similar to the chicken embryos. Animal care was in accordance with national and institutional guidelines and approved by the animal experiments committee of the Leiden University Medical Center (Permit Number 13067).

Serial sections were rehydrated and subjected to microwave antigen retrieval in citric acid buffer (pH = 6,0) before staining with the primary antibodies. Sections were incubated with primary antibodies against ISL1 (Clone 40.2d6, 1/100, Developmental Studies Hybridoma Bank, Iowa City, Iowa, USA), Troponin I, isoform 2 (TNNI2) (SC-15368, 1/200, Santa Cruz Biotechnology Inc., Dallas, Texas, USA), NKX2-5 (SC-8697, 1/500, Santa Cruz Biotechnology Inc., Dallas, Texas, USA) and HCN4 (APC-052, 1/2000, Alomone Labs, Jerusalem, Israel) overnight. Primary antibodies were diluted in phosphate buffered saline (PBS)-Tween-20 with 1% Bovine Serum Albumin (A8022, Sigma-Aldrich, St. Louis, Missouri, USA) to prevent non-specific binding. Between subsequent incubation steps all slides were rinsed in PBS (2x) and PBS-Tween-20 (1x). To enhance the signal of ISL1, Horse-Anti-Mouse (HAM)-Biotin (BA-2000, 1/200, Vector laboratories Inc., Burlingame, California, USA) in PBS-Tween-20 was added together with normal horse serum (6-S-2000, 1/66, Brunschwig Chemie, Switzerland) for 60 min. Visualization of the primary antibodies was achieved by incubation with fluorescently labeled secondary antibodies, diluted in PBS-Tween-20 (60 min). The following antibodies were used: Alexa Fluor® 488 Streptavidin Conjugate (S-11223, 1/200), Alexa Fluor® 555 Donkey Anti-Rabbit IgG (A-31572, 1/200) and Alexa Fluor® 647 Donkey Anti-Goat IgG (A-21447, 1/200). All secondary antibodies were purchased from Life technologies (Carlsbad, California, USA). DAPI (D3571, 1/1000, Life technologies, Carlsbad, California, USA) was used as a nuclear stain and the slides were mounted with Prolong gold (Life technologies, Carlsbad, California, USA). To reduce interfering autofluorescence (HH7-11),

small adjustments were made to the above described protocol. Sections were blocked (30 min) with a commercially available blocking reagent (Cat. No. 11 096 176 001, Roche, Mannheim, Germany), which was also used to dilute the primary and secondary antibodies. The sections were incubated with the primary antibody for 2 hrs. Sections were visualized using a Leica DM 5500 fluorescence microscope (Leica microsystems, Illinois, USA). ImageJ was used to process the pictures.

2.2. IN SITU HYBRIDIZATIONS

For detection of *HCN4* mRNA expression in the developing CCS, *in situ* hybridizations in chick embryos were performed (HH15-23) and analyzed as described previously.[23]

2.3. LASER CAPTURE MICRODISSECTION PROCEDURE

Laser capture microdissection (LCM) was performed in order to specifically isolate tissue of three distinct structures: 1. Myocardial continuity sinus venosus and AV canal (SV-AVC); 2. More caudal region of posterior AV canal (AVC); 3. Lateral wall right ventricle (RV). Embryos of HH21 were extracted and fixated for 24 hrs in 4% paraformaldehyde, embedded in paraffin and serially sectioned at 5µm. Sections were mounted on membrane-covered slides (MembraneSlide 1.0 PEN, Carl Zeiss Microscopy, Thornwood, NY, USA). Tissue from the different structures of interest was dissected using the PALM microbeam (Carl Zeiss Microscopy, NY, USA) and RoboSoftware package and subsequently transferred to AdhesiveCaps (Carl Zeiss Microscopy, Thornwood, NY, USA). After microdissection, the tissue was stored at -80°C. The outline of the dissected tissue was photographed in all embryos and examples of the different regions before and after dissection are shown in **Supplemental Fig. S1**.

2.4. RNA ISOLATION, CDNA SYNTHESIS AND QPCR OF LASER MICRODISSECTION TISSUE

After microdissection, RNA was isolated using the RecoverAll™ Total Nucleic Acid Isolation Kit for FFPE (Ambion, Life technologies, CA, USA). cDNA synthesis was performed with the iScript™ cDNA synthesis kit (Bio-rad, Hercules, CA, USA). After cDNA synthesis, qPCR was performed for *TNNT2*, *NKX2-5*, *HCN4* and *ISL1*. For *ISL1*, a nested approach was necessary in order to detect mRNA expression. After cDNA synthesis for *ISL1*, 15 cycles of pre-amplification were performed with 10µl SybrGreen Mastermix (Bio-Rad, Hercules, CA, USA), 8,5µl nuclease free water, 0,25µl forward and 0,25µl reverse primer and 1µl of cDNA (final volume of 20µl). For the other three genes, no pre-amplification was needed. The qPCR was performed with 10µl of SybrGreen Mastermix (Bio-Rad, Hercules, CA,

USA), 1µl of forward primer, 1µl of reverse primer, 1µl of cDNA (or 1µl nuclease free water as negative control) and 7µl nuclease free water per reaction (final volume 20µl). Reactions were carried out in triplicate for each sample. qPCR was performed on a Bio-Rad CFX96 real-time system. Melting curve analysis was performed to verify single PCR product amplification. Chicken GAPDH was used as the reference standard for normalization, and relative differences in mRNA expression were determined. The primers used are described in **Supplemental table 1**.

2.5. WHOLE MOUNT ISL1 STAINING

HH21 embryos were extracted and the heart was carefully removed from the thorax under the preparation microscope. The heart was fixated in DMSO:100% Methanol (ratio 4:1) for 2 hours at 4°C, after which the tissue was rehydrated in 75%, 50% and 25% methanol in PBS. After rinsing thoroughly with PBS for 30 minutes at room temperature, the tissue was permeabilized with PBS-Tween for 1 hour. Blocking was performed with PBS-Tween-20 with 1% BSA for 1 hour at room temperature. The ISL1 primary antibody (Clone 40.2d6, 1/100, Developmental Studies Hybridoma Bank, Iowa City, Iowa, USA) was dissolved in PBS-Tween-20 with 1% BSA and the tissue was incubated with the antibody overnight at 4°C in a shaking plate. The next morning, the tissue was rinsed with PBS and incubation with Vectastain ABC staining kit (PK- 6100, Vector Labs) was performed for 90 minutes at room temperature. After rinsing with PBS, the tissue was incubated for 30 minutes in 3-3'diaminobenzidine-tetrahydrochloride-dihydrate (DAB) (D5637, Sigma-Aldrich, St. Louis, MO) dissolved in Tris/Maleate (pH 7.6). Finally, a fresh solution of DAB with 5µl of H_2O_2 was added for a brief moment (+/- 5 seconds) to the tissue, after which the tissue was thoroughly rinsed in PBS to stop the visualization reaction.

2.6. SINGLE-CELL PATCH CLAMP RECORDINGS

Electrophysiological data was obtained by single-cell patch clamp of HH21-22 chick embryonic cardiomyocytes derived from the continuity between the sinus venosus and AV canal and compared to cardiomyocytes from the right ventricle. Whole mount ISL1 stained embryos were used to identify the ISL1+ continuity between the sinus venosus and AV canal, which aided in specifically dissecting this tissue under the preparation microscope (**Fig. 6a**). As control tissue, a piece of right ventricle was collected (**Fig. 6a**)**.** The dissected tissue was collected in 1,5ml tubes and 800µl of 0,05% Trypsin (Life technologies, Carlsbad, California, USA) was added. The tube was placed in a heated (37°C), shaking (850 rpm) plate for 10 minutes. After this, the tubes were vortexed until all tissue was dissociated and centrifuged at 1100 rpm for 5 minutes. The supernatant was removed and

the cells were resuspended in medium containing DMEM high glucose (Life technologies, Carlsbad, California, USA), 10% fetal calf serum (Sigma-Aldrich, St. Louis, Missouri, USA), 1% penicillin-streptomycin (Life technologies, Carlsbad, California, USA), 1% non-essential amino acids (Life technologies, Carlsbad, California, USA) and 1% L-Glutamine (Life technologies, Carlsbad, California, USA). Cells were plated on glass coverslips and used for single-cell patch clamp recording.

Recordings were performed on single cardiomyocytes, 1-2 days after cell dissociation. Action potential measurements of spontaneously contracting cells were recorded. Action potentials were recorded with the perforated patch clamp technique using an Axopatch 200B amplifier (Molecular Devices) and were filtered (5 kHz) and digitized (40 kHz). Data were acquired with pClamp10.1 (Axon Instruments) and analysis was performed with custom-made software. Potentials were corrected for the estimated change in liquid junction potential.
Action potentials were recorded at 37°C in Tyrode's solution. The pipette solution contained (mM): K-gluconate 125, KCl 20, NaCl 5, amphotericin-B 0.22, HEPES 10; pH 7.2 (KOH). The maximal diastolic potential (MDP), maximal upstroke velocity (V_{max}), action potential amplitude (APA), and action potential duration (APD) at 50% and 90% repolarization (APD_{50} and APD_{90}, respectively) were analyzed. Data from 8-9 consecutive action potentials were averaged.

2.7. MICROINJECTION PROCEDURE

A small window was created in the shell to gain access to the embryo (HH15-17). A 1:1 solution of two fluorescent dyes (DiI and 5-TAMRA) was used to label and follow cells during development. 2.5mg DiI (D-282, Life technologies, Carlsbad, California, USA) was dissolved in 50µl DMSO, which in turn was diluted in 950µl ethanol (100%). 2.5 mg 5-TAMRA (C-2211, Life technologies, Carlsbad, California, USA) was dissolved in 1000µl DMSO. The combined solution was loaded into a pulled glass needle and injected in different regions, using a programmable microinjector (IM-300 Narishige, Japan) and micromanipulator.

Medial labeling was performed by opening the coelomic cavity with subsequent injection in the ISL1+/TNNI2+ sinus venosus myocardium (**Fig. 1a-e**). To calculate the volume of labeling, all microscopic sections that contained DiI/5-TAMRA were photographed and ImageJ was used to calculate the volume of labeling. The total volume of labeling and the volume of labeling in the ISL1-/TNNI2+ atrial myocardium directly bordering the ISL1+/TNNI2+ sinus venosus myocardium were calculated for the 14 embryos that were analyzed in the medial group 1-2 hours after labeling.

Lateral, right-sided labeling of the mesenchyme and vessel wall of the right cardinal vein (RCV) was performed just caudal to the entrance of the RCV in the

sinus venosus (**Figure 1f-h**). Injection in this region was performed through the developing lateral body wall leaving the coelomic cavity intact. This injection site was chosen to assure lateral labeling of mesenchymal structures and to minimize leakage to other cardiac components. Embryos were collected at selected time points (HH15-25) to assess the location of labeling.

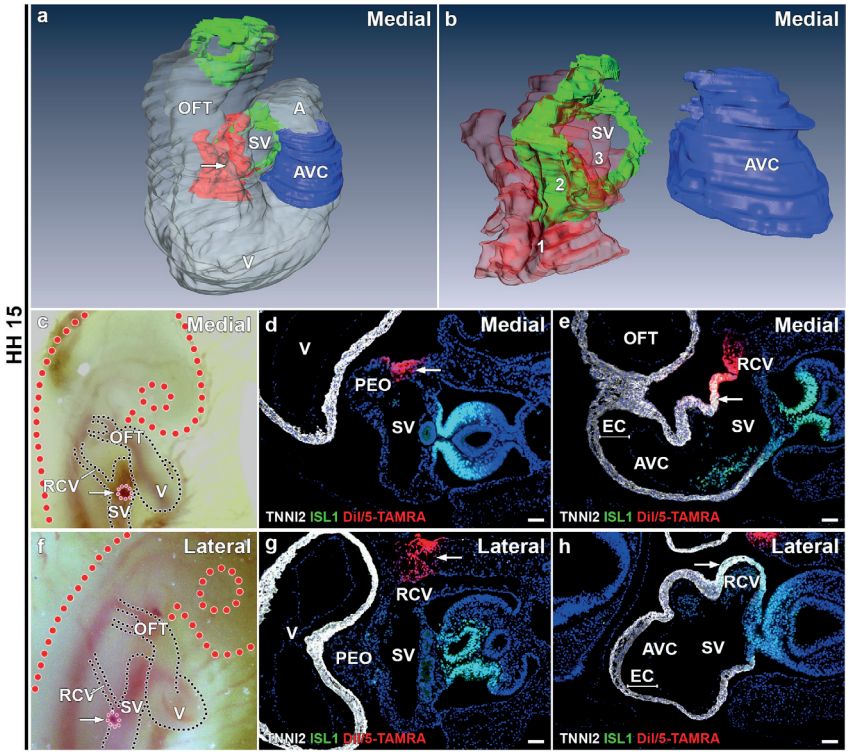

Figure 1. Medial and lateral labeling at HH15

a-b. 3D reconstructions of medial labeling, white: myocardium, blue: AV canal myocardium, green: ISL1+/TNNI2+ sinus venosus myocardium, red: DiI/5-TAMRA labeling **a.** Overview of PHT, arrow indicates labeling. **b.** All 14 microinjections are superimposed to clarify extend of total labeling. For separate labels see interactive PDF (**online 3D PDF S1,** available online or at request to the authors). No labeling of AV canal myocardium is seen and distance between myocardium of sinus venosus and AV canal is present. Labeling is found in mesenchyme RCV (1 in **b,** 100% of embryos), ISL1+/TNNI2+ sinus venosus myocardium (2 in **b,** 100% of embryos) and a small region of ISL1-/TNNI2+ myocardium directly bordering the ISL1+/TNNI2+ sinus venosus (3 in **b,** 64% of embryos). **c,f.** Directly after labeling demonstrates *in ovo* medial (**c**) and lateral (**f**) location of DiI/5-TAMRA (pink, arrow). **d,g.** DiI/5-TAMRA in mesenchyme RCV present in medial (**d**) and lateral (**g**) labeling. **e,h.** DiI/5-TAMRA present in ISL1+/TNNI2+ sinus venosus myocardium in medial labeling (DiI/5-TAMRA: arrow in **e**), not in lateral labeling (corresponding DiI/5-TAMRA negative region: arrow in **h**). AVC: atrioventricular canal, EC: endocardial cushion, OFT: outflow tract, PEO: proepicardial organ, RCV: right cardinal vein, SV: sinus venosus, V: ventricle. **d-e, g-h:** white: TNNI2, green: ISL1, red: DiI/5-TAMRA, blue: DAPI. Scale bars: 50μm.

2.8. 3D RECONSTRUCTIONS

AMIRA (Template Graphics Software, Inc.) reconstructions aided in clarifying the three-dimensional relationship between different structures. Embryos were serially sectioned and immunofluorescently stained for both TNNI2 and ISL1. The slides were photographed and processed with Adobe Photoshop CS6. Finally, the slides were stacked and aligned and structures of interest were labeled with the AMIRA software. A subset of reconstructions was converted to 3D interactive PDFs, which are available online or at request to the authors. Different functions (e.g. buttons to show, hide or make different structures transparent) were included in the interactive PDFs, using Javascript. The scripts that were used were previously written and published[24] and slightly modified for the current PDFs.

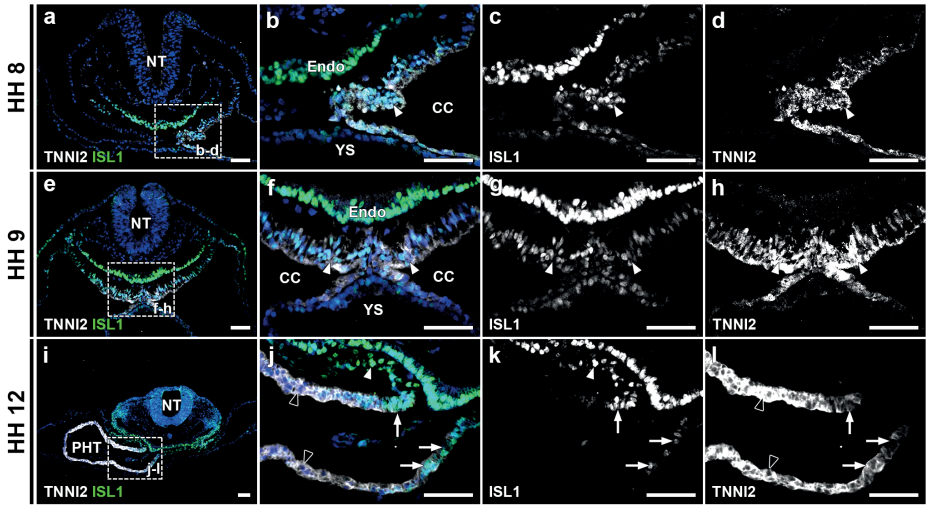

Figure 2. ISL1 and TNNI2 co-expression at HH stage 8-12

a. Overview of an HH8 embryo includes foregut and left-sided cardiogenic plate. The boxed region is enlarged in **b-d. b.** Co-expression of TNNI2 and ISL1 in cardiogenic plate (arrowheads in **b-d**). **c-d.** Separate channels in grey values. **e.** Overview of an HH9 embryo, with boxed region enlarged in **f-h**. Co-expression of ISL1 and TNNI2 in majority of cells in cardiogenic plate (arrowheads in **f-h**). **i.** Overview of an HH12 embryo. Boxed region is shown at higher magnification in **j-l**. **j.** ISL1+/TNNI2+ myocardium (arrows) is shown at arterial pole of PHT. white arrowheads show ISL1+/TNNI2- splanchnic mesoderm. Note lower expression of TNNI2 in ISL1+ cells. Black arrowheads show ISL1-/TNNI2+ myocardium PHT. **k**. ISL1 expression is shown. Arrowheads show ISL1+/TNNI2- splanchnic mesoderm and arrows show ISL1+/TNNI2+ myocardium of arterial pole. **l**. TNNI2 expression at arterial pole. Arrows show decreased TNNI2 expression in ISL1+ cells. Black arrowheads show ISL1-/TNNI2+ myocardium PHT. CC: coelomic cavity, Endo: endoderm, NT: neural tube, PHT: primary heart tube, YS: yolk sac. White: TNNI2, green: ISL1, blue: DAPI. Scale bars: 50μm.

2.9. STATISTICAL ANALYSIS

Results are expressed as mean ± SEM. Comparisons were made using unpaired Student's t-test (normal distribution) or Mann-Whitney U test when data were not normally distributed. $P<0.05$ was considered statistically significant.

3. RESULTS

3.1. IDENTIFICATION OF AN ISL1+/TNNI2+/HCN4+ MYOCARDIAL CONTINUITY BETWEEN SINUS VENOSUS AND POSTERIOR PORTION AV CANAL

This first phase of the study was aimed at analysis of expression patterns of ISL1, performing immunostaining at stages HH7-31. The first expression of TNNI2 was seen by HH8, within the medial borders of the bilateral cardiogenic plates, co-localizing with ISL1 (**Fig. 2a-d**). Strong expression of ISL1 was also found in the foregut endoderm (**Fig. 2a-c**). At HH9, the bilateral plates of mesoderm met in the midline, and started to fuse (**Fig. 2f**). TNNI2 expression increased and co-localization with ISL1 was still found in the majority of cells (**Fig. 2e-h**). By HH10, the bilateral plates had fused and formed a semitubular structure, with the ventral side formed by the TNNI2+ myocardium, and the dorsal side bordered by the ISL1+ foregut endoderm. By HH11-12, the heart was almost closed posteriorly, forming the primary heart tube. Most cardiomyocytes of the tube have lost ISL1 expression (**Fig. 2i-j**), except for populations of ISL1+/TNNI2+ cells at the arterial (**Fig. 2i-l**) and venous pole.

Analysis of ISL1 expression in subsequent developmental stages revealed ISL1/TNNI2 co-expression in the myocardium of the sinus venosus. At HH14-15, the myocardium connecting the atria to the AV canal is negative for ISL1 (**Fig. 3a-f**)**.** The AV canal was defined based on morphological criteria, i.e. the presence of thick endocardial cushions and less densely organized myocardium underlying the cushions (**Fig. 3e,i,k**). More caudally the sinus venosus myocardium is positive for ISL1 and TNNI2 (**Fig. 3g-h**). Thus, there is initially a region of ISL1-/TNNI2+ myocardium between the sinus venosus myocardium and the AV canal myocardium (**Fig. 3b-c**). To further clarify the relation between the different structures, an interactive PDF of the three-dimensional reconstruction shown in **Fig. 3** is available online (**online 3D PDF S1**, available online or at request to the authors). At this stage, the right and left venous valve are not evident, yet.

During further development, the right venous valve (RVV) becomes recognizable as a double myocardial leaflet, of which the inner leaflet (SV luminal side) shows co-expression of ISL1 and TNNI2. The outer leaflet is ISL1-/TNNI2+ (atrial luminal side) (**Fig. 3i-j**). An ISL1+/TNNI2+ continuity between the myocardium of the sinus venosus and the posterior part of the AV canal becomes apparent at HH16-17 (**Fig. 3k-l**).

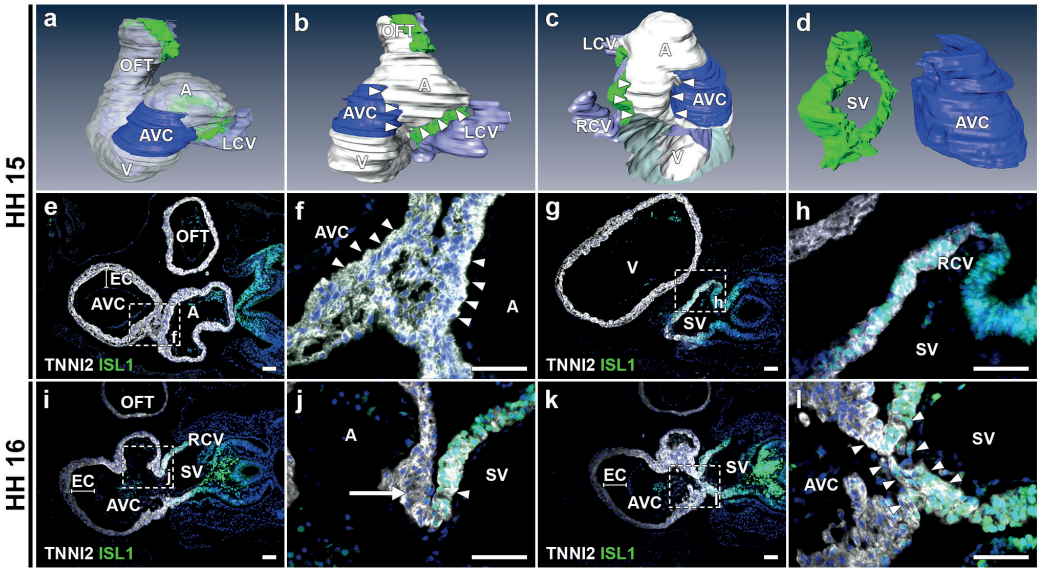

Figure 3. ISL1 and TNNI2 expression at the venous pole at HH15-16

a-d. 3D reconstructions, HH15 embryo. White: myocardium, blue: AV canal myocardium, green: ISL1+/TNNI2+ sinus venosus myocardium, purple: lumen **b.** Left lateral view showing ISL1-/TNNI2+ myocardium (between arrowheads) between myocardium of AV canal and sinus venosus. **c-d.** Right lateral view with (in **c,** part of ventricle and entire OFT are removed to expose right portion of inflow tract) and without (in **d**) myocardium reconstructed, demonstrating distance between sinus venosus and AV canal myocardium (between arrowheads). **e-f.** Transverse section at HH15 of ISL1-/TNNI2+ myocardial connection between AV canal (identified based on morphological criteria, i.e. presence of thick endocardial cushions and underlying spongious myocardium) and lower region of atrium (between arrowheads). **g-h.** ISL1+/TNNI2+ sinus venosus (including RCV myocardium) which is located caudally to connection between atrium and AV canal. **i-j.** At HH16, RVV is a double leaflet with ISL1+/TNNI2+ myocardium in inner leaflet (arrowhead) and ISL1-/TNNI2+ myocardium in outer leaflet (arrow). **k-l**. ISL1+/TNNI2+ continuity between the SV and AV canal (between arrowheads) is first seen at HH16. A: atrium, AVC: atrioventricular canal, EC: endocardial cushion, LCV: left cardinal vein, OFT: outflow tract, RA: right atrium, RCV: right cardinal vein, SV: sinus venosus. White: TNNI2, green: ISL1, red: NKX2-5, blue: DAPI. Scale bars: 50μm.

At HH21, this continuity still shows ISL1 and TNNI2 expression and is located between the posterior portion of the AV canal (region of the (putative) AVN) and the cranial portion of the sinus venosus at the level of the entrance of the cardinal veins in the sinus venosus (**Fig. 4c-e**). The AV canal is again characterized by the presence of thick endocardial cushions with spongious myocardium underlying the cushions (**Fig. 4g-j**). The ISL1+/TNNI2+ area includes the myocardium of the SAN, RCV, RVV and LCV, including the left SAN (**Fig. 4a-h**). The central part of the sinus venosus myocardium is connected to the myocardium of the posterior AV canal (**Fig. 4c,e,g**), where ISL1 expression is seen in the AV canal myocardium (**Fig. 4j-k**). An interactive PDF of the 3D reconstruction is available online or at request to the authors, which shows in further detail the continuity between the ISL1+/TNNI2+ sinus venosus myocardium and the posterior AV canal (**online 3D PDF S2**). An ISL1/NKX2-5/TNNI2 triple staining was performed and showed a gradient in ISL1 expression from the SV myocardium (strongest expression) towards the AV canal myocardium (decrease in expression) (**Fig. 4i-l**). NKX2-5 expression showed a similar but opposite gradient (**Fig. 4i-l**), suggesting differentiation of ISL1+/TNNI2+/NKX2-5- sinus venosus cardiomyocytes towards NKX2-5+/TNNI2+/ISL1- AV canal cardiomyocytes. During further development, ISL1 expression became confined to the myocardial sleeve of the RCV at the location of the future SAN (**Fig. 4m-p**), with no discernible expression of ISL1 in the continuity between the myocardium of the sinus venosus and AV canal any more.

To investigate whether the myocardial continuity between the sinus venosus and posterior AV canal indeed had a pacemaker-like phenotype, *in situ* hybridizations were performed in chick embryos for *HCN4*, which is used as a marker for the (developing) CCS.[23] The connection between the sinus venosus myocardium and the myocardium of the posterior portion of the AV canal (**Fig. 5a**) showed *HCN4* expression (**Fig. 5b**), shown at HH19. To verify the co-localization of ISL1, TNNI2 and HCN4 in this region in mammals, a triple staining for ISL1, TNNI2 and HCN4 was performed in wildtype mouse embryos. ISL1+/TNNI2+/HCN4+ cells were found in the region of the myocardial continuity between the sinus venosus and AV canal (shown at E11.5 in **Fig. 5c-f**). These results indicate that the cells of the myocardial continuity between the sinus venosus and posterior AV canal have a pacemaker-like phenotype.

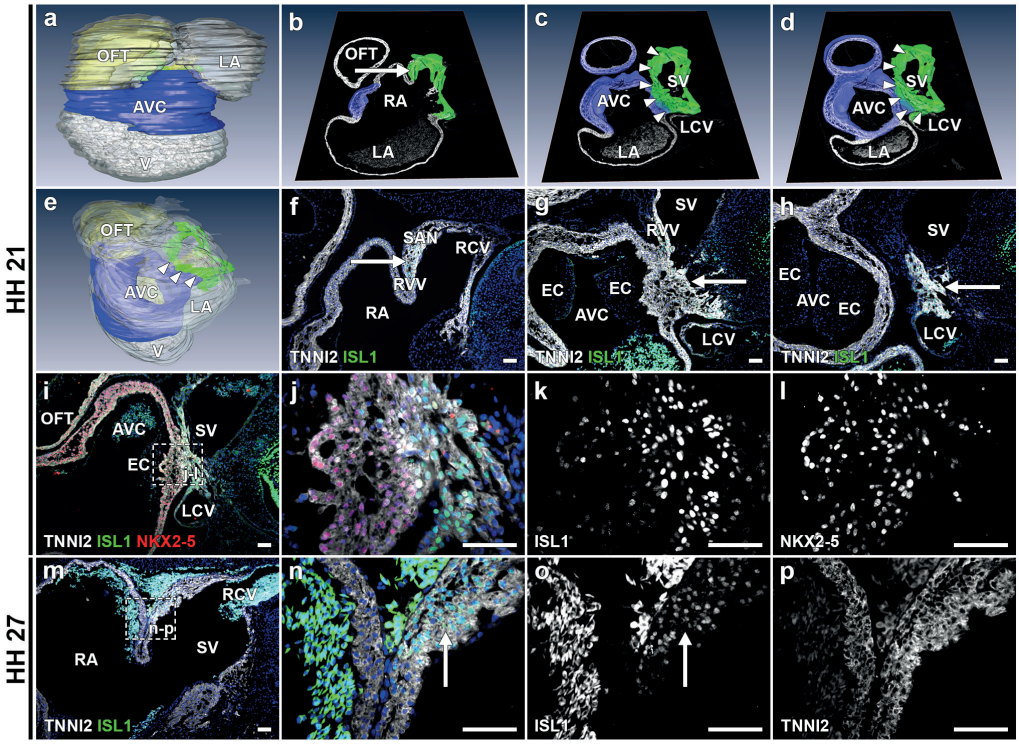

Figure 4. ISL1+/TNNI2+ continuity between myocardium of sinus venosus and AV canal

a-e. 3D reconstructions, HH21 embryo. white: myocardium, yellow: mesenchyme, blue: AV canal myocardium, green: ISL1+/TNNI2+ sinus venosus myocardium. **a.** Overview of heart. **e.** Arrowheads indicate continuity between sinus venosus and AV canal myocardium. **b-d.** 3D reconstructions of AV canal and sinus venosus myocardium with in white TNNI2 section from AMIRA. **b** to **d** is cranial to caudal. **f-h.** Corresponding TNNI2/ISL1 staining. **b.** Location of SAN and RVV (arrow). **f.** ISL1+/TNNI2+ connection between SAN and RVV (arrow). **c.** SAN and RVV are attached to myocardial continuity between sinus venosus and AV canal (arrowheads), arrow in **g**. AV canal identified by presence of endocardial cushions and spongious myocardium. **d.** Connection between LCV and ISL1+/TNNI2+ sinus venosus (arrowheads), arrow in **h**. **i-l.** ISL1/TNNI2/NKX2-5 staining of myocardial continuity between sinus venosus and AV canal. **k.** Decrease in ISL1 expression from sinus venosus towards AV canal. **l.** Opposite expression pattern for NKX2-5. **m-p.** ISL1 expression in SAN (arrows) at HH27. **o-p.** Grey values for ISL1 and TNNI2, showing ISL1+/TNNI2+ SAN. AVC: atrioventricular canal, EC: endocardial cushion, LA: left atrium, LCV: left cardinal vein, OFT: outflow tract, RA: right atrium, RCV: right cardinal vein, SV: sinus venosus. **f-p.** White: TNNI2, green: ISL1, red: NKX2-5, blue: DAPI. Scale bars: 50μm.

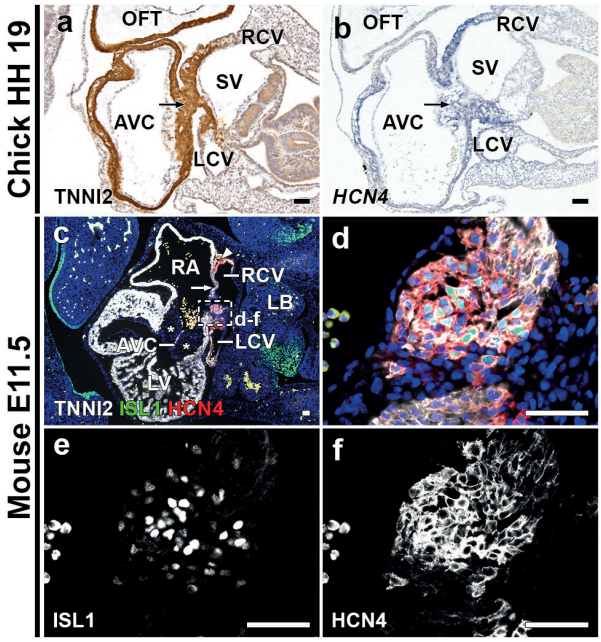

Figure 5. HCN4 expression in myocardial continuity sinus venosus and posterior AV canal
a. TNNI2 stain of HH19 chick embryo. Arrow indicates continuity between sinus venosus myocardium and posterior AV canal. **b.** *In situ* hybridization shows *HCN4* mRNA expression in continuity (arrow). **c.** Merge of ISL1, TNNI2, HCN4 and DAPI staining of E11.5 mouse embryo, showing the myocardial continuity between the sinus venosus and posterior AV canal. The ISL1+/HCN4+/TNNI2+ SAN (arrowhead) and RVV (arrow) are shown. Note the thick endocardial cushions (asterisks) in the AVC. **d-f.** Higher magnifications of boxed area in **c**. **d.** ISL1+/TNNI2+/HCN4+ cells are seen in the continuity between sinus venosus myocardium and posterior AV canal myocardium. **e-f.** grey values of ISL1 (**e**) and HCN4 (**f**). AVC: atrioventricular canal, LB: long bud, LCV: left cardinal vein, LV: left ventricle, OFT: outflow tract, RA: right atrium, RCV: right cardinal vein, SV: sinus venosus. **c-f.** White: TNNI2, green: ISL1, red: HCN4, blue: DAPI. Scale bars: 50μm.

3.2. CHARACTERIZATION MYOCARDIAL CONTINUITY CONFIRMS THE PACEMAKER-LIKE PHENOTYPE

Laser capture microdissection was performed in order to characterize the sinus venosus-AV canal continuity (SV-AVC in **Fig. 6**) and to quantify differences in expression levels of *TNNT2*, *NKX2-5*, *ISL1* and *HCN4* in this region. These results were compared to the more caudal tissue of the posterior AV canal and tissue from the lateral wall of the right ventricle to better identify the phenotype of the SV-AVC region.

Expression of *TNNT2* and *NKX2-5* was comparable between the different samples, confirming the myocardial identity of all tissue samples that were collected (**Fig. 6b-c**). Analysis of *HCN4* expression showed the highest relative

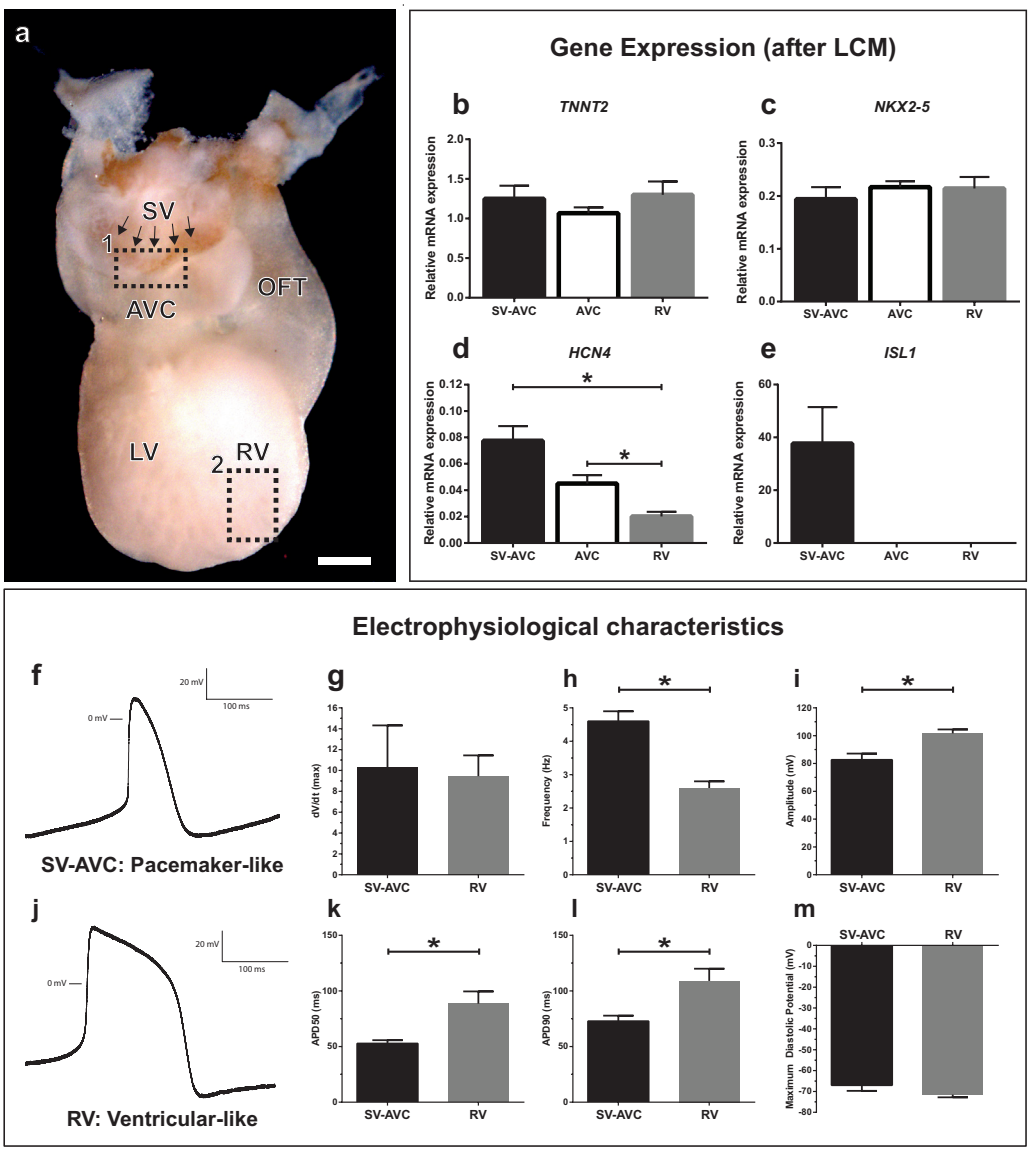

Figure 6. Characterization myocardial continuity between the sinus venosus and AV canal

a. Whole mount ISL1 staining, posterior view of the heart. Arrows indicate ISL1+ cells in continuity sinus venosus and AV canal. Rectangle 1 shows region from which SV-AVC continuity cells were collected for patch clamp. Rectangle 2 shows origin of right ventricular cells for patch clamp. **b-e.** mRNA expression after laser capture microscopy (LCM, see **Supplemental Fig. S1**) of *TNNT2, NKX2-5, HCN4* and *ISL1.* **f-m.** Results of single-cell patch clamp experiments. **f,j.** Representative tracing of SV-AVC continuity cells (**f,** pacemaker-like tracing) and RV cells (**j,** ventricular-like phenotype). **g-i, k-m.** graphs showing the difference in maximum upstroke velocity (**g**), frequency (**h**), amplitude (**i**), APD50 (**k**), APD90 (**l**) and maximum diastolic potential (**m**). * Indicates p<0,05. AVC: AV canal, LCM: laser capture microscopy, LV: left ventricle, OFT: outflow tract, RV: right ventricle, SV: sinus venosus, SV-AVC: myocardial continuity sinus venosus and AV canal. Scalebar: 250μm.

expression in the SV-AVC continuity, with a lower level of expression in the AV canal and right ventricle (**Fig. 6d**). The difference in expression levels between the myocardial continuity and the right ventricle was significant (p=0,008). There was a trend towards significance in the difference between the continuity and the AV canal samples (p=0,056). *ISL1* expression was only detectable in the samples taken from the SV-AVC continuity (**Fig. 6e**).

Single-cell patch clamp was performed to functionally characterize the cells of the myocardial continuity between the sinus venosus and AV canal. Whole mount ISL1 staining was performed to identify the region of the continuity between the sinus venosus myocardium and posterior portion of the AV canal (**Fig. 6a**). Cells from this region were compared to cells from the right ventricle (**Fig. 6a**). The action potential of cells from the SV-AVC continuity showed a pacemaker-like phenotype (**Fig. 6f**), while the action potential of cells from the right ventricle had a ventricular-like phenotype (**Fig. 6j**). The SV-AVC cells had a higher spontaneous beating frequency (**Fig. 6h**), a lower amplitude (**Fig. 6i**), a shorter APD50% (**Fig. 6k**) and APD90% (**Fig. 6l**), in line with what is expected from pacemaker-like cells. The results are summarized in **Table 1**.

Together these results confirm the pacemaker-like phenotype of the cells from the myocardial continuity between the sinus venosus and AV canal. Furthermore, results show that even during early development, it is possible to distinguish different cell populations within the region of the putative AVN.

Table 1. Electrophysiological characteristics.

Electrophysiological parameter	SV-AVC (n=8)	RV (n=6)	p-value
Vmax (V/s)	10.32±4	9.45±2	0,873
Frequency (Hz)	4.6±0.3	2.6±0.2	<0,001
APD50% (ms)	52.73±3	88.63±11	0,004
APD90% (ms)	72.79±5	109±11	0,007
Amplitude (mV)	82.66±4.5	101.67±2.8	0,006
MDP (mV)	-67±2.7	-71.5±1.3	0,209

APD: action potential duration, MDP: maximal diastolic potential, Vmax: maximal upstroke velocity, SV-AVC: cells from myocardial continuity sinus venosus and AV canal, RV: right ventricle.

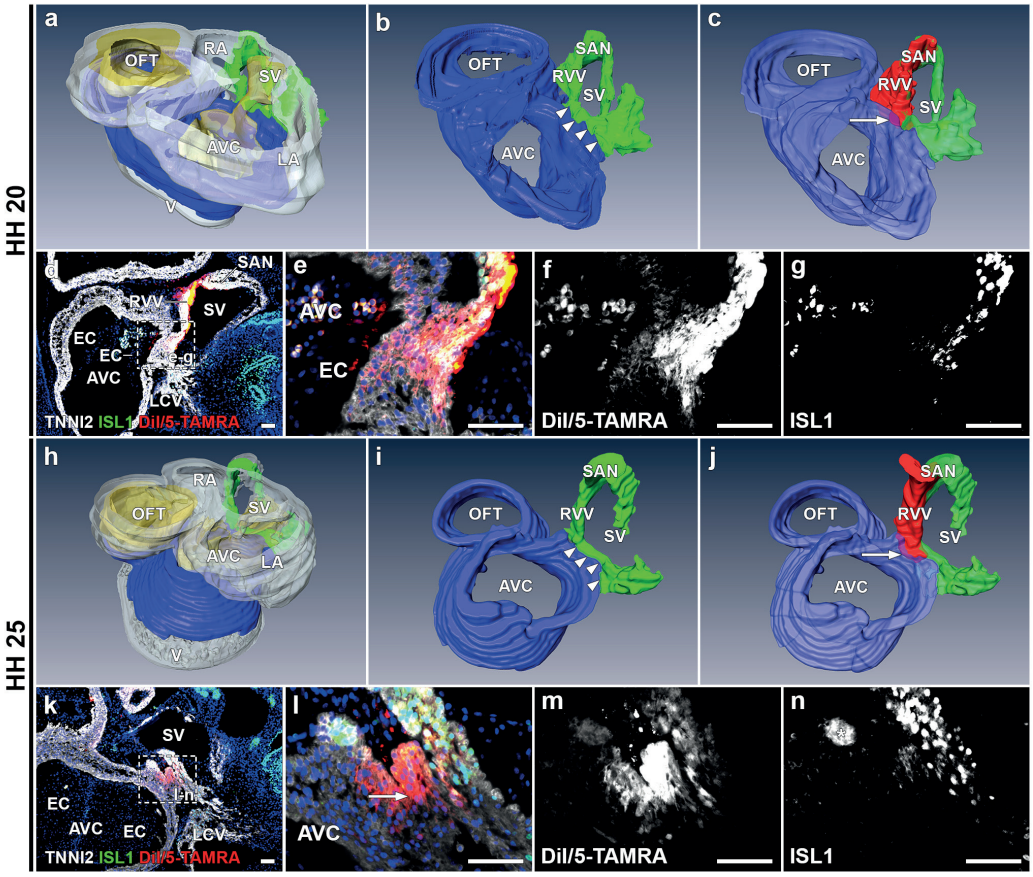

Figure 7. Tracing cells after medial labeling of ISL1+/TNNI2+ sinus venosus myocardium

a-c. 3D reconstruction, HH20 embryo. white: myocardium, yellow: mesenchyme, blue: AV canal myocardium, green: ISL1+/TNNI2+ sinus venosus myocardium, red: DiI/5-TAMRA **a.** Overview of HH20 heart. **b.** Detail of continuity (arrowheads) between AV canal and sinus venosus myocardium. **c.** DiI/5-TAMRA labels SAN, RVV and right side myocardial continuity sinus venosus and posterior region of the AV canal (arrow). **d.** Merge of DiI/5-TAMRA, ISL1, TNNI2 and DAPI. boxed area is shown at higher magnification in **e-g**. **e.** Labeling of continuity myocardium sinus venosus and AV canal **f-g**. Grey values of the fluorescent signal. **h.** Overview of HH25 heart. **i.** Myocardial continuity at HH25 (arrowheads). **j.** Labeling after 48 hrs is similar to 24 hrs and located in myocardial continuity sinus venosus and posterior part of the AV canal (arrow). **k.** Overview of labeling at HH25. Magnification in **l-n. l.** Shows DiI/5-TAMRA (arrow) in continuity between sinus venosus and AV canal myocardium. **m-n.** Grey values of fluorescent signal. **Asterisks** in **n**: background staining. AVC: atrioventricular canal, EC: endocardial cushion, LA: left atrium, LCV: left cardinal vein, OFT: outflow tract, RA: right atrium, RVV: right venous valve, SAN: sinoatrial node, SV: sinus venosus, V: ventricle. **d-g, k-n:** red: DiI/5-TAMRA, green: ISL1, white: TNNI2, blue: DAPI. Scale bars: 50µm.

3.3. LINEAGE TRACING SHOWS INCORPORATION OF SINUS VENOSUS MYOCARDIUM IN POSTERIOR REGION AV CANAL

The abovementioned results show the identification of an ISL1+/HCN4+/TNNI2+ myocardial continuity between the sinus venosus and posterior AV canal. At early developmental stages, ISL1-/TNNI2+ atrial myocardium is positioned between the ISL1+/TNNI2+ sinus venosus myocardium and the ISL1-/TNNI2+ AV canal myocardium. During further development, ISL1+/TNNI2+ myocardium is continuous with the ISL1-/TNNI2+ AV canal myocardium. To further study the possible contribution from the ISL1+/TNNI2+ sinus venosus myocardium to the posterior portion of the AV canal, lineage tracing experiments were performed. *In ovo* microinjection experiments were performed in chicken embryos with vital dyes (DiI-5-TAMRA) aimed at labeling the ISL1+/TNNI2+ sinus venosus myocardium at stages when this myocardium is not yet in contact with the AV canal (HH14-15). This myocardial labeling was termed medial labeling, since the labeling was applied more medial than the second group of labeling performed in the mesenchyme outside the sinus venosus myocardium (termed lateral labeling). First the results of the medial myocardial labeling will be discussed.

To confirm the location of the medial labeling, a group of embryos was harvested 1-2 hrs after microinjection (n=14). DiI/5-TAMRA was found in the myocardium of the sinus venosus and the myocardium surrounding the RCV, both positive for ISL1 and TNNI2 (**Fig. 1a-c,e**, 14/14 embryos, 100%; in **Fig. 1b** all 14 separate microinjections are superimposed to clarify the extent of the total labeling). Labeling was also present in the mesenchyme surrounding the RCV (**Fig. 1d,** 14/14 embryos, 100%). In 9/14 embryos (64%), a small area of labeling (on average 5,9% of total labeling) was also found in the ISL1-/TNNI2+ atrial myocardium directly bordering the ISL1+/TNNI2+ sinus venosus myocardium, but no leakage to the ISL1-/TNNI2+ connection between the inferior region of the atrium/sinus venosus and AV canal myocardium or the AV canal itself was seen. Limited leakage to other cardiac structures, such as the posterior OFT and ventricles was restricted to the upper layer of myocardial cells, while the labeling at the sinus venosus myocardium was applied to the full thickness of the myocardium. This first group of embryos therefore verified the correct location of injection. An interactive PDF of the three-dimensional reconstruction is available online, which shows the location of all separate initial microinjections (**online 3D PDF S1**, available online or at request to the authors).

Analysis of the embryos after 24 hrs of reincubation (n=10, HH19-22) revealed DiI/5-TAMRA in the sinus venosus myocardium (9/10 Embryos, 90%), putative SAN (10/10 embryos, 100%), RVV (10/10 embryos, 100%), right atrium (7/10 embryos, 70%) and the continuity between the sinus venosus myocardium and the posterior AV canal myocardium (8/10 embryos, 80%) (**Fig. 7a-g**). The labeled

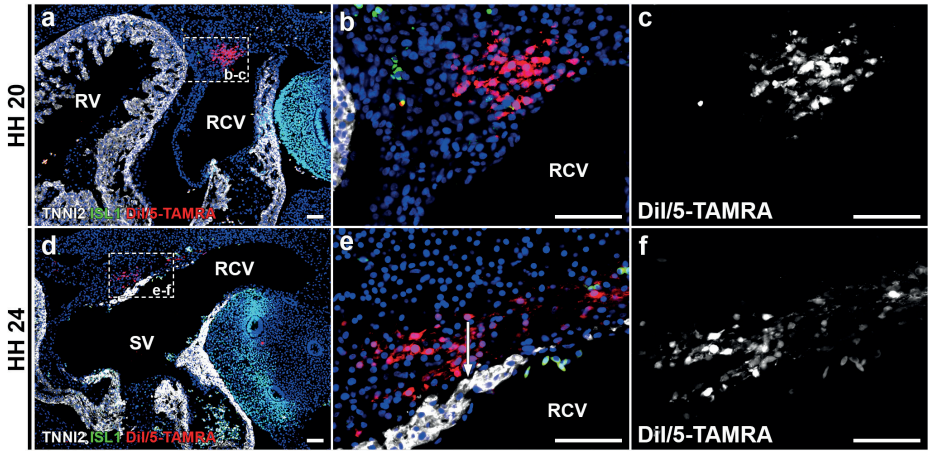

Figure 8. Tracing cells after lateral labeling of RCV mesenchyme

a. Overview, 24 hrs reincubation after labeling wall sinus venosus/RCV. Boxed area shown in **b-c**. **b-c**. No myocardial labeling, no ISL1+ cells labeled. **d.** Overview, 48 hrs reincubation. Boxed area shown in **d-f**. **d-f.** Comparable results. Labeling mesenchyme sinus venosus/RCV, no myocardial labeling. Note demarcation (arrow in **e**) between labeled mesenchyme and sinus venosus myocardium. No ISL1+ cells labeled. RCV: right cardinal vein, RV: right ventricle, SV: sinus venosus. Red: DiI/5-TAMRA, green: ISL1, white: TNNI2, blue: DAPI. Scale bars: 50µm.

area was largely positive for ISL1 and TNNI2 (**Fig. 7d-g**). Two embryos did not show DiI/5-TAMRA in the continuity between the myocardium of the sinus venosus and AV canal. In one of these embryos, initial labeling was applied more cranially, only resulting in labeling of the atrial myocardium. The other embryo showed DiI/5-TAMRA in the caudal portion of the sinus venosus myocardium. Here, initial injection was applied more caudally than in the 8 embryos that did show labeling of the continuity.

A third group of embryos was reincubated for 48 hrs (n=4, HH25). DiI/5-TAMRA was found in the myocardium of the putative SAN (3/4 embryos, 75%), the RVV (3/4 embryos, 75%), the sinus venosus myocardium (4/4 embryos, 100%), right atrium (3/4 embryos, 75%) and the myocardium of the posterior continuity between sinus venosus and AV canal (3/4 embryos, 75%) (**Fig. 7h-n**). In one embryo, labeling was not found in the continuity. This is explained by the more caudal initial injection that was performed, as was seen in one embryo in the second group.

3.4. LATERAL LABELING RCV MESENCHYME DOES NOT RESULT IN LABELING MYOCARDIUM SINUS VENOSUS OR AV CANAL

The above-described results showed that in all embryos, DiI/5-TAMRA was found in the mesenchyme of the RCV. The labeled cells that were found in the myocardial

continuity between sinus venosus and AV canal can therefore also be derived from this mesenchyme. To exclude this possibility, a second group of more lateral labeling of the RCV mesenchyme was performed at HH15-17 and the first group of embryos was harvested 1-2 hrs after injection (n=6). Analysis showed DiI/5-TAMRA in the RCV mesenchyme and lateral body wall (6/6 embryos, 100%) (**Fig. 1f-h**). None of the analyzed embryos showed leakage to myocardial structures.

Analysis after 24 hrs of reincubation (n=5, HH19-21), showed labeling in the lateral body wall and TNNI2- RCV mesenchyme in all cases (5/5 embryos, 100%, **Fig. 8a-c**), with no labeling of myocardial structures, such as the myocardium of the RCV, RVV or sinus venosus.

After 48 hrs of reincubation (n=5, HH24-25), DiI/5-TAMRA was found in the TNNI2- mesenchyme of the RCV (5/5 embryos, 100%, **Fig. 8d-f**). None of the embryos showed labeling of the SAN, RVV or sinus venosus myocardium.

Together, the medial and lateral labeling experiments show that ISL1+/ TNNI2+ myocardium of the sinus venosus is incorporated in the posterior region of the AV canal.

4. DISCUSSION

The adult AVN consists of multiple cell types (i.e. compact nodal cells, transitional cells and nodal extensions) with different morphological and electrophysiological characteristics. The initiation of AVNRT requires the presence of pathways with different electrophysiological characteristics, resulting in slow conduction in the so-called slow pathway, unidirectional conduction in the fast pathway and a central area of block. Cellular and functional heterogeneity of the node is thus a prerequisite for AVNRT to occur. A key finding of the current study was the demonstration of incorporation of sinus venosus myocardium in the AV canal in the posterior region of the AVN.

It has been suggested that the transitional cells of the AVN are an atrial contribution to the AVN.[25] The inferior nodal extension, which acts as the slow pathway in AVNRT, has been described as atrial myocardium, based on histologic criteria.[16] The CCS-LacZ[26,27] and HCN4nLacZ[28] mice, which were used to visualize the developing CCS, demonstrated that the sinus venosus myocardium, that includes the SAN at its proximal end as well as the left and right venous valves, is connected to the AVN. Analysis of protein expression of HNK-1 in human embryos[29], mRNA expression of *HCN4* in chicken embryos[23] and *Tbx3* in mice[30] showed the same connection between the sinus venosus myocardium and the AVN. More recently, it was established that Isl1+ cardiogenic mesoderm contributed to the AVN.[20] These results suggest that the sinus venosus myocardium and venous valves are connected with the AVN through specialized myocardium of the CCS. However, these studies did not show a direct embryonic contribution

from the sinus venosus myocardium to the developing AV canal. To overcome these limitations, it is necessary to directly label the cells from the sinus venosus myocardium and trace these cells during development.

Recently, two separate research groups performed vital dye labeling experiments and showed a very early contribution (4-6 somite stage in mouse[31] and HH8 in chick[32]) from a region posterior to the cardiac crescent to the AV canal myocardium. Dominguez *et al.* showed that the majority of cells comprising the murine AV canal are derived from an *Isl1*+ and *Mlc2a*- pool of cells.[31] Bressan *et al*. showed a contribution to the developing AV canal from an even more posteriorly located region, which is *Isl1*- and *Nkx2-5*-.[32] These experiments suggest that the AV canal myocardium, and thus the AVN, is derived from a larger population of cells than cardiac crescent cells alone. However, these results still do not prove the addition of cells from the sinus venosus myocardium to the developing AV canal.

The current study is aimed at the area of myocardial continuity between the sinus venosus and AV canal. Expression data show that in this tissue, ISL1 is strongly expressed in the sinus venosus myocardium and decreases towards the AV canal. NKX2-5 expression shows a similar but opposite pattern, with an increase in expression towards the AV canal myocardium, suggesting that ISL1+ cells are differentiating towards a more restricted cardiac fate in this region. The continuity between sinus venosus myocardium and the AV canal also showed *HCN4* mRNA expression and was identified in murine embryos co-expressing ISL1, TNNI2 and HCN4. HCN4 is responsible for the "funny current", enabling cardiomyocytes to depolarize spontaneously and HCN4 is known to be expressed in the (developing) CCS.[23] The pacemaker–like phenotype of the myocardial continuity was confirmed with single-cell patch clamp experiments and by qPCR. The different phenotype of this region compared to the more caudal, posterior region of the AV canal was demonstrated by the different levels of mRNA expression of *HCN4* and *ISL1*. These results suggest the presence of distinct, heterogenic cell populations within the region of the putative AVN and indicate a contribution of the sinus venosus during the development of the AVN.

Vital dye labeling of the ISL1+/TNNI2+ sinus venosus myocardium at HH15 (when this myocardium was not yet in contact with the AV canal) and follow-up of these cells during further development, showed that part of the sinus venosus myocardium becomes incorporated in the posterior region of the AV canal myocardium (putative AVN region). As mentioned, it was shown that in the region of the developing AVN, different cell populations (i.e. relative high expression of *HCN4* and *ISL1* in the myocardial continuity between the sinus venosus and AV canal as compared to the more caudal portion of the posterior AV canal) can be distinguished, even early in development.

These results combined with the co-expression studies support the hypothesis that the definitive AVN is derived from different sources of cells that are added at different time points. We hypothesize a relatively late (after HH15, when the PHT has been formed and dextral looping has progressed) contribution from the sinus venosus myocardium to the developing AVN, which results in the presence of multiple cell types in the adult AVN. Furthermore, we postulate that the cells from this sinus venosus-AV canal continuity contribute to the nodal extensions or transitional cells of the AVN, as the continuity is located posterosuperiorly in the AV canal.

Using a genetic lineage tracing approach in mice, Aanhaanen *et al*. described no contribution of Tbx18+ (used as a marker for the sinus horn myocardium and the epicardium) cells to the AVN or AV junction.[13] The current study describes a contribution from the sinus venosus myocardium to the AV canal. A possible explanation for this difference could be the different markers used to identify the sinus venosus myocardium. The Tbx18-Cre used will probably label a different pool of cells as compared to the ISL1+ cells that were labeled in the current study. Furthermore, it has been shown that inefficient recombination of the ROSA26R locus[33] (the reporter that was used in the Tbx18-Cre based genetic tracing experiments mentioned above was the $R26R^{LacZ}$ mouse) makes it difficult to interpret the results. Ma *et al*. reassessed the fate of Isl1+ and Nkx2-5+ cells and compared the results of a ROSA26R-based or GATA4-based reporter system. They found large differences in recombination domains between the two reporter systems, with a far larger recombination domain for the GATA4-based reporter experiments.[33] These results show that it is difficult to draw conclusions from the absence of reporter gene expression.

Two limitations of the vital dye experiments are the potential leakage of dye to adjacent structures and the impossibility to directly correlate the initial labeling to the fate of cells at a later time point within the same embryo. Leakage to the ISL1-/TNNI2+ atrial myocardium was calculated and showed that only a small percentage (on average 5,9%) of labeling was found in this region. Furthermore, labeling experiments in a large number of embryos and the high reproducibility of injections and pattern of distribution minimized these limitations.

In order to describe the dynamics of ISL1 expression, early stages of development were analyzed and co-expression of ISL1 and TNNI2 was found in the bilateral cardiogenic plates, before formation of the primary heart tube. Cells that contribute to the cardiac crescent and primary heart tube are considered to be derivatives of the first heart field. Mesodermal cells at both poles of the tube which differentiate and are recruited to the heart are considered to be derivatives of the second heart field.[34] *Isl1* is commonly used as a marker for the second heart field. However, co-expression of ISL1 and TNNI2 was found in the

majority of cells of the bilateral cardiogenic plates (first heart field derived) in chick, which is in agreement with expression of *ISL1* mRNA in this region.[35] As described above, Ma *et al*. showed that the majority of cardiac cells (including left ventricular cardiomyocytes) are derived from *Isl1*+ progenitors.[33] This shows that *Isl1* is not suitable as a second heart field marker.[33] These results raise the question whether the first and second heart field should be considered as truly distinct cell populations, or rather form a continuum and reflect different stages of differentiation of progenitor cells with a cardiac fate, as was mentioned previously.[33,36] Nevertheless, the analysis of ISL1 expression, which was performed in the current study, is crucial to identify cardiac progenitors and investigate the differentiation state of (pre)cardiac cells.

The current study describes co-expression of ISL1 and TNNI2 beyond HH12 in regions relevant for normal CCS development, but also in myocardial structures known to underlie common arrhythmias. Furthermore, it was shown that the myocardial continuity in the upper region of the developing AVN shows relative high expression of *HCN4* and *ISL1*. Our data and the results from other studies point towards an important link between ISL1 and the CCS. The primary pacemaker of the heart, the SAN, retains ISL1 expression until late stages of development, whereas in the remaining heart, ISL1 expression is downregulated after cells differentiate to working cardiomyocytes.[2] Previous inducible Cre-based genetic tracing experiments showed the contribution of Isl1+ progenitors to the SAN and AVN.[20] Also, a link between Shox2, a transcription factor essential in regulating the SAN gene expression program, and Isl1 has been shown.[37] Mice lacking Shox2 present with severe bradycardia and defects in SAN development, and show downregulation of Isl1 expression in the SAN. The Shox2-mediated bradycardia could be rescued by isl1 in a zebrafish model.[37] Zebrafish lacking isl1 expression show pacemaker dysfunction and the isl1+ cells from the inflow portion of the heart reveal pacemaker activity.[38] A possible mechanism by which ISL1 is involved in CCS functioning is by keeping cells in a primitive state, maintaining their pacemaker-like phenotype and preventing them from further differentiating towards working myocardium. The CCS consists of cells resembling a more primitive myocardium with slow conduction, high automaticity, and poor electrophysiological coupling.[10] We hypothesize that selected clinical arrhythmias could be explained by a local diminished or absent downregulation or re-expression of Isl1 resulting in areas with a more primitive, CCS-like phenotype, from which arrhythmias originate. Further experiments are needed to test this hypothesis.

5. CONCLUSION

Incorporation of sinus venosus myocardium in the posterior part of the AV canal myocardium was demonstrated. It is postulated that the sinus venosus myocardium contributes to the nodal extensions or transitional cells of the AVN. Multiple sources of cells contributing to the AVN may explain the heterogeneity of the node, and form the substrate underlying AVNRT.

REFERENCE LIST

1. Jongbloed, M. R. M. *et al.* Normal and abnormal development of the cardiac conduction system; implications for conduction and rhythm disorders in the child and adult. *Differentiation.* **84,** 131–148 (2012).

2. Vicente-Steijn, R. *et al.* Electrical activation of sinus venosus myocardium and expression patterns of RHOA and Isl-1 in the chick embryo. *J. Cardiovasc. Electrophysiol.* **21,** 1284–92 (2010).

3. Christoffels, V. M. *et al.* Formation of the venous pole of the heart from an Nkx2-5-negative precursor population requires Tbx18. *Circ. Res.* **98,** 1555–63 (2006).

4. Cai, C.-L. *et al.* Isl1 identifies a cardiac progenitor population that proliferates prior to differentiation and contributes a majority of cells to the heart. *Dev. Cell.* **5,** 877–89 (2003).

5. Blaschke, R. J. *et al.* Targeted mutation reveals essential functions of the homeodomain transcription factor Shox2 in sinoatrial and pacemaking development. *Circulation.* **115,** 1830–8 (2007).

6. Bax, N. A. M. *et al.* Cardiac malformations in Pdgfralpha mutant embryos are associated with increased expression of WT1 and Nkx2.5 in the second heart field. *Dev. Dyn.* **239,** 2307–17 (2010).

7. Hoogaars, W. M. H. *et al.* Tbx3 controls the sinoatrial node gene program and imposes pacemaker function on the atria. *Genes Dev.* **21,** 1098–112 (2007).

8. Mommersteeg, M. T. M. *et al.* Molecular pathway for the localized formation of the sinoatrial node. *Circ. Res.* **100,** 354–62 (2007).

9. Gittenberger-de Groot, A. C. *et al.* Nkx2.5-negative myocardium of the posterior heart field and its correlation with podoplanin expression in cells from the developing cardiac pacemaking and conduction system. *Anat. Rec.* **290,** 115–22 (2007).

10. Bakker, M. L., Christoffels, V. M. & Moorman, A. F. The cardiac pacemaker and conduction system develops from embryonic myocardium that retains its primitive phenotype. *J. Cardiovasc. Pharmacol.* **56,** 6–15 (2010).

11. James, T. N. The internodal pathways of the human heart. *Prog. Cardiovasc. Dis.* **43,** 495–535 (2001).

12. Aanhaanen, W. T. J. *et al.* The Tbx2+ primary myocardium of the atrioventricular canal forms the atrioventricular node and the base of the left ventricle. *Circ. Res.* **104,** 1267–74 (2009).

13. Aanhaanen, W. T. J. *et al.* Developmental origin, growth, and three-dimensional architecture of the atrioventricular conduction axis of the mouse heart. *Circ. Res.* **107,** 728–36 (2010).

14. Lee, P.-C., Chen, S.-A. & Hwang, B. Atrioventricular node anatomy and physiology: implications for ablation of atrioventricular nodal reentrant tachycardia. *Curr. Opin. Cardiol.* **24,** 105–12 (2009).

15. Katritsis, D. G. & Becker, A. The atrioventricular nodal reentrant tachycardia circuit: a proposal. *Heart Rhythm.* **4,** 1354–60 (2007).

16. Anderson, R. H. & Ho, S. Y. The morphology of the cardiac conduction system. *Novartis Found. Symp.* **250,** 6–17 (2003).

17. Greener, I. D. *et al.* Ion channel transcript expression at the rabbit atrioventricular conduction axis. *Circ. Arrhythm. Electrophysiol.* **2,** 305–15 (2009).

18. Li, J. *et al.* Computer three-dimensional reconstruction of the atrioventricular node. *Circ. Res.* **102,** 975–85 (2008).

19. Zhuang, S. *et al.* Expression of Isl1 during mouse development. *Gene Expr. Patterns.* **13,** 407–412 (2013).

20. Sun, Y. *et al.* Islet 1 is expressed in distinct cardiovascular lineages, including pacemaker and coronary vascular cells. *Dev. Biol.* **304,** 286–96 (2007).

21. Hamburger, V. & Hamilton, H. L. A series of normal stages in the development of the chick embryo. *J. Morphol.* **88,** 49–92 (1951).

22. Carmeliet, P. *et al.* Impaired myocardial angiogenesis and ischemic cardiomyopathy in mice lacking the vascular endothelial growth factor isoforms VEGF164 and VEGF188. *Nat. Med.* **5,** 495–502 (1999).

23. Vicente-Steijn, R. *et al.* Funny current channel HCN4 delineates the developing cardiac conduction system in chicken heart. *Heart Rhythm.* **8,** 1254–63 (2011).

24. de Boer, B. A. *et al.* The interactive presentation of 3D information obtained from reconstructed datasets and 3D placement of single histological sections with the 3D portable document format. *Development.* **138,** 159–67 (2011).

25. Argüello, C., Alanis, J. & Valenzuela, B. The early development of the atrioventricular node and bundle of His in the embryonic chick heart. An electrophysiological and morphological study. *Development.* **102,** 623–37 (1988).

26. Jongbloed, M. R. M. *et al.* Embryonic conduction tissue: a spatial correlation with adult arrhythmogenic areas. *J. Cardiovasc. Electrophysiol.* **15,** 349–55 (2004).

27. Rentschler, S. *et al.* Visualization and functional characterization of the developing murine cardiac conduction system. *Development.* **128,** 1785–92 (2001).

28. Liang, X. *et al.* HCN4 dynamically marks the first heart field and conduction system precursors. *Circ. Res.* **113,** 399–407 (2013).

29. Blom, N. A. *et al.* Development of the cardiac conduction tissue in human embryos using HNK-1 antigen expression: possible relevance for understanding of abnormal atrial automaticity. *Circulation.* **99,** 800–6 (1999).

30. Hoogaars, W. M. H. *et al.* The transcriptional repressor Tbx3 delineates the developing central conduction system of the heart. *Cardiovasc. Res.* **62,** 489–99 (2004).

31. Domínguez, J. N., Meilhac, S. M., Bland, Y. S., Buckingham, M. E. & Brown, N. A. Asymmetric fate of the posterior part of the second heart field results in unexpected left/right contributions to both poles of the heart. *Circ. Res.* **111,** 1323–35 (2012).

32. Bressan, M., Liu, G. & Mikawa, T. Early mesodermal cues assign avian cardiac pacemaker fate potential in a tertiary heart field. *Science.* **340,** 744–748 (2013).

33. Ma, Q., Zhou, B. & Pu, W. T. Reassessment of Isl1 and Nkx2-5 cardiac fate maps using a Gata4-based reporter of Cre activity. *Dev. Biol.* **323,** 98–104 (2008).

34. Buckingham, M., Meilhac, S. & Zaffran, S. Building the mammalian heart from two sources of myocardial cells. *Nat. Rev. Genet.* **6,** 826–835 (2005).

35. Yuan, S. & Schoenwolf, G. C. Islet-1 marks the early heart rudiments and is asymmetrically expressed during early rotation of the foregut in the chick embryo. *Anat. Rec.* **260,** 204–207 (2000).

36. Abu-Issa, R., Waldo, K. & Kirby, M. L. Heart fields: one, two or more? *Dev. Biol.* **272,** 281–5 (2004).

37. Hoffmann, S. *et al.* Islet1 is a direct transcriptional target of the homeodomain transcription factor Shox2 and rescues the Shox2-mediated bradycardia. *Basic Res. Cardiol.* **108,** 339 (2013).

38. Tessadori, F. *et al.* Identification and functional characterization of cardiac pacemaker cells in zebrafish. *PLoS One.* **7,** e47644 (2012).

SUPPLEMENTAL MATERIAL

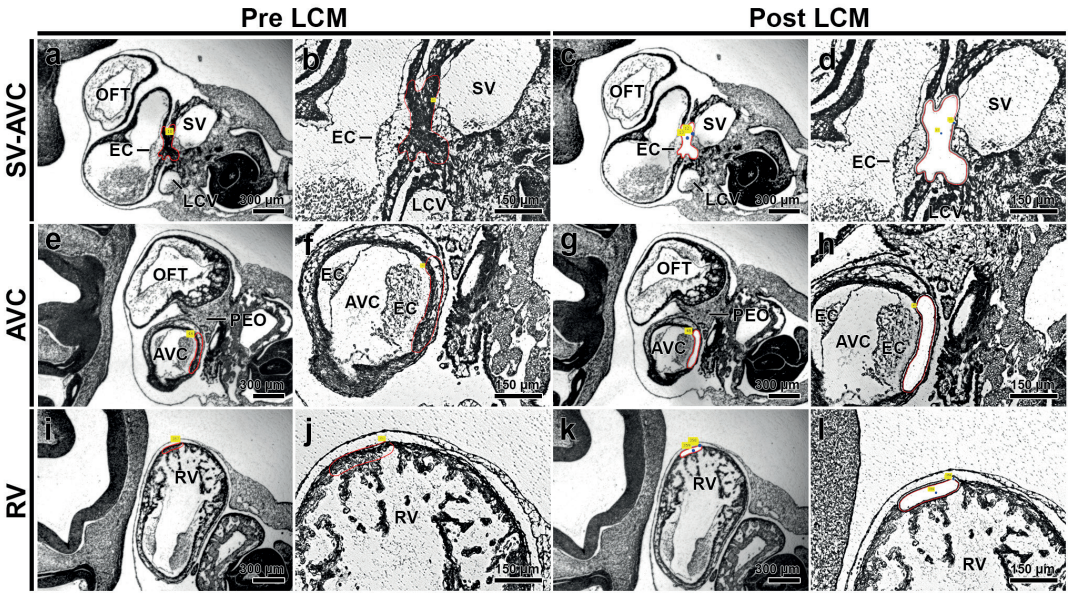

Supplemental figure S1. Representative images of regions collected by LCM

a-b. The myocardial continuity between the sinus venosus and AV canal is shown (SV-AVC) before LCM. The red line indicates the region where the laser will dissect. **c-d.** The same region is shown after dissection of the tissue. **e-g.** The more caudal posterior AV canal region (AVC,) before (**e-f**) and after (**g-h**) LCM. **i-l.** The right ventricular (RV) region where LCM was performed, before (**i-j**) and after (**k-l**) dissection. AVC: atrioventricular canal, EC: endocardial cushion, LCV: left cardinal vein, OFT: outflow tract, PEO: proepicardial organ, RV: right ventricle, SV: sinus venosus. Scale bars: length is depicted above bar.

Supplemental table 1. Primers used

Primer	Sequence
GAPDH forward	5'-CTAAGGCTGTGGGGAAGGT-3'
GAPDH reverse	5'-GTTGTTGACCTGACCTGCC-3'
TNNT2 forward	5'-AAGAAGGGTGGCAAGAAGCA-3'
TNNT2 reverse	5'-CTCGTGGTCACTGACACGATTT-3'
NKX2-5 forward	5'-CCCTACTACGTGAAGAGCTACG-3'
NKX2-5 reverse	5'-TCGGGATCCTCCAGCTCTCT-3'
HCN4 forward	5'-GCCTTCTGCTGTTGGCTCT-3'
HCN4 reverse	5'-GCTGCTGGATGTGGTAGGA-3'
ISL1 forward	5'-AAAAGAAGCATTATGATGAAGCAA-3'
ISL1 reverse	5'-CATGTCTCTCCGGACTAGCAG-3'
ISL1 nested forward	5'-AGCAACCCAATGACAAAAC-3'
ISL1 nested reverse	5'-TGTCTCTCCGGACTAGCAG-3'

5

LETTER TO EDITOR: DOES THE DORSAL MESENCHYMAL PROTRUSION ACT AS A TEMPORARY PACEMAKER DURING HEART DEVELOPMENT?

Tim P. Kelder, Rebecca Vicente-Steijn, Marco C. DeRuiter, Adriana C. Gittenberger-de Groot, Monique R.M. Jongbloed.

Modified after Journal of Biological Chemistry, 290: 8013-4 (2015)

LETTER TO EDITOR

Sun *et al.* report that the dorsal mesenchymal protrusion (DMP) acts as a temporary pacemaker during early development, prior to formation of the atrioventricular node (AVN).[1] We would like to question whether the anatomical designation of the DMP used in this paper is correct.

The DMP was originally described as a *mesenchymal* protrusion from the dorsal mesocardium towards the atrial cavity contributing to the base of the atrial septum along with the mesenchymal cap and atrioventricular (AV) cushions (see **Fig. 1**).[2] To differentiate between the DMP prior to muscularization (from approximately embryonic day (E)13 in mouse), and other structures in the AV junction during early development, stainings of myocardial markers are essential, which are lacking in the Sun paper.[1] In our opinion, the Shox2+ region described by Sun *et al.* as DMP at E11.5 and E12.5 corresponds to CTNI+/HCN4+/ISL1+ cells of the putative AVN region and not the DMP (CTNI-/HCN4-, ISL1+) (see **Fig. 1** and refs[3,4]). HCN4 expression to date has not been described in mesenchyme.[3–5] Co-expression of HCN4/TBX3 in cells in the AV junction, with nodal-like electrophysiological characteristics[1] corresponds to the (putative) AVN region instead of the DMP, which is in accordance with our own observations.[4] Misnaming the DMP during early development leads to the erroneous conclusion that this structure shows pacemaking properties.

Although we do not support the conclusion that the DMP acts as a temporary pacemaker, the results described by Sun *et al.* elegantly show an important role for the Shox2-BMP pathway during AVN development.

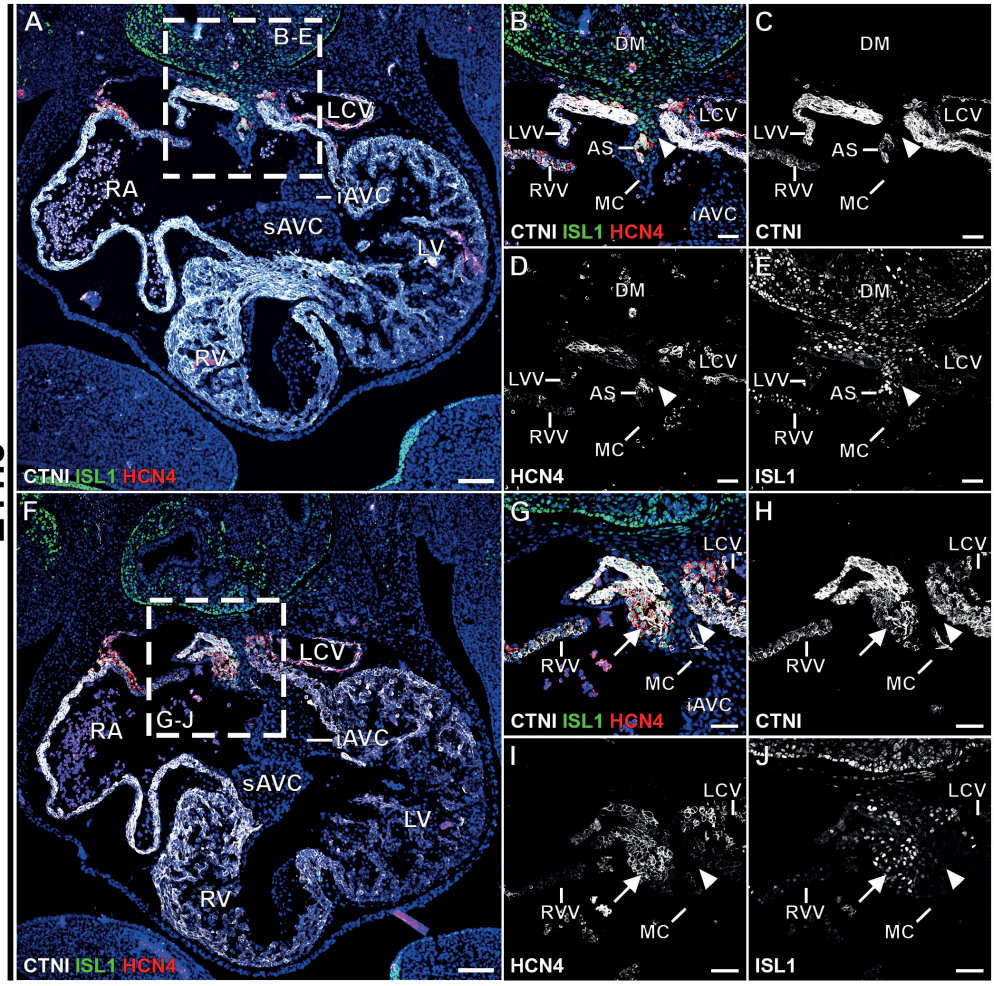

Figure 1. Structures in the atrioventricular junction at E11.5

Panels A-E show transverse sections just below the entrance of the pulmonary veins. **A.** Overview of CTNI/HCN4/ISL1 staining. Boxed area is shown in **B-E. B.** Merge of different channels showing the HCN4-/CTNI-/ISL1+ DMP (arrowhead) protruding from the dorsal mesocardium (DM) towards the atrial cavity. The close relation with the mesenchymal cap (MC) is shown. **C-E.** Separate grey values of CTNI (**C**), HCN4 (**D**), and ISL1 (**E**). **Panels F-J** show transverse sections at the level of the base of the atrial septum, more caudal to the level shown in panels **A-E. F.** Overview, with boxed region shown in **G-J. G.** the HCN4-/CTNI-/ISL1+ (low expression of ISL1 at this level) DMP (arrowhead) is continuous with the MC, which in turn is continuous with the inferior atrioventricular cushion (iAVC). The arrow indicates the HCN4+/CTNI+/ISL1+ region designated by Sun *et al.* as DMP. However, co-expression of markers and the location directly above the iAVC at the base of the right atrium shows that this region corresponds to the region of the future AVN. **H-J**. grey values of CTNI (**H**), HCN4 (**I**), and ISL1 (**J**). Scalebar in **A** and **F** 100μm, other panels 50μm. AS: atrial septum, CTNI: cardiac troponin-I, HCN4: hyperpolarization-activated cyclic nucleotide-gated channel 4, ISL1: Islet1, L/RCV: left/right cardinal vein, L/RV: left/right ventricle, L/RVV: left/right venous valve, RA: right atrium, sAVC: superior atrioventricular cushion.

REFERENCE LIST

1. Sun, C. *et al.* The short stature homeobox 2 (Shox2)-bone morphogenetic protein (BMP) pathway regulates dorsal mesenchymal protrusion development and its temporary function as a pacemaker during cardiogenesis. *J. Biol. Chem.* **290,** 2007–23 (2015).

2. Briggs, L. E., Kakarla, J. & Wessels, A. The pathogenesis of atrial and atrioventricular septal defects with special emphasis on the role of the dorsal mesenchymal protrusion. *Differentiation.* **84,** 117–30 (2012).

3. Liang, X. *et al.* HCN4 dynamically marks the first heart field and conduction system precursors. *Circ. Res.* **113,** 399–407 (2013).

4. Kelder, T. P. *et al.* The sinus venosus myocardium contributes to the atrioventricular canal: potential role during atrioventricular node development? *J. Cell. Mol. Med.* **19,** 1375–89 (2015).

5. Vicente-Steijn, R. *et al.* Funny current channel HCN4 delineates the developing cardiac conduction system in chicken heart. *Heart Rhythm.* **8,** 1254–63 (2011).

6

RHOA-ROCK SIGNALING IS NECESSARY FOR LATERALIZATION AND DIFFERENTIATION OF THE DEVELOPING SINOATRIAL NODE

Rebecca Vicente-Steijn, Tim P. Kelder, Leon G. Tertoolen, Lambertus J.Wisse, Daniel A. Pijnappels, Robert E. Poelmann, Martin J. Schalij, Marco C. DeRuiter, Adriana C. Gittenberger-de Groot, Monique R.M. Jongbloed

Modified after Cardiovascular Research, 113: 1186-97 (2017)

ABSTRACT

AIMS:

RHOA-ROCK signaling regulates cell migration, proliferation, differentiation and transcription. RHOA is expressed in the developing cardiac conduction system in chicken and mice. In early development, the entire sinus venosus myocardium, including both the transient left-sided and definitive right-sided sinoatrial node (SAN), has pacemaker potential. Later, pacemaker potential is restricted to the right-sided SAN. Disruption of RHOA expression in adult mice causes arrhythmias including bradycardia and atrial fibrillation, the mechanism of which is unknown but presumed to affect the SAN. The aim of this study is to assess the role of RHOA-ROCK signaling in SAN development in the chicken heart.

METHODS AND RESULTS:

ROCK signaling was inhibited chemically in embryonic chicken hearts using Y-27632. This prolonged the immature state of the sinus venosus myocardium, evidenced by up-regulation of the transcription factor *ISL1,* wide distribution of pacemaker potential and significantly reduced heart rate. Furthermore ROCK inhibition caused aberrant expression of typical SAN genes *ROCK1, ROCK2, SHOX2, TBX3, TBX5, ISL1, HCN4, CX40, CAV3.1* and *NKX2.5* and left-right asymmetry genes *PITX2C* and NODAL. Anatomical abnormalities in pulmonary vein development were also observed. Patch clamp electrophysiology confirmed the immature phenotype of the SAN cells and a residual left-sided sinus venosus myocardium pacemaker-like potential.

CONCLUSIONS:

RHOA-ROCK signaling is involved in establishing the right-sided SAN as the definitive pacemaker of the heart and restricts typical pacemaker gene expression to the right side of the sinus venosus myocardium.

1. INTRODUCTION

The RHOA-Rho kinase (ROCK1/2) signaling pathway is associated with multiple cardiovascular, metabolic and neurodegenerative diseases, and cancer.[1] RHOA is a member of a family of small GTPases that, together with downstream effector kinases ROCK1 and ROCK2, acts as a molecular switch regulating processes like cell migration, cytoskeletal reorganization and gene transcription.[1,2] RHOA-ROCK signaling has also been linked to early cardiogenesis and embryonic left-right asymmetry.[3-6] In addition, the function of the cardiac conduction system (CCS) likely depends on RHOA-ROCK signaling since (i) adult mice with altered RHOA expression present with bradycardia, atrial fibrillation and atrioventricular (AV) block[7,8] and (ii) expression of RHOA during chicken heart development is ultimately restricted to the sinoatrial node (SAN) and atrioventricular node (AVN).[9]

Supraventricular tachycardias (SVTs) are the most common cardiac arrhythmias in adults and children.[10] SVTs can originate from components of the adult CCS, but also from myocardial structures outside the CCS, such as the pulmonary venous myocardium.[11,12] To date, mechanisms underlying these arrhythmias have not been elucidated. Re-expression of embryonic genes or failure to mature so that the embryonic phenotype is retained, however may account for the development of specific arrhythmogenic sites within the heart.[9,13] In cardiomyopathy, pathophysiological remodeling occurs through re-expression of embryonic genes[14], a mechanism that could also apply to a specific subset of cardiac arrhythmias.

During early development, the heart is initially tubular, but loops and expands through continuous incorporation of cells from the mesoderm dorsal to the heart at the arterial and venous pole. Among the genes expressed by these actively proliferating cell populations is the LIM homeodomain transcription factor *Islet1* (*Isl1*), necessary for proper cellular proliferation, survival and migration.[15] *Isl1* has also been linked to the SAN as a direct downstream target of *Shox2* and is able to rescue the bradycardia in *Shox2* mutants.[16]

Early in development, the initial pacemaker signal originates from the left posterior portion of the venous pole of the heart[17], later corresponding to the sinus venosus myocardium covering the left cardinal vein. In adults, the SAN is located at the entrance of the right superior caval vein (embryonic right cardinal vein) in the right atrium (RA). Therefore, a shift in pacemaker location from the left towards the right side has to occur. During cardiogenesis, the sinus venosus myocardium covers the developing cardinal veins (adult caval veins) and includes a functional transient left-sided SAN and the definitive right-sided SAN.[9,18,19]

The developing sinus venosus myocardium, including the SAN, expresses

different genes than the atrial and ventricular working myocardium. These include PODOPLANIN[20], RHOA[9], *Shox2*[16, 21], *Tbx18*[22], *Tbx3*[23], ISL1[16], and *HCN4*[13] but NKX2.5 and connexin (Cx) 40 are absent[24] (reviewed in [25]). In contrast, atrial and ventricular myocardium does not express *Tbx3* or *Shox2* but does express NKX2.5.[20-22] While most of the key players in SAN differentiation have been identified, expression levels within the sinoatrial myocardium of the chicken during heart development are largely unknown.

Although the exact mechanism driving restriction of pacemaker function to the right side of the sinus venosus myocardium is unknown, recent studies suggest a role for right/left patterning factors like *PITX2C.* This gene is linked to a higher susceptibility for atrial arrhythmias[26] and acts as a direct suppressor of *Shox2* in the left atrium, inhibiting the SAN-specific genetic programme.[18,27]

Based on evidence linking RHOA to the CCS[7-9], we hypothesized that normal RHOA-ROCK signaling is essential for proper formation and differentiation of the SAN during embryonic development. Here, we disrupted ROCK signaling during development of the chicken heart and examined the consequences for gene expression and SAN function. We found that RHOA-ROCK signaling is important in establishing the right-sided SAN as the definitive pacemaker and restricts typical pacemaker gene expression to the right side of the sinus venosus myocardium.

2. METHODS

A detailed description of Experimental Methods used in this study is provided in the Data Supplement at the end of this chapter.

2.1. RHO-SIGNALING DISRUPTION, CARDIAC ELECTROPHYSIOLOGY AND GENE EXPRESSION

Animal experiments were performed in accordance with institutional guidelines of the Leiden University Medical Center. Rho signaling was disrupted by addition of the selective Rho kinase (ROCK) inhibitor compound Y-27632 (688000, Calbiochem, Massachusetts, USA) *in ovo* after 48 hrs of incubation (~ stage HH10/11). 2µl of 100µM Y-27632 or PBS (as control) was added to the surface of the embryo. A schematic representation of the experimental setup and survival rates of the embryos are provided in **Supplemental Fig. 2**. Extracellular microelectrode recordings and optical mapping recordings were conducted as described previously.[9,28]

RNA was isolated from control and ROCK inhibited hearts (for HH18-19 whole inflow tract portions were used, from HH20 onwards the inflow tract portion was divided into the right and the left side to assess gene expression separately) and gene expression was analyzed by quantitative Polymerase Chain Reaction (qPCR). Embryos were extracted 24 (stage HH18-19;n=6 controls (CTRL);n=8 ROCK inhibitions (ROCK)), 48 (stage HH21-22;n=7 CTRL;n=9 ROCK) and 96 (stage HH28-29;n=6 CTRL;n=8 ROCK) hrs after treatment. Chicken gene specific primers are provided in **Supplemental Table 1**.

2.2. MICROELECTRODE ARRAY ON ISOLATED CHICK CARDIOMYOCYTES

To study the direct effect of the ROCK inhibitor on rate and amplitude of cardiomyocytes, sinoatrial, atrial and ventricular cardiomyocytes of stage HH26-27 chicken embryos were cultured as described previously[29] and plated on microelectrode arrays (MEA) for electrophysiology. Time point zero was recorded before the ROCK inhibitor Y-27632 was added. Data points are displayed as % relative to time point zero (before application of inhibitory compound).

2.3. PATCH CLAMP ELECTROPHYSIOLOGY

Patch clamp electrophysiology was conducted on cardiomyocytes isolated from right/left or whole sinus venosus myocardium and right ventricular myocardium in control and *in ovo* ROCK-inhibited hearts as previously described.[29]

3. RESULTS

3.1. NORMAL SAN DEVELOPMENT: FROM BROAD PACEMAKING ACTIVITY TO RIGHT-SIDED RESTRICTION

Normal development of the SAN in the chicken embryo heart is summarized in **Fig. 1**. Early in development, just as looping of the heart tube has started (HH11), the first sinus venosus myocardium could be observed ventral to the cardinal veins, evidenced by expression of TNNI2 and absence of NKX2.5 (**Fig. 1A, A1-A6**). A cluster of cells at the entrance of the right cardinal vein (superior caval vein in the adult) corresponded to the putative right-sided SAN (**Fig. 1A1-A3**), whereas a cluster on the left side reflected the left-sided SAN (**Fig. 1A4-A6**). Previously, we showed that at these developmental stages the sinus venosus myocardium expresses *HCN*4 mRNA.[13] As the heart continued to grow and loop to adopt its mature four-chambered structure, the sinus venosus expanded considerably (**Fig. 1B,C**), still encompassing a right and left-sided SAN. Small differences between the right and left-sided SAN were already evident: the right-sided SAN was more compact than the left (although it still had larger intercellular spaces) and showed robust myocardial continuity with the atrial myocardium (compare **Fig. 1B1-B3** to **B4-B6**). At pre-hatching stages (HH42), the right side of the sinus venosus myocardium was the only region lacking NKX2.5 (**Fig. 1D**). The fully developed right-sided SAN expressed TNNI2 (**Fig. 1D1-D2**), and *HCN4 (***Fig. 1D4**) but not NKX2.5 (**Fig. 1D3**). In contrast to earlier stages, the myocardium medial to the left cardinal vein expressed TNNI2 (**Fig. 1D5-D6**) and NKX2.5 (**Fig. 1D7**), whereas *HCN4* expression (**Fig. 1D8**) was absent. Thus, although the developing SAN occupied a broad area of the heart early in development, it was restricted to the right side at later stages.

Figure 1. Normal development of the SAN (figure on page 123)

A-D. Posterior views of 3D reconstructions of HH11 (**A**), HH24 (**B**), HH35 (**C**), and HH42 (**D**) embryonic chicken hearts. NKX2.5-negative myocardium is depicted in lime green, right and left cardinal vein (R/LCV) lumen in transparent blue and pulmonary pit or vein in yellow. The numbered intersection lines refer to respective sections of the specific embryonic stage. **A1-A3.** HH11 heart showing TNNI2 (**A1-A2**) but no NKX2.5 (**A3**) expression in myocardium surrounding the RCV (**arrow**, putative right SAN). **A4-A6.** Sections showing a cluster of cells medial to the LCV (**arrow**, transient left SAN area) expressing TNNI2 (**A4-A5**) but no NKX2.5 (**A6**). **B1-B3.** HH24 heart showing TNNI2 (**B1**), *HCN4* (**B2**) but no NKX2.5 (**B3**) expression in the right-sided SAN. **B4-B6.** Cluster of cells medial to the LCV (**arrow**, transient left-sided SAN) expressing TNNI2 (**B3**), *HCN4* (**B5**) but no NKX2.5 (**B6**). The right-sided SAN is more compact and shows better myocardial continuity with the atrial myocardium than the left-sided SAN (compare **B1** with **B4**). **D1-D4.** Transverse sections of an HH42 chicken embryo depicting the right-sided SAN (arrows) which is TNNI2+ (**D1-D2**), NKX2.5- (**D3**) and *HCN4+* (**D4**). **D5-D8.** The majority of the sinus venosus myocardium including the left side (arrows) now expresses TNNI2 (**D5-D6**), NKX2.5 (**D7**) but no *HCN4* (**D8**). (L/R)A: left/right atrium. Scale bars**:** A-C: 200μm; D: 400μm, A1-D8: 100μm. HH11-31: n=40.

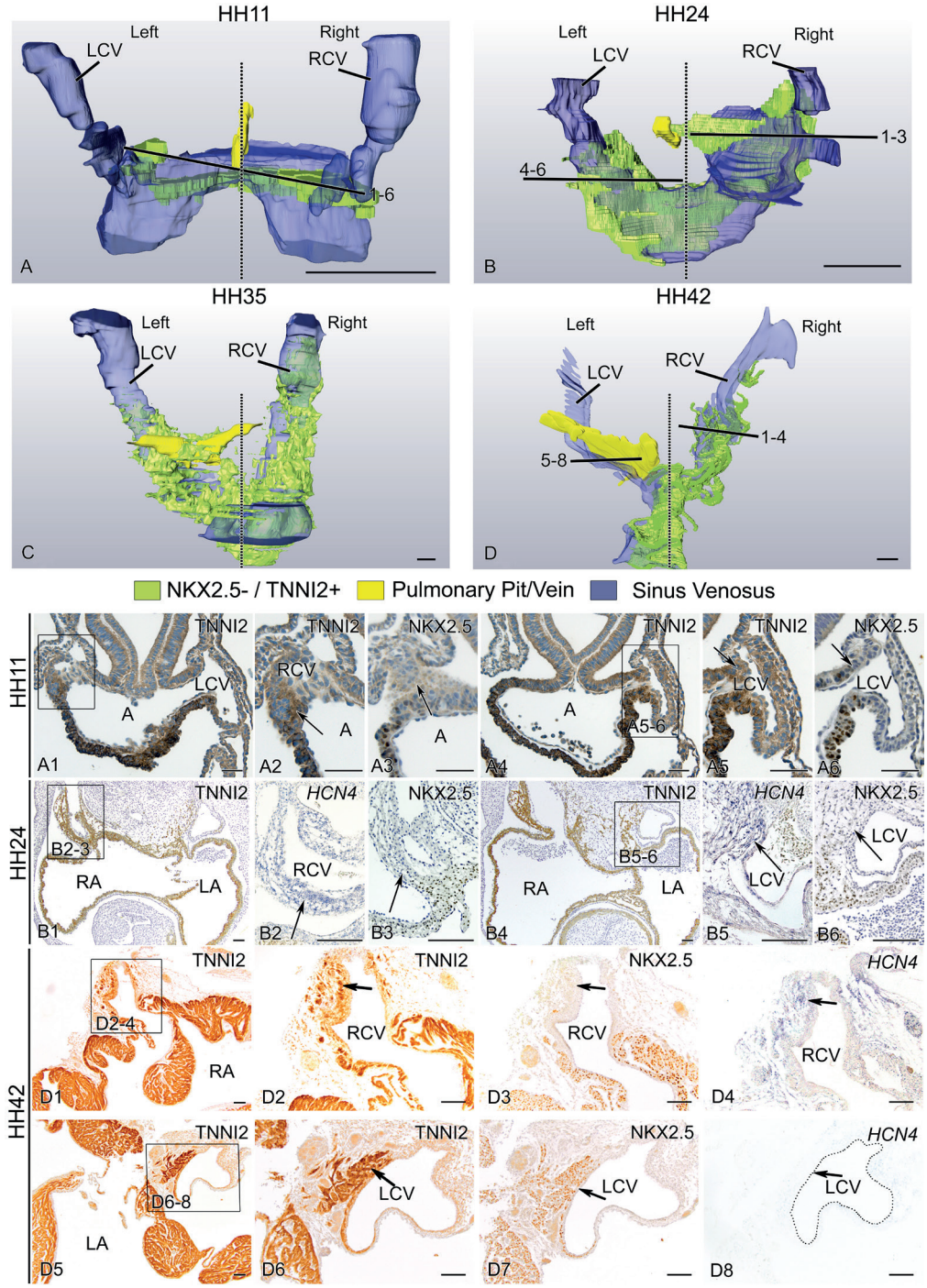

Figure 1. Normal development of the SAN (legend on page 122)

3.2. ROCK INHIBITION AND SAN FUNCTION: PERSISTENT IMMATURITY IN FUNCTION AND DEFICIENT LATERALIZATION

The ability of the entire sinus venosus myocardium to generate the first atrial activation signal has been previously demonstrated.[9, 18, 19] Electrophysiological measurements in the current study confirmed the presence of three atrial activation patterns during development: right side first activation pattern (RA signal precedes left atrium (LA), RA first, **Supplemental Fig. 3A-B**), left side first (LA signal precedes RA, LA first, **Supplemental Fig. 3C-D**) and concurrent activation (no distinction can be made between RA or LA (<1 ms difference), Concurrent). These activation patterns were confirmed by optical mapping recordings in which three preferential activation sites were observed: left, middle and right of the sinus venosus portion of the embryonic heart (**Fig. 2A-C**).

In light of restriction of RHOA expression to the SAN at HH28[9], hearts were divided into two groups for analysis: before (<) and at or after (≥) HH28. During early stages of normal heart development (<HH28, **Fig. 2D**) the RA first pattern was observed in 62% (63/95) of the cases, the LA first in 18% (18/95) and the concurrent pattern in 20% (20/95). Later (≥HH28, **Fig. 2D**), the RA first pattern represented 92% (24/31) of the observed patterns, LA first 4% (1/31) and concurrent 4% (1/31). Longitudinal analysis of activation patterns showed a significant difference between early and late developmental stages (p=0.014, <HH28 *vs* ≥HH28), demonstrating a shift towards right-sided pacemaking.

At early stages of development (<HH28, **Fig. 2D**), after ROCK signaling was inhibited, 39% (12/48) of cases showed the RA first pattern, 26% (8/48) the LA first pattern and 35% (11/48) the concurrent pattern. Differences with controls were not statistically significant (p=0.061). At later stages (≥HH28, **Fig. 2D**) ROCK inhibition resulted in 57% (8/18) of RA first cases and 21.5% (3/18) of both LA first and concurrent cases, significantly different (p=0.03) from the untreated group. Longitudinal analysis revealed no significant difference (p=0.099) in distribution of atrial activation sites before or after HH28 in the ROCK inhibition group.

During normal heart development, pacemaker cell differentiation could be monitored by electrophysiology *ex ovo*. One of the most striking electrical changes was a significant increase in heart rate in RA first hearts ≥HH28 compared to LA first hearts (**Fig. 2F**), compared to <HH28 (**Fig. 2E**). After ROCK inhibition, the heart rate at late stages (≥HH28) of RA first heart was significantly lower compared to controls (**Fig. 2F**). LA first hearts showed a significantly higher heart rate compared to its control counterpart and RA first control hearts (**Fig. 2F**). Overall, after ROCK inhibition, global pacemaking potential was maintained in the entire sinus venosus myocardium.

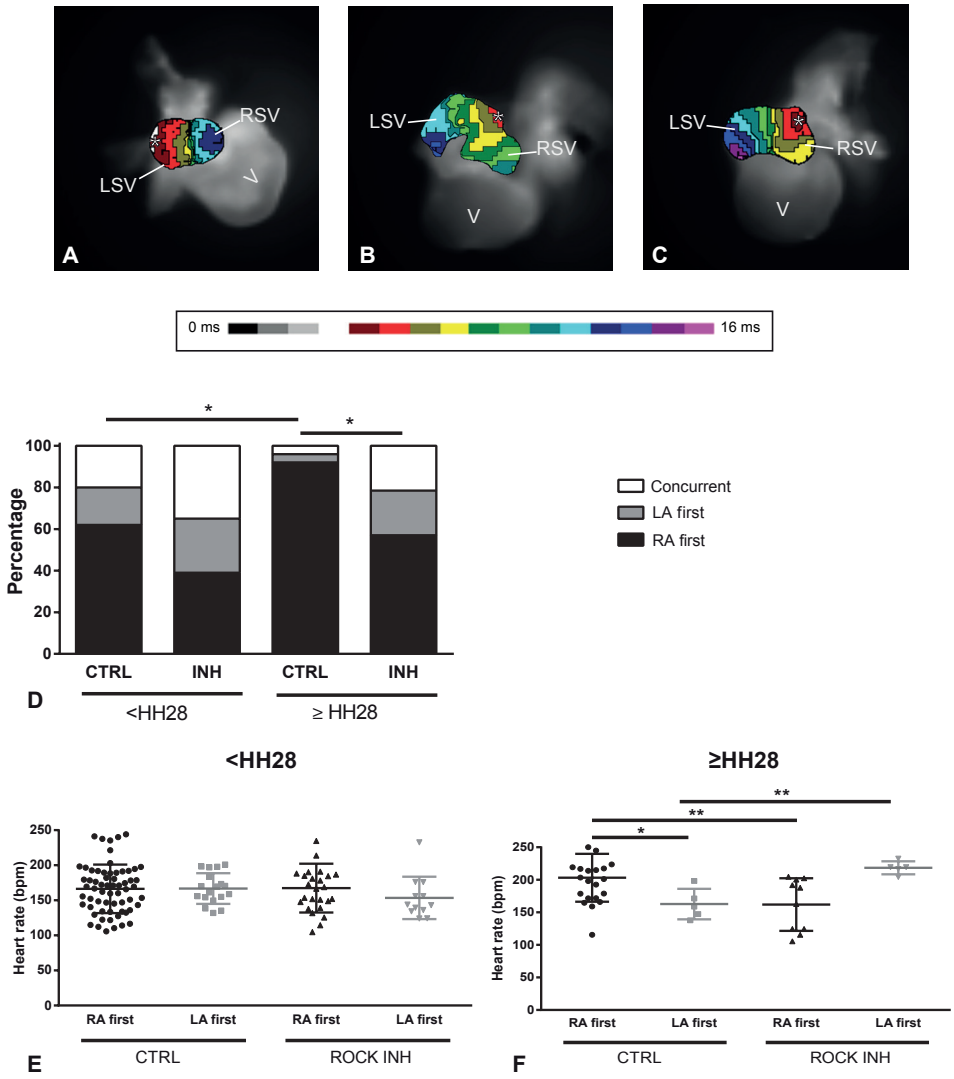

Figure 2. Persistent immaturity in function and deficient lateralization of the SAN

A-C. Optical mapping recordings of the dorsal portion of the heart of HH21 chick embryos showing first activation (white asterisk, color code red) of the heart from the left (**A**), middle (**B**) or right (**C**) side of the sinus venosus. Each color represents 1ms of propagation. **D**. Frequency distribution (in % of activation pattern) of different atrial activation patterns observed <or ≥ stage HH28 in controls or after ROCK inhibition (INH). **E**. Bar graph depicting significant changes in control heart rate (beats per minute, bpm) before stage HH28 between CTRL (n=95) and ROCK INH (n=48). **F**. Bar graph depicting significant changes in heart rate between CTRL (n=31) and ROCK INH (n=18) ≥HH28. L/RSV: left/right sinus venosus, V: ventricle. χ^2–test was performed for categorical values and two-way ANOVA with Bonferroni post-hoc test.*: p< 0.05; **: p< 0.005.

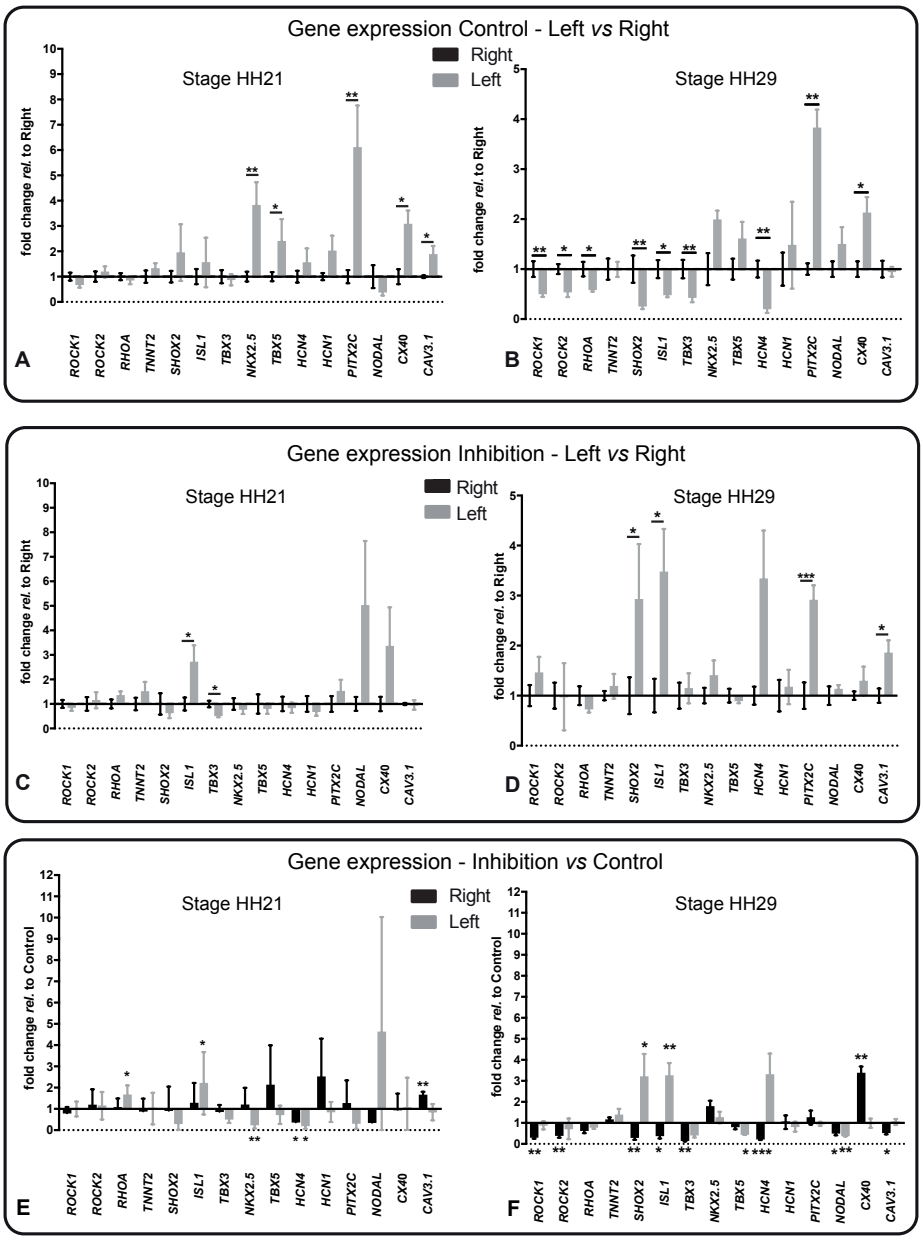

Figure 3. Hampered lateralization and pacemaker specification in sinoatrial myocardium

A. qPCR analysis of expression genes of interest, right (black bars) *vs* left (gray bars) sinoatrial myocardium, control HH21 chicken embryonic hearts (n=5-7). **B**. qPCR analysis of expression genes of interest, right (black bars) *vs* left (gray bars) sinoatrial myocardium, control HH29 chicken embryonic hearts (n=4-6). Levels shown relative to right side. **C,E**. qPCR analysis of expression genes of interest at stage HH21 after ROCK inhibition (n=4-8) for right (black bars) *vs* left (gray bars) sinoatrial myocardium. **D,F**. qPCR analysis of genes of interest at stage HH29 after ROCK inhibition (n=4-8) for the sinoatrial myocardium. In **C** and **D**, levels shown relative to right side. In **E** and **F**, levels shown relative to control counterpart. Dotted line represents 0. *, p<0.05; **, p<0.01; ***, p<0.001.

3.3. ROCK INHIBITION AND SAN DIFFERENTIATION: HAMPERED LATERALIZATION AND PACEMAKER SPECIFICATION

Based on the electrophysiology results, qPCR analysis was conducted on separate right and left portions of the sinoatrial myocardium to assess pacemaker gene expression patterns. The identity of the isolated portions was confirmed by expression of transcription factors important in SAN differentiation like *SHOX2*[21], *TBX3*[23], and *ISL1*[16], the ion channels necessary for pacemaking *HCN4* and *HCN1*[30, 31] and low levels of the SAN inhibitory transcription factor *NKX2.5*[24] and gap junction protein *Connexin (CX) 40,* highly expressed in atrial myocardium.[18,27]

Early in development, at HH21, control hearts showed that nearly all genes studied (i.e. genes of the ROCK pathway, transcription factors important in SAN differentiation) were equally expressed between right and left-sided sinoatrial myocardium (**Fig. 3A**). Significant differences encountered at this stage were higher expression of *NKX2.*5 (p=0.0087), *TBX5* (p=0.0159), *CX40* (p=0.0159), *CAV3.1* (p=0.0159) and the left-sided identity gene *PITX2C*[18,27] in the left side of the sinoatrial myocardium, as expected (p= 0.0023, **Fig. 3A**).

Later in development, at HH29, significant differences between the right and left sides of the sinoatrial myocardium became more apparent (**Fig. 3B**). The levels of expression of *RHOA*, *ROCK1* and *ROCK2* were significantly lower in the left side. The genetic profile of the inflow tract at HH29 on the right side of this region showed persistent expression of transcription factors and ion channels essential for proper SAN function, whereas the left side showed significantly lower levels of *SHOX2* (p=0.0087), *ISL1* (p=0.0173), *TBX3* (p=0.0079) and *HCN4* (p=0.0022) and significantly higher levels of *CX40* (p=0.0317), and *PITX2C* (p=0.0043) (**Fig. 3B**). Thus, functional and morphological changes showed that the definitive pacemaker of the normal heart will be right-sided.

At HH21 after ROCK inhibition, expression of *ISL1* was significantly higher (p=0.0401) and *TBX3* significantly lower on the left side of the sinus venosus (p=0.0148) (**Fig. 3C**). At HH29, levels of *SHOX2* (p=0.0186), *ISL1* (p=0.0293), *PITX2C* (p=0.0007) and *CAV3.1* (p=0.0451) were significantly higher in the left side compared to the right side (**Fig. 3D**).

Gene expression levels after ROCK inhibition were compared to control levels. At HH21, differences in gene expression levels after ROCK inhibition compared to control became apparent (**Fig. 3E**). *HCN4* (p=0.0293), and *NKX2.5* (p=0.0031) levels were lower in the left side, and *ISL1* (p=0.035) and *RHOA* expression were higher (p=0.037) (**Fig. 3E**). In the right side, only *HCN4* expression was significantly lower (p=0.0293) while *CAV3.1* expression was significantly higher in the right side (p=0.0079) (**Fig. 3E**). At HH29, levels of *SHOX2* (p=0.0173), and *ISL1* (p=0.0079) were significantly higher in the left side

whereas *TBX5* (p=0.0317) and *NODAL* (p=0.0043) were significantly lower. In the right side, levels of *SHOX2* (p=0.008), *ISL1* (p=0.02), *TBX3* (p=0.0025), *HCN4* (p=0.0007), and *CAV3.1* (p=0.0451), important for pacemaker development, were low relative to controls. Levels of *CX40* (p=0.0095), normally found in atrial myocardium, were high (**Fig. 3F**). In accordance with the functional data, after ROCK inhibition, the left-sided SAN region still showed a SAN-like phenotype (explaining the maintained pacemaker functionality in the left side) while the differentiation of the definitive right-sided SAN area was impaired (explaining the decreased heart rate observed in the inhibited hearts).

3.4. ABERRANT SINUS VENOSUS DIFFERENTIATION AND ABNORMAL PULMONARY VEIN DEVELOPMENT AFTER ROCK INHIBITION

Gene expression analysis revealed abnormal expression of *ISL1* after ROCK inhibition. During normal heart development, a portion of the sinus venosus myocardium including the definitive right-sided SAN expressed ISL1 (**Fig. 4A,G**) as well as a large proportion of the mesodermal cells dorsal to the heart (**Fig. 4C**). In controls, ISL1 expression was restricted to the right-sided SAN at late stages of differentiation (**Fig. 3B,F**, compare **4A** to **4G**). However, after ROCK inhibition, this *ISL1* balance was disrupted. At HH26 ROCK inhibition resulted in an overall increase in ISL1+ sinus venosus myocardium, especially in the left portion (compare **Fig. 4A** to **B**). This upregulation was still evident at HH29 (compare **Fig. 4G** to **H**), supporting the qPCR results (**Fig. 3E** and **F**).

Normally, the ISL1+ sinus venosus myocardium is negative for NKX2.5. In accordance with the gene expression analysis, ROCK inhibited hearts showed an increase in ISL1+/NKX2.5- myocardium on the left side and a decrease on the right side (compare **Fig. 4D** to **F**). At HH26, this increase in ISL1+ cells in ROCK inhibited hearts was also observed in the mesoderm dorsal to the heart, where the pulmonary vein is developing (compare **Fig. 4C** to **Fig. 4E**). Later in development (HH29), in 4/5 cases ROCK inhibition caused aberrant positioning of the entrance of the common pulmonary vein into the left atrium, including one case in which the right pulmonary veins entered the right portion of the sinus venosus (**Fig. 4H**).

3.5. THE EFFECT OF ROCK INHIBITION ON HEART RATE IS SPECIFIC FOR THE SINOATRIAL CARDIOMYOCYTES

Since ROCK inhibition was applied to the entire heart, we next examined whether effects observed on SAN function and development were specific for the sinoatrial myocardium. MEA experiments were performed on isolated sinoatrial and atrial (only appendages) cells of HH26-27 control and ROCK-inhibitor

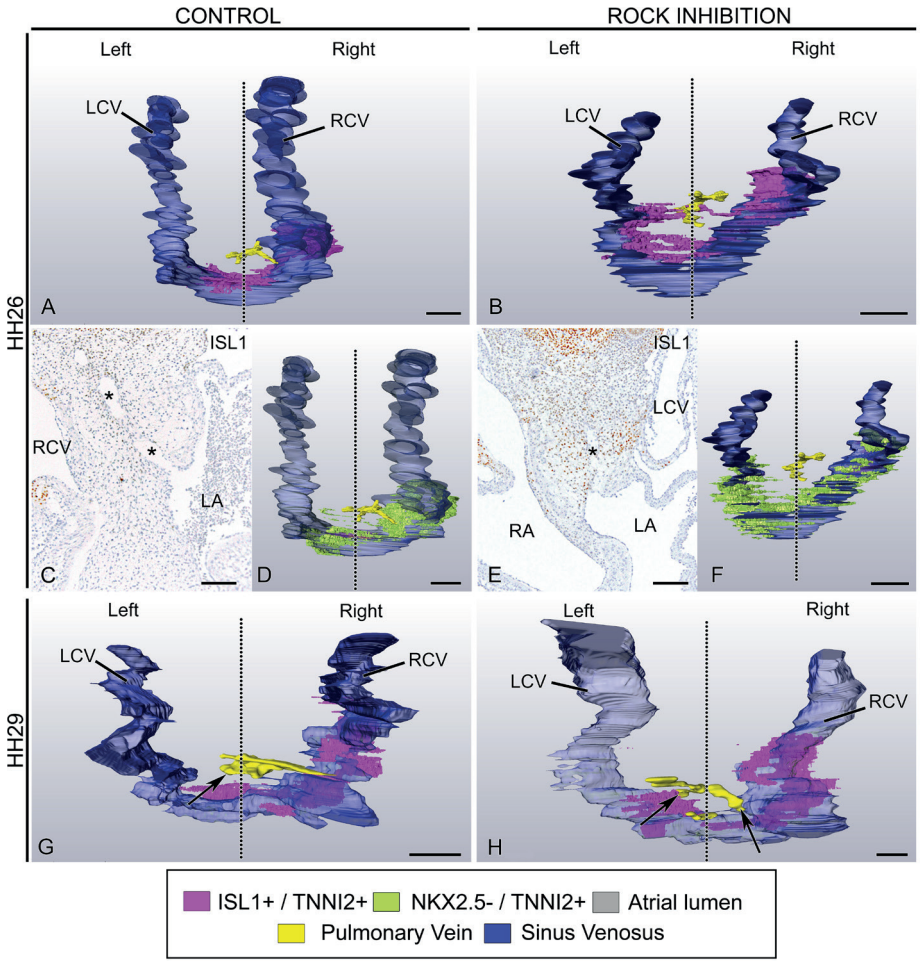

Figure 4. Aberrant sinus venosus differentiation and pulmonary vein formation after inhibition of ROCK signaling

Posterior view of 3D reconstructions of HH26 control (**A**) and ROCK inhibition (**B**). ISL1+/TNNI2+ myocardium is depicted in purple, right and left cardinal vein (R/LCV) lumen in transparent blue and pulmonary pit or vein in yellow. ISL1 staining of a HH26 control (**C**) and ROCK inhibition (**E**) heart showing ISL1 expression in non-myocardial area surrounding the lumen of the pulmonary vein (*). **D** and **F** show posterior views of the same 3D reconstruction as in **A** and **B** but with the NKX2.5 negative myocardium in lime green. Posterior view of 3D reconstructions of HH29 control (**G**) and ROCK inhibition (**H**) sinus venosus with the same color coding as in **A-B**. Dotted line in 3D reconstructions separates the right from the left sinus venosus portions. L/RA: left/right atrium, L/RCV: left/right cardinal vein. Scale bars: **A-B, G-H, G1-G2, H1-H2**: 200μm, **C-D**: 100μm.

treated embryonic chicken hearts. Results showed a decrease in heart rate (**Fig. 5A**) when ROCK signaling was inhibited in sinoatrial cardiomyocytes, but no effect on heart rate in atrial cardiomyocytes was observed (**Fig. 5B**). ROCK inhibition did affect signal amplitude in both sinoatrial and atrial cardiomyocytes (**Supplemental Fig. 4**). As an internal control, the same experiment was performed on ventricular cardiomyocytes and no effect on rate or amplitude was observed (**Supplemental Fig. 5**). This showed that the effect of inhibiting ROCK signaling was specific for the sinoatrial myocardium including the developing SAN.

3.6. ROCK INHIBITION DELAYS ACTION POTENTIAL MATURATION AND CAUSES PERSISTENT PACEMAKER POTENTIAL ON THE LEFT SIDE

To assess the electrophysiological maturation status of sinus venosus cardiomyocytes after ROCK inhibition, patch clamp electrophysiology was performed at HH29 (**Fig. 5C-J**). During normal development, maturation of the action potential was observed (compare **Fig. 5C** (HH29) to **Fig. 5E** (HH20)). After ROCK inhibition, the action potential of sinoatrial cardiomyocytes resembled that of HH20 sinoatrial cardiomyocytes more closely than HH29 untreated sinoatrial cardiomyocytes (**Fig. 5C-E**). This immaturity was confirmed by a significant decrease in maximal upstroke velocity (dV/dT, p=0.0035, **Fig. 5F**), action potential amplitude (p=0.011, **Fig. 5H**) and resting membrane potential (p=0.037, **Fig. 5J**), which bore more resemblance to early HH20 sinoatrial cardiomyocytes.

Right-left sinoatrial differences were also assessed after ROCK inhibition (**Fig. 6**). Immaturity was observed in both right and left-sided sinoatrial cardiomyocytes after ROCK inhibition (**Fig. 6A-D**). However, after ROCK inhibition, sinoatrial cardiomyocytes from the left side showed characteristics similar to that of the right side (definitive pacemaker), in concordance with the right-sided phenotype observed with qPCR. The action potential duration (APD90) was significantly increased (p=0.046) and the significant difference with the control group when compared to the right side (p<0.0001) was no longer apparent (p=0.307, **Fig. 6F**). The action potential amplitude was significantly lower on both sides after inhibition (p=0.014 for right and p<0.0001 for left, **Fig. 6G**) and the maximum diastolic potential significantly lower in the left-sided sinoatrial cardiomyocytes compared to control (p=0.0016).

Overall, the left-sided sinoatrial cardiomyocytes shared more properties of the right side after ROCK inhibition, indicative of persistent pacemaker potential on the left side.

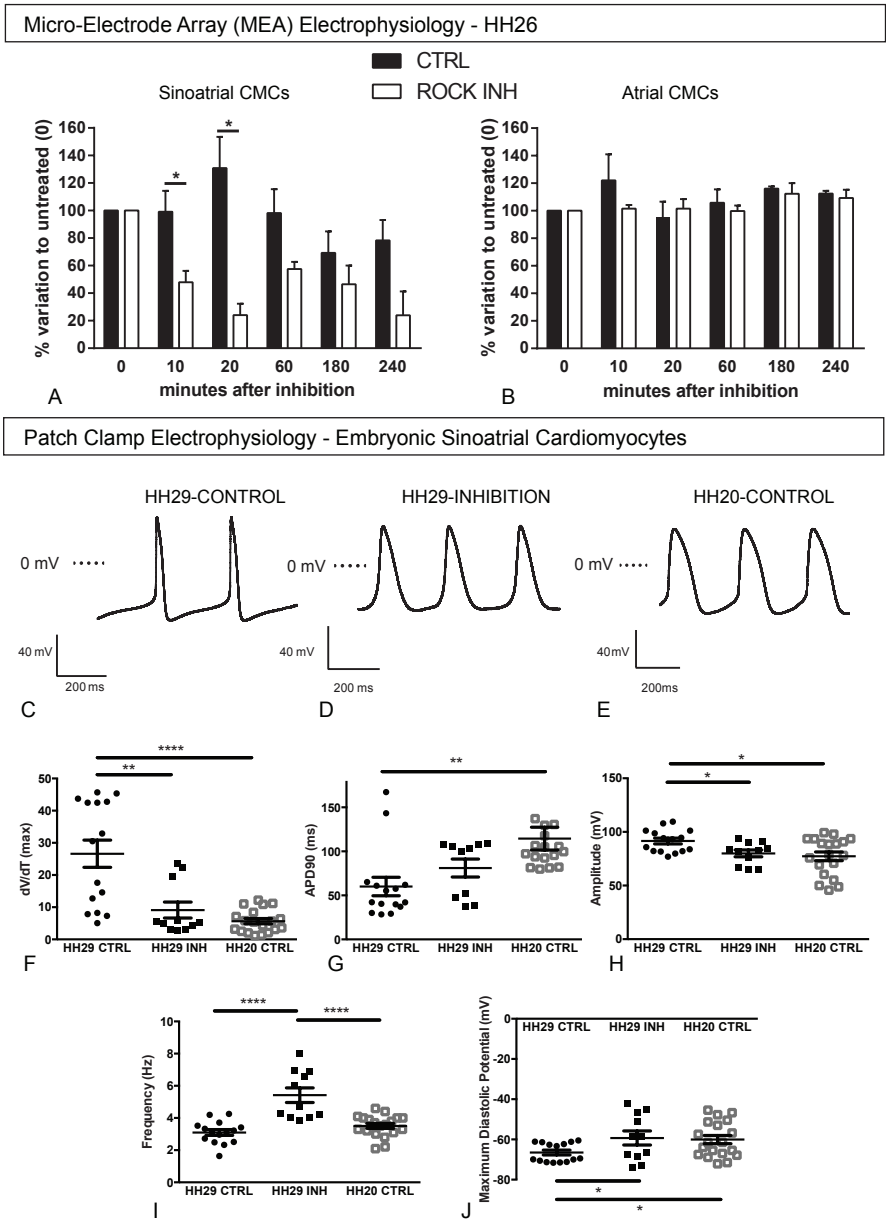

Figure 5. ROCK inhibition reduces the heart rate specifically in sinoatrial cardiomyocytes

A. % Of rate variation compared to time point zero (0) of sinoatrial cardiomyocyte cell cultures at various time points (up to 240 min) after treatment with ROCK inhibitor (ROCK INH; n=9) or PBS (CTRL; n=7). **B**. % Of rate variation compared to time point zero (0) of atrial cardiomyocytes (with no SAN cardiomyocytes) after treatment with ROCK inhibitor (ROCK INH; n=7) or PBS (CTRL; n=7). **C-E.** Representative tracings of sinoatrial cardiomyocytes from HH29 control (**C**, HH29 CTRL), HH29 ROCK inhibition (**D**, HH29 INH) and HH20 control (**E**, HH20 CTRL). 17-19 cells analyzed per group. **F-J.** Scatter plots showing maximum upstroke velocity (**F**), action potential duration (APD)90 (**G**), amplitude (**H**), frequency (**I**) and maximum diastolic potential (**J**). One or two-way ANOVA analyses were performed with Bonferroni post-hoc tests.*, p<0.05; ** p<0.01; ***, p<0.001; ****, p<0.0001.

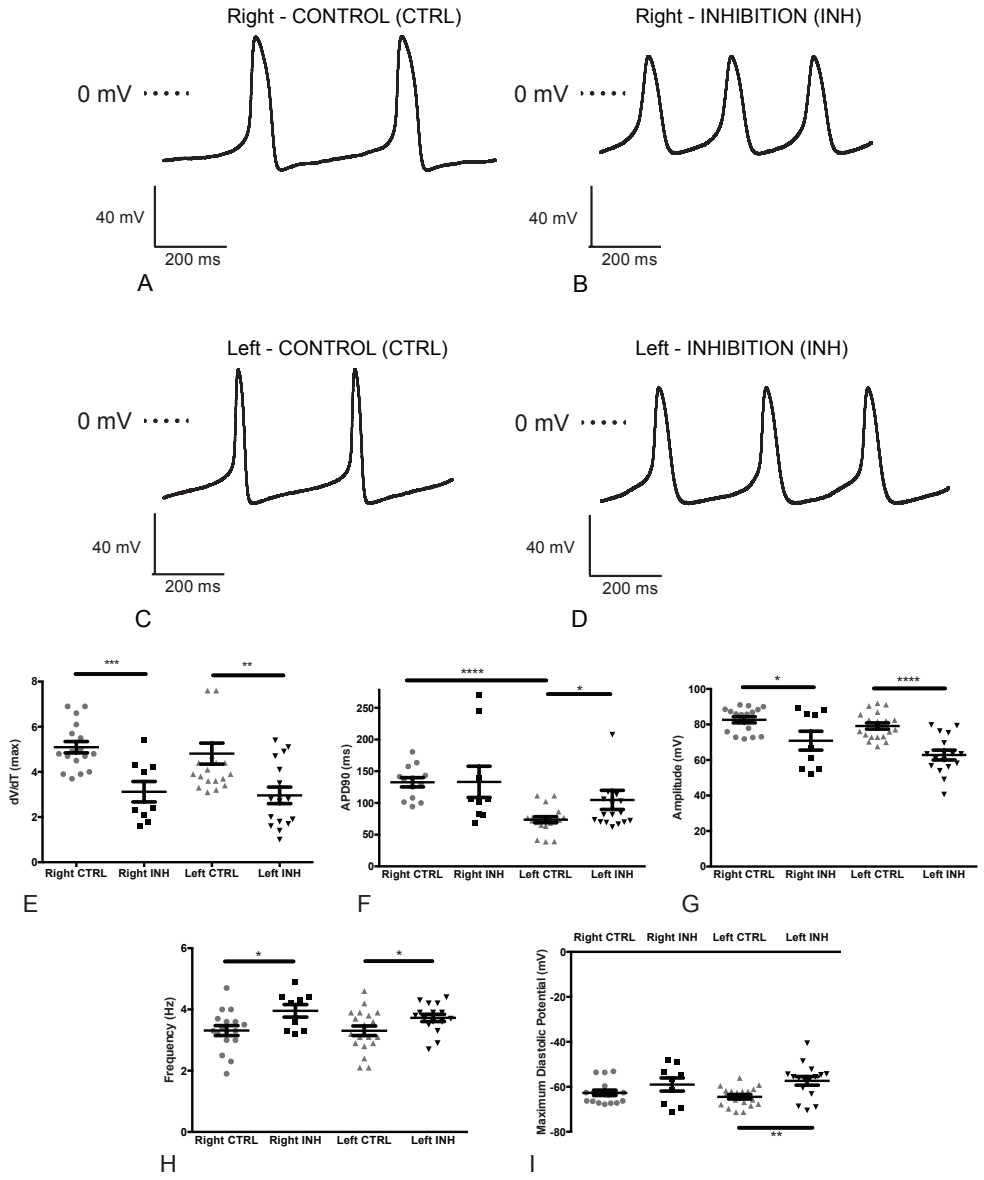

Figure 6. Right-left differences in sinus venosus cardiomyocytes after ROCK inhibition

A-D. Representative tracings of sinoatrial cardiomyocytes from right control (**A**), right ROCK inhibition (**B**), left control (**C**) and left ROCK inhibition (**D**). 17 to 19 cells were analyzed per group. **E-I**. Scatter plots showing maximum upstroke velocity (**E**), action potential duration (APD)90 (**F**), amplitude (**G**), frequency (**H**) and maximum diastolic potential (**I**). One-way ANOVA with Bonferroni post-hoc test was performed.*, p<0.05; ** p<0.01; ***, p<0.001; ****, p<0.0001.

4. DISCUSSION

In this study, changes in function and gene expression in the SAN region before full development of the definitive right-sided SAN were described. Rho kinase inhibitors wield a dual effect on the developing SAN. On the one hand, ROCK inhibition results in immaturity of the right-sided SAN and prolonged pacemaker potential of the transient left-sided SAN, reflecting overall immaturity of the sinus venosus myocardium. On the other hand, it results in gap junction and ion channel remodeling of the developing SAN, impairing proper conduction through this myocardium.

4.1. ROCK SIGNALING AND LATERALIZATION OF THE SAN

Left-right (LR) asymmetry is observed in the entire body plan; establishing this normal asymmetry correctly is essential in determining the position and structure of internal organs, including the heart. Abnormalities in LR asymmetry lead to laterality disorders including complex congenital heart diseases.[32,33] Asymmetric expression of *NODAL, LEFTY* and members of the *PITX2* gene family in the lateral plate mesoderm are essential for proper LR-asymmetry. This asymmetry is likely established early in development by the pre-determined antero-posterior and dorso-ventral axis in the embryonic plate.[33] Recently it was demonstrated that RHOA-ROCK signaling is involved in LR-asymmetry. *ROCK2B* knockdown in zebrafish resulted in abnormal asymmetric gene expression in the lateral plate mesoderm and abnormal LR-patterning in organs.[6] In mouse and chicken, disruption of ROCK signaling using the small molecule inhibitor Y-27632 results in cardiac defects and bilateral expression of *NODAL* in the lateral plate mesoderm in chicken embryos.[3]

Although Y-27632 has inhibitory effects on protein kinases other than ROCK1/2, its affinity for Rho kinases is more than 200-fold higher.[3,34] The present study showed that treatment with Y-27632 resulted in lower levels of *ROCK2* expression. However, further research is required to assess whether the effect of Y-27632 on SAN development is exclusively through downregulation of ROCK1/2. Chicken embryos studied here showed abnormal levels of *NODAL* in the left side of the sinoatrial myocardium. Thus, RHOA-ROCK signaling may play an important role in determining LR-asymmetry early in development, specifically in establishing right-sidedness in the sinus venosus myocardium, important for proper establishment of the right-sided SAN as definitive pacemaker of the heart.

4.2. ROCK SIGNALING AND SAN DIFFERENTIATION: GENE TRANSCRIPTION REGULATION AND FUNCTION

Inhibition of ROCK signaling during early developmental stages resulted in immature sinus venosus myocardium and abnormal SAN gene expression patterns. The definitive right-sided SAN is inefficient and its transient left-sided part retained its pacemaker potential. This results in impaired SAN function reflected by bradycardia at older developmental stages and in an immature area prone to arrhythmias, including structures with known arrhythmogenic potential like the pulmonary veins.[11, 12] Limited SAN function was already reported in mice with aberrant ROCK signaling, but the mechanism remains unknown.[7, 8] Based on results presented here, abnormal SAN function reflects abnormal differentiation of the SAN myocardium. A complex genetic transcriptional network involved in SAN differentiation was established over the past decade. However, new interactions and key players in SAN development keep arising. Among these are the transcription factors *Tbx3*[23], *Shox2*[21,35], *Nkx2.5*[24], *Pitx2c*[36] and *Isl1*[16,37] (reviewed in[25]). These are linked since they can exert inhibitory or activating effects on each another in complex feedback loops. Emerging evidence supports a role for RHOA-ROCK signaling in regulation of molecular pathways involved in early cardiogenesis.[3,5] More specifically Rho-Kinase inhibitors can either impair[5] or promote[38] cardiac differentiation *in vitro* altering the expression of key genes in early cardiac lineages like *GATA4, ISL1* and *TBX5*.[5, 38] In our study, at late developmental stages, low levels of *ROCK1* and *ROCK2* in the right portion of the sinoatrial myocardium were accompanied by low levels of expression of key transcription factors necessary for proper SAN differentiation (*ISL1, SHOX2*, *TBX3,* and *HCN4,* **Fig. 3**). Myocardial transcriptional targets of the RHOA-ROCK pathway are *SRF, GATA4, α-ACTIN, TBX5* and *ISL1.*[3,5,38] This signaling pathway may be involved in regulating the transcriptional network necessary for proper SAN differentiation, since dysregulation of this pathway in adult mice leads to several CCS abnormalities.[7,8] ROCK can control the activity of LIM kinases[1] and can therefore regulate proteins containing LIM domains, such as ISL1. A direct effect of ROCK on ISL1 expression has yet to be discovered. The dysregulation of *ISL1* expression is observed in both the myocardial (TNNI2+) as well as the TNNI2- cell population dorsal to the heart. Expression of *Isl1* in the developing SAN (i.e. the myocardial population) is important for proper SAN differentiation[37] and function.[16] Putative binding sites for *Isl1* were identified within the regulatory regions of *Tbx3* and *Hcn4*, suggesting a novel regulatory function of *Isl1* within the SAN gene program.[37]

ISL1 expression in the mesenchymal population is important for normal pulmonary vein development.[39] This is interesting in the light of the arrhythmogenic potential attributed to the pulmonary venous myocardial

sleeves, as well as the potential involvement of the RHOA-ROCK signaling pathway in anomalous pulmonary venous connections.[12] A well-kept Shox2 and Nkx2.5 balance has recently been described as the mechanism that ensures the non-pacemaker phenotype of the pulmonary venous myocardial sleeve during development.[40] In this study, *SHOX2* and *ISL1* are abnormally expressed in the venous pole of the heart, potentially leading to an increased arrhythmogenic potential due to abnormal/insufficient differentiation.

To ensure coordination between propagation of the pacemaking signal and contraction of the chambers, electrical heterogeneity of the myocardium is required. This is accomplished by differential expression of connexins and ion channels within the chambers.[41] For instance, high levels of Cx40 expression in the atrial myocardium ensure rapid propagation of the electrical impulse from the SAN to allow for simultaneous atrial contraction.[21,24,27] The abnormal conduction through the sinus venosus myocardium found in this study could be due to the effect of RHOA-ROCK signaling on ion channel expression or activity. This could account for the electrophysiological differences observed in SAN electrophysiology between whole-heart and single-cell measurements. Altered Rho-signaling has been associated with abnormalities in expression of Cx40[8] and 43[42], and L-type Ca2+ channels.[43] Expression of Cx40 was altered after Rho-kinase inhibition, resulting in high expression in the right-sided SAN (**Fig. 3**). In the chick heart, expression of connexins (40, 43, and 45) is different than in mammals.[44] Expression of all 3 connexins was studied but only Cx40 is of relevance in the developing chick SAN. Given the direct regulatory role of the RHOA-ROCK pathway on Cx43 expression in myocardial cells, this pathway could be involved in regulating Cx40 expression during development. In the mouse heart, L-type Cav1.2 and T-type Cav3.1 Ca2+ channels are highly expressed in the SAN.[45] Since RHOA has been found to regulate L-type Ca2+ currents in ventricular cardiomyocytes[43] and mice lacking T-type Cav3.1 Ca2+ channels show bradycardia[45], we studied its expression pattern in the developing SAN and the effects of ROCK inhibition. After ROCK inhibition, expression levels of Cav3.1 were altered, specifically in the right-sided SAN (**Fig. 3**). Additional experiments are necessary to unravel the mechanism by which RHOA can regulate Cav3.1 expression and/or activity, as observed in ventricular cardiomyocytes for Cav1.2.[43]

4.3. RHOA-ROCK SIGNALING IN HUMAN DISEASE

Human genetic studies have linked abnormal RHOA-ROCK signaling with several congenital heart abnormalities. Specifically, low frequency variants in the *ROCK1* gene have been associated with a higher risk of developing tetralogy of Fallot.[46] Mutations in the protein phosphatase *SHP-2* have been linked to Noonan

and Leopard syndrome, both frequently associated with congenital heart abnormalities like pulmonary valve stenosis, hypertrophic cardiomyopathy or conduction abnormalities. Missense mutations in *SHP-2* in these patients cause hyperactivation of the RHOA-ROCK pathway.[47] Additionally, trisomy 18 and 21 foetuses show higher levels of *ROCK1* RNA, and the *ROCK1* gene is located on chromosome 18 in humans.[48] RHOA was found to regulate Cx43 expression, providing a plausible disease mechanism for these patients.[42] These data suggest a role for RHOA-ROCK signaling in human cardiac diseases.

Overall, RHOA-ROCK signaling is essential for establishing the right-sided SAN as definitive pacemaker of the adult heart. Abnormal RHOA-ROCK signaling results in an immature sinus venosus myocardium, including the SAN, and ectopic maintenance of a pacemaker phenotype in the left-sided sinus venosus.

REFERENCE LIST

1. Amin E, Dubey BN, Zhang SC, Gremer L, Dvorsky R, Moll JM, Taha MS, Nagel-Steger L, Piekorz RP, Somlyo AV, Ahmadian MR. Rho-kinase: regulation, (dys) function, and inhibition. *Biol. Chem.* 2013;**394**:1399-1410.

2. Surma M, Wei L, Shi J. Rho kinase as a therapeutic target in cardiovascular disease. *Future Cardiol.* 2011;**7**:657-671.

3. Wei L, Roberts W, Wang L, Yamada M, Zhang S, Zhao Z, Rivkees SA, Schwartz RJ, Imanaka-Yoshida K. Rho kinases play an obligatory role in vertebrate embryonic organogenesis. *Development.* 2001;**128**:2953-2962.

4. Kaarbø M, Crane DI, Murrell WG. RHOA is highly up-regulated in the process of early heart development of the chick and important for normal embryogenesis. *Dev. Dyn.* 2003;**227**:35-47.

5. Kaarbø M, Crane DI, Murrell WG. RHOA regulation of cardiomyocyte differentiation. *ScientificWorldJournal.* 2013;**2013**:491546.

6. Wang G, Cadwallader AB, Jang DS, Tsang M, Yost HJ, Amack JD. The Rho kinase Rock2b establishes anteroposterior asymmetry of the ciliated Kupffer's vesicle in zebrafish. *Development.* 2011;**138**:45-54.

7. Sah VP, Minamisawa S, Tam SP, Wu TH, Dorn GW, Ross J, Jr., Chien KR, Brown JH. Cardiac-specific overexpression of RHOA results in sinus and atrioventricular nodal dysfunction and contractile failure. *J. Clin. Invest.* 1999;**103**:1627-1634.

8. Wei L, Taffet GE, Khoury DS, Bo J, Li Y, Yatani A, Delaughter MC, Klevitsky R, Hewett TE, Robbins J, Michael LH, Schneider MD, Entman ML, Schwartz RJ. Disruption of Rho signaling results in progressive atrioventricular conduction defects while ventricular function remains preserved. *FASEB. J.* 2004;**18**:857-859.

9. Vicente-Steijn R, Kolditz DP, Mahtab EA, Askar SF, Bax NA, van der Graaf LM, Wisse LJ, Passier R, Pijnappels DA, Schalij MJ, Poelmann RE, Gittenberger-de Groot AC, Jongbloed MR. Electrical activation of sinus venosus myocardium and expression patterns of RHOA and Isl-1 in the chick embryo. *J. Cardiovasc. Electrophysiol.* 2010;**21**:1284-1292.

10. Ko JK, Deal BJ, Strasburger JF, Benson DW, Jr. Supraventricular tachycardia mechanisms and their age distribution in pediatric patients. *Am. J. Cardiol.* 1992;**69**:1028-1032.

11. Shah DC, Jais P, Haissaguerre M, Chouairi S, Takahashi A, Hocini M, Garrigue S, Clementy J. Three-dimensional mapping of the common atrial flutter circuit in the right atrium. *Circulation.* 1997;**96**:3904-3912.

12. Haissaguerre M, Jais P, Shah DC, Takahashi A, Hocini M, Quiniou G, Garrigue S, Le MA, Le MP, Clementy J. Spontaneous initiation of atrial fibrillation by ectopic beats originating in the pulmonary veins. *N. Engl. J. Med.* 1998;**339**:659-666.

13. Vicente-Steijn R, Passier R, Wisse LJ, Schalij MJ, Poelmann RE, Gittenberger-de Groot AC, Jongbloed MR. Funny current channel HCN4 delineates the developing cardiac conduction system in chicken heart. *Heart Rhythm.* 2011;**8**:1254-63.

14. Harvey PA, Leinwand LA. The cell biology of disease: cellular mechanisms of cardiomyopathy. *J. Cell. Biol.* 2011;**194**:355-365.

15. Cai CL, Liang X, Shi Y, Chu PH, Pfaff SL, Chen J, Evans S. Isl1 identifies a cardiac progenitor population that proliferates prior to differentiation and contributes a majority of cells to the heart. *Dev. Cell.* 2003;**5**:877-889.

16. Hoffmann S, Berger IM, Glaser A, Bacon C, Li L, Gretz N, Steinbeisser H, Rottbauer W, Just S, Rappold G. Islet1 is a direct transcriptional target of the homeodomain transcription factor Shox2 and rescues the Shox2-mediated bradycardia. *Basic Res Cardiol.* 2013;**108**:339.

17. Kamino K, Hirota A, Fujii S. Localization of pacemaking activity in early embryonic heart monitored using voltage-sensitive dye. *Nature.* 1981;**290**:595-597.

18. Ammirabile G, Tessari A, Pignataro V, Szumska D, Sutera SF, Benes J, Jr., Balistreri M, Bhattacharya S, Sedmera D, Campione M. Pitx2 confers left morphological, molecular, and functional identity to the sinus venosus myocardium. *Cardiovasc. Res.* 2012;**93**:291-301.

19. Yi T, Wong J, Feller E, Sink S, Taghli-Lamallem O, Wen J, Kim C, Fink M, Giles W, Soussou W, Chen HS. Electrophysiological mapping of embryonic mouse hearts: mechanisms for developmental pacemaker switch and internodal conduction pathway. *J. Cardiovasc. Electrophysiol.* 2012;**23**:309-318.

20. Gittenberger-de Groot AC, Mahtab EAF, Hahurij ND, Wisse LJ, DeRuiter MC, Wijffels MCEF, Poelmann RE. Nkx2.5 negative myocardium of the posterior heart field and its correlation with podoplanin expression in cells from the developing cardiac pacemaking and conduction system. *Anat. Rec.* 2007;**290**:115-122.

21. Blaschke RJ, Hahurij ND, Kuijper S, Just S, Wisse LJ, Deissler K, Maxelon T, Anastassiadis K, Spitzer J, Hardt SE, Schöler H, Feitsma H, Rottbauer W, Blum M, Meijlink F, Rappold GA, Gittenberger-de Groot AC. Targeted mutation reveals essential functions of the homeodomain transcription factor Shox2 in sinoatrial and pacemaking development. *Circulation.* 2007;**115**:1830-1838.

22. Christoffels VM, Mommersteeg MT, Trowe MO, Prall OW, de Gier-de Vries C, Soufan AT, Bussen M, Schuster-Gossler K, Harvey RP, Moorman AF, Kispert A. Formation of the venous pole of the heart from an Nkx2-5-negative precursor population requires Tbx18. *Circ. Res.* 2006;**98**:1555-1563.

23. Hoogaars WM, Tessari A, Moorman AF, de Boer PA, Hagoort J, Soufan AT, Campione M, Christoffels VM. The transcriptional repressor Tbx3 delineates the developing central conduction system of the heart. *Cardiovasc. Res.* 2004;**62**:489-499.

24. Espinoza-Lewis RA, Liu H, Sun C, Chen C, Jiao K, Chen Y. Ectopic expression of Nkx2.5 suppresses the formation of the sinoatrial node in mice. *Dev. Biol.* 2011;**356**:359-369.

25. Jongbloed MR, Vicente-Steijn R, Hahurij ND, Kelder TP, Schalij MJ, Gittenberger-de Groot AC, Blom NA. Normal and abnormal development of the cardiac conduction system; implications for conduction and rhythm disorders in the child and adult. *Differentiation.* 2012;**84**:131-148.

26. Kirchhof P, Kahr PC, Kaese S, Piccini I, Vokshi I, Scheld HH, Rotering H, Fortmueller L, Laakmann S, Verheule S, Schotten U, Fabritz L, Brown NA. PITX2c is expressed in the adult left atrium, and reducing Pitx2c expression promotes atrial fibrillation inducibility and complex changes in gene expression. *Circ. Cardiovasc. Genet.* 2011;**4**:123-133.

27. Wang J, Klysik E, Sood S, Johnson RL, Wehrens XH, Martin JF. Pitx2 prevents susceptibility to atrial arrhythmias by inhibiting left-sided pacemaker specification. *Proc. Natl. Acad. Sci. USA.* 2010;**107**:9753-9758.

28. Calkoen EE, Vicente-Steijn R, Hahurij ND, van Munsteren CJ, Roest AA, DeRuiter MC, Steendijk P, Schalij MJ, Gittenberger-de Groot AC, Blom NA, Jongbloed MR. Abnormal sinoatrial node development resulting from disturbed vascular endothelial growth factor signaling. *Int. J. Cardiol.* 2015;**183**:249-257.

29. Kelder TP, Vicente-Steijn R, Harryvan TJ, Kosmidis G, Gittenberger-de Groot AC, Poelmann RE, Schalij MJ, DeRuiter MC, Jongbloed MR. The sinus venosus myocardium contributes to the atrioventricular canal: potential role during atrioventricular node development? *J. Cell. Mol. Med.* 2015**;19:**1375–89.

30. Stieber J, Herrmann S, Feil S, Loster J, Feil R, Biel M, Hofmann F, Ludwig A. The hyperpolarization-activated channel HCN4 is required for the generation of pacemaker action potentials in the embryonic heart. *Proc. Natl. Acad. Sci. USA.* 2003;**100**:15235-15240.

31. Fenske S, Krause SC, Hassan SI, Becirovic E, Auer F, Bernard R, Kupatt C, Lange P, Ziegler T, Wotjak CT, Zhang H, Hammelmann V, Paparizos C, Biel M, Wahl-Schott CA. Sick sinus syndrome in HCN1-deficient mice. *Circulation.* 2013;**128**:2585-2594.

32. Raya A, Izpisua Belmonte JC. Left-right asymmetry in the vertebrate embryo: from early information to higher-level integration. *Nat. Rev. Genet.* 2006;**7**:283-293.

33. Kato Y. The multiple roles of Notch signaling during left-right patterning. *Cell. Mol. Life. Sci.* 2011;**68**:2555-2567.

34. Uehata M, Ishizaki T, Satoh H, Ono T, Kawahara T, Morishita T, Tamakawa H, Yamagami K, Inui J, Maekawa M, Narumiya S. Calcium sensitization of smooth muscle mediated by a Rho-associated protein kinase in hypertension. *Nature.* 1997;**389**:990-994.

35. Espinoza-Lewis RA, Yu L, He F, Liu H, Tang R, Shi J, Sun X, Martin JF, Wang D, Yang J, Chen Y. Shox2 is essential for the differentiation of cardiac pacemaker cells by repressing Nkx2-5. *Dev. Biol.* 2009;**327**:376-385.

36. Lozano-Velasco E, Chinchilla A, Martinez-Fernandez S, Hernandez-Torres F, Navarro F, Lyons GE, Franco D, Aranega AE. Pitx2c modulates cardiac-specific transcription factors networks in differentiating cardiomyocytes from murine embryonic stem cells. *Cells Tissues Organs.* 2011;**194**:349-362.

37. Vedantham V, Galang G, Evangelista M, Deo RC, Srivastava D. RNA sequencing of mouse sinoatrial node reveals an upstream regulatory role for Islet-1 in cardiac pacemaker cells. *Circ. Res.* 2015;**116**:797-803.

38. Cheng YT, Yeih DF, Liang SM, Chien CY, Yu YL, Ko BS, Jan YJ, Kuo CC, Sung LY, Shyue SK, Chen MF, Yet SF, Wu KK, Liou JY. Rho-associated kinase inhibitors promote the cardiac differentiation of embryonic and induced pluripotent stem cells. *Int. J. Cardiol.* 2015;**201**:441-448.

39. Mommersteeg MT, Brown NA, Prall OW, de Gier-de Vries C, Harvey RP, Moorman AF, Christoffels VM. Pitx2c and Nkx2-5 are required for the formation and identity of the pulmonary myocardium. *Circ. Res.* 2007;**101**:902-909.

40. Ye W, Wang J, Song Y, Yu D, Sun C, Liu C, Chen F, Zhang Y, Wang F, Harvey RP, Schrader L, Martin JF, Chen Y. A common Shox2-Nkx2-5 antagonistic mechanism primes the pacemaking cell fate in the pulmonary vein myocardium and sinoatrial node. *Development.* 2015.

41. Kleber AG, Rudy Y. Basic mechanisms of cardiac impulse propagation and associated arrhythmias. *Physiol. Rev.* 2004;**84**:431-488.

42. Wang L, Liu S, Zhang H, Hu S, Wei Y. RHOA activity increased in myocardium of arrhythmogenic cardiomyopathy patients and affected connexin 43 protein expression in HL-1 cells. *Int. J. Clin. Exp. Med.* 2015;**8**:12906-12913.

43. Yatani A, Irie K, Otani T, Abdellatif M, Wei L. RHOA GTPase regulates L-type Ca2+ currents in cardiac myocytes. *Am. J. Physiol. Heart Circ. Physiol.* 2005;**288**:H650-H659.

44. Wiens D, Jensen L, Jasper J, Becker J. Developmental expression of connexins in the chick embryo myocardium and other tissues. *Anat. Rec.* 1995;**241**:541-553.

45. Marionneau C, Couette B, Liu J, Li H, Mangoni ME, Nargeot J, Lei M, Escande D, Demolombe S. Specific pattern of ionic channel gene expression associated with pacemaker activity in the mouse heart. *J. Physiol.* 2005;**562**:223-234.

46. Palomino DJ, Topf A, Bentham J, Bhattacharya S, Cosgrove C, Brook JD, Granados-Riveron J, Bullock FA, O'Sullivan J, Stuart AG, Parsons J, Relton C, Goodship J, Henderson DJ, Keavney B. Low-frequency intermediate penetrance variants in the ROCK1 gene predispose to Tetralogy of Fallot. *BMC Genet.* 2013;**14**:57.

47. Langdon Y, Tandon P, Paden E, Duddy J, Taylor JM, Conlon FL. SHP-2 acts via ROCK to regulate the cardiac actin cytoskeleton. *Development.* 2012;**139**:948-957.

48. Koide K, Slonim DK, Johnson KL, Tantravahi U, Cowan JM, Bianchi DW. Transcriptomic analysis of cell-free fetal RNA suggests a specific molecular phenotype in trisomy 18. *Hum. Genet.* 2011;**129**:295-305.

DATA SUPPLEMENT

ANIMAL PREPARATION AND RHO SIGNALING DISRUPTION

Animal experiments were performed in accordance to institutional guidelines of the Leiden University Medical Center, national guidelines and Directive 2010/63/EU of the European Parliament on the protection of animals used for scientific purposes. Fertilized White Leghorn chicken eggs were incubated horizontally at 37°C (80% humidity). Rho signaling was disrupted by addition of the selective Rho kinase (ROCK) inhibitor compound Y-27632 (688000, Calbiochem, Massachusetts, USA) *in ovo* after 48 hrs of incubation (~HH10-11). First, a window in the egg was made and the extraembryonic membranes were carefully opened. 2µl of 100µM Y-27632 or PBS was added to the surface of the embryo at a singular moment. qPCR analysis after 24 hrs of reincubation confirmed downregulation of *ROCK2* (p-value<0.05), with a trend towards lower expression of *RHOA* (**Supplemental Fig. 1**). A schematic representation of the experimental setup is provided in **Supplemental Fig. 2**. Y-27632 has a half-life of 12-16 hrs.[1] Embryos were extracted 1-4 days post-intervention, staged according to standard criteria[2] and euthanized by decapitation. For *ex ovo* extracellular microelectrode recordings hearts were isolated. The same experiments were performed for RNA isolation and for patch clamp electrophysiology. Survival rates of embryos treated with ROCK inhibitor was significantly different as compared to controls embryos (p=0.013, **Supplemental Fig. 2**).

EX OVO ELECTROPHYSIOLOGICAL RECORDINGS

To assess the effects of ROCK inhibition on sinoatrial node development, *ex ovo* electrophysiological recordings were conducted in 168 control and ROCK inhibited embryonic hearts (HH16 to HH31) during superperfusion with oxygenated Tyrode solution as previously described.[3] Briefly, hearts were placed in a temperature-controlled fluid-heated superperfused tissue bath (37±0.5°C), fixed with a wire through non-cardiac tissue near the outflow tract and allowed to equilibrate for 10 min. Heart rates (beats per minute, bpm) below the standard for their stage of development were excluded.[3] Tungsten recording electrodes were placed on the right atrium (RA) (near the entrance of the right cardinal vein), left atrium (LA) (near the entrance of the left cardinal vein), on the left side of the ventricular apex (V), and a reference electrode in the tissue bath. The electrical activity was confirmed visually by mechanical activity (contraction) of the atria and ventricles. A difference of ≥ 1ms in local depolarization time between the recording electrodes was considered significant. An example of an electrical recording is depicted in **Supplemental Fig. 3**. Heart rates were measured between two atrial signals. Interatrial conduction time was measured

as miliseconds (ms) between the RA and LA signal. Analysis was performed in two separate groups: <HH28 between control (n=95) and ROCK inhibition (n=48) and ≥HH28 between control (n=31) and ROCK inhibition (n=18).

OPTICAL MAPPING RECORDINGS

Optical mapping recordings were conducted as previously described.[3-5] Briefly, freshly isolated hearts from embryonic stages HH21-22 (n=9 chick embryos) were dissected in ice-cold Tyrode solution (to prevent any post-mortem ischemic damage) with the following composition: NaCl 145 mmol/l, KCl 5.9 mmol/l, $CaCl_2$ 1.1 mmol/l, $MgCl_2$ 1.2 mmol/l, glucose 11 mmol/l, HEPES 5 mmol/l; pH = 7.4. Hearts were isolated with abundant non-cardiac outflow tract tissue for fixation in the tissue bath and intact inflow tract region to ensure spontaneous pacemaking activity. These hearts were stained with 2.5 μmol/l di-4-ANEPPS (Invitrogen) for 10 minutes. Motion control was accomplished with 0.1μM blebbistatin (Sigma) and by pinning the heart by the non-cardiac outflow tract tissue to the bottom of the dish. The Ultima L high-speed camera and software were used for data acquisition and analysis was performed using the BV Analyzer software.[3-5]

IMMUNOHISTOCHEMISTRY AND NON-RADIOACTIVE IN SITU HYBRIDIZATION

For immunohistological analysis thoraxes were fixed in 4% paraformaldehyde for 24 hrs, embedded in paraffin and serially sectioned. Immunohistochemical stainings were conducted (HH16-HH31, n=40) as described[3] for primary antibodies: anti-TNNI2 (goat polyclonal antibody, sc-8118, Santa Cruz, 1/400), anti-NKX2.5 (goat polyclonal antibody, sc-8697, Santa Cruz, 1/4000), and anti-ISL1 (mouse monoclonal antibody, clone 39.4D5, Developmental Studies Hybridoma Bank, 1/400). Slides were incubated with biotin-conjugated secondary antibodies specific to the appropriate species (goat-α-rabbit (BA-1000); horse-α-goat (BA-9500), horse- α-mouse (BA-2000), all from Vector Labs), visualized by incubation with 3-3'diaminobenzidin tetrahydrochloride (DAB, D5637, Sigma-Aldrich), and counterstained with haematoxylin (0.1%, Merck). Nonradioactive *in situ* hybridization analysis for *HCN4* was conducted with a digoxigenin-labeled antisense RNA probe in 10μm embryo sections as described previously.[6] Briefly, a cDNA fragment corresponding to HCN4 amino acids 400–602 was used as template and digoxigenin-labeled probes were generated. A sense RNA probe was used as a negative control.

3D RECONSTRUCTIONS

3D reconstructions of atrial and ventricular myocardium of TNNI2-stained serial sections of HH11, HH24, HH26, HH29, HH35 and HH42 embryos were made as previously described[7] using the AMIRA v5.0 Software Package (Template Graphics Software, San Diego, USA). In the HH26 and HH29 reconstructions, ISL1-positive myocardial expression observed in immediate sister sections was superimposed. In the rest of the reconstructions, NKX2.5 negative myocardium observed in immediate sister sections was superimposed.

RNA ISOLATION, CDNA SYNTHESIS, REVERSE TRANSCRIPTASE PCR AND REAL TIME QPCR

Chicken embryos treated with 2µl of 100µM Y-27632 or PBS (as described before) were cultivated for RNA isolation. Embryos were extracted between 24 (stage HH18-19; n=6 controls (CTRL); n=6-7 ROCK inhibition (ROCK)), 48 (stage HH21-22; n=5-8 CTRL; n=4-8 ROCK) and 96 (stage HH28-29; n=4-8 CTRL; n=5-8 ROCK) hrs after treatment with the inhibitor for real time qPCR analysis. RNA was isolated from individual inflow tract regions of embryonic chicken hearts using the RNeasy Micro Kit (Qiagen) and treated with DNAse-I (Qiagen) according to the manufacturer's protocol. 200ng of RNA was reversely transcribed into cDNA using Superscript II reverse transcription-polymerase and random primers (Invitrogen). For HH18-19 specimens, whole inflow tract portions were used. From HH20 onwards, the inflow tract portion was divided into the right and the left side to assess gene expression separately.

For qPCR analysis, chicken gene specific primers for the genes of interest are shown in **Supplemental Table 1**. Primers for *HCN4*, *HCN1* and *GAPDH* have been already validated.[6] For each qPCR reaction 1µl of cDNA was used in a final volume of 20µl. Reactions were carried out in triplicate for each sample. Negative controls were reactions containing H_2O instead of cDNA. qPCR was performed on a Bio-Rad CFX96 Real Time System and a melting curve was produced to verify single qPCR product amplification. Efficiency of the PCR reaction was tested using a standard curve synthesized from a dilution series of cDNA. Chicken *GAPDH* was used as the reference standard for normalization and relative quantification of differences in mRNA expression was determined. Results were analyzed using Graphpad Prism software and are shown as fold change compared to the definitive right-sided SAN when showing only the control data or as fold change compared to the control group when showing the ROCK inhibition data. In the **Supplemental Excel file** (available online or at request to the authors), all raw qPCR values are provided. Furthermore, a step-by step overview is provided for the calculations that were performed.

The following steps were performed:

1. First, for every gene separately, the right (see **Supplemental qPCR data & Fig. 3A-3D**) or the control (see **Supplemental qPCR data & Fig. 3E-F**) average gene expression value was set to 1. This was achieved by dividing (for all genes separately) the values of either the right (**Supplemental qPCR data & Fig. 3A-3D**) or control (**Supplemental qPCR data & Fig. 3E-3F**) embryos by the average of the corresponding group. This results in an average value of expression of 1, and this value is used to calculate the fold change of expression for either the left side (**Supplemental qPCR data & Fig. 3A-3D**) or the inhibition group (**Supplemental qPCR data & Fig. 3E-F**).
2. To calculate the fold change between either the right *vs* the left side (**Supplemental qPCR data & Fig. 3A-3D)** or the control *vs* the inhibition (**Supplemental qPCR data & Fig. 3E-F**), for every gene the seperate values of the left side (**Supplemental qPCR data & Fig. 3A-D**) or the inhibition group (**Supplemental qPCR data & Fig. 3E-F**) were divided by the average of either the right side (**Supplemental qPCR data & Fig. 3A-D**) or the control group (**Supplemental qPCR data & Fig. 3E-F**).
3. These values (see also **Supplemental qPCR data** file, which also shows which values were used for the final statistical analysis) were used to perform Mann-Whitney U-tests in Graphpad. These values were also used to plot the graphs.
Missing data in the online Excel file is explained by a limited amount of cDNA available to perform qPCR (i.e. insufficient material to perform qPCR analysis for all the genes per embryo).

CELL CULTURE AND MICROELECTRODE ARRAY (MEA) ELECTROPHYSIOLOGY

To study the direct effect the ROCK inhibitor has on rate, sinoatrial, atrial (only appendages) and ventricular cardiomyocytes of HH26-27 chicken embryos were cultured as described previously[8] and plated for MEA electrophysiology. A total of 5 separate experiments were conducted. Each experiment consisted of a cardiomyocyte isolation of sinoatrial, atrial or ventricular cardiomyocytes pooled from 15-25 embryonic chicken hearts and plated into a minimum of 2-4 separate MEA chips. Experiments were always carried out with a control and treated group in parallel (n=7-9 per group). The culture medium used was our cardiomyocyte medium which contains DMEM high glucose (Life technologies, Carlsbad, California, USA), 10% fetal calf serum (Sigma-Aldrich, St. Louis, Missouri, USA), 1% penicillin-streptomycin (Life technologies, Carlsbad, California, USA), 1% non-essential amino acids (Life technologies, Carlsbad, California, USA) and 1% L-Glutamine (Life technologies, Carlsbad, California, USA). MEA chips

were plasma-cleaned and coated with fibronectin for 1 hour at 37°C. 80,000 to 100,000 isolated cardiomyocytes were plated on standard 60 electrode MEAs. After allowing the cells to settle and grow for 48 hours after plating, recordings were conducted using MEA1060INV MEA amplifier (Multi Channel Systems, Reutlingen, Germany) as described before.[9] Time point zero was recorded before the ROCK inhibitor Y-27632 (688000, Calbiochem, Massachusetts, USA) was added. Medium was refreshed in the MEAs with medium containing a final concentration of 10μM of Y-27632. Measurements were recorded at specific time intervals after inhibition (between 10 minutes and 4 hours after application of the inhibitor). During the recordings, temperature was kept at 37°C. Data were recorded using QT-screen (Multi Channel Systems,) and analyzed with QT-analyzer (Multi Channel Systems). Rate data from 3 independent electrodes were averaged using Graphpad Prism software. Data points are displayed as % relative to time point zero (before application of inhibitory compound).

PATCH CLAMP ELECTROPHYSIOLOGY

Patch clamp electrophysiological studies were performed on cardiomyocytes isolated from right/left or whole sinus venosus myocardium and right ventricular myocardium in control and *in ovo* ROCK-inhibited hearts as previously described.[10] A total of 3 separate experiments were performed. In each experiment sinus venosus or ventricular cardiomyoctes were isolated from a pool of 15-25 embryonic chicken hearts. Sinus venosus myocardium tissue was isolated the same way as for the qPCR analysis, maintained as a whole or divided into a right and a left portion. Tissue from the right ventricular free wall was isolated as internal control. The tissue was dissociated using 0.05% Trypsin (Life technologies, Carlsbad, California, USA) shaking (850 rpm) at 37°C, vortexed and then centrifuged for 5 minutes at 1100rpm (114g). The pellet was resuspended in our DMEM cardiomyocyte medium (with DMEM high glucose (Life technologies, Carlsbad, California, USA), 10% fetal calf serum (Sigma-Aldrich, St. Louis, Missouri, USA), 1% penicillin-streptomycin (Life technologies, Carlsbad, California, USA), 1% non-essential amino acids (Life technologies, Carlsbad, California, USA) and 1% L-Glutamine (Life technologies, Carlsbad, California, USA)). The cells were plated on glass coverslips. Recordings were performed on cardiomyocytes 24 hours after isolation at 37°C in Tyrode's solution of the following composition: NaCl 140 mM; KCl 5.4 mM; CaCl2 1.8 mM; MgCl2 1.0 mM, D-Glucose 5.5 mM; HEPES 5.0 mM adjusted to pH 7.4 with NaOH (all components from Sigma-Aldrich USA). Action potentials were recorded on spontaneously contracting cells with the perforated patch clamp technique using an Axopatch 200B amplifier (Molecular Devices Axon Instruments, USA) at 5 kHz in the fast current clamp mode. Cut-off seal resistance of 2GOhm or higher was

selected for further analysis. Data acquisition was obtained with DigiData 1550 under control of Clampex 10.0 software (Molecular Devices Axon Instruments, USA). Pipets had a resistance of ~2.4 MOhm and the buffer composition was the following: K-gluconate 125 mM; KCl 20 mM; NaCl 5 mM; HEPES 10 mM adjusted to pH 7.3 with KOH. Before measuring, Amphotericin-B (light protected, Sigma-Aldrich, USA) at a final concentration of 3µl/ml in DMSO was added.

The data was analyzed with custom developed software (L.G.J.T. under Labview development software, National Instruments, Austin, Texas, USA). A total of 17 to 19 cells were analyzed separately per treatment group. The Action Potential Duration (APD), maximal upstroke velocity (dV/dT), action potential amplitude, resting membrane potential and the spontaneous beating frequency were quantified.

STATISTICAL ANALYSIS

Data were analyzed using GraphPad Prism software (GraphPad Software, La Jolla, California, USA). Multiple comparisons between groups for the qPCR results were analyzed with the non-parametric Mann-Whitney U-test ($P<0.05$ was considered to be statistically significant). Additional one or two-way ANOVA analysis was performed with Bonferroni post-hoc tests in the data obtained from the MEA and patch clamp electrophysiology. For comparison of the activation pattern (categorical variable) χ^2 –test was performed. A p-value <0.05 was considered significant. Results are shown as mean ± SEM.

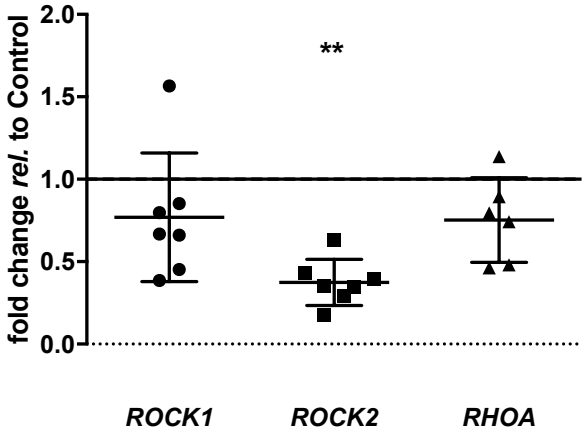

Supplemental Figure 1. *ROCK2* expression is reduced 24 hours after ROCK inhibition
qPCR analysis of induced gene expression changes for *RHOA, ROCK1* and *ROCK2* 24 hours after treatment with Y-27632 (6 controls *vs* 6-7 treated hearts). ** p<0.05.

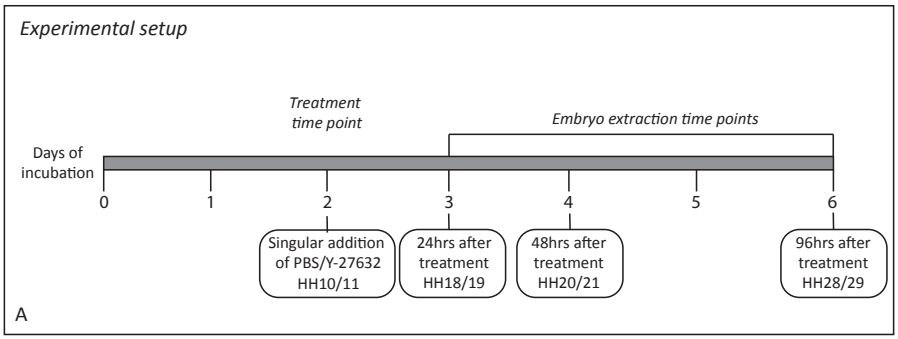

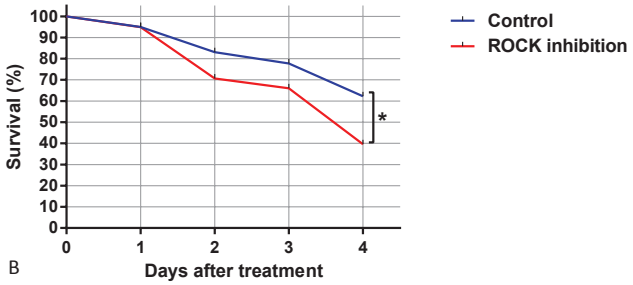

Supplemental Figure 2. ROCK inhibition results in higher mortality rates in embryos
A. Experimental setup of use of Rho-kinase inhibitor Y-27632. **B.** Survival curve of chick embryos after treatment with PBS (control) or with Y-27632 (ROCK inhibition). *p<0.05.

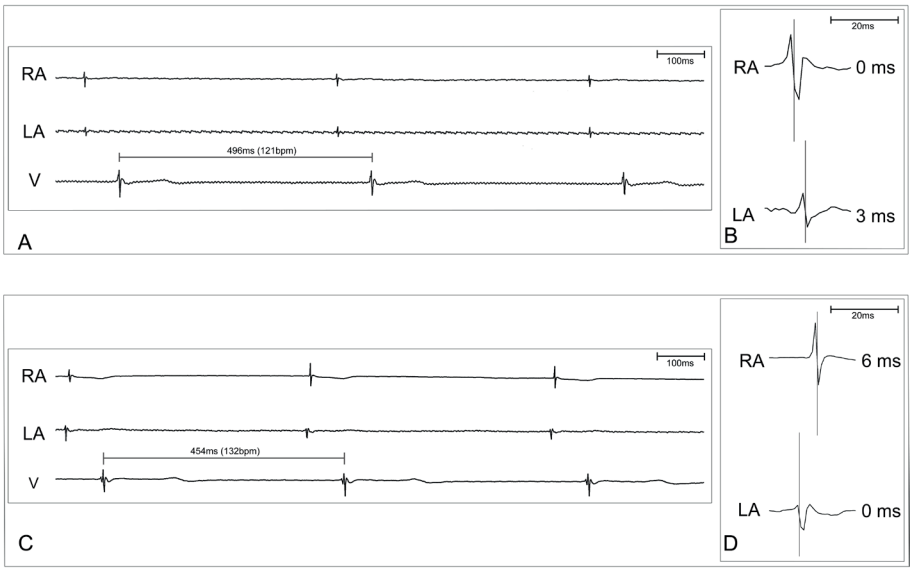

Supplemental Figure 3. Right and left-sided atrial activation patterns are observed throughout development

A-B. Representative example of a recording of an HH23 chicken heart showing pacemaking dominance in the right atrium (RA). **B**. Magnification of the atrial signals showing the RA signal preceding the left atrial (LA) signal by 3ms. **C-D**. Representative example of a recording of a chicken heart at HH24, showing pacemaking dominance in the LA. **D**. Magnification of the atrial signals showing the LA signal preceding the RA signal by 6ms.

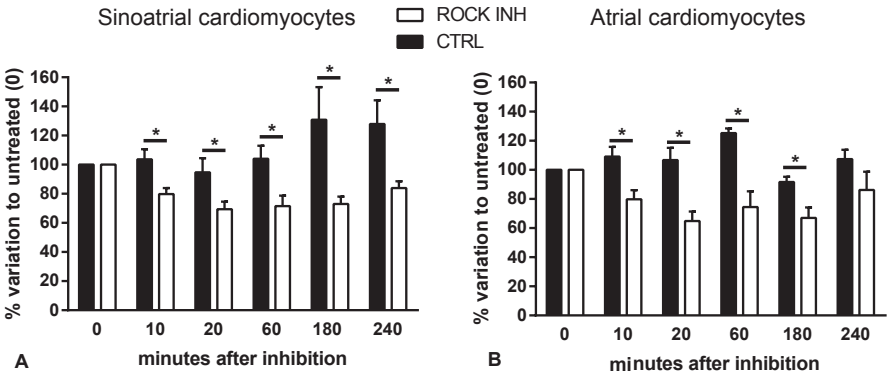

Supplemental Figure 4. ROCK inhibition results in a lower signal amplitude of sinoatrial cardiomyocytes

A. % Of amplitude variation compared to time point zero (0 min) of sinoatrial cardiomyocyte cell cultures at various time points (up to 240 min) after treatment with Y-27632, ROCK inhibitor (ROCK INH) or with PBS (control, CTRL). **B.** % Of amplitude variation compared to time point zero (0) of atrial cardiomyocytes (with no SAN cardiomyocytes) after treatment with ROCK inhibitor Y-27632 (ROCK INH) or with PBS (control, CTRL).*p< 0.05. n=7-9 per group (15-25 embryonic hearts pooled per MEA culture).

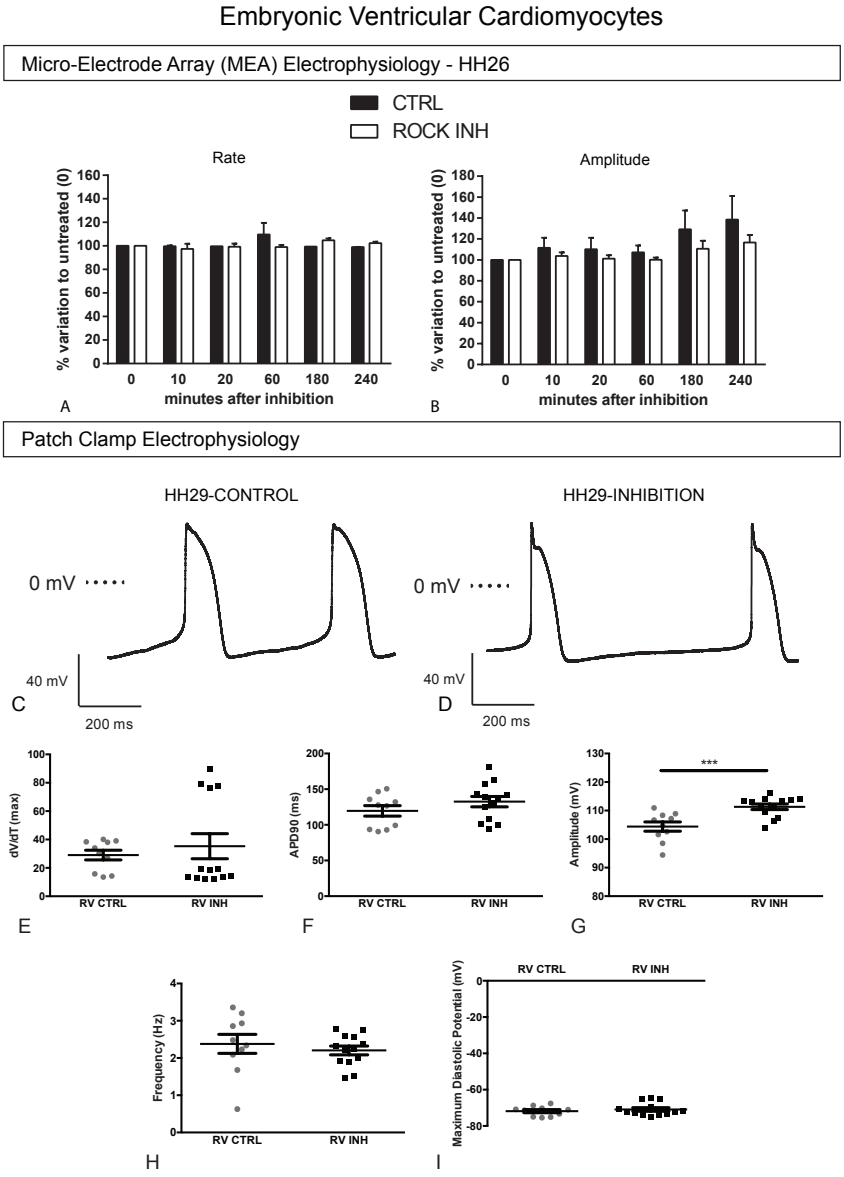

Supplemental Figure 5. ROCK inhibition does not affect electrophysiology ventricular cardiomyocytes

A. % Of rate variation compared to time point zero (0 min) of ventricular cardiomyocyte cell cultures at various time points (up to 240 min) after treatment with Y-27632, ROCK inhibitor (ROCK INH, n=10) or with PBS (control, CTRL, n=5). **B.** % Rate of amplitude variation compared to time point zero (0) of ventricular cardiomyocytes after treatment with ROCK inhibitor Y-27632 (ROCK INH) or with PBS (CTRL). **C-D.** Representative tracing of right ventricular cardiomyocytes from HH29 control (**C**, HH29 CTRL, n=10) and HH29 ROCK inhibition (**D**, HH29 INH, n=13). **E-I.** Scatter plots showing maximum upstroke velocity (**E**), action potential duration (APD)90 (**F**), amplitude (**G**), frequency (**H**) and maximum diastolic potential (**I**). ***p<0.001.

Supplemental table 1. Primer sequences used in qPCR analysis

Gene	Forward Primer (5'-3')	Reverse Primer (5'-3')
ROCK1	TGACTGGTGGTCAGTTGGAG	TAGAGATCTCGTTGTCATCAGG
ROCK2	GACTGGTGGTCCGTAGGAGT	GACAACATCCGAGAGACTGC
RHOA	GTTGGCTTTGTGGGATAC	CAGAAATGTTTCACTTCCG
TNNT2	AAGAAGGGTGGCAAGAAGCA	CTCGTGGTCACTGACACGATTT
SHOX2	AGGATGCGAAAGGCATGGAA	CCGGCATTTGGCTTTTCTGT
ISL1	AAAAGAAGCATTATGATGAAGCAA	CATGTCTCTCCGGACTAGCAG
TBX3	TCGTCCGAGCGAACGATATT	TCGTCCGAAGTGGGGTTTTC
NKX2.5	CCCTACTACGTGAAGAGCTACG	TCGGGATCCTCCAGCTCTCT
TBX5	AAGCTCGTAACATGGCGGAC	CCGCTCGTGCAAAAACACTT
HCN4	AAAAGGCTCCAGTCCCTGAT	CACCGCTCAGTCCCTGCT
HCN1	CTGCACCCAAGAATGAGGTT	ATCAGGGTGGAAATCTCGTG
PITX2C	CGATGAGTTGCATGAAGGAC	GAGATAGTGTGCACCTCCAGC
NODAL	CCAATCACGCGTACATGCAG	AGCATGGAGAGGGGACTCAT
CX40	CAGAGGTGGCCAGTGAATGT	CAAATCGTCTGACCTCGCCT
CAV3.1	CGTCTAATAGTCGGCCACCC	GCTAAGGCCACACAATTGGC

SUPPLEMENTAL REFERENCES

1. Oellers P, Schroer U, Senner V, Paulus W, Thanos S. ROCKs are expressed in brain tumors and are required for glioma-cell migration on myelinated axons. *Glia.* 2009;**57**:499-509.

2. Hamburger V, Hamilton HL. A series of normal stages in the development of the chick embryo. *J. Morphol.* 1951;**88**:49-92.

3. Vicente-Steijn R, Kolditz DP, Mahtab EA, Askar SF, Bax NA, van der Graaf LM, Wisse LJ, Passier R, Pijnappels DA, Schalij MJ, Poelmann RE, Gittenberger-de Groot AC, Jongbloed MR. Electrical activation of sinus venosus myocardium and expression patterns of RHOA and Isl-1 in the chick embryo. *J. Cardiovasc. Electrophysiol.* 2010;**21**:1284-1292.

4. Sankova B, Machalek J, Sedmera D. Effects of mechanical loading on early conduction system differentiation in the chick. *Am. J. Physiol. Heart. Circ. Physiol.* 2010;**298**:H1571-H1576.

5. Calkoen EE, Vicente-Steijn R, Hahurij ND, van Munsteren CJ, Roest AA, DeRuiter MC, Steendijk P, Schalij MJ, Gittenberger-de Groot AC, Blom NA, Jongbloed MR. Abnormal sinoatrial node development resulting from disturbed vascular endothelial growth factor signaling. *Int. J. Cardiol.* 2015;**183**:249-257.

6. Vicente-Steijn R, Passier R, Wisse LJ, Schalij MJ, Poelmann RE, Gittenberger-de Groot AC, Jongbloed MR. Funny current channel HCN4 delineates the developing cardiac conduction system in chicken heart. *Heart Rhythm.* 2011;**8**:1254-63.

7. Mahtab EA, Vicente-Steijn R, Hahurij ND, Jongbloed MR, Wisse LJ, DeRuiter MC, Uhrin P, Zaujec J, Binder BR, Schalij MJ, Poelmann RE, Gittenberger-de Groot AC. Podoplanin deficient mice show a RHOA-related hypoplasia of the sinus venosus myocardium including the sinoatrial node. *Dev. Dyn.* 2009;**238**:183-193.

8. Maltsev VA, Wobus AM, Rohwedel J, Bader M, Hescheler J. Cardiomyocytes differentiated in vitro from embryonic stem cells developmentally express cardiac-specific genes and ionic currents. *Circ. Res.* 1994;**75**:233-244.

9. Braam SR, Tertoolen L, van de Stolpe A, Meyer T, Passier R, Mummery CL. Prediction of drug-induced cardiotoxicity using human embryonic stem cell-derived cardiomyocytes. *Stem Cell Res.* 2010;**4**:107-116.

10. Kelder TP, Vicente-Steijn R, Harryvan TJ, Kosmidis G, Gittenberger-de Groot AC, Poelmann RE, Schalij MJ, DeRuiter MC, Jongbloed MR. The sinus venosus myocardium contributes to the atrioventricular canal: potential role during atrioventricular node development? *J. Cell. Mol. Med.* 2015**;19:**1375–89.

7

DISRUPTION OF RHOA-ROCK SIGNALING RESULTS IN ATRIOVENTRICULAR BLOCK AND DISTURBED DEVELOPMENT OF THE PUTATIVE ATRIOVENTRICULAR NODE

Tim P. Kelder, Rebecca Vicente-Steijn, Adriana C. Gittenberger-de Groot, Rob E. Poelmann, Martin J. Schalij, Marco C. DeRuiter, Monique R.M. Jongbloed

Submitted

ABSTRACT

INTRODUCTION:

The RHOA-ROCK signaling pathway is involved in numerous developmental processes, including cell proliferation and migration. RHOA is expressed in the atrioventricular node (AVN) and altered expression of RHOA results in atrioventricular (AV) conduction disorders in mice. The current study aims to elucidate the pathogenesis of AV conduction disorders after disturbing RHOA-ROCK signaling.

METHODS & RESULTS:

RHOA-ROCK signaling was inhibited chemically in avian embryos. *Ex ovo* microelectrode recordings showed first to third degree AV block. Morphological examination revealed hampered development of the myocardial continuity between the sinus venosus and posterior AV canal, including the AVN region. Laser capture microdissection and subsequent qPCR of tissue collected from this region revealed disturbed expression of *HCN1, ISL1* and *SHOX2*.

CONCLUSIONS:

RHOA-ROCK signaling is essential for normal morphological development and gene expression patterns of the myocardial continuity between the sinus venosus and posterior region of the AV canal, including the AVN region. Disturbing the RHOA-ROCK signaling pathway results in AV block. This is, at least in part, explained by the abnormal morphology of the AV transition and disturbed gene expression of key genes involved in normal CCS functioning. The RHOA-ROCK inhibition model can be used to further study the pathophysiology and therapeutic strategies for AV block.

1. INTRODUCTION

A proper functioning atrioventricular node (AVN) is essential for normal impulse propagation from the atria towards the ventricles, after allowing a delay of the electrical activation in the AVN. This delay must be long enough to ensure proper filling of the ventricles, and short enough to ensure maintenance of a sufficient heart rate. Disturbance of AV conduction may result in different degrees of AV block, ranging from first degree to complete (third degree) block requiring pacemaker implantation. The mechanisms of these different forms of AV block are still insufficiently understood. The AVN is a morphologically and functionally complex structure, consisting of multiple cell types. The compact portion of the node is covered by transitional cells with nodal extensions running towards the vestibules of the mitral and tricuspid valves.[1,2]

The exact origin of these different components of the AVN remains to be elucidated. It was suggested that at least the compact portion of the AVN is derived from the transcription factor T-box (Tbx)2^{+} myocardium of the AV canal.[3] We recently described another region that appears to be involved in AVN development.[4] This region consists of a myocardial continuity that is situated between the sinus venosus myocardium (containing the definitive right-sided and a transient left-sided sinoatrial node (SAN)), and the AVN, encompassing its posterior part. This area is characterized by expression of Islet1 (ISL1, marker for (pre)cardiac mesoderm and undifferentiated myocardium[5]), Troponin-I, isoform 2 (TNNI2, myocardial marker) and hyperpolarization-activated cyclic nucleotide-gated channel 4 (HCN4, marker for the (developing) CCS[6]).[4] In previously performed cell tracing studies, incorporation of the sinus venosus myocardium in the posterior region of the putative AVN (the region of the myocardial continuity) was shown.[4] This is in line with genetic tracing experiments of Isl1+ progenitors, which showed a contribution of Isl1+ progenitors to the AVN.[5] A dual origin for AVN cells (i.e. AVN cells deriving from the AV canal and the sinus venosus myocardium) helps to explain the cellular heterogeneity of the AVN region.

Further functional and genetic characterization of the continuity between the sinus venosus and AV canal showed that cells from this region had a pacemaker-like phenotype, which again implies a role for this region in CCS functioning.[4] However, whether this region is directly involved in normal and abnormal AV conduction was not studied.

The AVN region shows expression of the Ras homolog gene family, member A (RHOA). Expression is initially broadly present during development, but becomes restricted to the sinus venosus (including the SAN) during further development.[7] RHOA is a member of the family of Rho kinases, which are small GTPases, known to play an important role in cell migration, cell proliferation and apoptosis.[8] Interestingly, Rho-Kinase inhibitors have been shown to either

impair[9] or promote[10] cardiac differentiation *in vitro* altering the expression of key genes in early cardiac lineages like *GATA4, ISL1* and *TBX5*.[9,10] Normal RHOA-ROCK signaling is essential for normal development and functioning of the SAN, the pacemaker of the heart.[11] Inhibiting the RHOA-ROCK pathway in chick resulted in an immature right-sided SAN with residual pacemaker potential of the left-sided sinus venosus myocardium, indicating that the RHOA-ROCK pathway is crucial for establishing the SAN. In addition, it has been shown that cardiac specific overexpression of RHOA in mouse results in bradycardia, atrial fibrillation, first and second degree atrioventricular block and AVN dysfunction.[12] It was hypothesized that disruption of RHOA signaling affects the function of cardiac ion channels.[12] Interestingly, similar results were obtained when expression of RHOA was downregulated.[13] This indicates that strict regulation of RHOA expression is necessary for normal functioning of the AVN. However, these studies were performed in postnatal mice. The role of RHOA in developmental processes leading to AV conduction disturbances was not investigated. Furthermore, the morphology of the AV conduction axis after RHOA disruption has not been studied.

The current study aimed to first generate a novel model system to investigate AV conduction disturbances during development in chick embryos by *in ovo* inhibition of the RHOA-ROCK signaling pathway. Second, since RHOA is involved in cellular migration, it was hypothesized that AV block after RHOA inhibition may relate to a maldevelopment of the myocardial continuation between the sinus venosus and the AV canal (further referred to as SV-AVC continuity). Furthermore, we investigated RNA expression of a panel of key cardiac and conduction system genes in the region of the SV-AVC continuity and putative AVN after RHOA inhibition.

2. METHODS

A schematic representation of the experimental setup is provided in **Supplemental Fig. 1**.

2.1. EXPERIMENTAL PREPARATION

Fertilized White Leghorn chicken eggs were incubated horizontally at 37°C and 80% humidity, until they reached the desired developmental stage. Staging of embryos was performed according to the Hamburger and Hamilton (HH) criteria.[14] Embryos were either used as control or used for experiments as described in the following sections. After extraction from the egg, embryos were staged and euthanized by decapitation, and processed as described below. All animal experiments were in accordance with national and institutional guidelines.

2.2. IN OVO ROCK INHIBITION

The chick embryo is readily accessible for microsurgical procedures and follow-up after intervention is relatively easy. Inhibition of ROCK signaling was achieved as previously described.[11] Briefly, the Rho-kinase inhibitor compound Y-27632 (688000, Calbiochem, Massachusetts, USA) was administered *in ovo* once at ~HH10-11. ROCK inhibition was achieved by administering 2µl of 100µM Y-27632 directly to the surface of the embryo, or by placing heparin acryl beads loaded with compound at both sides of the inflow portion of the heart. As a control, PBS was administered directly to the surface of the embryo. After the procedure, eggs were reincubated and embryos were extracted from the egg at the desired time points.

2.3. EX OVO EXTRACELLULAR MICROELECTRODE RECORDINGS

Recordings were conducted in control (n=29) and ROCK inhibited (n=20) hearts (HH28-30) as described previously.[7,15,16] Hearts were placed in a temperature-controlled (37±0.1°C) superperfused (oxygenated Tyrode) tissue bath and allowed to equilibrate for 10 min. Heart rates (beats per minute, bpm) below the standard for their stage of development were excluded.[7] Tungsten recording electrodes were placed on the right atrium (RA) (near the entrance of the right cardinal vein), left atrium (LA) (near the entrance of the left cardinal vein), on the left side of the ventricular apex (V), and a reference electrode in the tissue bath. The time between the RA electrode and V electrode was considered the AV conduction time.

2.4. IMMUNOHISTOCHEMISTRY

Thoraxes of control (n=4) and ROCK inhibited (n=5) embryos of HH29-30 (corresponding with the stages used for microelectrode recordings) were fixed in 4% PFA for 24 hrs, embedded in paraffin and serially sectioned. Immunohistochemical stainings were conducted as described[4,7] for primary antibodies: anti-TNNI2 (goat polyclonal antibody, sc-8118, Santa Cruz, 1/400), anti-TNNI2 (rabbit polyclonal antibody, SC-15368, 1/200; Santa Cruz Biotechnology Inc., Dallas, TX, USA), and anti-ISL1 (mouse monoclonal antibody, clone 40.2d6, 1/100, Developmental Studies Hybridoma Bank, Iowa City, Iowa, USA). Slides were incubated with biotin-conjugated secondary antibodies (except for immunofluorescent staining of TNNI2, which was directly visualized with secondary antibody) specific to the appropriate species (horse-α-mouse (BA-2000) goat-α-rabbit (BA-1000); horse-α-goat (BA-9500), all from Vector Labs), and visualized by either incubation with 3-3'diaminobenzidin-tetrahydrochloride (DAB, D5637, Sigma-Aldrich) or fluorescently labeled

secondary antibodies (Alexa Fluor® 488 Streptavidin Conjugate (S-11223, 1/200) and Alexa Fluor® 647 donkey anti-goat IgG (A-21447, 1/200), all purchased from Life Technologies (Carlsbad, CA, USA)). Slides were either counterstained with haematoxylin (0.1%, Merck) or DAPI (used as a nuclear stain, D3571, 1/1000; Life Technologies).

2.5. 3D RECONSTRUCTIONS

3D reconstructions were made based on TNNI-stained serial sections of HH29-30 embryos which were representative for i. the control heart, ii. the mild phenotype, and iii. the severe phenotype. The AMIRA v4.0 software package (Template Graphics Software, San Diego, CA) was used as previously decribed.[17]

2.6. VITAL DYE LABELING STUDIES

Labeling of the sinus venosus myocardium with DiI/5-TAMRA was performed at HH15 as described previously.[4] Briefly, after windowing the egg the coelomic cavity was opened and the DiI/5-TAMRA was injected in the sinus venosus myocardium using a programmable microinjector (IM-300, Narishige, Tokyo, Japan) and micromanipulator. After injection of the vital dyes, 2µl of 100µM Y-27632 (n=5) or PBS (n=4) was injected into the pericardial cavity. Analysis of cellular fate was performed after 24 hrs of reincubation (HH19-20).

2.7. LASER CAPTURE MICRODISSECTION PROCEDURE

Laser capture microdissection (LCM) was performed in control (n=5) and ROCK inhibited (n=5) embryos at HH30-31 (corresponding with microelectrode recordings and immunohistochemical data) as described previously.[4] Two specific regions were isolated. First, the medial portion of the continuity between the sinus venosus myocardium and the posterior AV canal was isolated. The medial portion of the SV-AVC continuity is situated where the right venous valve (RVV) attaches to the base of the atrial septum ("SV-AVC", control: **Fig. 1A-D**, ROCK inhibition: **Fig. 1I-L**). The second set of samples collected was from the region of the (putative) AVN, which is situated just distal to the SV-AVC continuity ("AVN region", control: **Fig. 1E-H**, ROCK inhibition: **Fig. 1M-P**). After isolating the tissue using LCM, the tissue was stored at -80°C.

2.8. RNA ISOLATION, CDNA SYNTHESIS AND QPCR OF LASER MICRODISSECTION TISSUE

Gene expression of the following key genes was analyzed: 1. myocardial marker Troponin T, isoform 2 (*TNNT2*); 2. NK2 homeobox 5 (*NKX2-5)*, which is expressed in the cardiac mesoderm during early cardiac development and remains expressed in atrial and ventricular cardiomyocytes during adulthood. It

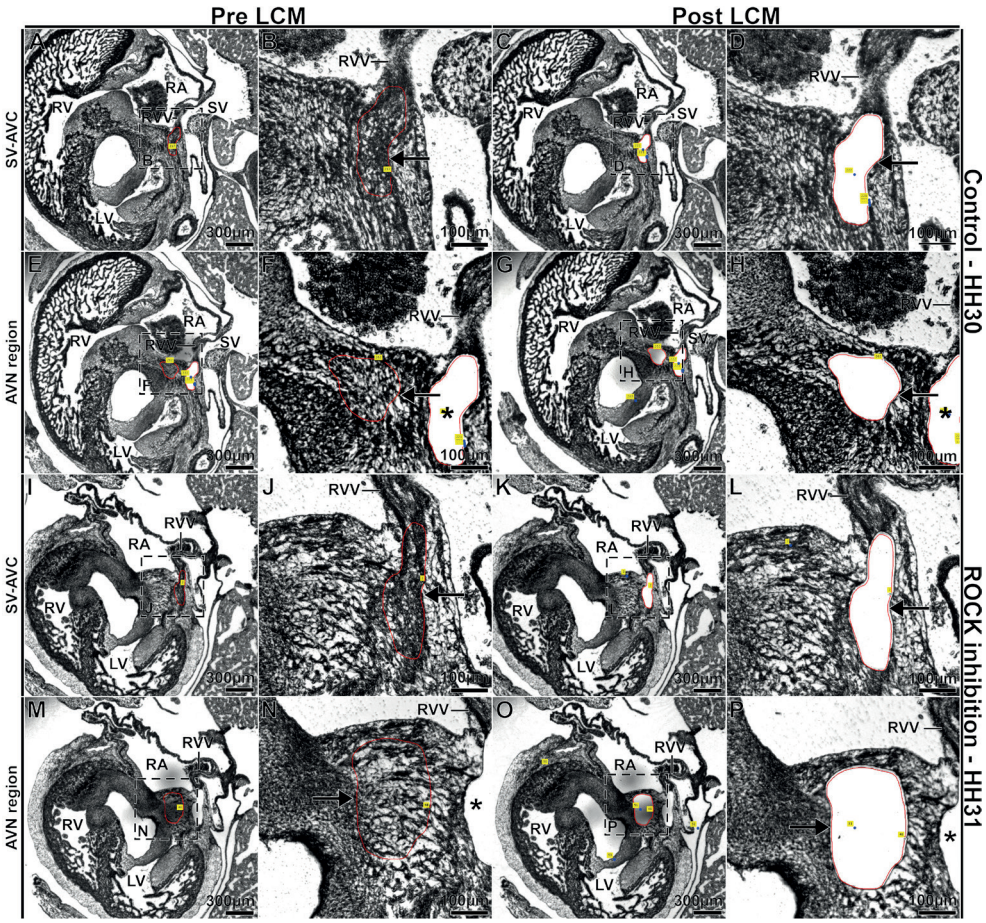

Figure 1. Laser capture microdissection to isolate specific regions of the AV conduction pathway

A-D. Control heart (HH30) before (**A-B**) and after (**C-D**) dissection of the myocardial continuity between sinus venosus and posterior AVC (SV-AVC). Boxed area in **A** and **C** are shown at higher magnification in resp. **B** and **D**. The excised region is located in the area where the right venous valve (RVV) attaches to the lower border of the atrial septum (arrows in **B** and **D**). **E-H.** Same heart before (**E-F**) and after (**G-H**) dissection of the region of the putative AVN. Boxed area in **E** and **G** are shown at higher magnification in resp. **F** and **H**. The excised region (arrows in **F** and **H**) is located just beneath the SV-AVC continuity (asterisk in **F** and **H**). Note the small strip of tissue that is located between the SV-AVC continuity and the AVN region. This was done to isolate different regions of tissue. **I-L.** Heart after ROCK inhibition, HH31, before (**I-J**) and after (**K-L**) dissection of the same region as in **A-D** (SV-AVC continuity). Boxed area in **I** and **K** are shown at higher magnification in resp. **J** and **L**. The excised region is indicated by arrows in **J** and **L**. **M-P.** Same heart (after ROCK inhibition) before (**M-N**) and after (**O-P**) dissection of the same region as in **E-H** (putative AVN region). Boxed area in **M** and **O** are shown at higher magnification in resp. **N** and **P**. The excised region is indicated by arrows in **N** and **P**. Excised SV-AVC tissue is marked by an asterisk in **N** and **P**. LV**:** left ventricle, RA: right atrium, RV: right ventricle, RVV: right venous valve, SV: sinus venosus.

is not expressed in the myocardium of the sinus venosus[18]; 3. hyperpolarization-activated cyclic nucleotide-gated channels (HCN)1 and 4, which are responsible for the "funny-current", also known as the pacemaker current and are used as markers for the (developing) CCS[6,19,20]; 4. T-box transcription factors (TBX)3 and 18. TBX3 is a transcriptional repressor which delineates the CCS and is essential for CCS function.[21,22] TBX18 is a marker for the sinus venosus and is essential for development of the venous pole and SAN[23,24]; 5. the short stature homeobox 2 (SHOX2) gene, which is also essential for SAN development.[25,26]

RNA was isolated with the RecoverAll™ Total Nucleic Acid Isolation Kit for FFPE (Ambion, catalog number AM1975, Life technologies, CA, USA). cDNA synthesis was generated using the iScript™ cDNA synthesis kit (Bio-rad, Hercules, CA, USA). For all genes, a nested approach was used as described[4], except for *GAPDH* and *TNNT2.* 10 Pre-amplification cycles were performed, using 10µl Sybr-Green Mastermix (Bio-Rad), 8.5µl nuclease-free water, 0.25µl forward and 0.25µl reverse primer and 10µl of cDNA (final volume of 20µl). qPCR was performed with for each reaction 5µl of SybrGreen Mastermix (Bio-Rad, Hercules, CA, USA), 0,5µl of forward primer, 0,5µl of reverse primer, 0,5µl of cDNA (or 0,5µl nuclease free water as negative control) and 3,5µl nuclease free water (final volume 10µl). Reactions were carried out in triplicate for each sample. qPCR was performed on a Bio-Rad CFX384 real-time system. Melting curve analysis was performed to verify single PCR product amplification. Chicken *GAPDH* was used as the reference standard for normalization, and relative quantification of differences in mRNA expression was determined. The primers used are described in **Supplemental table 1**.

2.9. STATISTICAL ANALYSIS

Data was analyzed with SPSS software (SPSS, Inc, Chicago, Ill). AV intervals were compared between groups with a 2-tailed Student's *t* test for normally distributed values. Levels of gene expression were compared using the Mann-Whitney U-test (non-normal data). A p-value <0.05 (2-tailed) was considered significant. Results are presented as mean ± SEM.

3. RESULTS

3.1. DISRUPTION OF THE ROCK PATHWAY RESULTS IN PROLONGED AV CONDUCTION TIME AND AV BLOCK

Ex ovo extracellular microelectrode recordings were performed at HH28-31 to investigate the effect of early ROCK inhibition on AV conduction in chick embryonic hearts. All control hearts showed a spontaneous, regular sinus rhythm, with atrial activation prior to ventricular activation for all contractions (**Fig. 2A**). After ROCK inhibition, the mean time between atrial and ventricular activation

(termed AV time) for the whole group was prolonged (control: 93.66±12.56 milliseconds, ROCK inhibition: 106.5±13.56 milliseconds, p=0.0031, **Fig. 2B**). Prolongation of the AV time is comparable to what is observed in first degree AV block.[27] Furthermore, after ROCK inhibition, 7/20 (35%) of the hearts displayed second (Wenkebach and Mobitz type) as well as third degree AV block[27] (see **Fig. 2C-E** and figure legend for details)**.** These results show that AV conduction is abnormal after ROCK inhibition in chick, confirming previous results found in postnatal mice.[12,13]

3.2. ROCK INHIBITION RESULTS IN DEFECTIVE DEVELOPMENT OF THE MYOCARDIAL CONTINUITY BETWEEN THE SINUS VENOSUS AND AV CANAL IN CHICK EMBRYONIC HEARTS

Next, we sought an explanation for the observed AV conduction disturbances. Previous work showed that during normal cardiac development, the sinus venosus myocardium is incorporated in the posterior region of the AV canal.[4] This myocardial continuity is situated in the region where the right venous valve (RVV) attaches to the lower rim of the atrial septum (putative AVN region).[4,28]

First, the morphology of the SV-AVC continuity after ROCK inhibition was studied. Examination of control hearts (n=4) showed the myocardial continuity between the sinus venosus myocardium (including the SAN, RVV, LVV and myocardium surrounding the cardinal veins) and the posterior region of the AV canal (putative AVN region), which in turn was continuous with the AV bundle (**Fig. 3A-F** and figure legend for detailed description).

After ROCK inhibition (n=5 analyzed), two phenotypes, that were designated "mild" and "severe", were seen. In the "mild" phenotype (3/5, 60%), the myocardial continuity could still be recognized. However, the continuity appeared smaller and the connection with the sinus venosus myocardium was displaced laterally and to the right (**Fig. 3G-L)**. A putative AVN region was distinguishable from the rest of the myocardium, similar to controls.

In the "severe" phenotype (2/5, 40%), the myocardial continuity between the sinus venosus and posterior AV canal was further displaced laterally and rightwards and consisted of only a strand of myocardial tissue, which was connected to the ventricular septum (**Fig. 3Q**). In contrast to the "mild" phenotype, the putative AVN was not distinguishable from the surrounding myocardium (**Fig. 3M-R**). These results show that after ROCK inhibition, the morphology of the AV conduction pathway is abnormal. Different phenotypes are present, indicating a variable degree of inhibition of the RHOA-ROCK pathway. This could explain the variable AV conduction disturbances that were found.

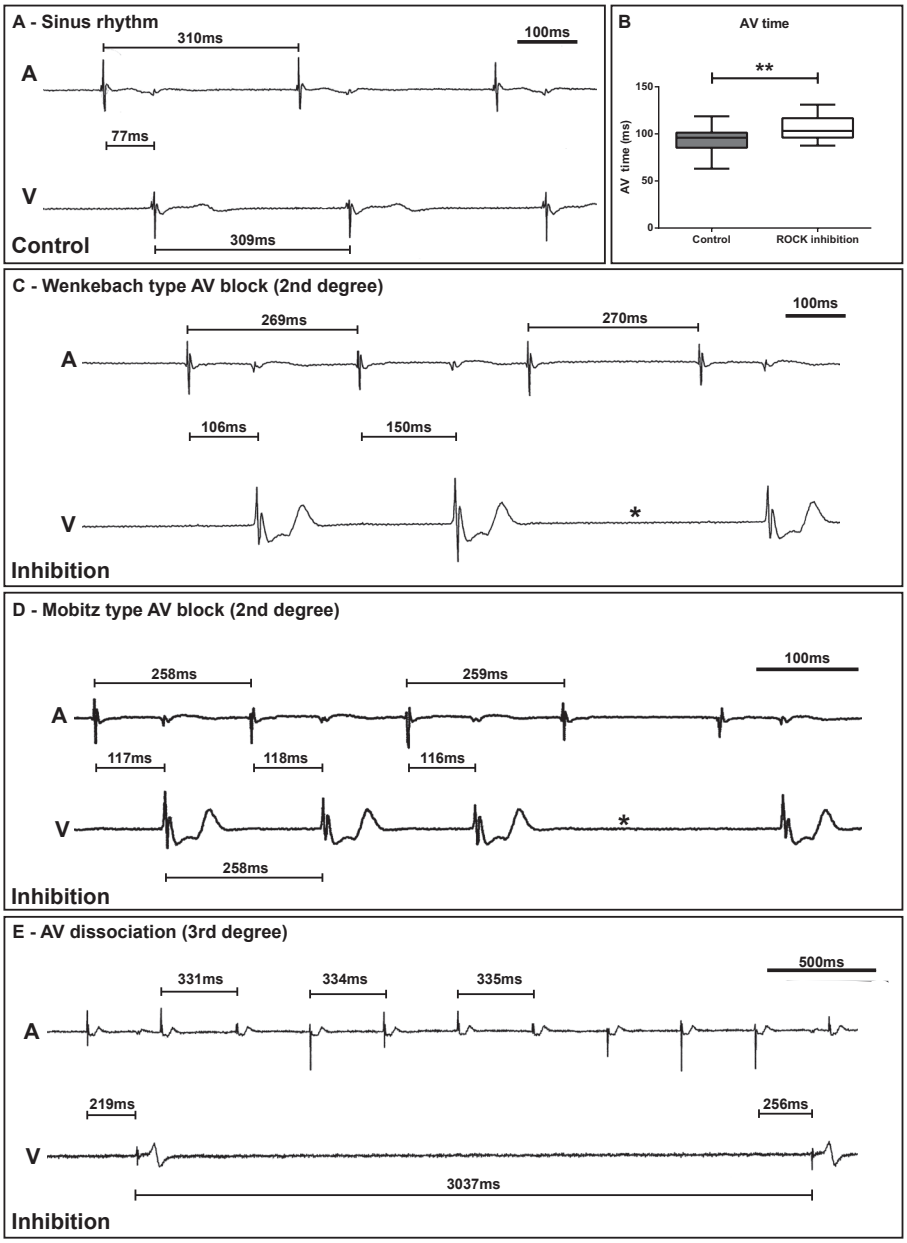

Figure 2. ROCK inhibition results in AV conduction disturbance

A. Normal AV conduction, atrial activation followed by ventricular activation. Time between subsequent ventricular activation waves is constant (309-310 milliseconds (ms)). **B.** AV time significantly prolonged after ROCK inhibition (**, p=0.0031). **C.** Example of Wenkebach type (second degree, type I) AV block, characterized by gradual prolongation of AV time, followed by complete AV block (asterisk). **D.** Example of Mobitz type (second degree, type II) AV block, characterized by sudden AV block (asterisk), without prolongation of AV time. **E.** Example of third degree AV block, characterized by dissociation between atrial and ventricular activation. Time between atrial activation constant (331-335ms), with variable AV time (219-256 ms). Note the low ventricular escape rhythm (+/- 20 beats per minute). A=atrial electrode, V=ventricular electrode.

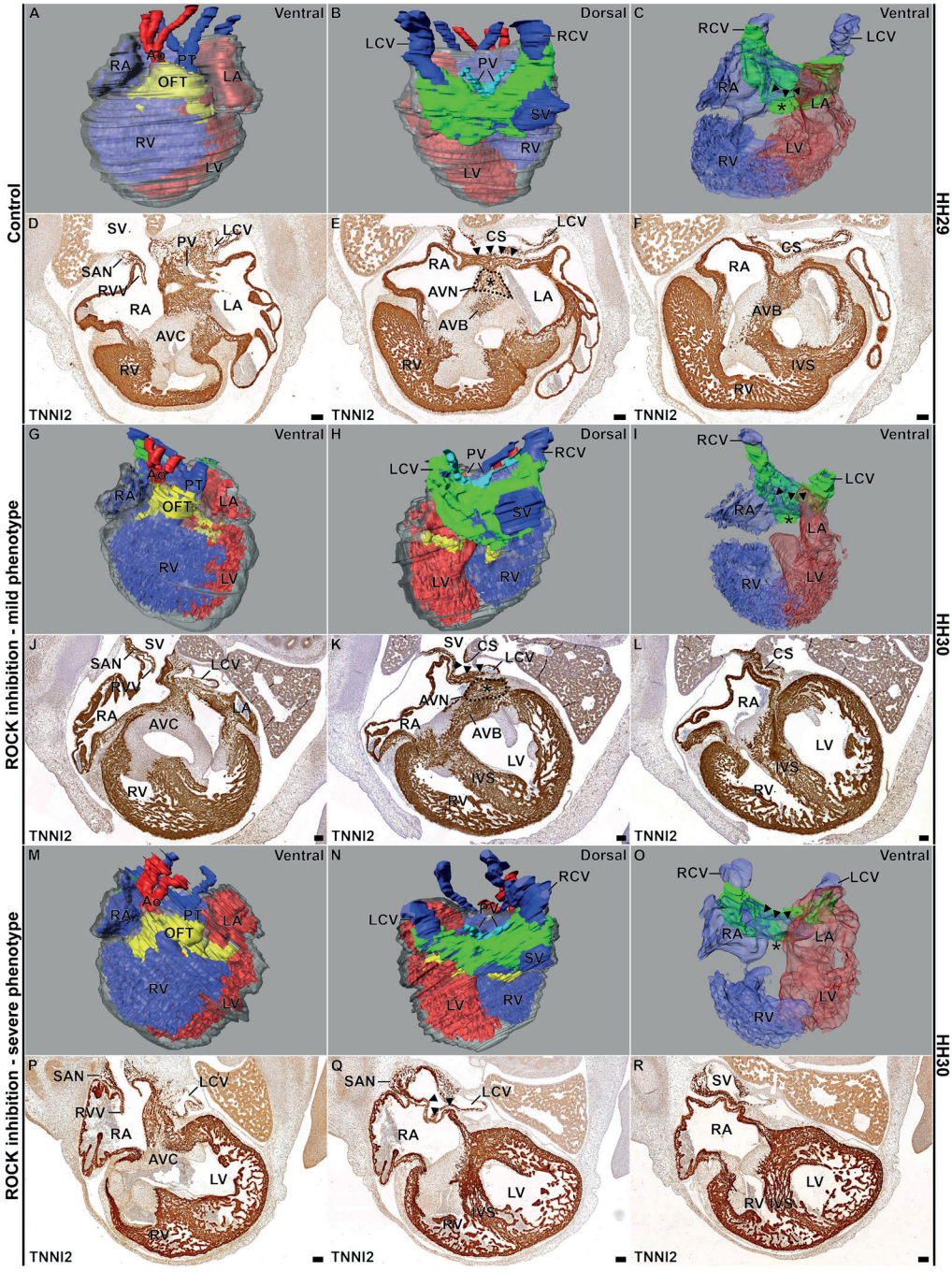

Figure 3. Development of the myocardial continuity between sinus venosus and posterior region of the AV canal is disturbed after ROCK inhibition (legend on page 162)

Figure 3. Development of the myocardial continuity between the sinus venosus and posterior region of the AV canal is disturbed after ROCK inhibition (figure on page 161)
A-C. 3D reconstructions (see below for color coding), control heart, HH29. Ventral (**A**) and dorsal (**B**) view. The sinus venosus (SV) myocardium, consisting of the myocardium of the SAN, the myocardium surrounding the cardinal veins and myocardium of the coronary sinus is shown in green. A ventral detail of the myocardial continuity between the SV and the posterior AV canal is provided in **C** (arrowheads). The putative AVN is shown (asterisk in **C**). **D-F.** Representative transverse sections of the same HH29 embryo, from cranial (**D**) to more caudal (**F**). The SV myocardium is shown. The myocardial continuity (arrowheads in **E**) between the sinus venosus and the putative AVN (dotted area with asterisk in **E**) is easily recognizabe. **G-I.** 3D reconstructions of the "mild phenotype" after ROCK inhibition, showing a smaller putative AVN region (asterisk in **I**). **J-L.** Representative transverse sections of the "mild phenotype", showing disturbed morphology of the myocardial continuity (compare arrows in **E** with arrows in **K**). Note the lateral displacement of the myocardial continuity between the SV and AV canal. Putative AVN is recognizable (dotted area with asterisk in **K**). **M-O.** 3D reconstructions of the "severe phenotype" after ROCK inhibition. The myocardial continuity is displaced laterally and is positioned more to the right (arrowheads in **O** and **Q**) and the putative AVN region (asterisk in **O**) is not recognizable. **P-R.** Representative transverse sections of the same embryo. Note the lateral and rightward displacement of the myocardial continuity (arrowheads in **Q**). The putative AVN is not recognizable and the connection between the sinus venosus and the posterior AV canal is smaller as compared to uninhibited hearts. Color coding 3D reconstructions: blue: lumen sinus venosus, right atrium, right ventricle and pulmonary artery; red: lumen left atrium, left ventricle, aorta; green: sinus venosus myocardium, yellow: mesenchymal tissue; light blue: pulmonary veins; transparent grey: myocardium. AVB: atrioventricular bundle, AVC: atrioventricular cushion, CS: coronary sinus, Ao: aorta, IVS: interventricular septum, LA: left atrium, LCV: left cardinal vein, LV: left ventricle, OFT: outflow tract, PV: pulmonary veins, RA: right atrium, RCV: right cardinal vein, RV: right ventricle, RVV: right venous valve, SAN: sinoatrial node, SV: sinus venosus. Scale bars: 100μm.

3.3. ROCK INHIBITION DOES NOT INTERFERE WITH INCORPORATION OF SINUS VENOSUS MYOCARDIUM IN THE POSTERIOR AV CANAL

In previous vital dye labeling studies, cells labeled with fluorescent dyes injected in the sinus venosus region could be traced to the posterior region of the AV canal, which corresponds to the region where the putative AVN develops.[4] As the RHOA-ROCK signaling pathway plays an important role during cell migration, proliferation, and motility[8,29], we hypothesized that inhibition of RHOA-ROCK signaling results in disturbed incorporation of the sinus venosus in the posterior AV canal, leading to disturbed AV conduction. To test this, the sinus venosus was labeled with vital dyes and labeling was assessed after 24 hrs of subsequent development.

In the control hearts (n=4), vital dye was seen in the region of the ISL1+/TNNI2+ myocardial continuity between the sinus venosus and the posterior AV

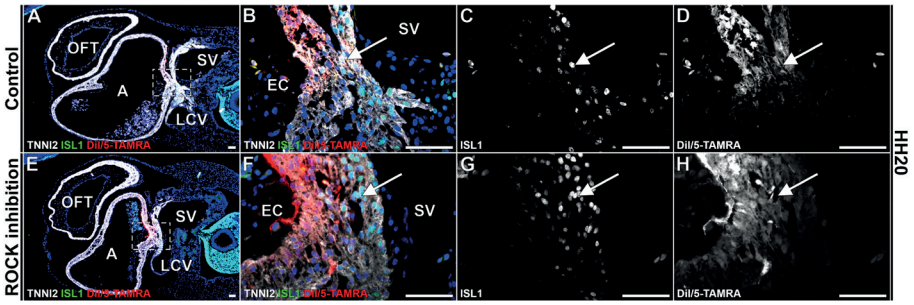

Figure 4. Incorporation of the sinus venosus myocardium in the posterior region of the AV canal is normal after ROCK inhibition

A. Overview of vital dye labeling after 24h in a control heart. The boxed area is shown at greater magnification in (**B-D**) **B.** Arrow shows ISL1+/TNNI2+ SV-AVC continuity with DiI/5-TAMRA labeling present in the continuity. Seperate grey values are shown for ISL1 (**C**, arrow = continuity) and DiI/5-TAMRA (**D**, arrow = continuity). **E.** Overview of labeling after ROCK inhibition. General morphology showed no apparent abnormalities at HH20. Boxed area is shown at greater magnification in (**F-H**). **F.** DiI/5-TAMRA is present in the SV-AVC continuity (arrows in **F-H**). Grey values for ISL1 (**G**) and DiI/5-TAMRA (**H**). A: atrium, EC: endocardial cushion, LCV: left cardinal vein, OFT: outflow tract, SV: sinus venosus. Scale bars: 50μm.

canal (**Fig. 4A-D**). After inhibition of the RHOA-ROCK pathway (n=5), no apparent morphological abnormalities were observed at HH20. Labeling was comparable to the control hearts. In the inhibited embryos, labeling was also present in the SV-AVC continuity (**Fig. 4E-H**), indicating that ROCK inhibition at HH15 does not interfere with incorporation of cells of the sinus venosus myocardium to the posterior region of the AV canal.

3.4. ROCK INHIBITION RESULTS IN ALTERED GENE EXPRESSION IN THE POSTERIOR AV CANAL

To investigate whether gene expression was disturbed after inhibition of the RHOA-ROCK pathway, qPCR was performed on specific regions of the heart at HH30-31 (corresponding with microelectrode recordings and immunohistochemical data) in control hearts and after ROCK inhibition.

ROCK inhibition resulted in alterations in gene expression in both regions extracted by LCM. In both groups of tissue ("SV-AVC" and "AVN region"), expression of *TNNT2* and *NKX2-5* (both expressed in high levels in myocardium) was comparable between control and ROCK inhibited embryos, confirming the myocardial identity of the isolated tissue (**Fig. 5A-B**). In the "SV-AVC" group, *HCN1* expression was detected in 4/5 (80%) of the control samples, whereas only 2/5 (40%) of the inhibited samples showed a detectable level of *HCN1* (**Fig. 5A**). The other genes showed no clear difference in expression between the two groups (**Fig. 5A**).

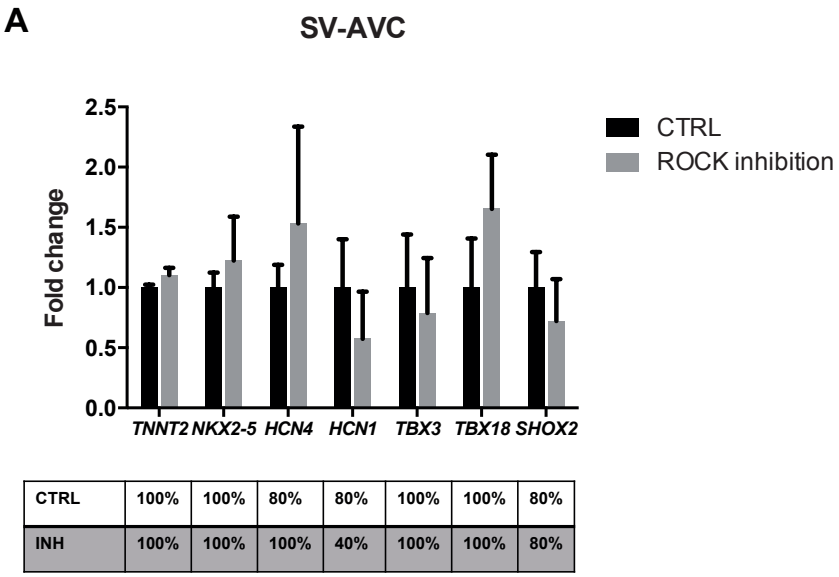

CTRL	100%	100%	80%	80%	100%	100%	80%
INH	100%	100%	100%	40%	100%	100%	80%

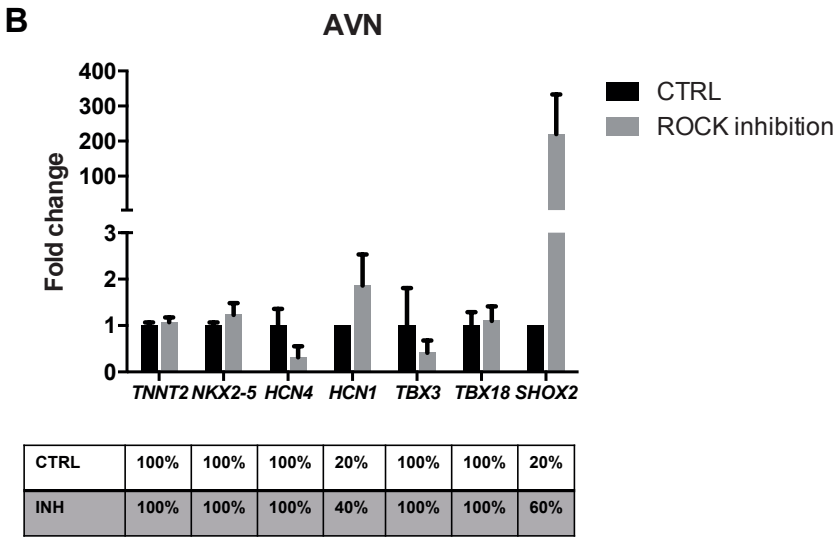

CTRL	100%	100%	100%	20%	100%	100%	20%
INH	100%	100%	100%	40%	100%	100%	60%

Figure 5. Disturbed gene expression after ROCK inhibition

A. qPCR results of tissue collected from the "SV-AVC" for the different genes of interest. The table underneath the graph shows the percentage of embryos in which expression of the corresponding gene could be detected. *HCN1* expression was found in 80% of control "SV-AVC" samples, compared to only 40% of samples after ROCK inhibition. **B.** qPCR results of tissue collected from the "AVN region" for the different genes of interest as in **A**, with the embryo percentage of the observed expression shown in the table underneath. *SHOX2* was found in 20% of control "AVN region" samples compared to 60% of "SV-AVC" samples. Expression appeared to be upregulated. Expression of *ISL1* was not shown in this figure, since none of the control embryos showed *ISL1* expression.

In the "AVN region" samples, no *ISL1* expression was detectable in the control group. However, in 2/5 (40%) of the ROCK inhibited samples, *ISL1* expression was detectable. *SHOX2* expression was detectable in 1/5 (20%) of the control hearts, compared to 3/5 (60%) of the inhibited samples (**Fig. 5B**). Expression appeared to be highly upregulated after ROCK inhibition (**Fig. 5B**). Unfortunately, statistical analysis was either not possible due to small numbers or showed no significant differences. However, the results do suggest abnormal differentiation of the AVN region after ROCK inhibition.

4. DISCUSSION

Understanding the developmental processes ultimately resulting in the mature AVN, is crucial to understand arrhythmias and conduction disturbances arising from this structure. Here we describe i. RHOA-ROCK inhibition in chick embryos as a novel model to study AV conduction disturbances; ii. Disturbed morphology of the myocardial continuity between the sinus venosus and the putative AVN in this model; iii. Altered gene expression in this region after disturbing RHOA-ROCK signaling.

Based on the findings in the current study, several explanations of the observed AV conduction disorders are possible. Morphological investigation of the AV transition after disturbing RHOA-ROCK signaling showed disturbed development of the myocardial continuity between the sinus venosus and the posterior region of the AV canal. Previous work showed that this continuity expresses HCN4 and ISL1 (both protein and mRNA), which are both important for normal functioning of the CCS.[4] Furthermore, cells extracted from this region showed a pacemaker-like electrophysiological phenotype, so it was concluded that this region is part of the CCS and likely plays a role in AV conduction.[4]

In the current study it was shown that ROCK inhibition results in a hypoplastic and laterally displaced SV-AVC continuity. In several hearts the AVN area could not be recognized at all. These morphological findings may well be related to the observed AV conduction disturbances. Stroud *et al.* described different degrees of AV conduction disturbances including AV block in cGATA6-Cre/Alk3-mice. Examination of the morphology of the AVN revealed an abnormally stretched and loosely organized AVN[30], indicating that abnormalities in morphology of the AVN coincide with AV conduction disturbances.

Although Rho-kinases are involved in cell motility[8], ROCK inhibition at HH15 did not interfere with incorporation of sinus venosus cells in the putative AVN region, as labeled cells could be traced towards the SV-AVC continuity. Cell tracing was performed at HH15, since this setup was previously validated. Incorporation of sinus venosus myocardium in the putative AVN region was confirmed with these experiments.[4]

In addition to aberrant development of the myocardial continuity between the sinus venosus and posterior AV canal and the putative AVN, gene expression was also disturbed. In the continuity between the sinus venosus and the posterior AV canal, *HCN1* expression was present in a higher percentage of control embryos as compared to ROCK inhibited embryos. The *HCN1* channel is expressed in the SAN and AVN[19] and mice deficient for *HCN1* display a phenotype resembling sick sinus syndrome[31], which suggests that *HCN1* is important for normal CCS functioning, and might help to explain the AV conduction disturbances after ROCK inhibition.

In the AVN region, *SHOX2* expression was found in a higher percentage of embryos, and *ISL1* was re-expressed after ROCK inhibition. Expression of *SHOX2* was increased after ROCK inhibition. These results correspond with previous data.[10,11] It was previously shown that ROCK inhibition resulted in disturbed lateralization of the SAN, with increased pacemaker potential at the left side of the sinus venosus myocardium and a more immature right side of the sinus venosus myocardium (the location where the SAN normally develops).[11]

Upregulation of *SHOX2* in the region of the AVN may be of interest to explain the observed phenotype. *Shox2* is important for normal development of the venous pole of the heart, including the SAN.[25,26] To date, focus has predominantly been on development of the SAN and the majority of studies have been performed in models where expression of *Shox2* is disturbed. However, previous work showed *Shox2* expression in the AV junction.[32] Furthermore, *Shox2* plays an important role in normal electrophysiological functioning within the AV junction.[33] Overexpression of *Shox2* in embryonic stem cells resulted in enhanced automaticity and an increase in pacing-ability of these cells.[34]. This is in line with the observed re-expression of *ISL1* in the putative AVN. *ISL1* is expressed in the developing SAN and is necessary for normal SAN development.[35,36] The increase in expression of SAN related genes (*ISL1/SHOX2*) in the region of the putative AVN might result in a more immature phenotype of the AVN, resulting in AV conduction disturbances. Furthermore, altered intercellular coupling and electrophysiological characteristics in this region could be of importance. ROCK inhibition hampers Connexin (Cx) 40 expression in the sinus venosus.[11] Cx40 is one of the major gap junction proteins.[37] These proteins are responsible for intercellular coupling, necessary for normal propagation of the action potential.[37] Altered differentiation and intercellular coupling in the region of the putative AVN might explain the observed AV conduction disorders after ROCK inhibition.

Finally, we described a “mild” and “severe” phenotype after ROCK inhibition. mRNA expression could only be tested in the “mild” phenotype, since the AVN region was not recognizable in the “severe” phenotype. Gene expression is expected to be more severely affected in the group with the “severe” phenotype, but quantification was not possible.

5. CONCLUSIONS

RHOA-ROCK signaling is essential for normal development of the myocardial continuity between the sinus venosus and posterior region of the AV canal, including the AVN region. Disturbing the RHOA-ROCK signaling pathway results in AV block, which, at least in part, can be explained by the abnormal morphology of the AV transition and abnormal differentiation of the putative AVN after inhibition.

The AV conduction disturbances found after ROCK inhibition mimic the classic clinical types of AV block (1st to 3rd degree AV block were found). This AV block model can therefore be used to further investigate the development of AV conduction disturbances and to study the effects of therapeutic strategies (including pharmacological interventions) aimed at treating these common clinical arrhythmias.

REFERENCE LIST

1. Mazgalev, T. N., Ho, S. Y. & Anderson, R. H. Anatomic-electrophysiological correlations concerning the pathways for atrioventricular conduction. *Circulation.* **103,** 2660–2667 (2001).

2. Inoue, S. & Becker, A. E. Posterior extensions of the human compact atrioventricular node : A neglected anatomic feature of potential clinical significance. *Circulation.* **97,** 188–193 (1998).

3. Aanhaanen, W. T. J. *et al.* Defective Tbx2-dependent patterning of the atrioventricular canal myocardium causes accessory pathway formation in mice. *J. Clin. Invest.* **121,** 534–44 (2011).

4. Kelder, T. P. *et al.* The sinus venosus myocardium contributes to the atrioventricular canal: potential role during atrioventricular node development? *J. Cell. Mol. Med.* **19,** 1375–89 (2015).

5. Sun, Y. *et al.* Islet 1 is expressed in distinct cardiovascular lineages, including pacemaker and coronary vascular cells. *Dev. Biol.* **304,** 286–96 (2007).

6. Vicente-Steijn, R. *et al.* Funny current channel HCN4 delineates the developing cardiac conduction system in chicken heart. *Heart Rhythm.* **8,** 1254–63 (2011).

7. Vicente-Steijn, R. *et al.* Electrical activation of sinus venosus myocardium and expression patterns of RHOA and Isl-1 in the chick embryo. *J. Cardiovasc. Electrophysiol.* **21,** 1284–92 (2010).

8. Riento, K. & Ridley, A. J. Rocks: multifunctional kinases in cell behaviour. *Nat. Rev. Mol. Cell Biol.* **4,** 446–56 (2003).

9. Kaarbø, M., Crane, D. I. & Murrell, W. G. RHOA regulation of cardiomyocyte differentiation. *Sci. World J.* **2013,** 1–12 (2013).

10. Cheng, Y.-T. *et al.* Rho-associated kinase inhibitors promote the cardiac differentiation of embryonic and induced pluripotent stem cells. *Int. J. Cardiol.* **201,** 441–448 (2015).

11. Vicente-steijn, R. *et al*. RHOA-ROCK signaling is necessary for lateralization and differentiation of the developing sinoatrial node. *Cardiovasc. Res.* **113,** 1186-97 (2017).

12. Sah, V. P. *et al.* Cardiac-specific overexpression of RHOA results in sinus and atrioventricular nodal dysfunction and contractile failure. *J. Clin. Invest.* **103,** 1627–34 (1999).

13. Wei, L. *et al.* Disruption of Rho signaling results in progressive atrioventricular conduction defects while ventricular function remains preserved. *FASEB J.* **18,** 857–9 (2004).

14. Hamburger, V. & Hamilton, H. L. A series of normal stages in the development of the chick embryo. *J. Morphol.* **88,** 49–92 (1951).

15. Kolditz, D. P. *et al.* Persistence of functional atrioventricular accessory pathways in postseptated embryonic avian hearts: implications for morphogenesis and functional maturation of the cardiac conduction system. *Circulation.* **115,** 17–26 (2007).

16. Kelder, T. P. *et al.* The epicardium as modulator of the cardiac autonomic response during early development. *J. Mol. Cell. Cardiol.* **89,** 251–9 (2015).

17. Jongbloed, M. R. M. *et al.* Embryonic conduction tissue: a spatial correlation with adult arrhythmogenic areas. *J. Cardiovasc. Electrophysiol.* **15,** 349–55 (2004).

18. Gittenberger-de Groot, A. C. *et al.* Nkx2.5-negative myocardium of the posterior heart field and its correlation with podoplanin expression in cells from the developing cardiac pacemaking and conduction system. *Anat. Rec.* **290,** 115–22 (2007).

19. Herrmann, S., Layh, B. & Ludwig, A. Novel insights into the distribution of cardiac HCN channels: an expression study in the mouse heart. *J. Mol. Cell. Cardiol.* **51,** 997–1006 (2011).

20. Garcia-Frigola, C., Shi, Y. & Evans, S. M. Expression of the hyperpolarization-activated cyclic nucleotide-gated cation channel HCN4 during mouse heart development. *Gene Expr. Patterns* **3,** 777–783 (2003).

21. Hoogaars, W. M. H. *et al.* The transcriptional repressor Tbx3 delineates the developing central conduction system of the heart. *Cardiovasc. Res.* **62,** 489–99 (2004).

22. Frank, D. U. *et al.* Lethal arrhythmias in Tbx3-deficient mice reveal extreme dosage sensitivity of cardiac conduction system function and homeostasis. *Proc. Natl. Acad. Sci. USA.* **109,** E154-63 (2012).

23. Christoffels, V. M. *et al.* Formation of the venous pole of the heart from an Nkx2-5-negative precursor population requires Tbx18. *Circ. Res.* **98,** 1555–63 (2006).

24. Kapoor, N., Liang, W., Marbán, E. & Cho, H. C. Direct conversion of quiescent cardiomyocytes to pacemaker cells by expression of Tbx18. *Nat. Biotechnol.* **31,** 54–62 (2013).

25. Blaschke, R. J. *et al.* Targeted mutation reveals essential functions of the homeodomain transcription factor Shox2 in sinoatrial and pacemaking development. *Circulation.* **115,** 1830–8 (2007).

26. Puskaric, S. *et al.* Shox2 mediates Tbx5 activity by regulating Bmp4 in the pacemaker region of the developing heart. *Hum. Mol. Genet.* **19,** 4625–33 (2010).

27. Da Costa, D., Brady, W. J. & Edhouse, J. Bradycardias and atrioventricular conduction block. *BMJ.* **324,** 535–8 (2002).

28. Blom, N. A. *et al.* Development of the cardiac conduction tissue in human embryos using HNK-1 antigen expression: possible relevance for understanding of abnormal atrial automaticity. *Circulation.* **99,** 800–6 (1999).

29. Amin, E. *et al.* Rho-kinase: regulation, (dys)function, and inhibition. *Biol. Chem.* **394,** 1399–410 (2013).

30. Stroud, D. M. *et al.* Abnormal conduction and morphology in the atrioventricular node of mice with atrioventricular canal targeted deletion of Alk3/Bmpr1a receptor. *Circulation.* **116,** 2535–43 (2007).

31. Fenske, S. *et al.* Sick sinus syndrome in HCN1-deficient mice. *Circulation.* **128,** 2585–94 (2013).

32. Sun, C., Zhang, T., Liu, C., Gu, S. & Chen, Y. Generation of Shox2-Cre allele for tissue specific manipulation of genes in the developing heart, palate, and limb. *Genesis.* **51,** 515–22 (2013).

33. Sun, C. *et al.* The short stature homeobox 2 (Shox2)-bone morphogenetic protein (BMP) pathway regulates dorsal mesenchymal protrusion development and its temporary function as a pacemaker during cardiogenesis. *J. Biol. Chem.* **290,** 2007–23 (2015).

34. Ionta, V. *et al.* SHOX2 overexpression favors differentiation of embryonic stem cells into cardiac pacemaker cells, improving biological pacing ability. *Stem Cell Reports.* **4,** 129–42 (2015).

35. Vedantham, V., Galang, G., Evangelista, M., Deo, R. C. & Srivastava, D. RNA sequencing of mouse sinoatrial node reveals an upstream regulatory role for Islet-1 in cardiac pacemaker cells. *Circ. Res.* **116,** 797–803 (2015).

36. Liang, X. *et al.* Transcription factor ISL1 is essential for pacemaker development and function. *J. Clin. Invest.* **125,** 3256–68 (2015).

37. Chaldoupi, S.-M., Loh, P., Hauer, R. N. W., de Bakker, J. M. T. & van Rijen, H. V. M. The role of connexin40 in atrial fibrillation. *Cardiovasc. Res.* **84,** 15–23 (2009).

SUPPLEMENTAL MATERIAL

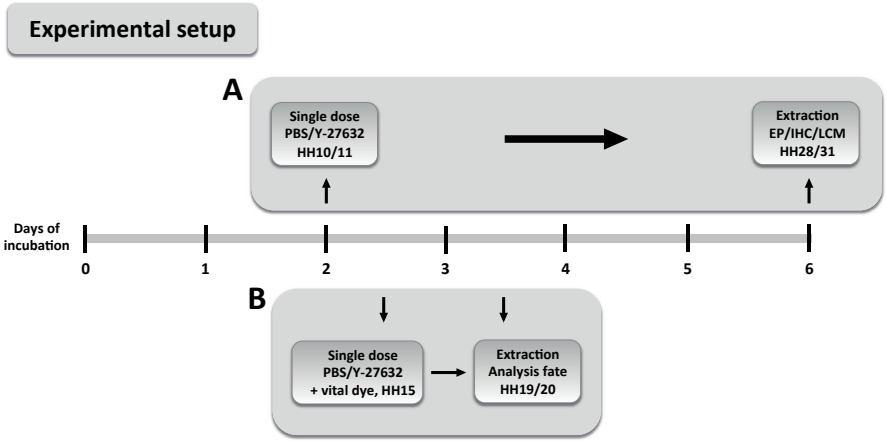

Supplemental Figure 1. Schematic representation of experimental setup

Two sets of time points were chosen for the experiments. **A.** Embryos were treated with either PBS or Y-27632 at HH10/11 (day 2 of incubation). The embryos were extracted at HH28-31 (day 6 of incubation) for electrophysiology (EP, microelectrode recordings), immunohistochemistry (IHC) or laser capture microdissection (LCM). **B.** Embryos were treated with either PBS or Y-27632 and the sinus venosus myocardium was labeled with vital dye at HH15 (2.5 days of incubation). The embryos were extracted at HH 19-20 (3.5 days of incubation) and the fate of the labeled cells was analyzed.

Supplemental table 1. Used primers

Primer	Sequence
GAPDH forward	5'-CTAAGGCTGTGGGGAAGGT-3'
GAPDH reverse	5'-GTTGTTGACCTGACCTGCC-3'
TNNT2 forward	5'-AAGAAGGGTGGCAAGAAGC-3'
TNNT2 reverse	5'-TGTCTTCGCTGAGGTGGTC-3'
NKX2-5 forward	5'-CCCTACTACGTGAAGAGCTACG-3'
NKX2-5 reverse	5'-TCGGGATCCTCCAGCTCTCT-3'
NKX2-5 nested forward	5'-GCTACGGGGAGATGGACAC-3'
NKX2-5 nested reverse	5'-GGGATCCTCCAGCTCTCTC-3'
HCN4 forward	5'-GCCTTCTGCTGTTGGCTCT-3'
HCN4 reverse	5'-GCTGCTGGATGTGGTAGGA-3'
HCN4 nested forward	5'-GCCTTCTGCTGTTGGCTCT-3'
HCN4 nested reverse	5'-GCTGCTGGATGTGGTAGGA-3'
HCN1 forward	5'-CTGCACCCAAGAATGAGGTT-3'
HCN1 reverse	5'-ATCAGGGTGGAAATCTCGTG-3'
HCN1 nested forward	5'-GCCCTCCACAACACCAAC-3'
HCN1 nested reverse	5'-TCAGGGTGGAAATCTCGTG-3'
ISL1 forward	5'-AAAAGAAGCATTATGATGAAGCAA-3'
ISL1 reverse	5'-CATGTCTCTCCGGACTAGCAG-3'
ISL1 nested forward	5'-AGCAACCCAATGACAAAAC-3'
ISL1 nested reverse	5'-TGTCTCTCCGGACTAGCAG-3'
TBX3 forward	5'-TCGTCCGAGCGAACGATATT-3'
TBX3 reverse	5'-TCGTCCGAAGTGGGGTTTTC-3'
TBX3 nested forward	5'-CATCGCAGTGACCGCATAC-3'
TBX3 nested reverse	5'-CCTCCTTCCATTCCCAGTG-3'
TBX18 forward	5'-GCTTTGGTGGAGTCTTACGC-3'
TBX18 reverse	5'-CAAAAGGTGAGGGTGGGTAG-3'
TBX18 nested forward	5'-ACGCCTTCTGGAGACCTTC-3'
TBX18 nested reverse	5'-GCACTCCACTGCCAGATCC-3'
SHOX2 forward	5'-AGGATGCGAAAGGCATGGAA-3'
SHOX2 reverse	5'-CCGGCATTTGGCTTTTCTGT-3'
SHOX2 nested forward	5'-TTCGACGAGACCCACTACC-3'
SHOX2 nested reverse	5'-TTTGGAACCAAACCTGCAC-3'

8

THE EPICARDIUM AS MODULATOR OF THE CARDIAC AUTONOMIC RESPONSE DURING EARLY DEVELOPMENT

Tim P. Kelder, Sjoerd N. Duim, Rebecca Vicente-Steijn, Anna M.D. Végh, Boudewijn P.T. Kruithof, Anke M. Smits, Thomas C. van Bavel, Noortje A. M. Bax, Martin J. Schalij, Adriana C. Gittenberger-de Groot, Marco C. DeRuiter, Marie-José Goumans, Monique R.M. Jongbloed

Modified after Journal of Molecular and Cellular Cardiology, 89: 251-9 (2015)

ABSTRACT

The cardiac autonomic nervous system (cANS) modulates the heart rate, contraction force and conduction velocity. The embryonic chicken heart already responds to epinephrine prior to establishment of the cANS. The aim of this study was to define the regions of the heart that might participate in modulating the early autonomic response to epinephrine. Immunofluorescence analysis revealed expression of neural markers tubulin beta-3 chain and neural cell adhesion molecule in the epicardium during early development. In addition, expression of the β2 adrenergic receptor, the receptor for epinephrine, was found in the epicardium. *Ex ovo* microelectrode recordings in hearts with inhibition of epicardial outgrowth showed a significantly reduced response of the heart rate to epinephrine compared to control hearts. This study suggests a role for the epicardium as autonomic modulator during early cardiac development.

1. INTRODUCTION

The cardiac autonomic nervous system (cANS) is essential in modulating cardiac function by altering heart rate (chronotropy), conduction velocity (dromotropy) and force of contraction (inotropy).[1] Dysfunctioning of the cANS plays a role in the pathogenesis of arrhythmias[1] and hypertension[2] and is involved in disease progression in heart failure.[3] Furthermore, normal functioning of the cANS is important for the prognosis of adult patients with congenital heart disease.[4] Understanding the processes that govern normal cANS development may help to unravel the pathophysiology of abovementioned disease processes and to develop targeted treatment options.

The cANS can be divided into a sympathetic and parasympathetic component. In general, sympathetic stimulation results in an increase of heart rate, conduction velocity and force of contraction, while parasympathetic stimulation has an opposing effect. Sympathetic neurons have their cell bodies primarily in the paravertebral stellate ganglion, whereas parasympathetic cell bodies are located in the cardiac ganglia.[5] The cells contributing to the cANS are derivatives of neural crest cells (NCCs) and cells of the nodose placode.[6,7] Kroese *et al.* demonstrated that prior to cardiac sympathetic innervation of the developing chicken embryo, the heart already responds to the catecholamine epinephrine.[8] This neurotransmitter binds to beta (β) adrenergic receptors, thereby activating cAMP dependent signaling[9], resulting in an increase in heart rate, conduction velocity and force of contraction.[5] It is remarkable that expression of enzymes necessary for production of catecholamines was found throughout the myocardium during cardiac development in rat[10], even before production is observed in the adrenal glands.[11,12] After addition of epinephrine in chick at Hamburger and Hamilton (HH[13]) stage 20-24, several hemodynamic parameters, including heart rate, increased significantly.[8] This supports an important role for catecholamines in the heart during early embryonic development. Furthermore, stimulation of chick embryos with isoproterenol (β-agonist) at embryonic day 7 (HH30-31) resulted in an increase in cAMP.[14] In addition to responding to β-adrenergic stimulation, the early embryonic chicken heart was also shown to respond to β-adrenergic receptor blockade by reducing heart rate and cardiac output.[15] Thus prior to establishment of the cANS, the heart already responds to autonomic stimulation and blockade.

Interestingly, Kroese *et al.* showed that after treatment with all-trans retinoic acid (RA) the reaction to epinephrine, including the increase in heart rate, was significantly reduced.[8] Normal RA signaling has been shown to be important for proper development of the epicardium.[16] This single layer of cells is derived from the proepicardial organ (PEO) and covers the initially bare primary myocardial heart tube. Cells derived from the epicardium are known to play an essential role

during normal cardiac development and defects in epicardial development result in cardiac malformations (reviewed in[17]).

The aim of the current study was to identify which cell population in the developing heart plays a role in modulating the autonomic response during early development. Our studies reveal unanticipated expression of neuronal markers in the epicardium during early cardiac development. To investigate a potential role of the epicardium, electrophysiological experiments were performed with and without inhibition of epicardial outgrowth.

2. MATERIAL AND METHODS

2.1. ANIMALS

Immunohistochemical analysis was performed in wild type mouse embryos with a mixed genetic background of different embryonic stages (E9.5-E17.5, mice described in[18]). The morning of the vaginal plug was considered E0.5. Pregnant mice were euthanized using CO_2 exposure and cervical dislocation. Animal care was in accordance with national and institutional guidelines and approved by the animal experiments committee of the Leiden University Medical Center.

To study protein expression in chick embryos, fertilized eggs of the White Leghorn chicken were incubated at 37°C and 80% humidity. Hearts were excised, and staged according to the Hamburger and Hamilton (HH) criteria.[13] Tissue was fixed in 4% paraformaldehyde for 24 hours and subsequently embedded in paraffin and sectioned (5µm) for immunohistochemical analysis.

2.2. HUMAN FETAL TISSUE

A 5-week-old human fetal heart was collected after elective abortion based on individual informed consent procedures conforming to the Declaration of Helsinki. Furthermore, the study was approved by the Medical Ethics committee of the Leiden University Medical Center. Tissue was treated as described above.

2.3. IMMUNOHISTOCHEMISTRY

The protocol used for immunohistochemical staining was described previously.[19] Briefly, slides were rehydrated, subjected to heat-induced epitope retrieval and incubated with the following list of antibodies: anti-cardiac Troponin I (CTNI) (myocardial marker, 1:1000, 4T21/2, HyTest Ltd), anti-Wilms' tumor-1 (WT1) (expressed in the epicardium, 1:1000, ab89901, Abcam), anti-tubulin beta-3 chain (TUBB3) (neuronal marker, 1:200, AB78078, Abcam), Neural Cell Adhesion Molecule (NCAM) (neuronal marker, 1:250, AB5032, Merck), anti-β1 adrenergic receptor (β1AR) (receptor for epinephrine, 1:200, PA528808, Thermo Scientific), and anti-β2 adrenergic receptor (β2AR) (receptor for epinephrine, 1:200, ab61778, Abcam). To amplify WT1 expression Tyramide Signal Amplification

(PerkinElmer) was used. Visualization was achieved by incubation with Alexa Fluor® 488 streptavidin (Invitrogen). The remainder of primary antibodies was visualized with Alexa-conjugated fluorescent secondary antibodies (Invitrogen) at a final concentration of 1:200. DAPI (D3571, 1/1000; Life Technologies) was used as a nuclear stain, after which slides were mounted with Prolong gold (Life Technologies).

2.4. MECHANICAL BLOCKING OF THE PROEPICARDIAL ORGAN

Mechanical inhibition of epicardial outgrowth in the chicken embryo was performed as described previously.[20] At HH15, a window was created in the eggshell, after which the embryonic membranes were opened. Subsequently, a small piece of eggshell membrane was placed between the PEO and developing heart tube, after which the egg was reincubated until the desired stage. In order to verify that outgrowth of the epicardial layer was hampered, hearts were sectioned and Haematoxylin and Eosin staining was performed.

2.5. EX OVO EXTRACELLULAR MICROELECTRODE RECORDINGS AND EPINEPHRINE ADMINISTRATION

To investigate the effect of epinephrine on heart rate, electrophysiological measurements were performed in embryonic chicken hearts at different developmental stages. After reaching the desired stage of development, embryos were extracted from the egg. The heart and some surrounding tissue was excised and placed in a temperature-controlled (37 ± 0.1°C) tissue bath containing Tyrode. Recordings were performed using a previously described protocol.[21] Recording electrodes were placed on the atrium and the ventricular apex, and a reference electrode in the tissue bath. The hearts of five groups of embryos were studied: 1. HH15 embryos (n=5), when the heart is not yet covered by epicardium; 2. HH19 embryos (n=3), when epicardial covering of the sinus venosus, atria and AV canal has commenced; 3. HH21 embryos (n=3), when migration of epicardial cells around the heart is (nearly) complete[22]; 4. HH24-25 control embryos (n=9, no surgical manipulation), when epicardial covering has been completed and subepicardial mesenchyme is present; 5. HH24-25 embryos (n=9) after inhibition of epicardial outgrowth.

The hearts were allowed to reach a stable baseline heart rate (which was comparable between all studied groups (**Supplemental Fig. 1**), after which 100µl of pre-warmed epinephrine (1mg/ml, Centrafarm, The Netherlands) was directly pipetted onto the heart. Pre-warmed Tyrode was administered as a negative control to HH24-25 hearts (n=6). The relative response to epinephrine was calculated by correcting the change in heart rate for the baseline heart rate. The heart rate was calculated every 10 seconds and plotted.

2.6. STATISTICAL ANALYSIS

The Mann-Whitney U-test (two groups) or Kruskal-Wallis test (>two groups) were used, since the data was not normally distributed. $P<0.05$ was considered statistically significant. Data shown is mean ± S.E.M. Statistical analysis was performed using the Graphpad Prism 6 software package (Graphpad Software).

3. RESULTS

3.1. DURING EARLY CARDIAC DEVELOPMENT THE NEURONAL MARKER TUBB3 IS EXPRESSED BY THE EPICARDIUM

In order to investigate which cell population plays a potential role in modulation of the early cardiac autonomic response, protein expression of the neuronal marker TUBB3 was analyzed during cardiogenesis.

At E9.5, the primary heart tube is not covered by epicardial cells and the PEO is recognizable (**Fig. 1a-d**). Co-expression of neuron-specific TUBB3 and WT1 was observed in a subset of cells in the PEO (**Fig. 1a-d**). WT1+/TUBB3- and WT1-/TUBB3+ cells were also present (**Fig. 1a-d**), confirming the heterogeneity of the PEO.[23] At E10.5, the epicardial layer started to envelope the heart and showed co-expression of TUBB3 and WT1 in most epicardial cells (**Fig. 1e-h**). Co-expression of TUBB3 and WT1 was still clearly present at E11.5 in the majority of epicardial cells (**Fig. 1i-l**). Strong expression of TUBB3 was observed in the mesenchyme of the endocardial cushions in the outflow tract (OFT) and AV canal, shown at E11.5 (**Fig. 1i-l**). TUBB3 expression in the epicardium decreased with ongoing development. At E12.5, only faint expression was observed in the epicardium (**Fig. 1m-p**), disappearing at E13.5 (**Fig. 1q-t**). At this stage, TUBB3 expression was only observed in subepicardial nerve fibers (**Fig. 1q-t**) and no co-expression of TUBB3 and WT1 was observed in the epicardium or subepicardium.

To confirm the neuronal phenotype of the epicardium, NCAM (neuronal marker) expression was analyzed. At E11.5, co-expression of NCAM and TUBB3 was seen in the nervous system, including the neural tube and dorsal root ganglion (**Supplemental Fig. S2a-d**). Furthermore, NCAM expression was seen in the epicardium, co-localizing with TUBB3 (**Supplemental Fig. S2e-h**), thereby confirming the neuronal phenotype of the epicardium.

In addition, TUBB3 expression was analyzed during early human fetal development. A subset of epicardial cells and cells in the endocardial cushions showed expression of TUBB3 (**Supplemental Fig. S3b-c**). Furthermore, cells in the subepicardial space showed TUBB3 expression (**Supplemental Fig. S3d-e**).

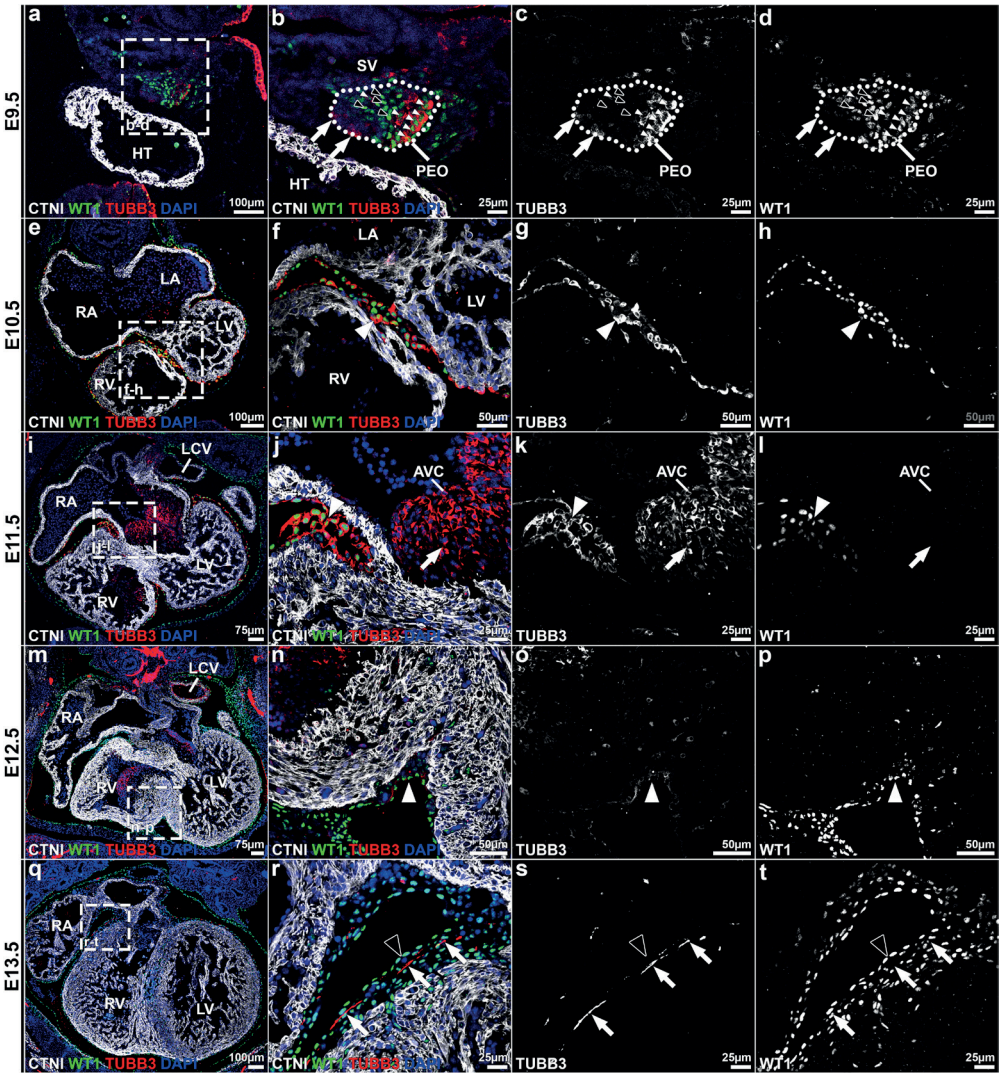

Figure 1. The neuronal specific marker TUBB3 is expressed in the epicardium and subepicardium during early development

a-d. At E9.5, the PEO (dotted line) is recognizable and the heart tube is not covered by epicardium. WT1+/TUBB3+ cells (white arrowheads in **b-d**), WT1+/TUBB3- cells (black arrowheads in **b-d**) and WT1-/TUBB3+ cells (arrows in in **b-d**) are observed within the PEO. **e-h.** At E10.5 the heart is partially surrounded by epicardial cells and co-expression of TUBB3 with WT1 is seen in most epicardial cells (arrowheads in **f-h**). **i-l.** Co-expression of TUBB3 and WT1 in the epicardium is still present at E11.5 (arrowheads in **j-l**). TUBB3 expression is also seen in the endocardial cushions (arrows in **j-l**), shown here at E11.5. **m-p.** Co-expression of TUBB3/WT1 decreases from E12.5 (compare white arrowhead in **k** with white arrowhead in **o**). **q-t.** At E13.5 the expression of TUBB3 in the WT1+ epicardium (black arrowheads in **r-t**) is lost but is now present in subepicardial nerve fibers (arrows in **r-t**). AVC: atrioventricular cushion, HT: heart tube, LA: left atrium, LCV: left cardinal vein, LV: left ventricle, PEO: proepicardial organ, RA: right atrium, RV: right ventricle, SV: sinus venosus.

3.2. A SUBPOPULATION OF CELLS IN THE CENTRAL NERVOUS SYSTEM CO-EXPRESSES WT1 AND TUBB3

The neuronal marker TUBB3 showed protein expression in the epicardium, co-expressing with WT1. In order to provide possible evidence that these proteins are involved in normal neuronal function, expression of TUBB3 and WT1 was studied in the nervous system. At E11.5, the developing nervous system showed expression of TUBB3 (**Fig. 2a-d**). No WT1 expression was found (**Fig. 2a-d**). Microscopic analysis at E13.5 revealed co-expression of TUBB3 and WT1 in the ventral region of the neural tube, as well as the roof of the 4th ventricle of the brain (**Fig. 2e-g**). WT1 expression was observed along the entire length of the neural tube (**Fig. 2e**). Co-expression of TUBB3 and WT1 in the spinal cord was still present at E17.5 (**Fig. 2h-k**).

3.3. DURING EARLY CARDIAC DEVELOPMENT THE CATECHOLAMINE RECEPTOR β2AR IS EXPRESSED BY THE EPICARDIUM

To further confirm a potential neuronal phenotype of the epicardium, expression of the beta1 (β1) and beta2 (β2) adrenergic receptors (AR) was studied. To confirm neural co-expression of TUBB3 and β2AR, these markers were studied at E11.5 in the nervous system. Co-labeling of TUBB3 and β2AR was seen in the dorsal root ganglion and neural tube (**Fig. 3a-d**).

In murine embryos at E11.5, most epicardial cells are TUBB3+, and a subpopulation of epicardial cells showed co-expression with β2AR (**Fig. 3e-h**). β2AR+ cells were found throughout the epicardial layer, predominantly seen in the AV sulcus (arrowheads in **Fig. 3e**) and interventricular sulcus (**Fig. 3e-h**). Furthermore, expression of β2AR was seen in endocardial cells and a subpopulation of cells in the endocardial cushions (**Fig. 3e**). Expression of TUBB3 and β2AR was seen in the subepicardium at E12.5, with a subset of cells co-expressing both markers (**Fig. 3i-l**). β1AR expression was not observed in these stages (not shown).

3.4. INHIBITION OF EPICARDIAL OUTGROWTH RESULTS IN A DIMINISHED RESPONSE TO EPINEPHRINE

At HH21 of chick development, expression of β2AR was found in the epicardium, PEO and endocardium (**Supplemental Fig. S4**), which is in agreement with the β2AR expression found in mice. First, the role of the epicardial layer in the response of the heart to epinephrine was studied. For this purpose, chick hearts from embryos of subsequent stages of epicardial development were analyzed using *ex ovo* microelectrode recordings (**Fig. 4** and **Supplemental Fig. S5**). The relative increase ((maximal heart rate – baseline)/(baseline)) * 100%) in heart

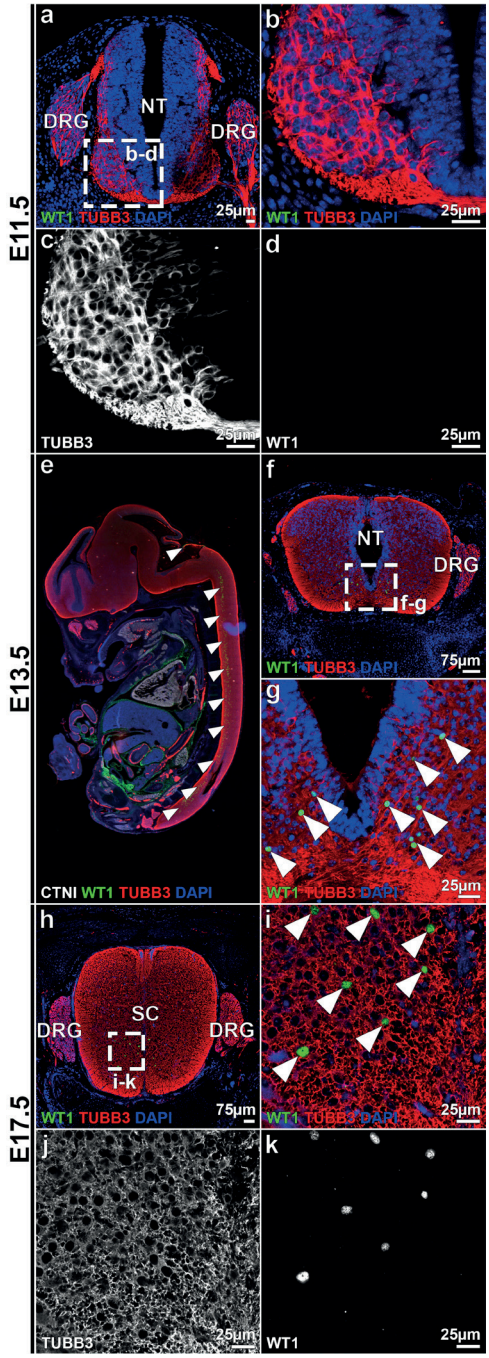

Figure 2. WT1 is expressed in the ventral horn of the spinal cord

a-d. At E11.5 TUBB3 is present in the neural tube. However, no co-expression with WT1 is found. **e-g.** At E13.5 co-expression of WT1 and TUBB3 is observed in the ventral horn of the neural tube and the roof of the 4th ventricle of the brain (arrowheads). **h-k.** Co-expression of TUBB3/WT1 is still present in the spinal cord at E17.5 (arrowheads in **i**). DRG: dorsal root ganglion, NT: neural tube, SC: spinal cord.

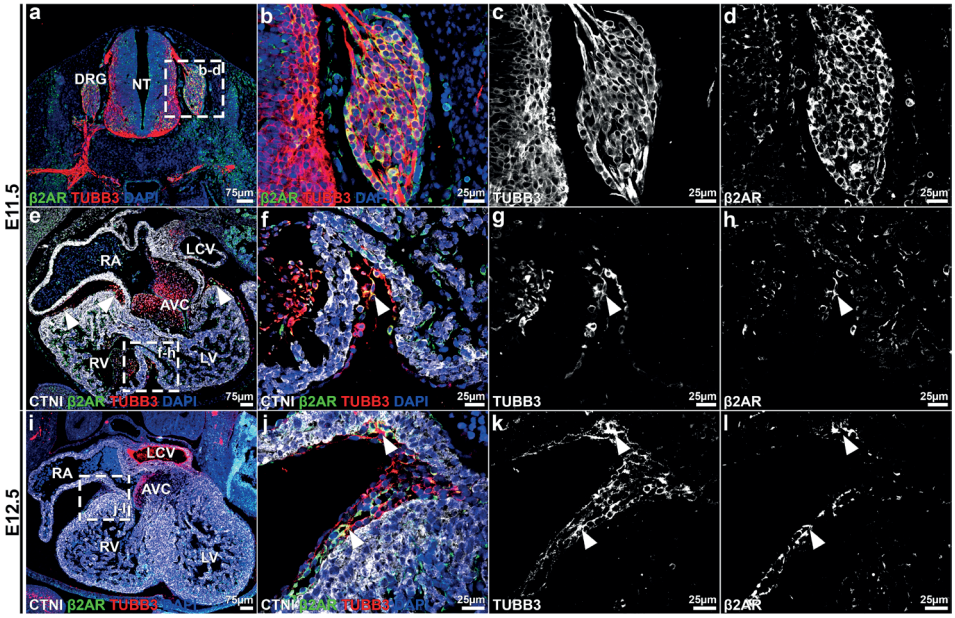

Figure 3. β2 adrenergic receptor expression in epicardium and subepicardium during development

a-d. Co-expression of β2AR (green) and TUBB3 (red) is found in the dorsal root ganglia during murine embryonic development from E11.5 onwards. Separate grey values are shown for TUBB3 (**c**) and β2AR (**d**). **e-h.** At E11.5, a subpopulation of TUBB3+ epicardial cells is positive for β2AR (arrowheads in **f-h**). **i-l.** At E12.5 co-expression of TUBB3 and β2AR in the epicardium is lost. There is, however, expression of β2AR in the subepicardium of which a subset shows co-labeling with TUBB3 (arrowheads in **j-l**). AVC: atrioventricular cushion, DRG: dorsal root ganglion, LCV: left cardinal vein, LV: left ventricle, NT: neural tube, RA: right atrium, RV: right ventricle.

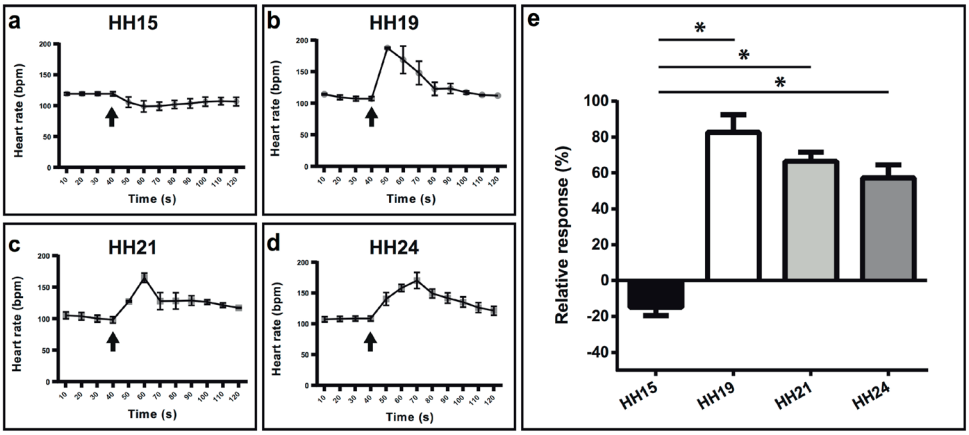

Figure 4. The epicardium modulates the response to epinephrine during early development

a. Administration of epinephrine to isolated hearts at HH15 results in a slight decrease in heart rate. **b-d.** Administration of epinephrine to isolated hearts at HH19, HH21 and HH24 results in a strong increase in heart rate. **e.** Relative response of hearts at HH19, HH21 and HH24 is significantly increased compared to the response of hearts at HH15. *p<0.05

rate after administration of epinephrine was calculated. HH15 hearts, which lack epicardial covering, showed no increase in heart rate after administration of epinephrine (**Fig. 4a** and **Supplemental Fig. S5a**). A significant increase in heart rate was observed in hearts of HH19 (when epicardial covering of the sinus venosus, atria and AV canal has initiated), HH21 (epicardial covering is (nearly) finished) and HH24 (the occurrence of subepicardial mesenchyme) embryos compared to HH15 (**Fig. 4b-e** and **Supplemental Fig. S5b**). This indicates that the presence of epicardium is required for the response to epinephrine during early developmental stages.

To further substantiate the role of the epicardium in the response to epinephrine, an experimental model was used in which outgrowth of the epicardium was inhibited in chick embryos. To confirm epicardial inhibition, hearts were analyzed histologically, after the electrophysiological measurements. Analysis of the epicardial response to epinephrine was conducted at stage HH24, when the effects of the epicardial inhibition are clearly observed. At HH24, control hearts showed epicardial covering of the entire heart, with a cell-rich subepicardial space (**Supplemental Fig. S6a**). After epicardial inhibition, large portions of the heart were not covered by epicardium and the regions covered with epicardium showed less subepicardial cells (**Supplemental Fig. S6b**). Furthermore, compaction was hampered, as shown by a less dense compact myocardial layer compared to controls (**Supplemental Fig. S6b**).

Ex ovo microelectrode recordings were performed after administration of epinephrine in control and inhibited hearts. After administration of epinephrine to control hearts (n=9), a fast increase in heart rate was observed (**Fig. 5a** and **Supplemental Fig. S5b**). The relative increase in heart rate was 57,2 ± 7,20%. After epicardial inhibition (n=9) however, this response was decreased (**Fig. 5b,d** ($p = 0,03$) and **Supplemental Fig. S5d**), with a relative increase in frequency of 24,8 ± 4,33%. Pre-warmed Tyrode served as a negative control. Upon administration a short decrease in heart rate was observed, after which the heart rate returned to the baseline frequency (**Fig. 4c** and **Supplemental Fig. S5c**).

The earliest electrical activity is generated in the myocardium of the sinus venosus (SV).[21] Since the response to epinephrine was altered after epicardial inhibition, the next step was to evaluate epicardial covering of the SV myocardium in these hearts. Hearts that were classified as successful inhibition of epicardial outgrowth in **Fig. 4** were microscopically subdivided into two categories based on epicardial covering of the SV. Hearts were classified as “mild inhibition” (n=4) when the myocardium of the SV was covered by epicardium, but no subepicardial cells were present (**Fig. 6a,b**). Hearts were classified as “severe inhibition” (n=5) when the myocardium of the SV was (largely) devoid of epicardium and

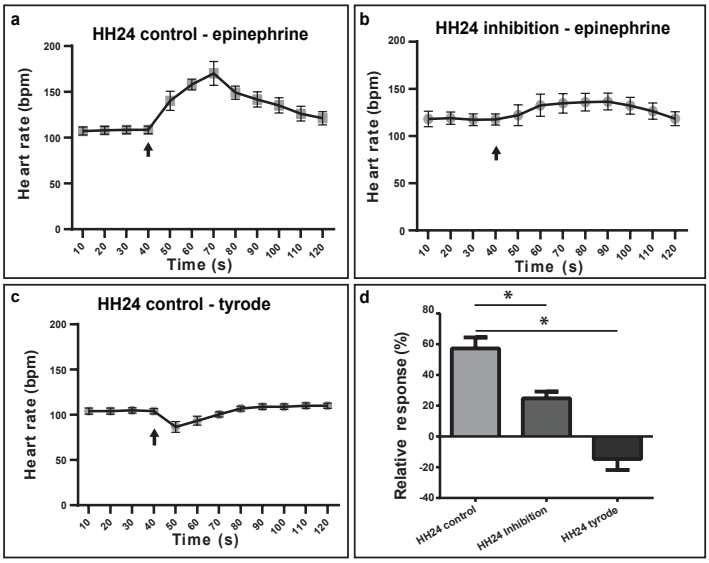

Figure 5. Repression of epicardial covering reduces cardiac response to epinephrine

a. Fast increase in heart rate after administration of epinephrine to isolated control hearts at HH24. **b.** Response strongly reduced after epicardial inhibition **c.** Administration of Tyrode to isolated control hearts results in a slight decrease in heart rate. **d.** Relative response of hearts after epicardial inhibition is significantly reduced compared to the response of control hearts, *p<0,05.

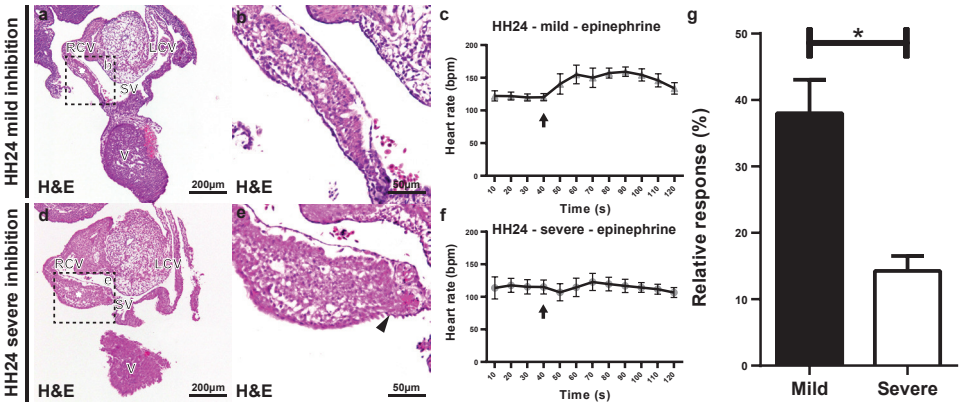

Figure 6. Severity inhibition epicardial covering sinus venosus correlates to response to epinephrine

Hearts microscopically subdivided based on covering of sinus venosus (SV). **a-b.** Mild inhibitions show epicardial covering of myocardium SV, subepicardial cells not present. * in **a** = SAN, higher magnification in **b. d-e.** Severe inhibition lack epicardial covering myocardium SV, subepicardial cells not present.* in **d** = SAN, higher magnification in **e.** Arrowhead in **e** shows boundary epicardial covering. **c.** Response to epinephrine after mild inhibition is hampered (compare with **4a**) **f.** Administration of epinephrine to hearts with severe inhibition (HH24) does not result in increase in heart rate. **g.** Relative response in severe *vs* mild inhibition significantly reduced, *p=0,016. R/LCV: right/left cardinal vein, V: ventricle.

subepicardial cells were not present (**Fig. 6d,e**). Microelectrode recordings revealed that the relative response to epinephrine was hampered in the mild inhibition group. The increase in heart rate was less pronounced and it took longer to return to the baseline heart rate after epinephrine administration compared to the control group (**Fig. 6c**). In the severely inhibited group, virtually no response to epinephrine was observed (**Fig. 6f**). The relative response to epinephrine was significantly decreased in the group classified as "severe inhibition" as compared to the "mild inhibition" group (p=0,016 **Fig. 6g**).

4. DISCUSSION

Autonomic modulation is essential for proper functioning of the heart and contributes to the prognosis of patients with heart failure and congenital heart disease. Early in development, the heart already responds to sympathetic stimulation, even prior to the presence of sympathetic nerve fibers.[8] The exact mechanism behind this early response is poorly understood. The current study provides new evidence that can account for this response. Key findings of this study are: 1) the epicardium expresses TUBB3, NCAM and β2AR during early development, which are known neuronal markers; 2) inhibition of epicardial outgrowth results in a disturbed response to epinephrine; 3) the severity of inhibition of epicardial covering of the sinus venosus myocardium correlates to the severity of disturbance in the response to epinephrine. Together, these results suggest a role for the epicardium in autonomic modulation of the heart during early development.

The current work describes expression of proteins known to be of importance in the nervous system in the epicardium. The tubulin isoform TUBB3 is primarily expressed in neurons and is important for axonal guidance and maintenance.[24] Expression however is not limited to neurons, since melanocytes (derived from the neural crest, as do neurons) also show TUBB3 expression.[25,26] To ensure the neuronal phenotype, staining of another neural marker, neural cell adhesion molecule (NCAM) was performed. NCAM expression was also present in the epicardium, confirming the neuronal phenotype of the epicardial layer. More indirect evidence suggesting a possible role for the epicardium in neural function is the co-expression of WT1 and TUBB3 in the central nervous system. WT1, a transcription factor expressed in the embryonic PEO and epicardium, is necessary for normal epicardial and cardiac development.[27] The current manuscript shows WT1/TUBB3 co-expression in the central nervous system, which is in agreement with previous reports demonstrating an important role for WT1 in neural functioning.[28–32]

In addition to epicardial expression of NCAM and TUBB3, the receptor for epinephrine, β2AR, was expressed in the epicardium. Epinephrine binds to β2AR,

which activates adenyl cyclase, resulting in cAMP-dependant signaling[9], which leads to sympathetic modulation of the heart rate, conduction velocity, and force of contraction.

To investigate the functional role of the epicardium in autonomic modulation, the response to epinephrine was analyzed in an experimental model in which normal outgrowth of the epicardium was inhibited. Results showed a significantly reduced response to epinephrine after epicardial inhibition. To further validate these results, epinephrine was administered in control chicken embryos at HH15, a stage in which no epicardial cells are present on the heart tube. Interestingly, these embryos did not show a response to epinephrine, confirming the data seen after epicardial inhibition. These results show that epicardial covering of the heart is (at least partially) responsible for a normal response to epinephrine during early cardiogenesis.

Absence of epicardial covering of the sinus venosus myocardium, as was described in the "severe inhibition group", results in absence of the epicardial β2AR. If epinephrine cannot bind to this receptor, cAMP mediated signaling is likely to be hampered, resulting in an absent response to epinephrine. Furthermore, it was recently shown that the β2AR forms protein complexes with the "funny current" ion channel HCN4, responsible for spontaneous depolarization of pacemaker cells. Disturbing the formation of the β2AR/HCN4 protein complexes results in a hampered response to sympathetic stimulation[33], a result also observed after epicardial inhibition (this study).

Kroese *et al.* showed that disturbance of retinoic acid signaling results in a hampered response to epinephrine. Disturbing RA signaling in the epicardium by epicardial deletion of the retinoid X receptor-α (RXRα), results in defective epithelial-to-mesenchymal transition (EMT), thinning of the myocardium, disturbed coronary arteriogenesis and ventricular pre-excitation.[34,35] This phenotype is also seen after disturbance of epicardial outgrowth in avian embryos[36] and in *Wt1*-null mice.[27,37] Wt1 regulates RA signaling by activating RALDH2, the enzyme involved in RA synthesis[38], and Wt1-null mice show downregulation of RALDH2.[27] Vice versa, induction of RA signaling results in upregulation of Wt1 expression in chick epicardium-derived cells.[39] Therefore, disturbing the normal outgrowth of the epicardium could result in hampering of RA signaling. Previous data showed that RA treatment *in vitro* results in neuronal differentiation, with an increase in β2AR expression.[40] This indicates that RA signaling is important for normal β2AR expression. Disturbing this by epicardial inhibition (or administration of teratogenic concentrations of all-trans RA[8]) could therefore result in aberrant β2AR expression and an impaired response to its ligand, epinephrine.

Finally, recent work showed that normal development of the cardiac veins

is required for normal development of the sympathetic nervous system of the heart.[41] This process is driven by nerve growth factor (NGF), secreted by vascular smooth muscle cells in subepicardial blood vessels.[41] Interestingly, the smooth muscle cells in the coronary vasculature derive from the epicardium after EMT.[42,43] Disturbing epicardial outgrowth results in abnormal development of the coronary vasculature.[36] The hampered response to epinephrine described in the current study could possibly be explained by disruption of the earliest stages of blood vessel formation and NGF production, which is required for normal development of the autonomic nervous system.[41]

The current study has several limitations. It cannot be excluded that inhibition of the outgrowth of the epicardium has secondary effects on the heart which can affect cardiac functioning, since epicardial cells are important for differentiation and maturation of cardiomyocytes.[44] However, our results show that epicardial covering is important for the response to epinephrine, since normal hearts without epicardium (HH15) do not respond to epinephrine. As soon as cardiac outgrowth of epicardial cells has commenced (HH19), the heart shows a rapid response to epinephrine. The early response seen at HH19, makes it unlikely that myocardial differentiation is responsible for the change in heart rate seen after administration of epinephrine. Furthermore, the response seen in normal hearts at HH15 was comparable to the response seen in epicardially inhibited hearts. This again shows that it is not myocardial differentiation, but the presence of epicardium which is responsible for the response to epinephrine. Although the chicken model demonstrates highly reproducible results, the results described in the current work could possibly be strengthened by electrophysiological testing in a mammalian model, which shows defects in epicardial covering. However, up to date there is no mouse model specifically affecting outgrowth of the epicardium, since the genes commonly used for epicardium-specific expression of Cre are known to be expressed more broadly throughout the fetus during development.[19,45]

In conclusion, the current study provides evidence indicating a role for the epicardium in autonomic modulation during early development. Autonomic modulation is essential for proper cardiac functioning and dysfunctioning of the autonomic nervous system is implicated in several diseases, such as cardiac arrhythmias, heart failure, congenital heart disease and hypertension.[1–3] Further research is required to investigate the role of the epicardium in autonomic dysfunction seen in common cardiac disorders, and to explore the mechanisms responsible for the early heart rate response mediated by the epicardium.

REFERENCE LIST

1. Shen, M. J. & Zipes, D. P. Role of the autonomic nervous system in modulating cardiac arrhythmias. *Circ. Res.* **114,** 1004–1021 (2014).

2. Mancia, G. & Grassi, G. The autonomic nervous system and hypertension. *Circ. Res.* **114,** 1804–1814 (2014).

3. Florea, V. G. & Cohn, J. N. The autonomic nervous system and heart failure. *Circ. Res.* **114,** 1815–1826 (2014).

4. Diller, G.-P. *et al.* Heart rate response during exercise predicts survival in adults with congenital heart disease. *J. Am. Coll. Cardiol.* **48,** 1250–1256 (2006).

5. Hasan, W. Autonomic cardiac innervation: development and adult plasticity. *Organogenesis.* **9,** 176–93 (2013).

6. Hildreth, V., Anderson, R. H. & Henderson, D. J. Autonomic innervation of the developing heart: origins and function. *Clin. Anat.* **22,** 36–46 (2009).

7. Verberne, M. E., Gittenberger-de Groot, A. C., Van Iperen, L. & Poelmann, R. E. Contribution of the cervical sympathetic ganglia to the innervation of the pharyngeal arch arteries and the heart in the chick embryo. *Anat. Rec.* **255,** 407–19 (1999).

8. Kroese, J. M., Broekhuizen, M. L. A., Poelmann, R. E., Mulder, P. G. H. & Wladimiroff, J. W. Epinephrine affects hemodynamics of noninnervated normal and all-trans retinoic acid-treated embryonic chick hearts. *Fetal Diagn. Ther.* **19,** 431–9 (2004).

9. McGraw, D. W. & Liggett, S. B. Molecular mechanisms of beta2-adrenergic receptor function and regulation. *Proc. Am. Thorac. Soc.* **2,** 292-296-312 (2005).

10. Ebert, S. N. & Thompson, R. P. Embryonic epinephrine synthesis in the rat heart before innervation : association with pacemaking and conduction tissue development. *Circ. Res.* **88,** 117–124 (2001).

11. Ebert, S. N., Baden, J. M., Mathers, L. H., Siddall, B. J. & Wong, D. L. Expression of phenylethanolamine n-methyltransferase in the embryonic rat heart. *J. Mol. Cell. Cardiol.* **28,** 1653–1658 (1996).

12. Teitelman, G., Baker, H., Joh, T. H. & Reis, D. J. Appearance of catecholamine-synthesizing enzymes during development of rat sympathetic nervous system: possible role of tissue environment. *Proc. Natl. Acad. Sci. USA.* **76,** 509–13 (1979).

13. Hamburger, V. & Hamilton, H. L. A series of normal stages in the development of the chick embryo. *J. Morphol.* **88,** 49–92 (1951).

14. Ostádal, B., Krause, E. G., Beyerdörfer, I., Pelouch, V. & Wollenberger, A. Effect of intra-amnial administration of a cardiotoxic dose of isoproterenol on cyclic AMP levels in the chick embryo heart. *J. Mol. Cell. Cardiol.* **11,** 1183–7 (1979).

15. Kockova, R. *et al.* Heart rate changes mediate the embryotoxic effect of antiarrhythmic drugs in the chick embryo. *Am. J. Physiol. Heart Circ. Physiol.* **304,** H895-902 (2013).

16. Hoover, L. L., Burton, E. G., Brooks, B. A. & Kubalak, S. W. The expanding role for retinoid signaling in heart development. *ScientificWorldJournal.* **8,** 194–211 (2008).

17. Gittenberger-de Groot, A. C. *et al.* The arterial and cardiac epicardium in development, disease and repair. *Differentiation.* **84,** 41–53 (2012).

18. Carmeliet, P. *et al.* Impaired myocardial angiogenesis and ischemic cardiomyopathy in mice lacking the vascular endothelial growth factor isoforms VEGF164 and VEGF188. *Nat. Med.* **5,** 495–502 (1999).

19. Duim, S. N., Kurakula, K., Goumans, M.-J. & Kruithof, B. P. T. Cardiac endothelial cells express Wilms' tumor-1. *J. Mol. Cell. Cardiol.* **81,** 127–135 (2015).

20. Männer, J. Experimental study on the formation of the epicardium in chick embryos. *Anat. Embryol.* **187,** 281–289 (1993).

21. Vicente-Steijn, R. *et al.* Electrical activation of sinus venosus myocardium and expression patterns of RHOA and Isl-1 in the chick embryo. *J. Cardiovasc. Electrophysiol.* **21,** 1284–92 (2010).

22. Vrancken Peeters, M. P. F. M., Mentink, M. M. T., Poelmann, R. E. & Gittenberger-de Groot, A. C. Cytokeratins as a marker for epicardial formation in the quail embryo. *Anat. Embryol.* **191,** 503–8 (1995).

23. Katz, T. C. *et al.* Distinct compartments of the proepicardial organ give rise to coronary vascular endothelial cells. *Dev. Cell.* **22,** 639–650 (2012).

24. Tischfield, M. A. *et al.* Human TUBB3 mutations perturb microtubule dynamics, kinesin interactions, and axon guidance. *Cell.* **140,** 74–87 (2010).

25. Locher, H. *et al.* Class III β-tubulin, a novel biomarker in the human melanocyte lineage. *Differentiation.* **85,** 173–181 (2013).

26. Locher, H., Frijns, J. H. M., Huisman, M. A. & Chuva de Sousa Lopes, S. M. TUBB3: neuronal marker or melanocyte mimic? *Cell Transplant.* **23,** 1471–3 (2014).

27. von Gise, A. *et al.* WT1 regulates epicardial epithelial to mesenchymal transition through β-catenin and retinoic acid signaling pathways. *Dev. Biol.* **356,** 421–431 (2011).

28. Armstrong, J. F., Pritchard-Jones, K., Bickmore, W. A., Hastie, N. D. & Bard, J. B. L. The expression of the Wilms' tumour gene, WT1, in the developing mammalian embryo. *Mech. Dev.* **40,** 85–97 (1992).

29. Rackley, R. R. *et al.* Expression of the Wilms' tumor suppressor gene WT1 during mouse embryogenesis. *Cell Growth Differ.* **4,** 1023–31 (1993).

30. Wagner, N. *et al.* A splice variant of the Wilms' tumour suppressor Wt1 is required for normal development of the olfactory system. *Development.* **132,** 1327–1336 (2005).

31. Wagner, K.-D. *et al.* The Wilms' tumor gene Wt1 is required for normal development of the retina. *EMBO J.* **21,** 1398–1405 (2002).

32. Parenti, R. *et al.* Immunolocalization of Wilms' Tumor protein (WT1) in developing human peripheral sympathetic and gastroenteric nervous system. *Acta Histochem.* **116,** 48–54 (2014).

33. Greene, D., Kang, S., Kosenko, A. & Hoshi, N. Adrenergic regulation of HCN4 channel requires protein association with β2-adrenergic receptor. *J. Biol. Chem.* **287,** 23690–23697 (2012).

34. Merki, E. *et al.* Epicardial retinoid X receptor alpha is required for myocardial growth and coronary artery formation. *Proc. Natl. Acad. Sci. USA.* **102,** 18455–18460 (2005).

35. Lie-Venema, H. *et al.* Origin, fate, and function of epicardium-derived cells (EPDCs) in normal and abnormal cardiac development. *ScientificWorldJournal.* **7,** 1777–98 (2007).

36. Gittenberger-de Groot, A. C., Vrancken Peeters, M. P. F. M., Bergwerff, M., Mentink, M. M. T. & Poelmann, R. E. Epicardial outgrowth inhibition leads to compensatory mesothelial outflow tract collar and abnormal cardiac septation and coronary formation. *Circ. Res.* **87,** 969–971 (2000).

37. Kreidberg, J. A. *et al.* WT-1 is required for early kidney development. *Cell.* **74,** 679–691 (1993).

38. Guadix, J. A. *et al.* Wt1 controls retinoic acid signaling in embryonic epicardium through transcriptional activation of Raldh2. *Development.* **138,** 1093–1097 (2011).

39. Braitsch, C. M., Combs, M. D., Quaggin, S. E. & Yutzey, K. E. Pod1/Tcf21 is regulated by retinoic acid signaling and inhibits differentiation of epicardium-derived cells into smooth muscle in the developing heart. *Dev. Biol.* **368,** 345–357 (2012).

40. Fennell, M., Khawaja, X. Z., Cockett, M. I. & Wood, A. Enhanced neuronal differentiation of NTera-2 cells expressing neuronally restricted β2 adrenergic receptor. *Brain Res.* **799,** 243–249 (1998).

41. Nam, J. *et al.* Coronary veins determine the pattern of sympathetic innervation in the developing heart. *Development.* **140,** 1475–85 (2013).

42. Vrancken Peeters, M. P. F. M., Gittenberger-de Groot, A. C., Mentink, M. M. T. & Poelmann, R. E. Smooth muscle cells and fibroblasts of the coronary arteries derive from epithelial-mesenchymal transformation of the epicardium. *Anat. Embryol.* **199,** 367–378 (1999).

43. Mikawa, T. & Gourdie, R. G. Pericardial mesoderm generates a population of coronary smooth muscle cells migrating into the heart along with ingrowth of the epicardial organ. *Dev. Biol.* **174,** 221–232 (1996).

44. Weeke-Klimp, A. *et al.* Epicardium-derived cells enhance proliferation, cellular maturation and alignment of cardiomyocytes. *J. Mol. Cell. Cardiol.* **49,** 606–16 (2010).

45. Christoffels, V. M. *et al.* Tbx18 and the fate of epicardial progenitors. *Nature.* **458,** E8-9-10 (2009).

SUPPLEMENTAL MATERIAL

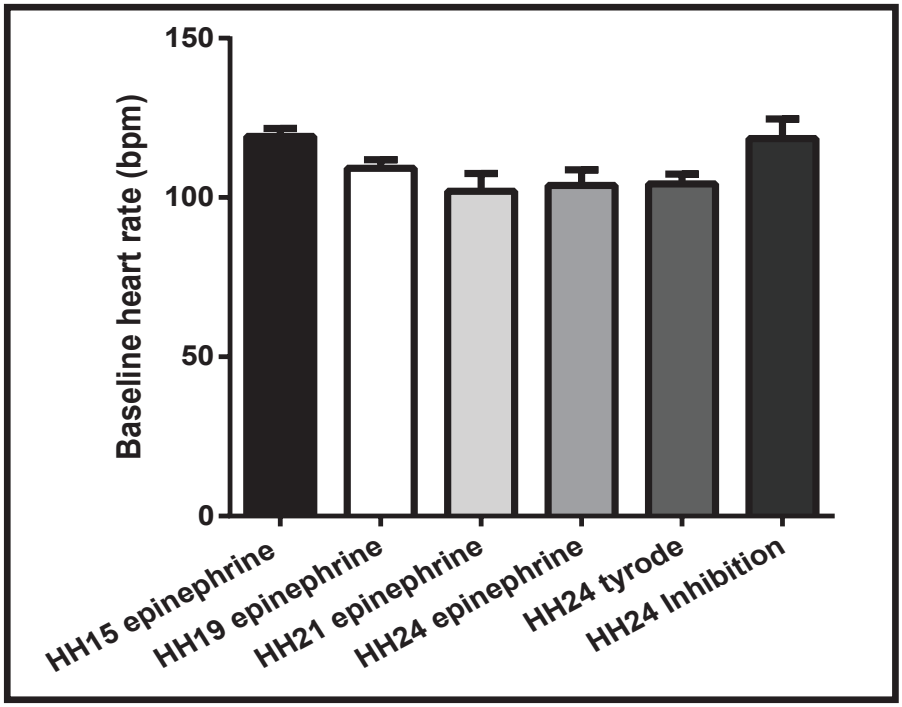

Supplemental Figure 1. Baseline heart rate of the experimental groups does not differ between the groups

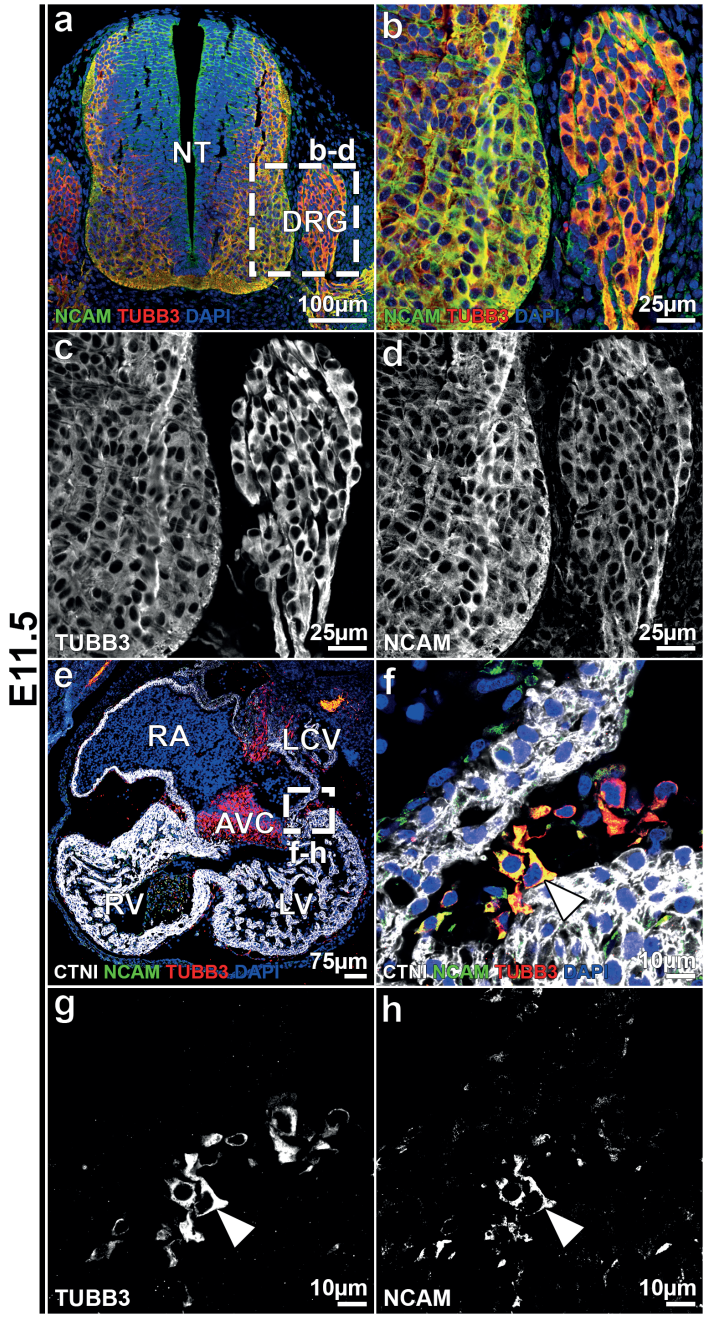

Supplemental Figure 2. Epicardial co-expression of the neuronal markers NCAM and TUBB3 confirms the neuronal phenotype of the epicardium

a-d. NCAM and TUBB3 are co-expressed in the nervous system, shown here in the neural tube (NT) and dorsal root ganglia (DRG). **e-h.** A subpopulation of epicardial cells co-express TUBB3 and NCAM (white arrowheads in **f-h**). AVC: atrioventricular cushion, LCV: left cardinal vein, LV: left ventricle, RA: right atrium, RV: right ventricle.

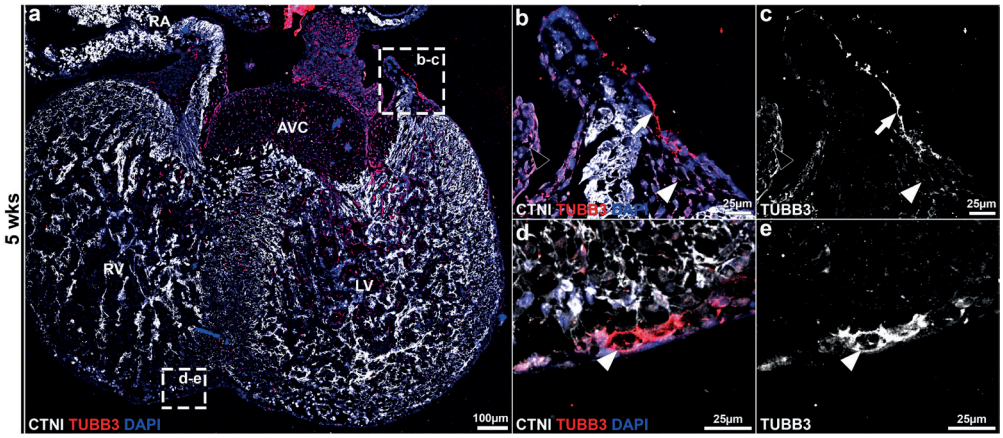

Supplemental Figure 3. The neuronal marker TUBB3 is expressed in the epicardium and subepicardium during early human development

a-c. Expression of TUBB3 is found in the epicardial layer (arrows in **b,c**), the subepicardium (white arrowheads in **b,c**) and the endocardial cushions (black arrowheads in **b,c**) of the human embryonic heart at week 7. **a, d-e.** Expression of TUBB3 is found in the subepicardial layer of the human embryonic heart (white arrowheads in **d,e**). AVC: atrioventricular cushion, LV: left ventricle, RV: right ventricle.

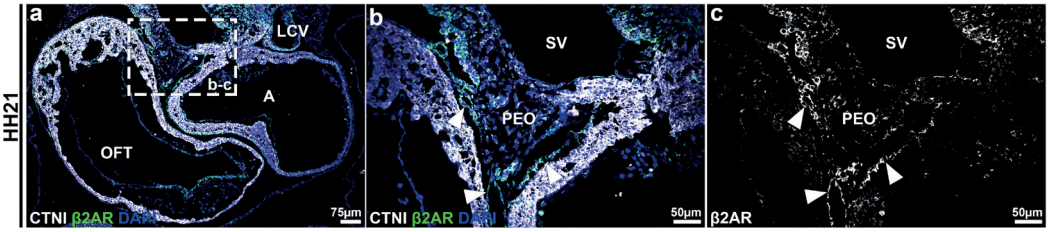

Supplemental Figure 4. β2AR expression in the epicardium in chick

a-c. At HH21 in chicken, expression of β2AR is present in the proepicardial organ (PEO), epicardium (arrowheads in **b-c**) and endocardium. A: atrium, LCV: left cardinal vein, OFT: outflow tract, SV: sinus venosus.

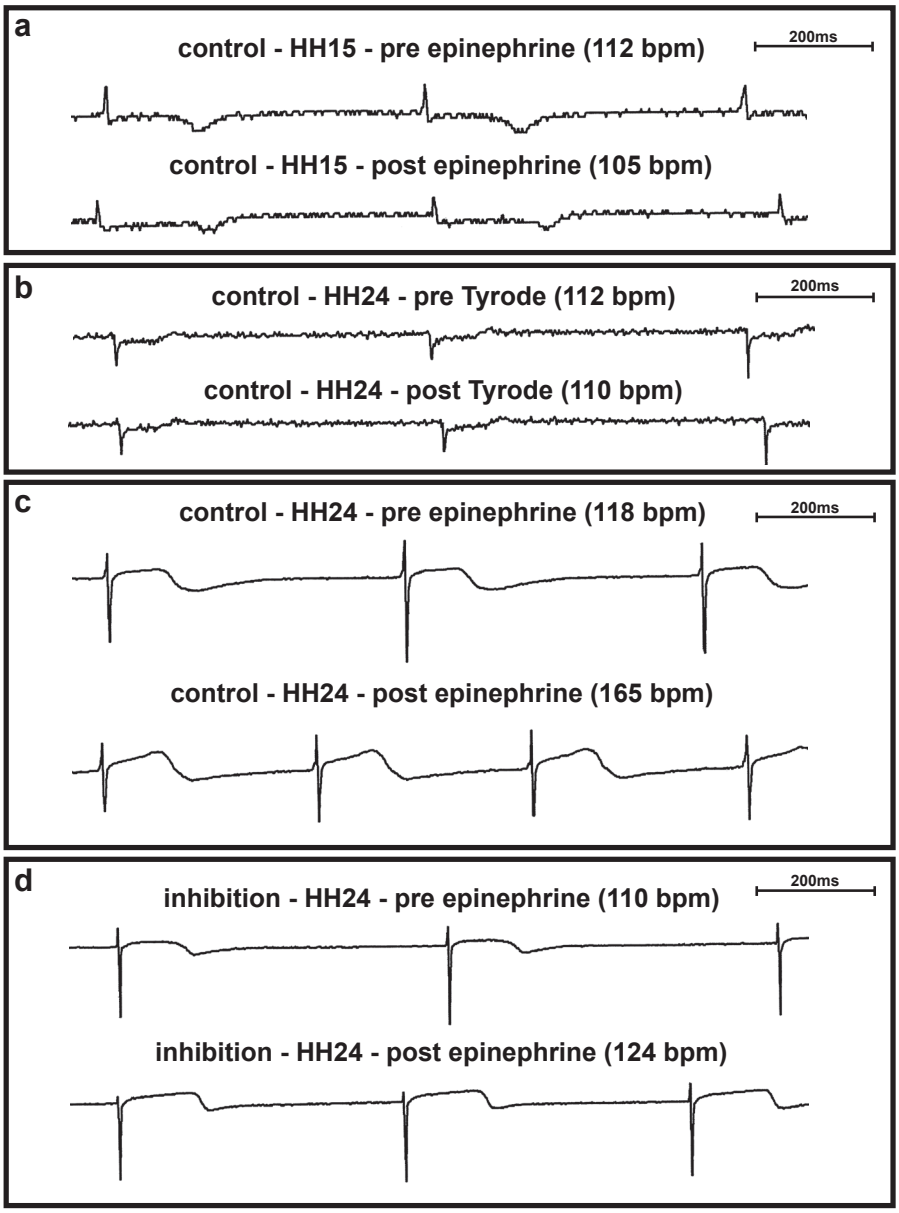

Supplemental Figure 5. Representative electrode recordings

a. The heart rate at HH15 did not increase after administration of epinephrine. **b.** The heart rate at HH24 did not increase after administration of Tyrode. **c.** The heart rate at HH24 increased after administration of epinephrine. **d.** The heart rate at HH24 after epicardial inhibition showed a decreased response to epinephrine.

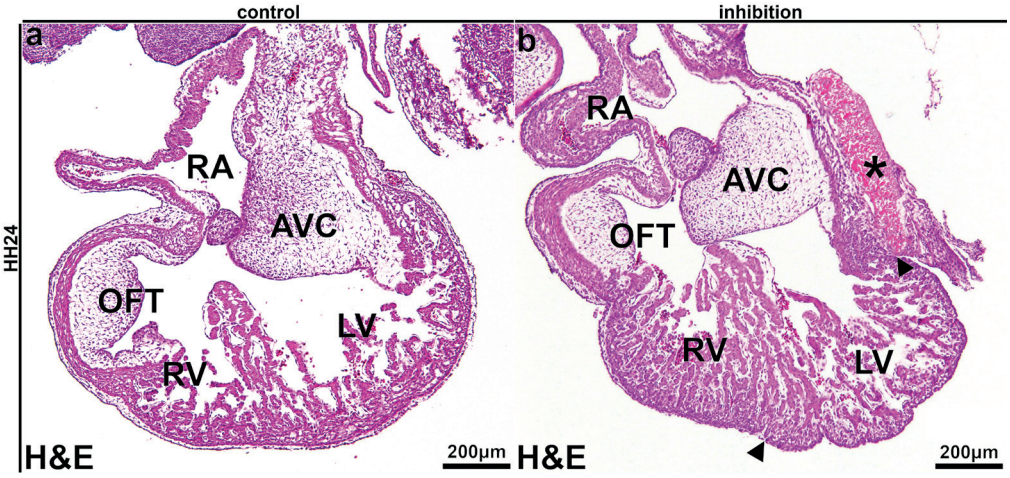

Supplemental Figure 6. Inhibition of epicardial outgrowth in chicken embryos

a. Control heart at stage HH24 showing epicardial covering and a thick, cell-rich subepicardial space. **b.** Inhibition of epicardial outgrowth results in incomplete epicardial covering of the heart and a thin subepicardial space at stage HH24. Black arrowheads demarcate the border of the epicardial lining. Note the abnormal shape of the ventricle with a thin compact myocardium in the region where epicardial covering is absent (between arrowheads). AVC: atrioventricular cushion, LA: left atrium, LV: left ventricle, OFT: outflow tract, RA: right atrium, RV: right ventricle. * Eggshell membrane.

9

LESSONS LEARNED FROM CELL TRACING AND FATE MAPPING EXPERIMENTS AIMED AT ELUCIDATING THE DEVELOPMENTAL ORIGIN OF THE CARDIAC CONDUCTION SYSTEM

Tim P. Kelder, Rebecca Vicente-Steijn, Marie-José Goumans, Marco C. DeRuiter, Monique R. M. Jongbloed

Submitted

ABSTRACT

The current work provides an overview of the different fate mapping and cell tracing techniques aimed at elucidating the developmental origin of the cardiac conduction system. Special focus will be on the specific limitations and advantages of these techniques. The data obtained from the different fate mapping and cell tracing techniques will be evaluated critically and a possible working model for the development of the cardiac conduction system is generated.

1. GENERAL INTRODUCTION

The cardiac conduction system (CCS) consists of specialized cardiomyocytes that initiate, propagate and modulate electrical activation of the heart. Disturbances in this system lead to cardiac arrhythmias, an important cause of morbidity and mortality worldwide. Understanding the embryological origin and molecular mechanisms underlying normal CCS development contributes to elucidating the etiology and pathophysiologic mechanisms that ultimately lead to cardiac arrhythmias. Historically, the developing CCS has been studied using classical light microscopy, histological stainings and electron microscopy.[1–4] A comprehensive basis providing insight in sequential stages of CCS development was founded using these techniques. Unfortunately, analyzing the developmental origin of the CCS is not possible using these methods. To answer these questions, several techniques such as genetic tracing and vital dye labeling have been developed. After an introduction of the basic processes of CCS development, this review will provide an overview of current available data on fate mapping and cell tracing of the CCS, highlighting advantages but also pitfalls in interpretation of these techniques. The results are used to generate a working model on CCS development.

1.1. BASIC CARDIAC DEVELOPMENT AND ANATOMY OF THE CCS

The heart is derived from the mesodermal layer of the embryonic plate. During gastrulation, mesodermal cells arise from the primitive streak and subsequently migrate cranially and laterally to form the cardiogenic plates. The first sign of cardiomyocyte differentiation is seen in this region at Hamburger and Hamilton (HH) stage 8-9 in chick and between E6.5-7.5 in mice, when cardiac troponin-I (cTnI) and sarcomeric myosin (MF20) are first detected. Fusion of the bilateral plates of splanchnic mesoderm establishes the primary heart tube (PHT).[5,6] During further development, cells from the splanchnic mesoderm differentiate and are added to the PHT at the venous and arterial pole. A controversial, but popular view in cardiac developmental biology is the distinction between a first and second heart field. In this view, the cardiomyocytes of the cardiac crescent and PHT are derivatives of the first heart field (FHF). The FHF will contribute to the atria, atrioventricular (AV) canal and ventricles.[5] The cells that are added to the PHT at the venous and arterial pole are considered to derive from a distinct cardiogenic field, the second heart field (SHF).[5] The SHF will contribute to the outflow tract and all cardiac structures except a part of the left ventricle (LV).[5,7] Whether the distinction between FHF and SHF is valid is not the focus of the current review. In addition to cardiac growth at the arterial and venous poles, several processes, including cardiac looping, septation, outgrowth

and remodelling of the different chambers, will establish the mature electro-mechanically functional 4-chambered heart with separated pulmonary and systemic circulations (reviewed in[8,9]).

The CCS is of myocardial origin[10] and consists of cardiomyocytes with a distinct differentiation program compared to the working myocardium cardiomyocytes (reviewed in[11]). During early development, the entire myocardium of the PHT displays a pacemaker-like phenotype (e.g. relatively high automaticity, slow conduction, poor electrical coupling).[12] However, even at early stages of development, the first electrical activation of the heart is already preferentially at the inflow of the heart, also called the sinus venosus myocardium.[13] The heartbeat is initiated by the sinoatrial node (SAN), which is derived from the sinus venosus myocardium. During embryonic stages, a transient left-sided SAN can be distinguished.[13,14] In the adult, the definitive right-sided SAN is a comma-shaped structure located with its "head" at the entrance of the superior caval vein in the right atrium, and the "tail" is situated along the terminal crest (i.e. the adult counterpart of the embryonic right venous valve) (**Fig. 1**).[15]

The second key structure of the CCS is the atrioventricular node (AVN), which is situated on the right side of the base of the atrial septum in the triangle of Koch (formed by i. the tendon of Todaro, ii. the septal leaflet of the tricuspid valve, and iii. the ostium of the coronary sinus) (**Fig. 1**).[16] The adult AVN is a complex, heterogeneous structure, consisting of a compact node, covered with transitional cells (which show a transition in gene and protein expression between the atrial and nodal myocardium) at the atrial side of the node.[17] Furthermore, nodal extensions run from the AVN towards the vestibules of the tricuspid and mitral valve.[17–21] The AVN delays the depolarization wave after fast electrical activation of the atria, thus ensuring adequate filling of the ventricles. The atria and ventricles are electrically insulated by the annulus fibrosus (**Fig. 1**).

After delay in the AVN the electrical impulse accelerates and traverses the annulus fibrosus through the common AV bundle, also known as bundle of His. From the AV bundle, the depolarization wave reaches the left and right bundle branches, after which it is passed to the ventricular cardiomyocytes through the Purkinje fiber network. The Purkinje fiber network consists of specialized cardiac muscle fibres that guarantee fast electrical activation of the ventricular cardiomyocytes (**Fig. 1**). The AV bundle, bundle branches and Purkinje fiber network together are called the ventricular conduction system (VCS).[22]

To be able to study cardiac development, several techniques have been used to trace the origin and fate of CCS cells. These experiments have resulted in advances in our knowledge on development of the CCS. An overview of these techniques and what can be concluded from these experiments with respect to development of the CCS will be described in the subsequent paragraphs.

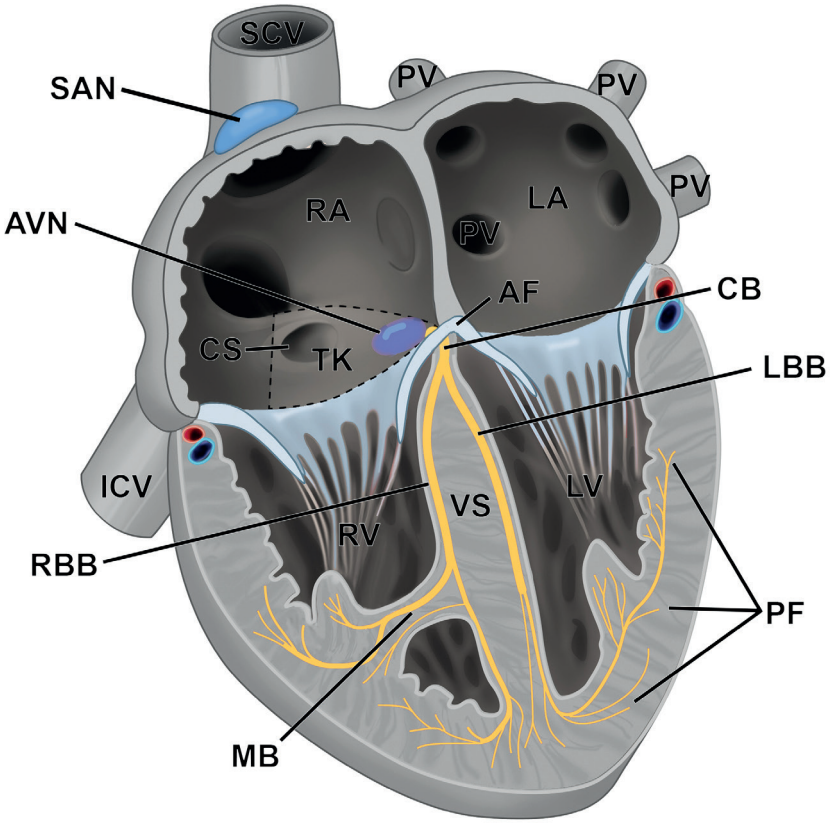

Figure 1. The adult cardiac conduction system

Different components of the adult CCS. AF: annulus fibrosus, AVN: atrioventricular node, CB: common bundle, CS: coronary sinus, ICV: inferior caval vein, LA: left atrium, LBB: left bundle branch, LV: left ventricle, MB: moderator band, PF: Purkinje fiber network, PV: pulmonary vein, RA: right atrium, RBB: right bundle branch, RV: right ventricle, SAN: sinoatrial node, SCV: superior caval vein, TK: triangle of Koch, VS: ventricular septum.

2. CELL TRACING TECHNIQUES APPLIED TO CCS DEVELOPMENT

A recent review provided an overview of the available techniques to trace the fate of cells.[23] A number of these techniques have also been used to identify progenitors of the CCS. In the next section the different methods used to study CCS development will be introduced and discussed.

2.1. GENETIC TRACING

A widely used tool in developmental biology is based on site-specific recombination of the genome. Most mouse models developed utilize the P1 Bacteriophage derived enzyme Cre-recombinase, which recognizes a 34-bp sequence called the *loxP* site, and induces recombination between pairs of these sites.[24] The Cre-*loxP* system, combined with the ability to knock-in sequences at specific sites in the genome has been used to study the origin of the developing CCS. See **Table 1** for an overview of Cre lines used for these experiments**.**

Table 1. Overview Cre lines used to study development of CCS

Genotype	Reporter	Used to study	Ref
$Tbx18^{Cre}$	$R26R^{lacZ}$; $R26R^{mT/mG}$	SAN, AVN, VCS	1,2,3
$HCN4^{CreErt2}$	$R26R^{lacZ}$; $R26R^{mT/mG}$	SAN, AVN, VCS	2
$Isl1^{Cre}$	$R26R^{mT/mG}$; $Gata4^{flap}$	SAN, AVN, VCS	2,4
$Isl1^{MerCreMer}$	$R26R^{lacZ}$	SAN, AVN	5
$Nkx2\text{-}5^{Cre}$	$R26R^{mT/mG}$	SAN, AVN, VCS	2
$Shox2^{Cre}$	$R26R^{lacZ}$	SAN, AVN	6,7
$Tbx2^{Cre}$	$R26R^{lacZ}$; Z/EG	AVN, VCS	3,8
$cGATA6^{Cre}$	$R26R^{lacZ}$	AVN	9
Mef2c-AHF-Cre	Z/EG	AVN, VCS	3
$Cx40^{CreERT2}$	$R26R^{lacZ}$	VCS	10
$Wnt1^{Cre}$	$CAG\text{-}CAT^{eGFP}$;$R26R^{lacZ}$	VCS	11,12,13

References: 1. Wiese, C. *et al. Circ. Res.* **104**, 88–97 (2009), 2. Liang, X. *et al. Circ. Res.* **113,** 399–407 (2013), 3. Aanhaanen, W.T.J. *et al. Circ. Res.* **107**, 728-36 (2010), 4. Ma, Q. *et al. Dev. Biol.*, **323**, 98-104 (2008), 5. Sun, Y. *et al. Dev. Biol.* **304,** 286–96 (2007), 6. Sun, C. *et al. Genesis.* **51,** 515–522 (2013), 7. Sun, C. *et al. J. Biol. Chem.*, **290**, 2007-23 (2015), 8. Aanhaanen, W.T.J. *et al. Circ. Res.*, **104**, 1267-74 (2009), 9. Davis, D.L. *et al. Mech. Dev.*, **108**, 105-19 (2001), 10. Miquerol *et al. Circ. Res.* **107**, 153-161 (2010), 11. Nakamura, T. *et al. Circ. Res.* **98**, 1547-1554 (2006), 12. Poelmann, R. *et al. Anat. Embryol.*, **208,** 389-393 (2004), 13. Miquerol, L. *et al. Dev. Dyn.* **242,** 665-677 (2013)

2.1.1. BASICS OF GENETIC TRACING

To use the Cre-*loxP* system for genetic tracing, several steps are necessary (**Fig. 2**). The basis of the Cre-*loxP* system is crossing a Cre transgenic mouse strain with a mouse in which a reporter gene is flanked by *LoxP* sequences ("floxed"). First, the sequence coding for Cre-recombinase is knocked into the locus of the gene of interest, for example Isl1. The next step is crossing the $Isl1^{Cre}$ mouse line with a reporter line (**Fig. 2A**). The genetic tracing experiments in this review

were mostly performed in reporter lines that utilize the Rosa26 locus (R26R), but different loci (e.g. Gata4[25]) are used. Important characteristics of a potential reporter locus are ubiquitous expression of the gene and viability and fertility of the mouse strain after homozygous inactivation of the reporter locus by insertion of a reporter gene, such as lacZ or a single or multiple fluorescent proteins. To control expression of the reporter gene, a floxed sequence preventing transcriptional read-through (also referred to as a "stop-cassette") is placed before the reporter gene sequence (**Fig. 2A**).

Crossing the reporter line with the Cre line results in offspring carrying both constructs (**Fig. 2B**). Cells expressing the gene of interest will produce Cre-recombinase, which will result in permanent deletion of the stop-cassette and expression of the reporter gene (**Fig. 2C**). Since expression is under control of the Rosa26 promoter, these cells and their progeny will retain reporter gene expression, thereby enabling tracing of these cells. The above-described method is referred to as "*constitutive*" genetic tracing in this review (**Fig. 2D**).

With another form of genetic tracing, referred to as "*inducible*" genetic tracing, it is possible to gain temporal control of recombination (**Fig. 2D**). This system is based on fusion of a mutated ligand-binding domain (LBD) of the human estrogen receptor (ER) and Cre-recombinase. The resulting protein is only sensitive to the anti-estrogen tamoxifen, not to the endogenously present estradiol.[26] The fusion gene is inserted in the locus of the gene of interest, which results in production of the fusion protein upon expression of the gene of interest. The Cre fusion protein is located in the cytoplasm and is unable to enter the nucleus, due to the presence of the mutated LBD. Administration of tamoxifen results in binding to the LBD, which enables translocation of Cre-recombinase to the nucleus, where it induces gene specific recombination.[27] Thus, recombination can only occur after administration of tamoxifen, resulting in temporal control of lineage labeling (**Fig. 2D**).

2.1.2. ADVANTAGES OF GENETIC TRACING

The most important advantage is the ability to investigate which genes are expressed by the structure of interest's progenitor pool. Combining these results with known expression patterns of the gene of interest (e.g. based on immunohistochemical staining patterns) and with other cell tracing techniques has provided important information on the developmental origin of the CCS.

Furthermore, genetic lineage tracing is non-invasive, in contrast to e.g. performing prospective tracing with microinjection of vital dyes or viral constructs. In chick, the egg has to be opened and the dye or viral construct has to be administered directly to live cells, frequently accompanied by extra microsurgical manipulation. After these steps, the egg can be reincubated.[28]

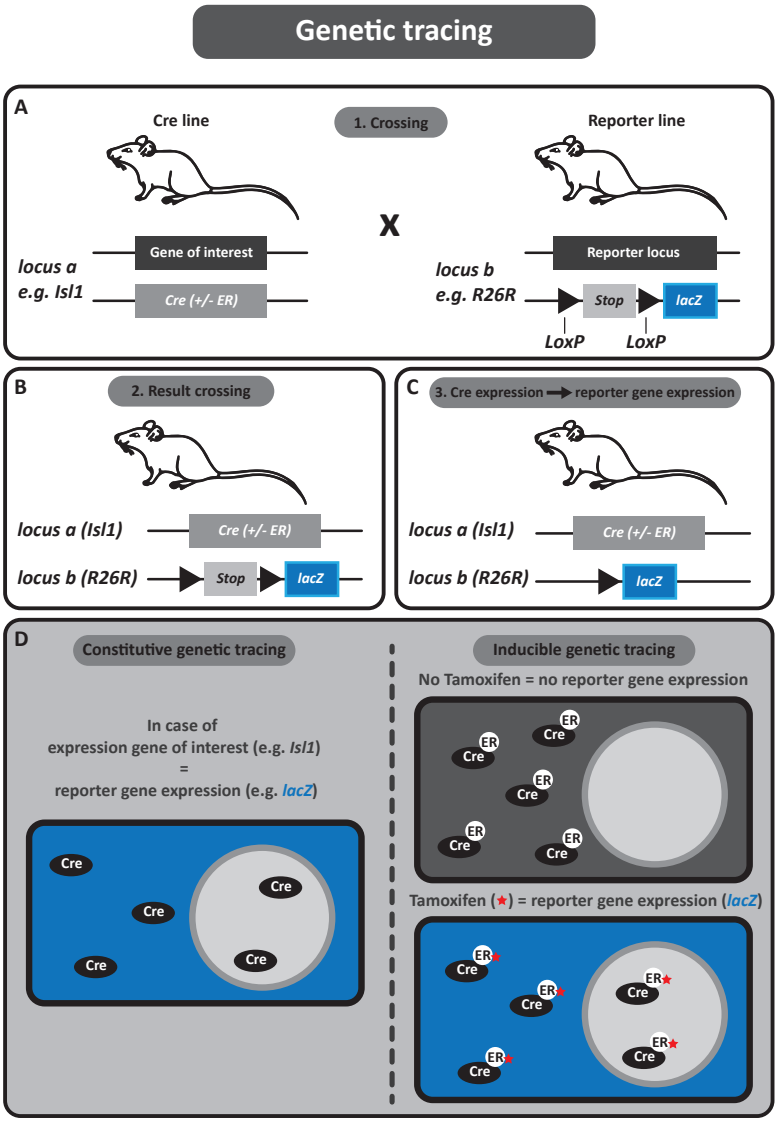

Figure 2. The Cre-lox system

A. Genetic tracing with Cre line in which one allele of gene of interest (here "locus a", e.g. Isl1) is replaced by coding sequence Cre-recombinase (fused with estrogen receptor (ER) if aim is inducible genetic tracing). Crossed with reporter mouse with floxed (between black triangles) stop codon and reporter gene (e.g. lacZ) inserted in reporter locus (here "locus b", e.g. R26R). **B**. Crossing results in offspring with coding sequence Cre-recombinase on locus gene of interest ("locus a", e.g. Isl1) and floxed stop codon and reporter gene in reporter locus ("locus b", e.g. R26R). **C**. Expression gene of interest results in synthesis Cre-recombinase enzyme, which removes floxed stop codon. **D**. Difference between constitutive (left) and inducible (right) tracing. Constitutive tracing: expression of gene of interest results in Cre-recombinase (indicated in **Fig.** as Cre) expression, which enters nucleus and induces reporter gene expression. Inducible tracing: in absence of tamoxifen, the estrogen receptor prohibits Cre-recombinase to enter the nucleus. In presence tamoxifen, Cre-recombinase enters nucleus and induces reporter gene expression.

In murine embryos it is necessary to extract the embryo from the uterus, followed by culturing the embryo in for example a rolling culture system.[29] The time of follow-up is therefore hampered in murine embryos and extracting the embryo is an extra invasive procedure. Genetic tracing on the other hand is non-invasive, as long as insertion of the sequence for Cre does not impair normal development of the embryo.

Inducible genetic tracing has an important advantage over constitutive genetic tracing, namely temporal control of Cre expression. With constitutive genetic tracing there is no control of timing of Cre expression. Expression of the gene of interest at any given (and frequently unknown) time point will result in reporter gene expression (if the level of Cre expression is sufficient to induce reporter gene expression, see below). With inducible tracing, reporter gene expression will only occur in the presence of tamoxifen.[26]

2.1.3. DISADVANTAGES OF GENETIC TRACING

Common pitfalls in interpretation of results from genetic lineage tracing are given in **Fig. 3.** Finding reporter gene expression in the tissue or structure of interest can result from several scenarios. In the ideal situation, depicted in **Fig. 3A**, it can show that at time point 0, a certain structure with known expression of the gene of interest is a progenitor for the structure with reporter gene expression at a later time point (**Fig. 3A**). However, it can also reflect expression of the gene of interest at the later time point, since active expression of the gene will also result in reporter gene expression (**Fig. 3B**). Finally, expression of the gene of interest in an entirely different progenitor pool (e.g. different tissue or at a different time point) can contribute to the structure of interest (**Fig. 3C**). The latter two scenarios could lead to a wrong conclusion on the lineage of the structure of interest. The difficulty in interpretation of genetic tracing experiments was demonstrated by constitutive genetic tracing of *Tbx18*. *Tbx18* is commonly used as a marker for the sinus venosus and epicardium. Constitutive genetic tracing was performed with a $Tbx18^{Cre}$ in the $R26R^{lacZ}$ background and reporter gene expression was found in myocardial cells, which led to the conclusion that these cardiomyocytes derived from epicardial cells.[30] However, later experiments showed active expression of *Tbx18* in cardiomyocytes, which was put forward as an explanation for the observed reporter gene expression.[31] Using constitutive genetic tracing, reporter gene expression in cells shows that either these cells have expressed the gene of interest at an unknown time during development, or still express this gene.

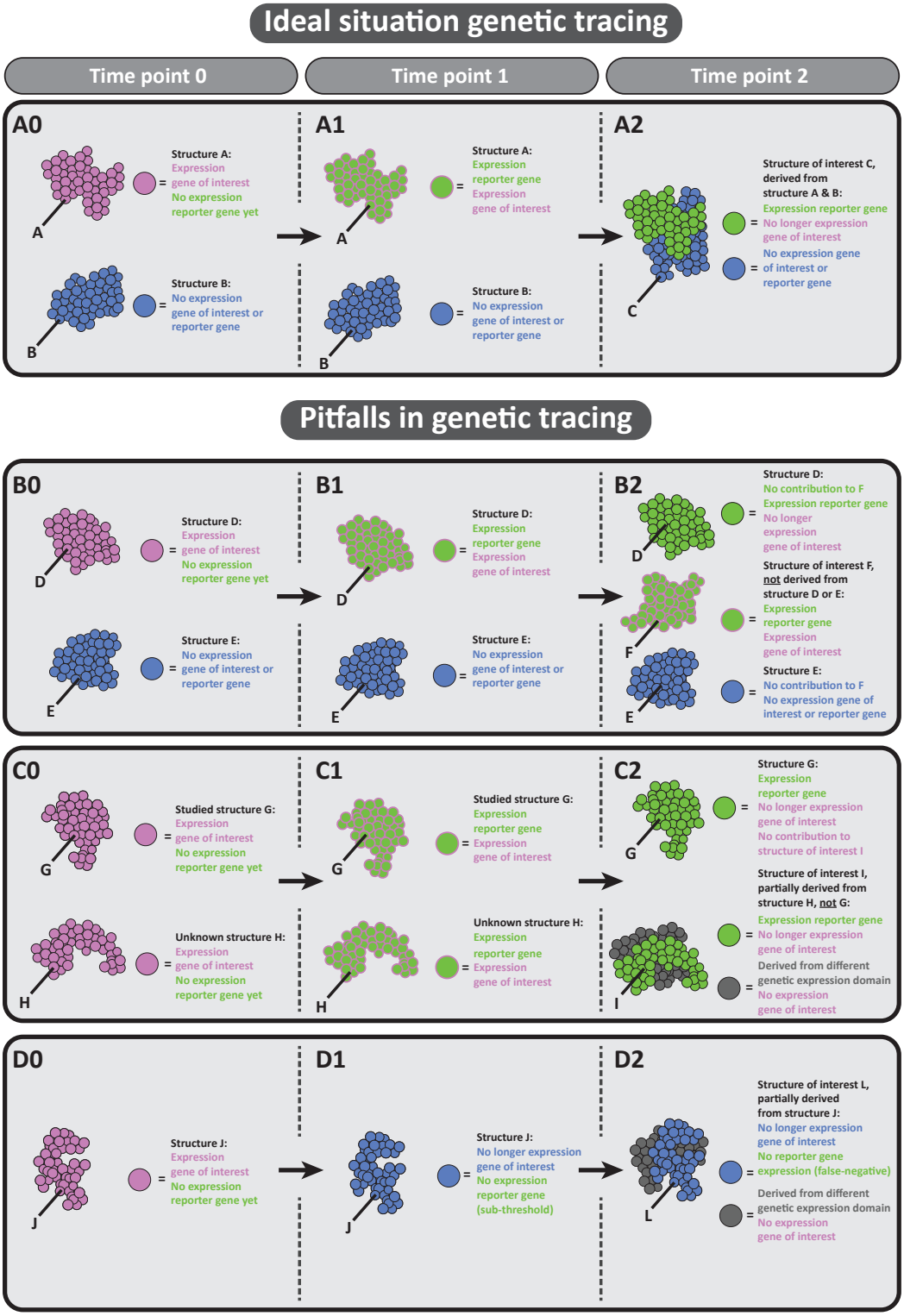

Figure 3. Pitfalls of the Cre-lox system (legend on page 207)

Even though timing is far more accurately determined using inducible genetic tracing, exact timing of recombination and reporter gene expression remains difficult. It was shown that after intraperitoneal injection of tamoxifen at E8.5 in pregnant dams, the first signs of lacZ activity in the embryos were seen 6 hrs after injection, with an increase in expression at 12, 24, and 48 hrs.[32] Analysis of reporter gene expression after tamoxifen injection therefore is dependent on the *duration* of tamoxifen exposure, which complicates exact timing. Furthermore, the *dosage* of tamoxifen has also been shown to influence reporter gene expression, with higher doses resulting in reporter gene expression in more cells.[32] This shows that analysis of reporter gene expression and interpretation of these results can be problematic.

In genetic tracing experiments, interpreting positive results can be problematic, but a far more complex problem arises in case of lack of reporter gene expression (**Fig. 3D**). A large number of genetic tracing experiments utilize the R26R locus, which is also the most commonly used reporter locus described in the current review. Genetic tracing experiments comparing the R26R locus with a Gata4 based reporter system showed differences in reporter gene expression

Figure 3. Pitfalls of the Cre-lox system (figure on page 206)
Ideal situation shown in **A0-2**. At time point 0 (**A0**), structure of interest A expresses gene of interest, but not yet reporter gene. Other tissue (e.g. structure B) does not express gene of interest (or reporter gene). At later time point 1 (**A1**), structure A expresses gene of interest and reporter gene. Structure B shows no expression of gene of interest or reporter gene. At final time point 2 (**A2**), structure of interest C shows reporter gene expression, no expression of gene of interest and is derived from structure A and B, with reporter gene expression only being derived from structure A. **B0-2**. At time point 0 (**B0**), structure of interest D expresses gene of interest (not yet reporter gene), while other tissue (e.g. structure E) does not express gene of interest or reporter gene. At time point 1 (**B1**), reporter gene expression is seen in structure D, not structure E. However, structure D and E both do not contribute to final structure of interest F (**B2**). At time point 2 (**B2**), structure of interest F actively expresses gene of interest, resulting in reporter gene expression. This could result in falsely concluding that structure F receives a cellular contribution from structure D. **C0-2**. At time point 0 (**C0**) structure of interest G and unknown structure H (i.e. expression of gene of interest was not studied in this structure) both express gene of interest (no reporter gene expression yet). At time point 1, reporter gene expression is present in both structures G and H. At time point 2 (**C2**), final structure of interest I shows reporter gene expression (**C2**). However, cells expressing reporter gene derive from unknown structure H, not initial structure of interest G. This results in falsely concluding that final structure of interest I receives contribution from structure G. **D0-D2**. At time point 0 (**D0**) structure of interest J expresses gene of interest (no reporter gene yet). At later time point 1 (**D1**) structure J loses expression gene of interest. However, expression gene of interest is too low to induce recombination at level high enough to detect reporter gene expression, resulting in lack of reporter gene expression. At time point 2 (**D2**), final structure of interest L (partially derived from structure J), shows no reporter gene expression due to sub-threshold level of expression to induce expression of reporter gene (i.e. false-negative cells). This could result in the incorrect conclusion that structure J does not contribute to structure L.

between the two lines.[25] Constitutive genetic tracing of *Isl1* and *Nkx2-5* (both genes are discussed in more detail below) showed more extensive reporter gene expression in the Gata4 reporter line, indicating that the Gata4 locus was more sensitive to recombination than the R26R locus.[25] The difference in reporter gene expression shows that different reporter strains have different thresholds for reporter gene expression, resulting in different conclusions based on the reporter used. An example of the importance of this is shown by reassessment of the fate of *Isl1*+ progenitors.[25] This gene is commonly used as marker for the SHF.[7,33] However, the expanded pattern of reporter gene expression in the Gata4 reporter line showed that nearly all cells (including the LV, which is commonly described as being derived from the FHF) of the heart derive from an *Isl1+* progenitor. This shows that Isl1 is not suitable as a SHF marker.[25] mRNA[34] and protein[35] expression of Isl1 in the cardiac crescent, classically considered to be a FHF structure, further substantiates this.

The absence of reporter gene expression is also an important difficulty in interpreting results from inducible genetic tracing experiments, since reporter gene expression is dependent on dosage of tamoxifen.[32] This shows that it is very difficult to draw conclusions from tissue lacking reporter gene expression, since absence of reporter gene expression can be caused by absence of expression of the gene of interest, or absence of recombination due to sub-threshold levels of Cre expression, not sufficient to induce reporter gene expression.

Therefore, when performing constitutive or inducible genetic tracing experiments, one should be cautious with interpretation of the results. In constitutive genetic tracing, reporter gene expression demonstrates that labeled cells have expressed or still actively express the gene of interest. It does not provide information on the initial source/location of the progenitor cells. With inducible genetic tracing, temporal control of Cre expression is possible. Expression of the reporter gene shows that Cre is present in the labeled cell *between* the time of tamoxifen administration and the moment of analysis. Finally, interpretation of negative results in genetic tracing is challenging and results need to be verified by additional tracing techniques and gene/protein expression experiments at sequential stages of development.

2.2. VITAL DYE AND VIRAL LABELING EXPERIMENTS

With vital dye and viral labeling it is possible to directly label clusters of cells. This method is widely used in developmental biology in several species, and has provided essential information on the developmental origin of the CCS.

2.2.1. BASICS OF VITAL DYE AND VIRAL LABELING EXPERIMENTS

To perform microinjection of minute quantities of either vital dye or viral

constructs, the embryo needs to be exposed. The technique to expose the chick embryo was described recently in detail elsewhere.[28] An important advantage of chick embryos is the easy accessibility of the embryo in the egg, which allows long-term reincubation after labeling. In mice, it is first necessary to extract the embryo from the uterus, followed by reincubation in culture medium, for example in rolling bottles.[29] Labeling of cells is performed with a glass capillary mounted to micromanipulators, and a pneumatic microinjector to inject small amounts of dye or virus in the region of interest.

Vital dye labeling is performed with lipophilic dyes which can label distinct cell compartments (**Fig. 4A**).[35] Commercial dyes are available in different colors, which enables simultaneous labeling of different clusters of cells and studying the direction of migration and potential intermingling of different cell clusters.

Viral labeling experiments are aimed at induction of reporter gene expression in specific regions of the embryo. This technique utilizes the ability of retroviruses to infect the cell and to incorporate its genome in the genome of the infected cell.[36–38] Retroviral vectors driving the expression of a reporter gene (such as LacZ) enable cell tracing of infected cells (**Fig. 4B**). More targeted viral tracing can be performed by placing expression of the reporter gene under the transcriptional control of a specific promoter, which enables tracing of cells that express the gene of interest (**Fig. 4C**).[39]

2.2.2. ADVANTAGES OF VITAL DYE LABELING EXPERIMENTS

With physical labeling of a progenitor pool, it is possible to select the progenitor pool based on location and to time the moment of labeling. An important advantage of this technique is the opportunity to select a physical cluster of cells, rather than a genetic expression domain (as is the case with genetic tracing). An important drawback of genetic tracing therefore does not apply to physical labeling of cells. The pitfall described in **Fig. 3C**, in which a distinct progenitor population is missed, will not occur in physical labeling, since location of labeling is known. Combining physical labeling with a viral vector in which reporter gene expression is driven by a specific promoter results in selection of an even smaller domain of cells. Selecting this population is then based on location and gene expression of a gene of interest, while minimizing the risk of missing a distinct progenitor pool (**Fig. 3C**).

Performing physical labeling experiments is relatively cost efficient and easy, especially in chick embryos. Working with mice in general, and complex transgenic mouse strains in particular, requires advanced biotechnical and animal care facilities, which are not needed when working with chick embryos. Furthermore, labeling can be combined with other microsurgical procedures.

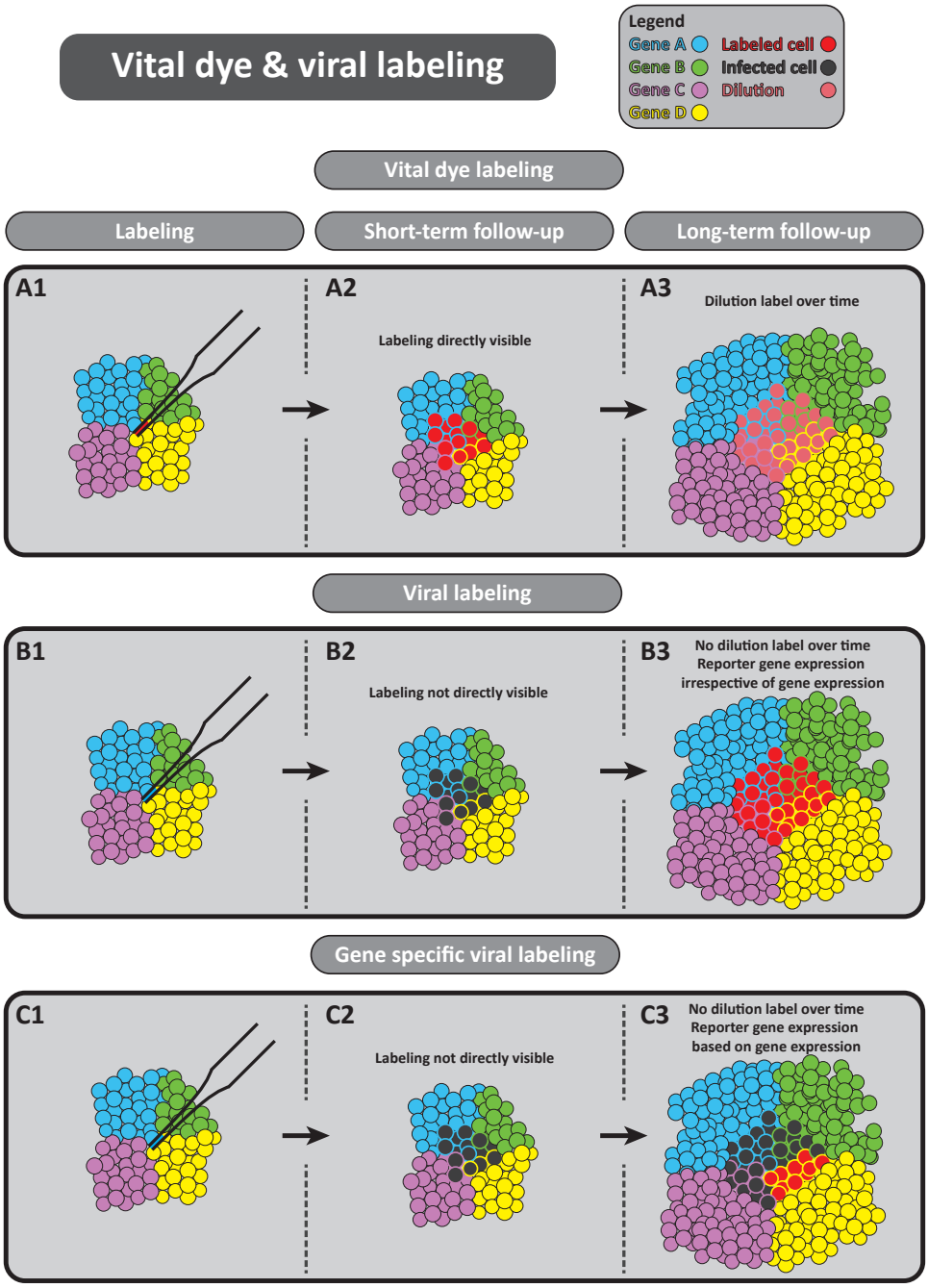

Figure 4. Vital dye and viral labeling

A1. Vital dye labeling of structure expressing 4 genes. **A2.** Label (red cells) directly visible on all cell types. **A3.** Disadvantage is dilution (pink cells) of label during further development. **B1.** Viral labeling of same structure. **B2.** Disadvantage is that label is not visible directly after infection (dark grey cells), all cell types infected. **B3.** No dilution of labeling (red cells) during long-term follow-up, labeling seen in all cell types. **C1.** Gene-specific (for gene D) viral labeling of same structure. **B2.** Infection (dark grey) of all cell types, labeling not visible directly. **C3.** Labeling only seen in cells expressing gene D (red cells), no dilution, no labeling in other cell types (dark grey). See legend for color coding.

2.2.3. LIMITATIONS OF VITAL DYE AND VIRAL LABELING

As with genetic tracing, physical labeling experiments start with selection of the progenitor population, which results in only tracing this cluster of cells. Knowledge about the possible progenitor pool is necessary to perform the experiment and unexpected contributions are easily missed with this technique.

Furthermore, physically labeling cells is relatively invasive and manipulation of the embryo can result in developmental defects. It is therefore necessary to carefully select embryos that show no macroscopic abnormalities and use appropriate control embryos when indicated. Toxicity of the dyes itself appears to be negligible.[40,41] With viral labeling, there is random integration of the viral genome in the host cells DNA, which could result in damage or abnormal functioning of the infected cell.[23]

When performing physical labeling experiments in murine embryos, culturing the embryo *ex utero* results in limited follow-up, since simple diffusion of oxygen and nutrients is only sufficient during early development. When using the chick as a model, approaching the desired structure can be a challenge depending on the anatomical location, since the embryo is positioned on the left side. *Ex ovo* culturing offers alternatives but, as with the murine model, the culture is time-limited.

Leakage of dye or infection of cells in the vicinity of the designated progenitor pool could result in incorrect conclusions about the fate of the progenitor cells. It is therefore essential to analyze in detail the location of dye directly after administration.[35,42] Histological evaluation of embryos directly after labeling is crucial, but follow-up is impossible after histological evaluation. Live-imaging of vital dyes[41,43,44] could help to minimize this limitation. Furthermore, delay in reporter gene expression with viral labeling omits direct evaluation of the location of labeling. In addition, efficiency of the reporter gene expression in the desired cells has to be previously tested to ascertain activation of expression in the specific cell type within the animal model (i.e. species differences in expression levels in specific cell types).

Rapid cell division in early embryos results in dilution of the vital dyes, which complicates long-term follow-up of the labeled cells.[45] The extent of dilution is dependent on the rate of proliferation and the amount of dye administered, which therefore necessitates titration of the dye with every new experiment. With retroviral labeling, integration of the reporter gene in the host cells DNA results in stable and high expression of the reporter gene in the daughter cells[46], which overcomes the problem of dilution.

In conclusion, the disadvantage of vital dye labeling is dilution, while the possibility of direct evaluation after labeling is an important advantage. The opposite is true for viral labeling, where direct evaluation is not possible, but

dilution of dye does not occur after stable integration of the viral vector. Therefore, a possible solution to overcome these limitations is to combine vital dye labeling with viral labeling.

Finally, to perform viral labeling experiments, advanced biosafety laboratories are crucial to safely perform experiments with potentially hazardous viral constructs.

2.3. RETROSPECTIVE CLONAL ANALYSIS

The above-mentioned techniques can be described as prospective fate mapping techniques. Knowledge on gene and protein expression profile, timing of expression and/or location of progenitors is necessary to perform subsequent prospective labeling of this progenitor pool.[23] The following section focuses on retrospective clonal analysis.

2.3.1. BASICS OF RETROSPECTIVE CLONAL ANALYSIS

Retrospective clonal analysis is based on infrequent and spontaneous recombination of the *nLaacZ* reporter.[47] This reporter gene encodes the *LacZ* gene, with an inactivating duplication inserted in the reading frame, thereby inhibiting transcription of functional β-galactosidase. A spontaneous and rare recombination event can result in removal of the duplication and subsequent production of β-galactosidase (**Fig. 5A**).[47] Reporter gene expression can be followed in progeny of cells in which spontaneous recombination of the *nLaacZ* construct occurred.[47] Targeting of this construct to an allele highly expressed in cardiac muscle (e.g. α-cardiac-actin), enables retrospective clonal analysis of cardiac cells, irrespective of gene expression.[48–50]

Clonal analysis is based on statistical evaluation of the chance that reporter gene expression in different cells is based on separate spontaneous recombination events, or that these different cells are progeny of one recombination event (and thus share a common progenitor during development). A statistical method commonly used is the fluctuation test of Luria and Delbrück.[51] This famous experiment showed that mutations in bacteria occur spontaneously (not induced by selection) and at a constant rate, which was used to formulate a probability distribution.[51] This distribution is used to calculate the probability of one or more recombination events, and will therefore determine whether cells showing reporter gene expression are most likely clonally related or are derived from different recombination events (**Fig. 5B**).[47–49,52] Early recombination (i.e. during early stages of development) will give large clusters of cells with reporter gene expression (**Fig. 5C**), while late spontaneous recombination will give smaller clusters of *lacZ* positive cells (**Fig. 5D**).

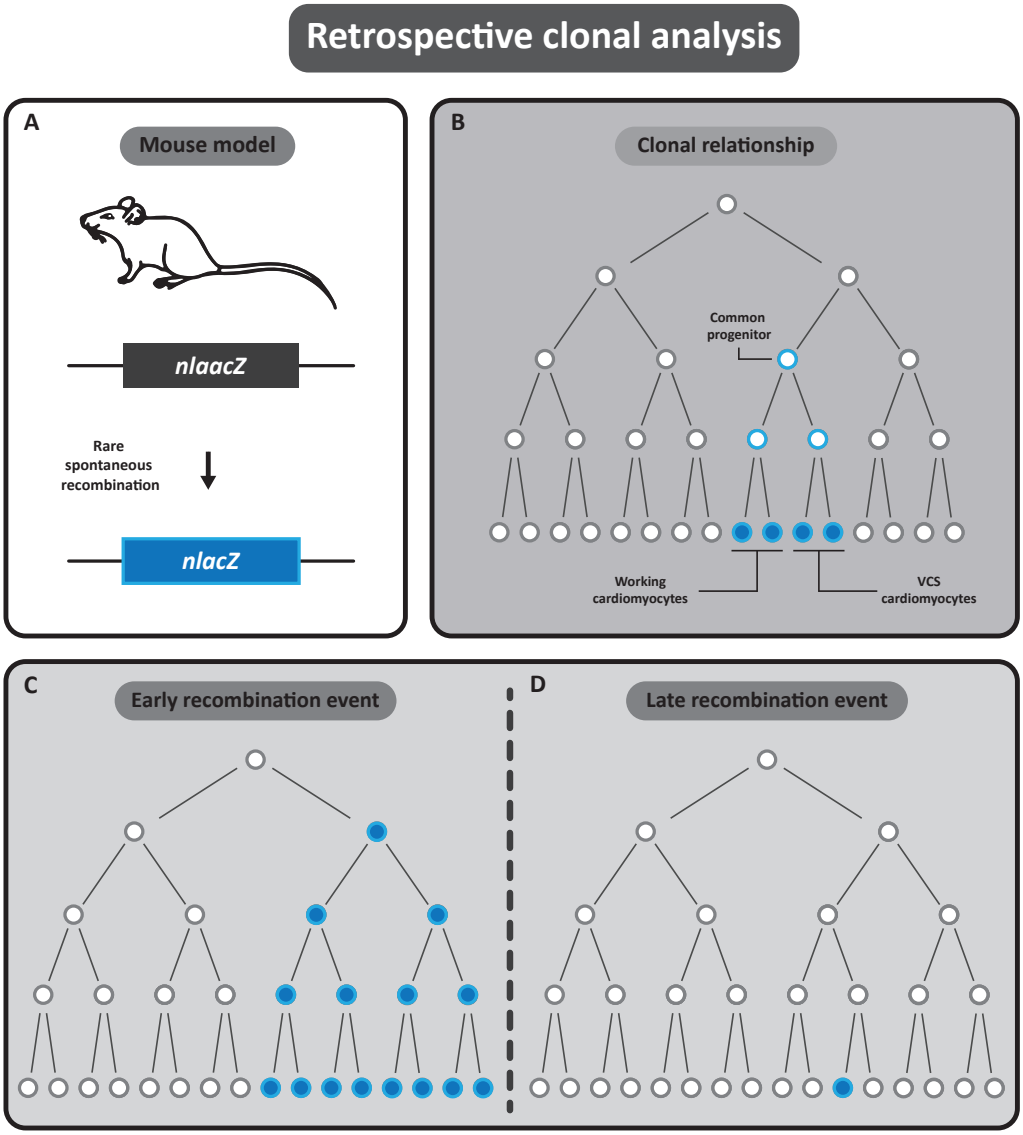

Figure 5. Retrospective clonal analysis

A. Shows mouse model used. Rare, spontaneous recombination results in deletion of an intragenic duplication in the *nlaacZ* gene, resulting in reporter gene expression of the *nlacZ* gene. **B.** Reporter gene expression in this example is seen in VCS and working cardiomyocytes (dark blue with light blue stroke), which, based on statistical analysis is most likely based on one spontaneous recombination event in a common progenitor for both cell types (and not two unrelated spontaneous recombination events).[49] **C-D.** Early spontaneous recombination will result in a large clone (**C**), while late recombination will result in a small clone (**D**).

2.3.2. ADVANTAGES OF RETROSPECTIVE CLONAL ANALYSIS

To perform prospective lineage tracing, some basic knowledge on the progenitor population that will be traced is required. This information is not necessary when performing retrospective clonal analysis. Studying whether certain structures or clusters of cells are clonally related is done independent of gene expression or any other preconceived idea of a possible progenitor pool. Retrospective clonal analysis can therefore establish clonal relationships that are less apparent at first sight, such as the clonal relationship between head musculature and cardiomyocytes from the outflow tract and right ventricle.[53]

Furthermore, as described previously, prospective genetic tracing is hampered by the difficulty to draw conclusions from the absence of reporter gene expression. With the retrospective clonal approach, analysis is based on *lacZ* positive cells. *LacZ* expression in different structures or tissues is mapped and statistical analysis is performed to calculate whether these different tissues or structures are clonally related.

Finally, as with genetic tracing, retrospective clonal analysis is non-invasive.

2.3.3. LIMITATIONS OF RETROSPECTIVE CLONAL ANALYSIS

The retrospective approach has several drawbacks. Since data is analyzed retrospectively, it is not possible to locate the common progenitor, either in time or space. Therefore it is not possible to perform further experiments with these progenitors (e.g. characterization or ablation). Retrospective clonal analysis has to be performed in conjunction with other fate mapping techniques to build the complete lineage tree of a structure or organ. In this sense, the most important advantage of this technique is also its most important drawback. Starting with a certain progenitor pool based on timing, location and/or gene/protein expression profile excludes contributions from other (sometimes unexpected) progenitors, but does directly pinpoint a possibly important progenitor pool for the structure/tissue of interest.

Spontaneous recombination of the *nlaacZ* gene is rare and it is therefore necessary to obtain a large library of embryos with *lacZ* positive clones. Thousands of embryos or adult mice will have to be sacrificed and analyzed. Although this is laborious and causes distress to the animals, it is important to realize that after establishing this large library of clones, answers to numerous scientific questions in all fields of developmental biology can potentially be found.

3. THE SINOATRIAL NODE

Several techniques have been used to investigate the progenitors that will ultimately form the adult SAN. The next section gives an overview of these techniques, which are summarized in **Table 2**.

3.1. GENETIC TRACING AND SAN DEVELOPMENT

Several Cre-based genetic tracing studies have been performed to identify SAN progenitors. An important gene studied in sinus venosus and SAN development is T-box transciption factor gene 18 (Tbx18). Tbx18 is linked to the embryonic venous pole and is involved in development of the epicardium and sinus venosus myocardium, including the SAN.[54] $Tbx18^{Cre}$:$R26R^{lacZ}$ tracing experiments showed lacZ staining of the SAN head and tail at E17.5, which indicated that the progenitors of the SAN express Tbx18 at some time point during development. Since atrial myocardium lacked lacZ staining, the authors concluded that atrial myocardium is not derived from Tbx18+ progenitors.[15] In a recent study, genetic tracing experiments were performed, utilizing several constitutive and inducible Cre lines.[55] In this study, the derivation of the SAN head and tail from a Tbx18+ progenitor pool was confirmed using a different $Tbx18^{Cre}$, crossed with the $R26R^{mT/mG}$ reporter line.[55] This reporter construct utilizes the R26R locus and expresses the membrane-bound fluorescent protein Tomato in all cells.[56] Cre-mediated excision of mTomato results in expression of membrane-bound GFP.[56]

Another important gene studied extensively in CCS function and development is the hyperpolarization-activated cyclic nucleotide-gated channel 4 (HCN4). This channel delineates the (developing) CCS[14] and is the main driving force behind the "funny current", which enables pacemaker cells to depolarize spontaneously.[57] Genetic tracing experiments were performed with an inducible $HCN4^{CreERT2}$ line, which was crossed with the $R26R^{lacZ}$ reporter mouse.[55] Induction with tamoxifen at E6.5 and analysis at E16.5 revealed lacZ expression in the coronary sinus, but not the SAN. Induction at E7.5 showed lacZ expression in a larger region, with staining present in the SAN tail at E16.5. With inductions from E8.5 onwards, the entire SAN showed lacZ activity, indicating that from ~E7.5-8.5 onwards, SAN precursors express HCN4.[55]

Constitutive and inducible tracing of Islet1 (Isl1), a LIM homeodomain transcription factor important for cell proliferation, differentiation and survival[58] and known to be essential for normal development and function of the SAN[59,60], was also performed. Constitutive tracing with $Isl1^{Cre}$:$R26R^{mT/mG}$ showed that the SAN is derived from Isl1+ progenitors.[44] Inducible genetic tracing was performed with the $Isl1^{MerCreMer}$ mouse line. Induction of Cre-recombinase at E9 and analysis of lacZ staining at E11 revealed lacZ expression in the SAN, which shows that around E9, SAN progenitors express Isl1.[7]

Table 2. Overview cell tracing experiments aimed at the sinoatrial node

Genetic tracing					
Genotype	**C vs I***	**Induction at**	**Analysis at**	**Conclusion authors**	**Ref**
$Tbx18^{Cre}$:$R26R^{lacZ}$	C	n.a.	E17.5	SAN progenitors express Tbx18	1
$Tbx18^{Cre}$:$R26R^{mT/mG}$	C	n.a.	E16.5	SAN derived from Tbx18+ progenitors	2
$HCN4^{CreErt2}$:$R26R^{lacZ}$	I	E6.5-9.5, E11.5-12.5	E16.5	Induction E6.5: no labeling SAN, E7.5 labeling SAN tail, later inductions entire SAN[#]	2
$HCN4^{CreErt2}$:$R26R^{mT/mG}$	I	E7.5, 9.5, 12.5, 16.5	E16.5, P1	[#]Same pattern with different reporter (lacZ vs mT/mG, both R26R locus)	2
$Isl1^{Cre}$:$R26R^{mT/mG}$	C	n.a.	E16.5	SAN derived from Isl1+ progenitors	2
$Isl1^{MerCreMer}$:$R26R^{lacZ}$	I	E9	E11	At ~E9 SAN progenitors express Isl1	3
$Nkx2\text{-}5^{Cre}$:$R26R^{mT/mG}$	C	n.a.	E16.5	SAN tail partially derived from Nkx2-5+ progenitors	2
$Shox2^{Cre}$:$R26R^{lacZ}$	C	n.a.	E9.5-11.5	SAN shows lacZ expression	4
Vital dye labeling					
Location of labeling		**Time point labeling**	**Time point analysis**	**Conclusion authors**	**Ref**
ISL1/NKX2-5 negative lateral plate mesoderm		HH5, 8, 10	HH18	Pacemaker precursors positioned in right side *ISL1/NKX2-5* negative lateral plate mesoderm, termed the tertiary heart field	5
ISL1/TNNI2 positive sinus venosus myocardium		HH15-17	HH20, 25	SAN derived from sinus venosus myocardium	6

*C = constitutive, I = inducible, see text for explanation, E = embryonic day, P = postnatal day, n.a. = not applicable

References: 1. Wiese, C. *et al. Circ. Res.* **104**, 88–97 (2009), 2. Liang, X. *et al. Circ. Res.* **113,** 399–407 (2013). 3. Sun, Y. *et al. Dev. Biol.* **304,** 286–96 (2007). 4. Sun, C. *et al. Genesis.* **51,** 515–522 (2013). 5. Bressan, M. *et al. Science.* **340**, 744-748 (2013). 6. Kelder, T.P. *et al. J. Cell. Mol. Med.* **19**, 1375-1379 (2015).

Nkx2-5, which is commonly used as an early precardiac marker[61], was studied using constitutive tracing with Nkx2-5^{Cre}:R26R$^{mT/mG}$ mice.[55] The SAN head showed no reporter gene expression. A subpopulation of cells in the SAN tail did show GFP expression, and the authors therefore concluded that these cells are derived from an Nkx2-5+ precursor.[55] As mentioned, active expression of *Nkx2-5* could also result in reporter gene expression (**Fig. 3**).

Finally, the Shox2^{Cre} mouse line was used to investigate whether Shox2 expressing progenitors contributed to the SAN.[62] Shox2 is important for recruitment of sinus venosus myocardium during early development[61] and is necessary for pacemaker differentiation and normal SAN function.[63–66] The R26R^{LacZ} mouse was used as reporter and analysis of β-galactosidase staining was performed between E9.5-11.5.[62] Reporter expression was seen in the SAN. However, at these stages, the SAN actively expresses Shox2.[61,62] Reporter gene expression is therefore likely the result of active expression of Shox2 by the cells from the SAN and does not give lineage information.

3.2. VITAL DYE LABELING AND SAN PRECURSORS

Elegant vital dye labeling experiments were performed by Bressan *et al.*, aimed at identifying the precursor cells of the SAN.[42] Labeling was performed during the first stages of embryonic development in chick (HH5-10). Results showed that during early embryonic stages, pacemaker precursor cells are positioned in the *NKX2-5/ISL1* negative portion of the right lateral plate mesoderm.[42] This region was posterior to the *ISL1/NKX2-5* expressing heart field.[42] Furthermore, labeling cells within the left portion of the inflow and subsequent follow-up showed that these cells did not contribute to the right-sided SAN.[42]

Tracing the fate of cells deriving from the *NKX2-5-/ISL1-* right lateral plate mesoderm showed that cells arising from this mesoderm also contribute to the atria, AV junction and proepicardial organ. Since this region showed no expression of *NKX2-5* and *ISL1* (markers commonly used to define the FHF and SHF), the authors termed this region the tertiary heart field. However, as described above, Isl1 has been shown to be unsuitable as marker for the SHF. It remains therefore the question whether the different (i.e. first, second and tertiary) heart fields represent true distinct cell populations, or that they form a continuum and reflect different stages of differentiation of progenitor cells with a cardiac fate.[25,35,67]

Another series of vital dye labeling experiments was aimed at tracing the fate of sinus venosus myocardium.[35] *In ovo* labeling of ISL1+/TNNI2+ sinus venosus myocardium at HH15 resulted in SAN labeling after 24-48h of follow-up. This confirms that the SAN is derived from the sinus venosus myocardium (**Table 2**).

3.3. CONCLUSION TRACING EXPERIMENTS AIMED AT THE DEVELOPMENTAL ORIGIN OF THE SAN

The tracing experiments support the now widely accepted idea that SAN precursors reside in the myocardium of the sinus venosus. Furthermore, pacemaker cell fate is established during the first stages of embryonic development, even prior to formation of the heart tube.[42]

4. THE ATRIOVENTRICULAR NODE

The AVN is a complex heterogeneous structure and the developmental origin is still subject of debate. The following section focuses on the genetic tracing and fate mapping experiments that were performed to identify progenitors of the AVN. Results are summarized in **Table 3**.

4.1. GENETIC TRACING AND THE AVN

An essential gene in AVN development is the gene encoding the T-box transcription factor (Tbx) 2. Tbx2 is a repressor of transcription and during development is expressed in the myocardium of the outflow tract and AV canal.[68] Constitutive genetic tracing with the $Tbx2^{Cre}$ was performed using either the $R26R^{lacZ}$ or Z/EG reporter mouse.[69] The Z/EG mouse expresses lacZ in a varying degree in different tissues. Cre mediated excision of the lacZ gene results in irreversible expression of eGFP in cells expressing Cre, making this model suitable for genetic tracing.[70] No clear distinction was made between the results obtained from the different reporter constructs. At E8-8.5, reporter gene expression (and *Tbx2* mRNA expression) was seen in the inflow tract.[69] Unfortunately, the exact description of the inflow tract (either anatomical or based on marker expression) was not provided. Analysis at E9.25 revealed reporter gene expression (and *Tbx2* mRNA expression) in the AV canal.[69] The authors concluded that the AV canal is derived from the Tbx2+ inflow tract.[69] Analysis of Tbx2+ lineage data at E17.5 showed expression of eGFP (reporter gene) in the complete AVN and AV ring bundle.[69] It was concluded that the AVN and AV ring bundle derive from the AV canal.[69] Reporter gene expression (in the Z/EG line) at P14 was found in all *Hcn4+/Tbx3+* atrial cells at the AV junction. The authors concluded that this could indicate that the AV canal contributes to the atrial components of the AV conduction axis, including the transitional cells and nodal extensions.[71] It is important to mention that active expression of *Tbx2* mRNA (which was found in cells of the AV canal up till E17.5, later stages not described[69]) could also result in reporter gene expression, which complicates the analysis of the described experiments.

Another series of genetic tracing experiments were performed with a GATA6-gene heart-region-specific enhancer.[72] The GATA6 gene is an evolutionary conserved gene encoding a transcription factor important for early specification

of cardiac progenitors.[73,74] Genetic tracing was performed with the gene encoding Cre inserted at the locus of this enhancer, combined with the $R26R^{lacZ}$ reporter mouse. Analysis of reporter gene expression was performed at E8.5, E9.5, E12.5 and in the neonatal stage.[72] The embryonic stages showed expression in the AV canal. In neonatal hearts, reporter gene expression was found in the AVN and AV bundle and a subset of cells in the LV and atria also showed lacZ-staining.[72] However, expression of this enhancer (as shown by inserting the gene encoding lacZ in the locus for the cardiac enhancer) was found in the AV canal at E14. No data is presented on neonatal expression of the enhancer itself. This could mean that reporter gene expression merely reflected active expression of the GATA6 enhancer, which does not give lineage information. It is therefore difficult to interpret the results from the genetic tracing experiments performed in this study.

The genes used for genetic tracing experiments aimed at the precursors of the SAN were also used to study the developmental origin of the AVN. Constitutive genetic tracing with two different $Tbx18^{Cre}$ mouse models[55,71], crossed with either $R26R^{lacZ}$, [71] or $R26R^{mT/mG}$, [55] showed no reporter expression in the compact portion of the AVN at E16.5-17.5. It was concluded that the atrial portion of the AV conduction axis[71] or the AVN in general[55] is not derived from Tbx18 positive progenitors. Again, it is important to mention that negative results are difficult to interpret in genetic lineage tracing experiments (see **Section 2.1.3.**).

Inducible genetic tracing with HCN4 to study the developmental origin of the AVN has also been performed.[55] The $HCN4^{CreERT2}$ mouse was bred with either $R26R^{lacZ}$ or $R26R^{mT/mG}$ reporter mice. Tamoxifen was administered at E6.5-9.5 and E11.5-12.5 in the $R26R^{lacZ}$ reporter and at E7.5, 9.5, 12.5 and 16.5 in the $R26R^{mT/mG}$ reporter. Analysis was performed at E16.5 and P1. After induction at E6.5, only a small number of positive cells was found in the coronary sinus and AV region, but not the AVN. Induction from E7.5 onwards resulted in reporter gene expression in the AVN, and later inductions resulted in more positive labeling of the AVN.[55] This shows that the precursors of the AVN start expressing HCN4 from ~E7.5-8.5.[55]

Contribution of Isl1+ precursors to the AVN was investigated with constitutive and inducible genetic tracing. Inducible tracing with the $Isl1^{MerCreMer}$ mouse and $R26R^{lacZ}$ reporter line showed that induction with tamoxifen at E9 resulted in reporter gene expression in a subset of AVN cells.[7] The results from earlier inductions did not mention the AVN explicitly in this study.[7] Constitutive genetic tracing with the $Isl1^{Cre}$ combined with the $R26R^{mT/mG}$ reporter mouse confirmed the R26R-based inducible genetic tracing, showing that approximately 9.4% of AVN cells are derived from an Isl1+ progenitor.[55] These results indicate that at least a part of the AVN is derived from Isl1+ progenitors. However, as described

Table 3. Overview cell tracing experiments aimed at the atrioventricular node

Genetic tracing					
Genotype	**C vs I***	**Induction at**	**Analysis at**	**Conclusion authors**	**Ref**
$Tbx2^{Cre}$:$R26R^{lacZ}$; Z/EG	C	n.a.	E8.5, E9.25, E17.5, P14	1. AVC is derived from Tbx2+ myocardium IFT 2. AVN is derived from AVC	1,2
$cGATA6^{Cre}$: $R26R^{lacZ}$	C	n.a.	E8.5, E9.5, E12.5, P(?)	LacZ expression in AVC/AVN, AV bundle, left ventricle and atria	3
$Tbx18^{Cre}$:$R26R^{lacZ}$	C	n.a.	E17.5	No contribution Tbx18+ progenitors to atrial component AV conduction axis	2
$Tbx18^{Cre}$:$R26R^{mT/mG}$	C	n.a.	E16.5	No contribution Tbx18+ progenitors to AVN	4
$HCN4^{CreErt2}$:$R26R^{lacZ}$	I	E6.5-12.5	E16.5	AVN precursors start expressing HCN4 at ~E7.5-8.5#	4
$HCN4^{CreErt2}$:$R26R^{mT/mG}$	I	E7.5-16.5	E16.5, P1	#same pattern as described for lacZ reporter	4
$Isl1^{Cre}$:$R26R^{mT/mG}$	C	n.a.	E16.5	Subset of AVN cells derived from Isl1+ progenitor	4
$Isl1^{MerCreMer}$:$R26R^{lacZ}$	I	E9	E11	At ~E9 AVN progenitors express Isl1	5
$Isl1^{Cre}$:$Gata4^{flap}$	C	n.a.	E9.5, P(?)	(Nearly) all cells of the heart are derived from Isl1+ progenitors	6
$Nkx2\text{-}5^{Cre}$:$R26R^{mT/mG}$	C	n.a.	E16.5	AVN is derived from the first heart field	4
$Shox2^{Cre}$:$R26R^{lacZ}$	C	n.a.	E12.5, E18.5, P7	No contribution Shox2+ progenitors to AVN	7
Mef2c-AHF-Cre:Z/EG	C	n.a.	E14.5, P14	AV conduction axis not derived from ventricular myocardium, AV bundle or DMP	2

Vital dye labeling				
Location of labeling	**Labeling**	**Analysis**	**Conclusion authors**	**Ref**
pSHF mesoderm(*Isl1+/Fgf10-*)	2, 4, 6 somites	20-25 somites	Cells from "pSHF" contribute to AV canal	8
Lateral plate mesoderm	HH5, 8, 10	HH18	Right lateral plate mesoderm contributes to AV junction	9
ISL1/TNNI2 positive sinus venosus myocardium	HH15-17	HH20, 25	Sinus venosus myocardium contributes to pacemaker-like cells putative AVN region	10

***C = constitutive, I = inducible, see text for explanation, E = embryonic day, P = postnatal day (? = unknown), n.a. = not applicable**

References: 1. Aanhaanen, W.T.J. *et al. Circ. Res.* **104**, 1267-74 (2009), 2. Aanhaanen, W.T.J. *et al. Circ. Res.* **107**, 728-36 (2010), 3. Davis, D.L. *et al. Mech. Dev.* **108**, 105-19 (2001), 4. Liang, X. *et al. Circ. Res.* **113,** 399–407 (2013), 5. Sun, Y. *et al. Dev. Biol.* **304,** 286–96 (2007), 6. Ma, Q. *et al. Dev. Biol.* **323**, 98-104 (2008), 7. Sun, C. *et al. J. Biol. Chem.* **290**, 2007-23 (2015), 8. Domínguez, J. *et al. Circ. Res.* **111,** 1323-1335 (2012), 9. Bressan, M *et al. Science.* **340**, 744-748 (2013), 10. Kelder, T.P. *et al. J. Cell. Mol. Med.* **19**, 1375-1389 (2015).

above, Gata4-based constitutive tracing revealed that (nearly) all cardiomyocytes are derived from Isl1+ progenitors, including the cardiomyocytes of the AV canal.[25] This again demonstrates the importance of the reporter line used and underlines the difficulty of interpreting genetic tracing experiments.

Constitutive genetic tracing experiments were also performed for Nkx2-5. Crossing the Nkx2-5^{Cre} with the R26R$^{mT/mG}$ showed that most cells of the AVN (+/- 98%) at E16.5 show reporter gene expression. The authors concluded that the AVN is derived from the FHF.[55] However, according to the used definition of the FHF and SHF, Nkx2-5 is expressed in both FHF and SHF progenitors and derivatives.[5] Therefore, Nkx2-5 is not suitable as lineage marker for the FHF. Furthermore, Nkx2-5 is actively expressed in the AV conduction system.[75] Therefore, reporter gene expression is likely to reflect active expression of Nkx2-5, rather than informing on the fate of Nkx2-5+ precursors.

Since Shox2 is expressed in the AV conduction system[62], constitutive genetic tracing was performed by Sun *et al.* with a Shox2^{Cre} mouse line, combined with the R26R^{lacZ} reporter line.[76] Reporter gene expression was analyzed at E12.5, E18.5 and P7. The authors conclude that the AVN does not receive cellular contributions from Shox2+ progenitors.[76] Instead, it was concluded that the cells derived from a Shox2+ lineage contribute to the dorsal mesenchymal protrusion (DMP).[76] The DMP is a mesenchymal protrusion from the dorsal mesocardium which plays an important role during AV septation by contributing to the base of the atrial septum, together with the mesenchymal cap and AV cushions.[77] The Shox2+ cells in the AV junction showed expression of *Hcn4* and *Tbx3,* and had a pacemaker-like genetic profile with nodal-like electrophysiological characteristics.[76] However, we proposed that the anatomical designation of the DMP and developing AVN may be questioned as the *Hcn4+/Tbx3+* cells in the AV junction with nodal-like electrophysiological characteristics and a pacemaker-like genetic profile may well correspond to the putative AVN, and not the DMP.[78]

The final Cre-line that has been used to perform genetic tracing of the AVN is the Mef2c-AHF-Cre.[71] Mef2c is an important cardiac transcription factor and R26R-based fate map previously showed reporter gene expression in the outflow tract, right ventricle (RV), ventricular septum and DMP.[79,80] The constitutive genetic tracing experiments aimed at the AVN were performed in the Z/EG line.[71] No eGFP expression was found in the atrial part of the AV conduction axis. The authors concluded that the outflow tract, RV, ventricular septum and DMP do not contribute to the AVN (**Table 3**).[71]

4.2. VITAL DYE LABELING STUDIES AND AVN PROGENITORS

Analysis of the fate of cells from the posterior SHF in mouse embryos resulted in findings which could be of importance to AV canal and AVN development.[29] The

posterior SHF was defined in this study as the region that was positive for *Islet1* and negative for *Fgf10*. Vital dye labeling of the left and right side of this region was performed in mouse embryos of 2, 4 and 6 somites and analyzed at the 20-25 somite stage.[29] The results show that cells from the *Islet1*+/*Fgf10*- region, which is distant from the cardiac crescent and PHT, contribute to the sinus venosus, atria and AV canal in a craniocaudal fashion. This means that the cranial portion of the *Islet1*+/*Fgf10*- region will contribute to the AV canal and the more caudal region will contribute to the sinus venosus, with atrial progenitors in between.[29] It was not investigated whether the cells from the posterior SHF will contribute to the AVN. The results however show that Islet1+ cells outside the cardiac crescent and PHT will contribute to the AV canal.

In chick it was shown that at HH8, the progenitors of the AV junction reside in the *ISL1*/*NKX2-5* negative lateral plate mesoderm.[42] Even though the AVN itself was not investigated, it does show that during early development AV canal/junction progenitors are found outside the cardiac crescent or PHT.[29,42]

Vital dye labeling at older stages in chick were aimed at investigating a possible contribution from sinus venosus myocardium to the developing AVN.[35] Labeling of the ISL1+/TNNI2+ myocardium of the sinus venosus was performed at HH15-17 and the location of cells was traced after 24 and 48 hours.[35] Labeled cells could be traced to a myocardial continuity between the myocardium of the sinus venosus and posterior region of the AV canal. qPCR analysis of this continuity showed mRNA expression of *ISL1* and *HCN4*. Furthermore, single-cell patch clamp experiments showed pacemaker-like electrophysiological characteristics.[35] Together, these results show that the sinus venosus myocardium contributes to the posterior AV canal and the cells from this region show a pacemaker-like phenotype.[35] Based on the location of the myocardial continuity between the sinus venosus and AV canal, it was postulated that the continuity contributes to the nodal extensions or transitional cells of the AVN (**Table 3**).[35]

4.3. CONCLUSION FATE MAPPING AND CELL TRACING AIMED AT THE AVN

Based on the results from the above-described lineage tracing experiments (summarized in **Table 3**), we propose the following working model for AVN development. During early development, the progenitors of the AV canal are positioned outside the cardiac crescent and PHT, in the lateral plate mesoderm.[42] During early development, no *ISL1, NKX2-5*[42] and *Hcn4*[55] expression is seen. Perhaps *Tbx2* expression can already be found at this stage, but this was not investigated. During further development, the cells from this region are sequentially incorporated in the inflow tract/sinus venosus and start to express Isl1, Hcn4, and Tbx2.[35,55,69] The cells from the inflow tract[69] and sinus venosus[35]

are incorporated in the AV canal. Interestingly, in the *mef2c*$^{-/-}$ mouse line, this sequential incorporation of inflow tract was shown to be disturbed.[81] After targeted deletion of *mef2c*, precursors of the AV canal (as labeled by *cGATA6* expression) remained in the sinoatrial region.[81] The *Tbx2+/cGATA6+* AV canal will form (at least) the compact AVN.[69] The craniocaudal patterning of the *Isl1+/Fgf10-* splanchnic mesoderm[29] and late incorporation of sinus venosus myocardium[35] could help to explain the different cell types present in the adult AVN. We hypothesize that the most cranial part of the inflow tract will generate the compact AVN, whereas more caudal cells from the sinus venosus contribute to the nodal extensions and/or transitional cells. However, further research is needed. We propose combining early dye/viral labeling of AV canal/junction progenitors with live imaging, long-term follow-up and characterization of these cells. This could prove the gradual incorporation of cells from outside the cardiac crescent and PHT in the AV canal and AVN. Characterization of labeled cells could help to understand the origin of the different components of the AVN.

5. THE VENTRICULAR CONDUCTION SYSTEM

The ventricular conduction system (VCS) ensures rapid and synchronous electrical activation of the ventricles and consists of the AV bundle, the left and right bundle branches (LBB/RBB) and Purkinje fiber (PF) network (**Fig. 1**).[22] The following section provides an overview of experiments aimed at investigating the cellular origin of the VCS, which are summarized in **Table 4**.

5.1. GENETIC TRACING AND VCS ORIGIN

Intercellular communication between cardiomyocytes is necessary for electrical coupling and is achieved by gap junctions. An important marker for the VCS is Connexin40 (Cx40), which is one of the major gap junction proteins, and is expressed in the atrial working myocardium, the AVN, and the fast conducting cells of the VCS.[82,83] To perform prospective tracing experiments, a transgenic mouse line was generated in which the tamoxifen inducible CreERT2 was placed in the Cx40 locus.[49] The mice were crossed with the R26R^{lacZ} line and tamoxifen was administered between E10.5-18.5 followed by analysis of reporter gene expression at P7. Interestingly, inducing translocation of Cre to the nucleus with tamoxifen at E10.5-E14.5 resulted in lacZ expression in both conductive as well as working cardiomyocytes at P7.[49] However, after induction with tamoxifen from E16.5 onwards, reporter gene expression was almost entirely restricted to conduction system cardiomyocytes.[49] This study indicates that around E16.5, Cx40+ progenitors start to generate progeny with a more restricted conductive fate, as compared to Cx40+ progenitors during earlier developmental stages.[49]

In addition, several of the Cre lines described for the SAN and AVN have also

Table 4. Overview cell tracing experiments aimed at the ventricular conduction system

Genetic tracing					
Genotype	**C vs I***	**Induction**	**Analysis**	**Conclusion authors**	**Ref**
$Cx40^{CreERT2}$:$R26R^{lacZ}$	I	E10.5-E18.5	P7	Induction <E16.5: working + conductive VCS, >E16.5: conductive cells VCS	1
$Tbx18^{Cre}$:$R26R^{lacZ}$	C	n.a.	E10.5, E17.5	No contribution Tbx18+ progenitors to VCS	2
$Tbx18^{Cre}$:$R26R^{mT/mG}$	C	n.a.	E16.5	No contribution Tbx18+ progenitors to VCS	3
$HCN4^{CreErt2}$:$R26R^{lacZ}$	I	E6.5-12.5	E16.5	All components except RBB and subset PFs RV derive from FHF#	3
$HCN4^{CreErt2}$:$R26R^{mT/mG}$	I	E7.5-16.5	E16.5, P1	#same pattern as described for lacZ reporter	3
$Isl1^{Cre}$:$R26R^{mT/mG}$	C	n.a.	E16.5	RBB and subset RV Purkinje fibers derived from SHF	3
$Isl1^{Cre}$:$Gata4^{flap}$	C	n.a.	E9.5, P(?)	(Nearly) all cells of the heart are derived from Isl1+ progenitors	4
$Nkx2\text{-}5^{Cre}$:$R26R^{mT/mG}$	C	n.a.	E16.5	AV bundle, LBB, and PF network LV (and PFs RV partially) derive from FHF	3
Mef2c-AHF-Cre:Z/EG	C	n.a.	E14.5, P14	Focus on AVN. Not possible to draw lineage conclusions for VCS	2
$Tbx2^{Cre}$:Z/EG	C	n.a.	E17.5, P14	No contribution of Tbx2+ progenitors to AV bundle or bundle branches	2,5
$Wnt1^{Cre}$:CAG-CAT^{eGFP};$R26R^{lacZ}$	C	n.a.	E17.5	NCCs contribute to Purkinje fiber network	6
$Wnt1^{Cre}$:$R26R^{lacZ}$	C	n.a.	E12.5-17.5	NCCs are contiguous with VCS	7
$Wnt1^{Cre}$:$R26R^{lacZ}$:$Cx40^{GFP}$	C	n.a.	E14.5, 18.5 P7	NCCs are in close vicinity to VCS, but do not contribute to VCS	8
Viral labeling					
Location of labeling	**Labeling**	**Analysis**	**Conclusion authors**		**Ref**
Ventricular wall	E3	E14, 18	Purkinje fibers derive from cardiomyocytes of ventricular wall		9
Pericardial cavity	E2.5-3	E4.5, E10-19	VCS derives from cardiomyocytes of PHT		10
Retrospective clonal analysis					
Genotype	**Analysis**	**Conclusion authors**			**Ref**
α-cardiac $actin^{n1aacZ}$:$Cx40^{GFP}$	P 3 wks	VCS shares common progenitor with working myocardium; After lineage restriction still proliferation; Different progenitor pool conductive/working cardiomyocytes for LV as compared to RV			1
α-cardiac $actin^{n1aacZ}$:$Cx40^{GFP}$	P 3 wks	VCS shares common progenitor with working myocardium; Left and right VCS derive from a different progenitor pool; Both progenitor pools contribute to AVB and RBB			8

***C = constitutive, I = inducible, see text for explanation, E = embryonic day, P = postnatal age (? = unknown), n.a. = not applicable**

References: 1. Miquerol, L. *et al. Circ. Res.* **107**, 153-161 (2010), 2. Aanhaanen, W.T.J. *et al. Circ. Res.* **107,** 728-736 (2010), 3. Liang, X. *et al. Circ. Res.* **113,** 399–407 (2013), 4. Ma, Q. *et al. Dev. Biol.* **323,** 98-104 (2008), 5. Aanhaanen, W.T.J. *et al. Circ. Res.* 104, 1267-74 (2009), 6. Nakamura, T. *et al. Circ. Res.* **98**, 1547-1554 (2006), 7. Poelmann, R. *et al. Anat. Embryol.* **208,** 389-393 (2004), 8. Miquerol, L. *et al. Dev. Dyn.* **242,** 665-677 (2013), 9. Gourdie, R. *et al. Development.* **121,** 1423-1431 (1995), 10. Cheng, G. *et al. Development.* **126,** 5041-5049 (1999).

been used to study the origin of the VCS. Constitutive tracing with the $Tbx18^{Cre}$, either in the $R26R^{lacZ}$ or $R26R^{mT/mG}$ strain was performed. Analysis of reporter gene expression was performed at E10.5[71], E16.5[55] and E17.5.[71] No reporter gene expression was found in the components of the VCS in either of the studies.[55,71]

Inducible genetic tracing experiments were performed with the $HCN4^{CreERT2}$ mouse line combined with either the $R26R^{LacZ}$ or $R26R^{mT/mG}$.[55] Tamoxifen inductions were performed at different developmental stages and analyzed at either E16.5 or P1. Inductions at E6.5 showed no reporter gene expression in the components of the VCS at E16.5. Inductions at E7.5 resulted in labeling of the LBB, PF network of the LV and sporadic labeling in the PF network of the RV. [55] Tamoxifen administration at E8.5 resulted in additional labeling in the His bundle. Interestingly, absent or reduced expression in the PF network, His bundle and LBB was seen when inductions were performed at E9.5-E12.5. Labeling at E16.5 resulted in labeling of all the components of the CCS, including the RBB and PF network.[55] The authors concluded that all components of the VCS derive from the FHF, except the RBB and a subset of PFs of the RV, which are derived from the SHF. Furthermore, components of the CCS show *de novo* or re-expression of HCN4 (as shown by inductions performed at E16.5) according to the authors.[55] However, absent reporter gene expression could also be explained by Cre expression below the threshold to induce reporter gene expression.[25] As described above, previous work showed that R26R-based genetic tracing is susceptible to this problem, with a higher recombination threshold for the RV.[25] Furthermore, reporter gene expression in the performed experiments could also reflect active expression of HCN4 in the components of the CCS, which complicates tracing the HCN4+ lineage, again stressing the need for careful interpretation of results obtained by genetic lineage tracing.

Constitutive genetic tracing of Isl1+ progenitors was performed in different reporter strains. R26R-based constitutive tracing with the $R26R^{mT/mG}$ line showed reporter gene expression in the RBB and PFs of the RV at E16.5.[55] Interestingly, only a small number of cells in the His bundle, PFs of the LV and cells from the LBB showed expression of eGFP.[55] Based on these results and HCN4 genetic tracing, it was concluded that the VCS is derived from the FHF, except the RBB. The latter is suggested to be derived from the SHF.[55] However, since Isl1 is not suitable as SHF marker and lack of reporter gene expression can result from sub-threshold levels of Cre-expression to induce recombination, these results need further confirmation.

To perform constitutive genetic tracing of Nkx2-5+ progenitors, the $Nkx2\text{-}5^{Cre}$ was combined with the $R26R^{mT/mG}$ line.[55] Analysis at E16.5 revealed reporter gene expression in the majority of cells from the His bundle, LBB, and PF network (both from the LV/RV). Far less reporter gene expression was found in the RBB.

The authors conclude that this is in line with derivation of the majority of the VCS from the FHF.[55] However, Nkx2-5 is not solely a marker for the FHF and eGFP expression can also be explained by active expression of Nkx2-5 in the cells from the VCS. Again, sub-threshold levels of Cre expression in the RBB could also explain the difference in reporter gene expression.[25]

The Mef2c-AHF-Cre was combined with the Z/EG reporter line to perform constitutive genetic tracing.[71] Analysis of reporter expression at E14.5 showed labeling of the AV bundle. However, Cre expression was also found in the AV bundle. Therefore, reporter gene expression likely reflects active expression of the Mef2c-AHF gene. At P14 reporter gene expression was found in the AV bundle as well as the lower nodal cells.[71] Unfortunately, Cre expression was not assessed, which is necessary to discriminate between active expression of Cre or follow-up of cells after irreversible excision of the *lacZ* gene (and subsequent continuous expression of eGFP).

Constitutive genetic tracing for Tbx2 was performed in the Z/EG background at E17.5 and P14.[69,71] Both studies report absence of reporter gene expression in the components of the VCS[69,71], indicating that either the progenitors of the VCS do not express Tbx2 or express Tbx2 at levels too low to reach the threshold to induce recombination of the reporter construct. The former possibility would indicate that the AVN and the proximal components of the VCS derive from a different genetic expression domain.

Constitutive tracing of neural crest cells (NCCs) was performed using the $Wnt1^{Cre}$. The *Wnt1* gene is expressed in the neural plate, dorsal neural tube and in early migratory cells from the neural crest.[84] The migratory NCCs migrate to the heart where they, together with cells from the nodose placode, form the cardiac autonomic nervous system.[85,86] Furthermore, NCCs play an important role during development of the pharyngeal arch arteries, outflow tract septation and evidence has been found that NCCs play an important role during lamellar organization and compaction of the His bundle.[87,88] Genetic tracing experiments were performed with the $Wnt1^{Cre}$ combined with the CAG-CAT^{eGFP} or $R26R^{lacZ}$ reporter lines to trace the fate of NCCs.[89] Cells in the CAG-CAT-eGFP line start expressing eGFP after Cre-mediated excision of the CAT gene.[89] Results are described to be identical between the two reporter lines.[89] Analysis of reporter gene expression was performed at E17.5 and showed positive labeling in the region of the proximal VCS (posterior nodal tract, His bundle, and bundle branches).[89] Based on these results the authors concluded that NCCs contribute to the proximal VCS. However, previous constitutive genetic tracing experiments performed with a $Wnt1^{Cre}$ and the $R26R^{lacZ}$ reporter indicated that NCCs were contiguous with the VCS, but did not contribute to the VCS.[87] In addition, more recent tracing experiments with a $Wnt1^{Cre}$ combined with the $R26R^{lacZ}$ reporter

argue against a contribution from NCCs to the proximal VCS.[50] Tracing was performed using the Cx40-GFP line as background, which expresses GFP in the Cx40+ cells of the VCS.[50] No co-expression of lacZ (the reporter gene) and GFP (delineating the VCS) was seen. Reporter gene expression was seen in close proximity to the AV bundle[50], which is in agreement with previous constitutive genetic tracing experiments.[87] These results indicate that cells from the VCS do not originate from a *Wnt1*+ progenitor pool (**Table 4**).

5.2. VCS PROGENITORS AND VIRAL LABELING

Targeted labeling of cells using genetically modified retroviruses has been performed in order to understand the cellular origin of the VCS. Over two decades ago, *in ovo* microinjection experiments were performed in chick embryos, utilizing 2 different viral vectors, which either induced expression of β-galactosidase in nuclei (SNTZ virus) or the cytoplasm (CXL virus) of infected cells.[90] Either the neural tube was labeled at E2 to trace the fate of cardiac NCCs, or the ventricular wall was labeled at E3. Analysis of β–gal expression at E14 or E18 showed that labeling of the neural tube did not result in labeling of the VCS, indicating that (conform more recent genetic tracing studies, see above[50,87]) NCCs do not contribute to the VCS.[90] Positive labeling was found in ALD58+ cells surrounding the coronary vessels, which were designated to be PFs.[90] No contribution to the AV ring tissue, AV bundle, or bundle branches was found.[90] Furthermore, labeling of myocytes at E3 resulted in β-gal expression in working and conductive cardiomyocytes. Finally, between E14 and E18, an increase in total β–gal+ cells was found, while the number of cells contributing to the PFs remained constant.[90] These results indicate that the PFs derive from cardiomyocytes of the ventricular wall at E3. Furthermore, working myocardium and PFs derive from a common precursor at E3, with PFs committing earlier to a non-proliferative phenotype.[90]

The results of this study are largely in agreement with later performed adenoviral and retroviral labeling experiments.[10] Again, in a larger dataset, no contribution from NCCs to the CCS was found.[10] Injection of these viral vectors at E2.5-3 in the pericardial cavity resulted in reporter gene expression in cardiomyocytes of the atria, ventricles and outflow tract at E4.5. At E10-19, expression was found in EAP-300+ cells, which were designated to be PFs.[10] Interestingly, in a small number of embryos (~5% of total embryos) in this larger dataset with additional adenoviral tracing constructs, expression was found in AV ring tissue, the His bundle and bundle branches.[10] Expression was also present in working myocardium. Together, these results indicate that the proximal and distal components of the VCS derive from the myocardium of the early tubular heart.[10] Unfortunately, the SAN and AVN are not mentioned specifically in the

results. Important to note is that administering viral vectors in the pericardial cavity resulted in reporter gene expression in cardiomyocytes of the atria, ventricles and outflow tract (the sinus venosus myocardium is not mentioned specifically). Therefore, the viral labeling experiments cannot be used to answer the question which of these initially labeled structures ultimately gave rise to the proximal components of the VCS (**Table 4**).

5.3. RETROSPECTIVE CLONAL ANALYSIS AND VCS PRECURSORS

Retrospective clonal analysis was performed with the *nlaacZ* gene under transcriptional control of the *α-cardiac actin* locus, which restricts expression of *nlacZ* (after spontaneous recombination) to cardiomyocytes.[49] This reporter line was bred into the *Cx40*^{GFP} line, which delineates the *Cx40+* cells of the central (His bundle, bundle branches) and proximal (PF network of the RV and LV) VCS.[49] Analysis of reporter gene expression was performed at a postnatal age of 3 weeks. Mixed (GFP+ and GFP- β-galactosidase+ cells) and unmixed (either GFP+ or GFP- β-galactosidase+ cells) clusters were found. The mixed clusters indicate that working (*Cx40-*) and conductive (*Cx40+*) cardiomyocytes derive from a common progenitor.[49] Furthermore, the occurrence of unmixed clusters of conductive cells shows that after lineage restriction, cells still proliferate.[49] The results are in agreement with the inducible genetic tracing results (from the same study) in the Cx40^{CreERT2} mouse line, which showed progressive lineage restriction to either working or conductive cardiomyocytes during development.[49] Interestingly, while the number of conductive cardiomyocytes in mixed clusters between the RV and LV were comparable, the number of working cardiomyocytes was significantly higher in mixed clusters of the LV.[49] This indicates that the progenitor population for conductive and working cardiomyocytes of the LV is different to that of the RV. The mechanisms leading to this difference remain to be elucidated.

A more recent study by the same group also reports on retrospective clonal analysis in *α-cardiac actin*^{nlaacZ}*:Cx40*^{GFP} mice, aimed at elucidating the mechanism of development of the VCS.[50] In a small number (18/912 hearts) of 3-week-old mice, large clusters of β-galactosidase+ cells (>1000 cells) were found. Large clusters of β-galactosidase+ cells indicate that the spontaneous recombination occurred during early development (see **Fig. 4C**). β-gal expression in conductive cardiomyocytes was found in 16/18 of the hearts analyzed, combined with expression in working cardiomyocytes.[50] This again indicates that working cardiomyocytes and conductive cardiomyocytes of the VCS share a common progenitor. Reporter gene expression was found in all components of the VCS. Within one heart, expression was mostly found in two or more separate components of the VCS. Interestingly, no hearts were found with simultaneous

expression of *nlacZ* in the AV bundle, LBB and RBB.[50] Two separate groups could be identified, based on either β-galactosidase+ cells in the PF network of the RV, or β-galactosidase+ cells in the LBB, corresponding to contribution from either a right or left lineage.[50] These results indicate that the left and right VCS derive from a different progenitor population. Reporter gene expression in the AV bundle and RBB was found together with β-gal expression in either the LBB/PF network of the LV or the PF network of the RV, which indicates that both lineages contribute to the AV bundle and RBB (**Table 4**).[50]

5.4. CONCLUSION FATE MAPPING AND CELL TRACING AIMED AT THE ORIGIN OF THE VCS

The above-described results are summarized in **Table 4**. The cells contributing to the VCS are of myocardial origin and share a common progenitor with working cardiomyocytes. The cells contributing to the VCS derive from *Cx40*+ progenitors, which initially produce working and conductive cardiomyocytes. From E16.5 onwards, predominantly conductive cardiomyocytes are produced by *Cx40*+ progenitors. The cardiomyocytes of the left and right portion of the VCS derive from a different progenitor pool. An important question that still needs to be answered is whether continuity between (the primordia of) the AVN and the VCS is present from the onset of development or that these structures are initially separate and connect during further development. During early development in mouse embryos (E8-10), no clear AVN or AV bundle could be discriminated.[2] However, the region of the putative AVN and primitive interventricular septum (the location of the future proximal VCS) showed continuity at these early developmental stages.[2] Furthermore, from E11 onwards, the AVN and AV bundle are distinguishable and are continuous as well.[3,69] Finally, discontinuity between the AVN and VCS in human is rare, even in complex structural heart disease affecting cardiac septation, such as (atrio)ventricular septal defects and congenitally corrected transposition of the great arteries.[11] In left isomerism of the atrial appendages discontinuation between the AVN and the VCS is found.[91] However, damage to the normal continuity of the AVN and VCS rather than failure of the AVN and VCS to fuse is suggested as causative mechanism for the discontinuation.[91] The available data therefore appears to point towards the hypothesis that (the progenitors of) the AVN and VCS are already continuous from the onset of development. However, since the exact location of AV bundle progenitors has not been mapped to date[92], further research is needed to provide a final answer to this question.

6. SUMMARY AND CONCLUSIONS

This review provides an overview of cell tracing and fate mapping techniques used to study the developmental origin of the CCS (**Fig. 6**) and advantages and limitations of these techniques were discussed. One of the conclusions that must be drawn is that caution is necessary when performing cell tracing or fate mapping. Analysis of results must be performed keeping the specific advantages and limitations of the used technique in mind. Omitting this can lead to false conclusions about clonal relationships or lineage information. Combining different techniques and the use of live imaging will help to minimize this risk.

Even though every technique has its limitations, immense progress has been made in understanding the developmental origin of the CCS. Based on the results described here, the following working model (**Fig. 6**) on general CCS development is proposed:

The inflow tract and sinus venosus myocardium will give rise to the SAN (that is initially dual in Anlage with a transient left SAN) and myocardium of the AV canal. The AV canal will generate the compact portion of the AVN and possibly a portion of the transitional cells and/or nodal extensions. The sinus venosus contributes cells to the nodal extensions and transitional cells. The primordia of the AVN (posterior AV canal) and AV bundle and bundle branches (primitive interventricular septum crest and septum) are continuous from the onset of development, and therefore no fusion of these structures is needed. Further differentiation of ventricular cardiomyocytes (which are connected to the surrounding myocardium and bundle branches) towards PFs establishes the final connection between the proximal and distal components of the VCS, thereby completing the electrical wiring of the adult heart.

Figure 6. Summary of cell tracing and fate mapping experiments aimed at elucidating the developmental origin of the CCS (figure on page 231)

The results from the different techniques used to investigate the embryological origin of the different components of the CCS are summarized. Based on these results, the (possible) developmental origin of the different structures is provided.

Figure 6. Summary of cell tracing and fate mapping experiments aimed at elucidating the developmental origin of the CCS (legend on page 230)

REFERENCE LIST

1. Wenink AC. Development of the human cardiac conducting system. *J. Anat.* 1976;121:617–31.

2. Virágh S, Challice CE. The development of the conduction system in the mouse embryo heart. I. The first embryonic A-V conduction pathway. *Dev. Biol.* 1977;56:382–96.

3. Virágh S, Challice CE. The development of the conduction system in the mouse embryo heart. II. Histogenesis of the atrioventricular node and bundle. *Dev. Biol.* 1977;56:397–411.

4. Virágh S, Challice CE. The development of the conduction system in the mouse embryo heart. *Dev. Biol.* 1982;89:25–40.

5. Buckingham M, Meilhac S, Zaffran S. Building the mammalian heart from two sources of myocardial cells. *Nat. Rev. Genet*. 2005;6:826–835.

6. Abu-Issa R, Kirby ML. Heart field: from mesoderm to heart tube. *Annu. Rev. Cell Dev. Biol.* 2007;23:45–68.

7. Sun Y, Liang X, Najafi N, Cass M, Lin L, Cai C-L, Chen J, Evans SM. Islet 1 is expressed in distinct cardiovascular lineages, including pacemaker and coronary vascular cells. *Dev. Biol.* 2007;304:286–96.

8. Gittenberger-de Groot AC, Bartelings MM, Poelmann RE, Haak MC, Jongbloed MRM. Embryology of the heart and its impact on understanding fetal and neonatal heart disease. *Semin. Fetal Neonatal Med.* 2013;18:237–44.

9. Gittenberger-de Groot AC, Calkoen EE, Poelmann RE, Bartelings MM, Jongbloed MRM. Morphogenesis and molecular considerations on congenital cardiac septal defects. *Ann. Med.* 2014;46:640–52.

10. Cheng G, Litchenberg WH, Cole GJ, Mikawa T, Thompson RP, Gourdie RG. Development of the cardiac conduction system involves recruitment within a multipotent cardiomyogenic lineage. *Development*. 1999;126:5041–9.

11. Jongbloed MRM, Vicente-Steijn R, Hahurij ND, Kelder TP, Schalij MJ, Gittenberger-de Groot AC, Blom NA. Normal and abnormal development of the cardiac conduction system; implications for conduction and rhythm disorders in the child and adult. *Differentiation*. 2012;84:131–148.

12. Bakker ML, Christoffels VM, Moorman AF. The cardiac pacemaker and conduction system develops from embryonic myocardium that retains its primitive phenotype. *J. Cardiovasc. Pharmacol*. 2010;56:6–15.

13. Vicente-Steijn R, Kolditz DP, Mahtab EAF, Askar SFA, Bax NAM, van der Graaf LM, Wisse LJ, Passier R, Pijnappels DA, Schalij MJ, Poelmann RE, Gittenberger-de Groot AC, Jongbloed MRM. Electrical activation of sinus venosus myocardium and expression patterns of RHOA and Isl-1 in the chick embryo. *J. Cardiovasc. Electrophysiol.* 2010;21:1284–92.

14. Vicente-Steijn R, Passier R, Wisse LJ, Schalij MJ, Poelmann RE, Gittenberger-de Groot AC, Jongbloed MRM. Funny current channel HCN4 delineates the developing cardiac conduction system in chicken heart. *Heart Rhythm*. 2011;8:1254–63.

15. Wiese C, Grieskamp T, Airik R, Mommersteeg MTM, Gardiwal A, de Gier-de Vries C, Schuster-Gossler K, Moorman AFM, Kispert A, Christoffels VM. Formation of the sinus node head and differentiation of sinus node myocardium are independently regulated by Tbx18 and Tbx3. *Circ. Res.* 2009;104:388–97.

16. Kozlowski D, Kozluk E, Adamowicz M, Grzybiak M, Walczak F, Walczak E. Histological examination of the topography of the atrioventricular nodal artery within the triangle of Koch. *Pacing Clin. Electrophysiol.* 1998;21:163–7.

17. Mazgalev TN, Ho SY, Anderson RH. Anatomic-electrophysiological correlations concerning the pathways for atrioventricular conduction. *Circulation*. 2001;103:2660–2667.

18. Billette J. What is the atrioventricular node? Some clues in sorting out its structure-function relationship. *J. Cardiovasc. Electrophysiol.* 2002;13:515–8.

19. Anderson RH, Boyett MR, Dobrzynski H, Moorman AF. The anatomy of the conduction system: implications for the clinical cardiologist. *J. Cardiovasc. Transl. Res*. 2013;6:187–196.

20. Inoue S, Becker AE. Posterior extensions of the human compact atrioventricular node : A neglected anatomic feature of potential clinical significance. *Circulation*. 1998;97:188–193.

21. Yanni J, Boyett MR, Anderson RH, Dobrzynski H. The extent of the specialized atrioventricular ring tissues. *Heart Rhythm*. 2009;6:672–80.

22. Miquerol L, Beyer S, Kelly RG. Establishment of the mouse ventricular conduction system. *Cardiovasc. Res*. 2011;91:232–242.

23. Buckingham ME, Meilhac SM. Tracing cells for tracking cell lineage and clonal behavior. *Dev. Cell*. 2011;21:394–409.

24. Sauer B. Inducible gene targeting in mice using the Cre/lox system. *Methods*. 1998;14:381–92.

25. Ma Q, Zhou B, Pu WT. Reassessment of Isl1 and Nkx2-5 cardiac fate maps using a Gata4-based reporter of Cre activity. *Dev. Biol*. 2008;323:98–104.

26. Feil R, Brocard J, Mascrez B, LeMeur M, Metzger D, Chambon P. Ligand-activated site-specific recombination in mice. *Proc. Natl. Acad. Sci. USA.* 1996;93:10887–90.

27. Indra AK, Warot X, Brocard J, Bornert JM, Xiao JH, Chambon P, Metzger D. Temporally-controlled site-specific mutagenesis in the basal layer of the epidermis: comparison of the recombinase activity of the tamoxifen-inducible Cre-ER(T) and Cre-ER(T2) recombinases. *Nucleic Acids Res.* 1999;27:4324–7.

28. Kelder TP, Vicente-Steijn R, Poelmann RE, Mummery CL, DeRuiter MC, Jongbloed MRM. The avian embryo to study development of the cardiac conduction system. *Differentiation.* 2016;91:90–103.

29. Domínguez JN, Meilhac SM, Bland YS, Buckingham ME, Brown NA. Asymmetric fate of the posterior part of the second heart field results in unexpected left/right contributions to both poles of the heart. *Circ. Res.* 2012;111:1323–35.

30. Cai C-L, Martin JC, Sun Y, Cui L, Wang L, Ouyang K, Yang L, Bu L, Liang X, Zhang X, Stallcup WB, Denton CP, McCulloch A, Chen J, Evans SM. A myocardial lineage derives from Tbx18 epicardial cells. *Nature*. 2008;454:104–8.

31. Christoffels VM, Grieskamp T, Norden J, Mommersteeg MTM, Rudat C, Kispert A. Tbx18 and the fate of epicardial progenitors. *Nature*. 2009;458:E8-9-10.

32. Hayashi S, McMahon AP. Efficient recombination in diverse tissues by a tamoxifen-inducible form of Cre: a tool for temporally regulated gene activation/inactivation in the mouse. *Dev. Biol.* 2002;244:305–18.

33. Cai C-L, Liang X, Shi Y, Chu P-H, Pfaff SL, Chen J, Evans S. Isl1 identifies a cardiac progenitor population that proliferates prior to differentiation and contributes a majority of cells to the heart. *Dev. Cell*. 2003;5:877–89.

34. Yuan S, Schoenwolf GC. Islet-1 marks the early heart rudiments and is asymmetrically expressed during early rotation of the foregut in the chick embryo. *Anat. Rec*. 2000;260:204–207.

35. Kelder TP, Vicente-Steijn R, Harryvan TJ, Kosmidis G, Gittenberger-de Groot AC, Poelmann RE, Schalij MJ, DeRuiter, MC, Jongbloed MRM. The sinus venosus myocardium contributes to the atrioventricular canal: potential role during atrioventricular node development? *J. Cell. Mol. Med.* 2015;19:1375–89.

36. Sanes JR. Analysing cell lineage with a recombinant retrovirus. *Trends Neurosci.* 1989;12:21–28.

37. Sanes JR, Rubenstein JL, Nicolas JF. Use of a recombinant retrovirus to study post-implantation cell lineage in mouse embryos. *EMBO J.* 1986;5:3133–3142.

38. Price J, Turner D, Cepko C. Lineage analysis in the vertebrate nervous system by retrovirus-mediated gene transfer. *Proc. Natl. Acad. Sci. USA.* 1987;84:156–160.

39. Pacak CA, Byrne BJ. AAV vectors for cardiac gene transfer: experimental tools and clinical opportunities. *Mol Ther.* 2011;19:1582–90.

40. Honig MG, Hume RI. Fluorescent carbocyanine dyes allow living neurons of identified origin to be studied in long-term cultures. *J. Cell. Biol.* 1986;103:171–87.

41. Progatzky F, Dallman MJ, Lo Celso C. From seeing to believing: labeling strategies for in vivo cell-tracking experiments. *Interface Focus*. 2013;3:20130001.

42. Bressan M, Liu G, Mikawa T. Early mesodermal cues assign avian cardiac pacemaker fate potential in a tertiary heart field. *Science.* 2013;340:744–748.

43. Lo Celso C, Fleming HE, Wu JW, Zhao CX, Miake-Lye S, Fujisaki J, Côté D, Rowe DW, Lin CP, Scadden DT. Live-animal tracking of individual haematopoietic stem/progenitor cells in their niche. *Nature*. 2009;457:92–6.

44. Sipkins DA, Wei X, Wu JW, Runnels JM, Côté D, Means TK, Luster AD, Scadden DT, Lin CP. In vivo imaging of specialized bone marrow endothelial microdomains for tumour engraftment. *Nature*. 2005;435:969–73.

45. Honig MG, Hume RI. Dil and DiO: versatile fluorescent dyes for neuronal labeling and pathway tracing. *Trends Neurosci.* 1989;12:333–5,340–1.

46. Mikawa T, Hyer J, Itoh N, Wei Y. Retroviral vectors to study cardiovascular development. *Trends Cardiovasc. Med.* 1996;6:79–86.

47. Bonnerot C, Nicolas JF. Clonal analysis in the intact mouse embryo by intragenic homologous recombination. *CR. Acad. Sci. III.* 1993;316:1207–17.

48. Meilhac SM, Kelly RG, Rocancourt D, Eloy-Trinquet S, Nicolas J-F, Buckingham ME. A retrospective clonal analysis of the myocardium reveals two phases of clonal growth in the developing mouse heart. *Development*. 2003;130:3877–3889.

49. Miquerol L, Moreno-Rascon N, Beyer S, Dupays L, Meilhac SM, Buckingham ME, Franco D, Kelly RG. Biphasic development of the mammalian ventricular conduction system. *Circ. Res.* 2010;107:153–161.

50. Miquerol L, Bellon A, Moreno N, Beyer S, Meilhac SM, Buckingham M, Franco D, Kelly RG. Resolving cell lineage contributions to the ventricular conduction system with a Cx40-GFP allele: a dual contribution of the first and second heart fields. *Dev. Dyn*. 2013;242:665–677.

51. Luria SE, Delbrück M. Mutations of bacteria from virus sensitivity to virus resistance. *Genetics*. 1943; 28: 491–511.

52. Lescroart F, Mohun T, Meilhac SM, Bennett M, Buckingham ME. Lineage tree for the venous pole of the heart: clonal analysis clarifies controversial genealogy based on genetic tracing. *Circ. Res.* 2012;111:1313–22.

53. Lescroart F, Kelly RG, Le Garrec J-F, Nicolas J-F, Meilhac SM, Buckingham M. Clonal analysis reveals common lineage relationships between head muscles and second heart field derivatives in the mouse embryo. *Development*. 2010;137:3269–79.

54. Greulich F, Rudat C, Kispert A. Mechanisms of T-box gene function in the developing heart. *Cardiovasc. Res.* 2011;91:212–22.

55. Liang X, Wang G, Lin L, Lowe J, Zhang Q, Bu L, Chen Y, Chen J, Sun Y, Evans SM. HCN4 dynamically marks the first heart field and conduction system precursors. *Circ. Res.* 2013;113:399–407.

56. Muzumdar MD, Tasic B, Miyamichi K, Li L, Luo L. A global double-fluorescent Cre reporter mouse. *Genesis*. 2007;45:593–605.

57. DiFrancesco D. The role of the funny current in pacemaker activity. *Circ. Res.* 2010;106:434–46.

58. Zhuang S, Zhang Q, Zhuang T, Evans SM, Liang X, Sun Y. Expression of Isl1 during mouse development. *Gene Expr. Patterns*. 2013;13:407–412.

59. Liang X, Zhang Q, Cattaneo P et al. Transcription factor ISL1 is essential for pacemaker development and function. *J. Clin. Invest.* 2015;125:3256–68.

60. Vedantham V, Galang G, Evangelista M, Deo RC, Srivastava D. RNA sequencing of mouse sinoatrial node reveals an upstream regulatory role for Islet-1 in cardiac pacemaker cells. *Circ. Res.* 2015;116:797–803.

61. Blaschke RJ, Hahurij ND, Kuijper S et al. Targeted mutation reveals essential functions of the homeodomain transcription factor Shox2 in sinoatrial and pacemaking development. *Circulation*. 2007;115:1830–8.

62. Sun C, Zhang T, Liu C, Gu S, Chen Y. Generation of Shox2-Cre allele for tissue specific manipulation of genes in the developing heart, palate, and limb. *Genesis*. 2013;51:515–22.

63. Hashem SI, Lam ML, Mihardja SS, White SM, Lee RJ, Claycomb WC. Shox2 regulates the pacemaker gene program in embryoid bodies. *Stem Cells Dev.* 2013;22:2915–26.

64. Liu H, Espinoza-Lewis RA, Chen C, Hu X, Zhang Y, Chen Y. The role of Shox2 in SAN development and function. *Pediatr. Cardiol.* 2012;33:882–9.

65. Liu H, Chen C-H, Ye W, Espinoza-Lewis RA, Hu X, Zhang Y, Chen Y. Phosphorylation of shox2 is required for its function to control sinoatrial node formation. *J. Am. Heart. Assoc.* 2014;3:e000796.

66. Espinoza-Lewis RA, Yu L, He F, Liu H, Tang R, Shi J, Sun X, Martin JF, Wang D, Yang J, Chen Y. Shox2 is essential for the differentiation of cardiac pacemaker cells by repressing Nkx2-5. *Dev. Biol.* 2009;327:376–85.

67. Abu-Issa R, Waldo K, Kirby ML. Heart fields: one, two or more? *Dev. Biol.* 2004;272:281–5.

68. Christoffels VM, Hoogaars WMH, Tessari A, Clout DEW, Moorman AFM, Campione M. T-box transcription factor Tbx2 represses differentiation and formation of the cardiac chambers. *Dev. Dyn.* 2004;229:763–70.

69. Aanhaanen WTJ, Brons JF, Domínguez JN, Rana MS, Norden J, Airik R, Wakker V, de Gier-de Vries C, Brown NA, Kispert A, Moorman AFM, Christoffels VM. The Tbx2+ primary myocardium of the atrioventricular canal forms the atrioventricular node and the base of the left ventricle. *Circ. Res.* 2009;104:1267–74.

70. Novak A, Guo C, Yang W, Nagy A, Lobe C. G. Z/EG, a double reporter mouse line that expresses enhanced green fluorescent protein upon Cre-mediated excision. *Genesis*. 2000;28:147–55.

71. Aanhaanen WTJ, Mommersteeg MTM, Norden J, Wakker V, de Gier-de Vries C, Anderson RH, Kispert A, Moorman AFM, Christoffels VM. Developmental origin, growth, and three-dimensional architecture of the atrioventricular conduction axis of the mouse heart. *Circ. Res.* 2010;107:728–36.

72. Davis DL, Edwards AV, Juraszek AL, Phelps A, Wessels A, Burch JBE. A GATA-6 gene heart-region-specific enhancer provides a novel means to mark and probe a discrete component of the mouse cardiac conduction system. *Mech. Dev.* 2001;108:105–119.

73. Jiang Y, Evans T. The Xenopus GATA-4/5/6 genes are associated with cardiac specification and can regulate cardiac-specific transcription during embryogenesis. *Dev. Biol.* 1996;174:258–70.

74. Jiang Y, Tarzami S, Burch JB, Evans T. Common role for each of the cGATA-4/5/6 genes in the regulation of cardiac morphogenesis. *Dev. Genet.* 1998;22:263–77.

75. Bakker ML, Moorman AFM, Christoffels VM. The atrioventricular node: origin, development, and genetic program. *Trends Cardiovasc. Med.* 2010;20:164–71.

76. Sun C, Yu D, Ye W, Liu C, Gu S, Sinsheimer NR, Song Z, Li X, Chen C, Song Y, Wang S, Schrader L, Chen Y. The short stature homeobox 2 (Shox2)-bone morphogenetic protein (BMP) pathway regulates dorsal mesenchymal protrusion development and its temporary function as a pacemaker during cardiogenesis. *J. Biol. Chem.* 2015;290:2007–23.

77. Briggs LE, Kakarla J, Wessels A. The pathogenesis of atrial and atrioventricular septal defects with special emphasis on the role of the dorsal mesenchymal protrusion. *Differentiation.* 2012;84:117–30.

78. Kelder TP, Vicente-Steijn R, DeRuiter MC, Gittenberger-de Groot AC, Jongbloed MRM. Does the dorsal mesenchymal protrusion act as a temporary pacemaker during heart development? *J. Biol. Chem.* 2015;290:8013–8014.

79. Verzi MP, McCulley DJ, De Val S, Dodou E, Black BL. The right ventricle, outflow tract, and ventricular septum comprise a restricted expression domain within the secondary/anterior heart field. *Dev. Biol.* 2005;287:134–45.

80. Goddeeris MM, Rho S, Petiet A, Davenport CL, Johnson GA, Meyers EN, Klingensmith J. Intracardiac septation requires hedgehog-dependent cellular contributions from outside the heart. *Development*. 2008;135:1887–95.

81. Vong L, Bi W, O'Connor-Halligan KE, Li C, Cserjesi P, Schwarz JJ. MEF2C is required for the normal allocation of cells between the ventricular and sinoatrial precursors of the primary heart field. *Dev. Dyn.* 2006;235:1809–1821.

82. Benes J, Ammirabile G, Sankova B, Campione M, Krejci E, Kvasilova A, Sedmera D. The role of connexin40 in developing atrial conduction. *FEBS. Lett.* 2014;588:1465–9.

83. Miquerol L, Meysen S, Mangoni M, Bois P, Van Rijen HVM, Abran P, Jongsma H, Nargeot J, Gros D. Architectural and functional asymmetry of the His-Purkinje system of the murine heart. *Cardiovasc. Res.* 2004;63:77–86.

84. Jiang X, Rowitch DH, Soriano P, McMahon AP, Sucov HM. Fate of the mammalian cardiac neural crest. *Development*. 2000;127:1607–16.

85. Hildreth V, Anderson RH, Henderson DJ. Autonomic innervation of the developing heart: origins and function. *Clin. Anat.* 2009;22**:**36–46.

86. Verberne ME, Gittenberger-de Groot AC, Van Iperen L, Poelmann RE. Contribution of the cervical sympathetic ganglia to the innervation of the pharyngeal arch arteries and the heart in the chick embryo. *Anat. Rec.* 1999;255**:**407–19.

87. Poelmann RE, Jongbloed MRM, Molin DGM, Fekkes ML, Wang Z, Fishman GI, Doetschman T, Azhar M, Gittenberger-de Groot AC. The neural crest is contiguous with the cardiac conduction system in the mouse embryo: a role in induction? *Anat. Embryol.* 2004;208**:**389–93.

88. Gurjarpadhye A, Hewett KW, Justus C, Wen X, Stadt H, Kirby ML, Sedmera D, Gourdie RG. Cardiac neural crest ablation inhibits compaction and electrical function of conduction system bundles. *Am. J. Physiol. Heart Circ. Physiol.* 2007;292**:**H1291-300.

89. Nakamura T, Colbert MC, Robbins J. Neural crest cells retain multipotential characteristics in the developing valves and label the cardiac conduction system. *Circ. Res.* 2006;98**:**1547–54.

90. Gourdie RG, Mima T, Thompson RP, Mikawa T. Terminal diversification of the myocyte lineage generates Purkinje fibers of the cardiac conduction system. *Development*. 1995;121**:**1423–31.

91. Ho SY, Fagg N, Anderson RH, Cook A, Allan L. Disposition of the atrioventricular conduction tissues in the heart with isomerism of the atrial appendages: its relation to congenital complete heart block. *J. Am. Coll. Cardiol.* 1992;20**:**904–10.

92. van Weerd JH, Christoffels VM. The formation and function of the cardiac conduction system. *Development*. 2016;143**:**197–210.

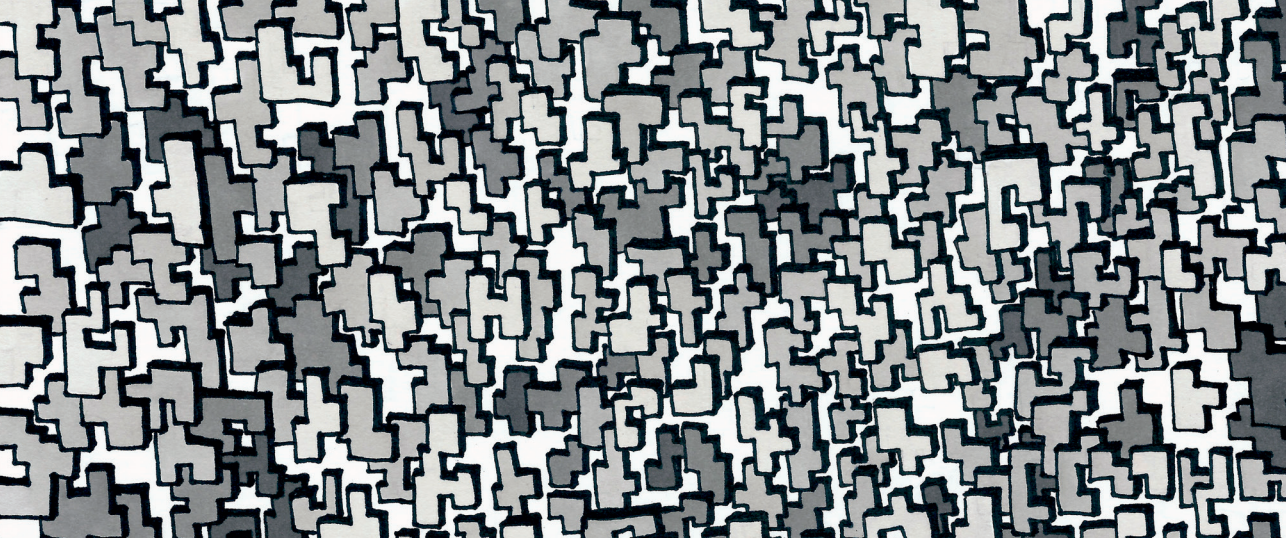

10

SUMMARY & FUTURE PERSPECTIVES

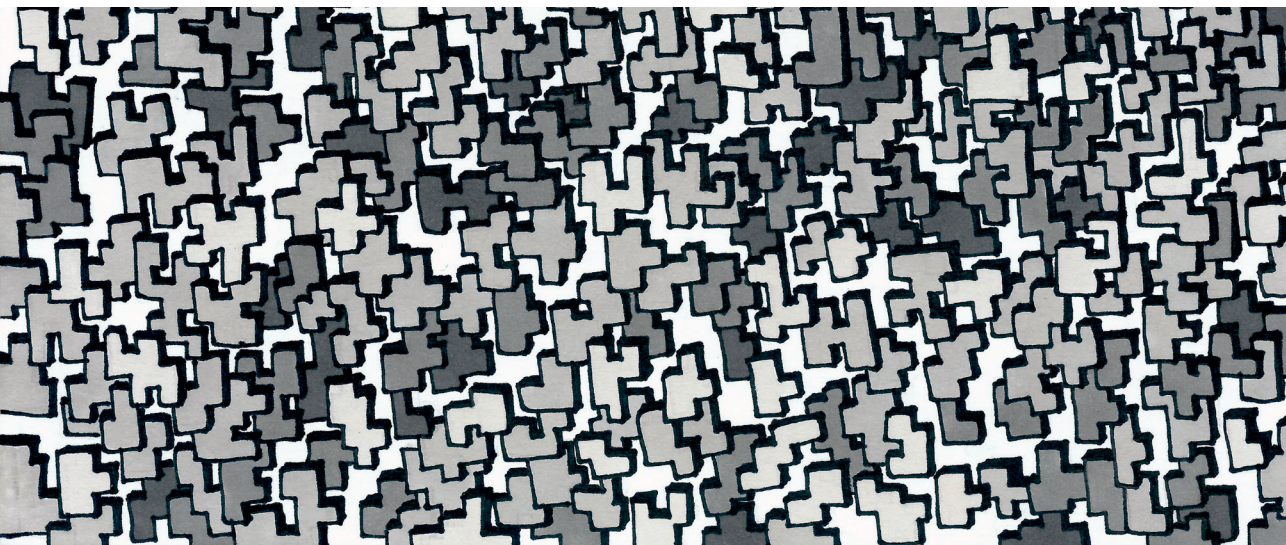

SUMMARY & FUTURE PERSPECTIVES

SUMMARY

In the current thesis the embryological origin of the developing atrioventricular (AV) canal and atrioventricular node (AVN) was investigated, using different techniques, including immunohistochemical staining, lineage tracing and genetic characterization. In addition, the role of the RHOA-ROCK signaling pathway on development of key components of the cardiac conduction system (CCS) was studied. Finally, the potential role of the epicardium in autonomic modulation of the heartbeat was investigated.

In **chapter 2,** a general introduction on cardiac and CCS development was provided. Development of the CCS was linked to clinical arrhythmias found in the pediatric and adult population. Furthermore, arrhythmias occurring in the setting of congenital heart disease were discussed. Finally, a working model for the developmental background of cardiac arrhythmias was generated. In this working model, embryological structures were linked to their adult counterparts and the arrhythmias arising from these structures.

Chapter 3 described the specific advantages and limitations of the avian embryo as model system in developmental biology, also based on experience obtained from the experiments described in the current thesis. Furthermore, the techniques that were performed in avian embryos to understand the development of the CCS were discussed. The results from these experiments showed that the avian embryo was and still is an essential tool to study developmental biology.

In **chapter 4**, lineage tracing of the AVN area was performed. An important finding was protein expression of ISL1 (commonly used as second heart field marker) in the chick cardiac crescent. In literature, this structure is described to be part of the first heart field. This indicates that ISL1 is unsuitable as a marker for the second heart field. Immunohistochemical analysis of the embryonic heart at later stages of development revealed a myocardial continuity between the myocardium of the sinus venosus and posterior portion of the AV canal. This region showed protein and mRNA expression of TNNI2, HCN4 and ISL1 and single-cell patch clamp revealed pacemaker-like electrophysiological characteristics. Lineage tracing using vital dye labeling showed that the myocardium of the sinus venosus was incorporated in the region of the myocardial continuity between the sinus venosus and posterior AV canal. Based on the superioposterior location of this myocardial continuity in relation to the AV canal, it was postulated that cells from the sinus venosus contribute to the transitional cells and/or nodal extensions of the AVN.

Recently, it was suggested by a report in literature that the dorsal mesenchymal protrusion (DMP), a mesenchymal structure contributing to the base of the atrial septum, acts as a temporary pacemaker during development. In **chapter 5**, we have questioned this, as we believe that the anatomical description of the DMP is not correct. The region designated as DMP in early mouse embryos in the specific report is in our opinion more likely to be the putative AVN, based on expression profile and electrophysiological characteristics.

In **chapter 6**, the role of the RHOA-ROCK signaling pathway on sinus venosus and sinoatrial node (SAN) development was studied. This pathway has important functions in a.o. cell migration and gene transcription. RHOA-ROCK signaling was chemically inhibited during early chick development. This resulted in prolongation of the immature state of the sinus venosus, shown by an increase in *ISL1* expression, persisting pacemaker potential in the entire sinus venosus and a significantly reduced heart rate. Furthermore ROCK inhibition caused aberrant expression of typical SAN genes like *ROCK1, ROCK2, SHOX2, TBX3, TBX5, ISL1, HCN4, CAV3.1, CX40* and *NKX2.5* and the left-right asymmetry genes *PITX2C* and NODAL. The immature phenotype of the right-sided SAN and residual pacemaker potential of the left side of the sinus venosus was confirmed with patch clamp electrophysiology. Together these results showed that RHOA-ROCK signaling is involved in establishing the right-sided SAN as the definitive pacemaker of the heart and restricts typical pacemaker gene expression to the right side of the sinus venosus myocardium.

The experiments performed in **chapter 6** showed that normal RHOA-ROCK signaling is essential in SAN development. However, previous research showed that disturbing RHOA-ROCK signaling also resulted in AV conduction disturbances in adult mice. In **chapter 7**, we have examined the effect of ROCK inhibition on AVN development and have shown that inhibition during early chicken development results in different degrees of AV block, ranging from first degree AV block to advanced grades of block, including AV dissociation. This novel model system can be used to investigate the developmental background of AV block. Furthermore, the development of the myocardial continuity in the region of the putative AVN (described in detail in **chapter 4**) was shown to be disturbed, which may, at least in part, explain the AV block observed in this model. Finally, evidence was found that expression of *SHOX2* and *ISL1* was disturbed in the region of the putative AVN. The consequence of disturbed gene expression in this region warrants further investigation.

For proper physiological responses, the SAN and AVN depend on innervation by the autonomic nerve system. In the adult heart, both the SAN and AVN are richly supplied by autonomic nerve fibers. Development of cardiac autonomic innervation is established by major contributions of the cardiac neural crest cells. However, during early cardiac development, when autonomic innervation has not yet been established, the heart already responds to catecholamines such as epinephrine. In **chapter 8** we showed expression of neuronal markers, as well as the β2 adrenergic receptor (one of the receptors for epinephrine) in the epicardium. Specifically inhibiting the outgrowth of the epicardial layer during development resulted in a reduced heart rate response to epinephrine. The more severely the epicardial covering of the sinus venosus was disturbed, the more severely the heart rate response to epinephrine was hampered. Our results show that the epicardium is (at least partially) responsible for autonomic modulation of the early embryonic heart.

FUTURE PERSPECTIVES

The cell tracing and fate mapping experiments aimed at elucidating the origin of the components of the CCS (described in more detail in **chapters 3, 4, 7** and **9**), share that they provide a static representation of a dynamic process. Combining live-imaging, high-resolution confocal microscopy and either physical or genetic labeling of cells would enable "four-dimensional" analysis of the fate of these cells. If for example a fluorescent label is applied to the sinus venosus myocardium, the active incorporation of this structure in the region of the putative AVN could be verified, thereby dynamically confirming the static observation described in **chapter 4**.

We have shown that the RHOA-ROCK signaling pathway plays an essential role in normal development of the CCS. Future research could focus on identifying the exact molecular pathway by which RHOA-ROCK signaling influences SAN and AVN development. It would be interesting to perform microarray analysis on (control and ROCK inhibited) tissue isolated from specific key CCS regions (such as the right and left-sided SAN and the putative AVN), using the laser capture microdissection technique described in this thesis. This genetic characterization will shed light on the mechanisms leading to pacemaker dysfunction and AV block after inhibition of the RHOA-ROCK pathway.

Finally, the current thesis describes a novel and important role for the epicardium in modulation of the autonomic response prior to establishment of the cardiac autonomic nervous system (**chapter 8**). Epicardial cells have already been shown capable of secreting different factors and to become reactivated in response to damage. The exact mechanism by which the epicardium regulates autonomic responses remains to be elucidated. Future experiments could be

aimed at the *in vitro* neurogenic potential of epicardial and epicardium-derived cells. Furthermore, (single-cell) microarray analysis could help to identify genes that are involved in epicardial modulation of the autonomic response. Finally, it would be interesting to confirm the results in mammals as well as in adult stages, for example after damage. Epicardium-specific knockdown of the β2 adrenergic receptor, followed by microelectrode recordings would be interesting to confirm the importance of the epicardium in general and the epicardial β2 adrenergic receptor in particular in autonomic modulation of the heart.

11

NEDERLANDSE SAMENVATTING

NEDERLANDSE SAMENVATTING

In dit proefschrift werd de embryonale ontwikkeling van het atrioventriculaire kanaal en de atrioventriculaire knoop onderzocht. Hiervoor werden verschillende technieken gebruikt, waaronder *cell tracing* en genetische karakterisatie. Hiernaast werd gekeken naar de rol van de RHOA-ROCK signalerings-cascade tijdens ontwikkeling van het cardiale geleidingssysteem. Tot slot werd er onderzoek verricht naar de relatie tussen de ontwikkeling van het epicard en het cardiale autonome zenuwstelsel.

In **hoofdstuk 2** werd een algemene inleiding gegeven over de ontwikkeling van het hart en het cardiale geleidingssysteem. Er werd getracht specifieke ritmestoornissen te verklaren vanuit de ontwikkeling van het cardiale geleidingssyteem. Verder werd in dit hoofdstuk aandacht besteed aan ritmestoornissen die optreden bij aangeboren hartafwijkingen. Deze informatie werd gebruikt om een model te creëren waarbij embryonale structuren en de "volwassen" structuren die hieruit ontstaan, werden gekoppeld aan ritmestoornissen.

Hoofdstuk 3 beschreef de voor- en nadelen van het aviaire embryo als modelsysteem binnen de ontwikkelingsbiologie. Verder werd een overzicht gegeven van de verschillende technieken die werden verricht met behulp van dit modelsysteem om inzicht te krijgen in de ontwikkeling van het cardiale geleidingssysteem. De resultaten van deze experimenten laten zien dat het aviaire embryo een essentieel modelsysteem is binnen de ontwikkelingsbiologie.

In **hoofdstuk 4** werd de embryonale oorsprong van de atrioventriculaire knoop onderzocht. Een belangrijke vondst was eiwit-expressie van ISL1 (frequent beschreven als marker voor het *second heart field*) in de *cardiac crescent*. Echter, in de literatuur wordt de *cardiac crescent* gerekend tot het *first heart field*. Deze bevinding laat zien dat ISL1 ongeschikt is als marker voor het *second heart field*. Immunohistochemische analyse van het embryonale hart tijdens latere embryonale stadia liet een myocardiale verbinding zien tussen de sinus venosus en de achterzijde van het atrioventriculaire kanaal. Deze verbinding liet mRNA expressie van *TNNI2*, *HCN4* en *ISL1* zien, met pacemaker-achtige elektrofysiologische eigenschappen. Met behulp van *vital dye lineage tracing* experimenten werd aangetoond dat het myocard van de sinus venosus wordt geïncorporeerd in de myocardiale verbinding tussen de sinus venosus en het atrioventriculaire kanaal. Op basis van de lokatie van de myocardiale verbinding werd gepostuleerd dat het sinus venosus myocard bijdraagt aan de transitionele cellen en/of de nodale extensies van de atrioventriculaire knoop.

In een recent artikel werd gesuggereerd dat de *dorsal mesenchymal protrusion (DMP)*, een mesenchymale structuur die bijdraagt aan de basis van het atrium septum, als een tijdelijke pacemaker fungeert tijdens de hartontwikkeling. In **hoofdstuk 5** werd dit door ons in twijfel getrokken, aangezien wij geloven dat de anatomische beschrijving van de DMP in dit artikel niet correct is. De structuur die wordt beschreven als DMP is naar onze mening waarschijnlijk de (toekomstige) atrioventriculaire knoop, gezien het (eiwit en mRNA) expressie-profiel en de elektrofysiologische eigenschappen van de desbetreffende structuur.

In **hoofdstuk 6** werd de rol van de RHOA-ROCK signalerings-cascade tijdens ontwikkeling van de sinus venosus en sinus knoop onderzocht. Deze cascade speelt een belangrijke rol tijdens onder andere cel migratie en gentranscriptie. RHOA-ROCK signalering werd chemisch geremd tijdens de vroege embryonale ontwikkeling in de kip. Dit resulteerde in langer immatuur blijven van de sinus venosus, hetgeen bleek uit een toename van *ISL1* expressie, persisteren van een pacemaker-achtig fenotype van de gehele sinus venosus en een significante reductie van het hartritme. Remming van de RHOA-ROCK signaleringscascade resulteerde verder in afwijkende expressie van zowel genen die typisch zijn voor de sinus knoop, zoals *ROCK1, ROCK2, SHOX2, TBX3, TBX5, ISL1, HCN4, CAV3.1, CX40* en *NKX2.5,* als *PITX2C* en *NODAL*, genen die een belangrijke rol spelen bij het ontstaan van asymmetrie van de organen. Het immature fenotype van de rechtszijdige sinus knoop en het aanhoudende pacemaker-achtige fenotype van de linkerzijde van de sinus venosus werd verder bevestigd met *patch clamp* experimenten. Tezamen lieten de resultaten zien dat RHOA-ROCK signalering noodzakelijk is voor de normale ontwikkeling van de (rechtsgelegen) sinus knoop.

Hoofdstuk 6 liet zien dat RHOA-ROCK signalering van belang is tijdens de normale ontwikkeling van de sinus knoop. Echter, eerder uitgevoerde experimenten in volwassen muizen lieten zien dat het verstoren van RHOA-ROCK signalering ook in AV geleidingsstoornissen resulteerde. Daarom werd in **hoofdstuk 7** het effect van inhibitie van de RHOA-ROCK signalerings-cascade op de ontwikkeling van de atrioventriculaire knoop onderzocht. Chemische remming van RHOA-ROCK signalering in kippenembryo's resulteerde in verschillende gradaties van AV-blok, variërend van eerstegraads AV-blok tot hooggradig AV-blok (inclusief AV dissociatie). De morfologie van de myocardiale verbinding tussen de sinus venosus en het atrioventriculaire kanaal (uitgebreid beschreven in **hoofdstuk 4**) was verstoord, hetgeen de gevonden AV geleidingsstoornis in ieder geval deels verklaart. Genexpressie van *SHOX2* en *ISL1* leek ook verstoord te zijn in de (toekomstige) atrioventriculaire knoop. De consequentie van deze verstoorde

genexpressie moet verder onderzocht worden. Een interessante bijkomstigheid is dat het in **hoofdstuk 6** en **7** beschreven nieuwe modelsysteem kan worden gebruikt om de pathofysiologie en behandeling van AV-blok te onderzoeken.

Voor een normale fysiologische respons van het hart op externe stimuli moeten de sinus en atrioventriculaire knoop geïnnerveerd worden door het autonome zenuwstelsel. Het cardiale autonome zenuwstelsel is afkomstig van cardiale neurale lijst cellen. Tijdens de embryonale ontwikkeling reageert het hart al op catecholamines (zoals epinefrine) met o.a. een stijging van de hartfrequentie vóórdat innervatie door het cardiale autonome zenuwstelsel is bewerkstelligd. In **hoofdstuk 8** werd aangetoond dat het epicard zowel neuronale markers als de β2 adrenerge receptor (één van de receptoren voor epinefrine) tot expressie brengt. Remming van de uitgroei van het epicard tijdens de vroege embryonale ontwikkeling resulteerde in een verminderde respons van de hartfrequentie op epinefrine. Hoe minder epicardiale cellen gezien werden in het gebied van de sinus venosus, hoe minder het hart reageerde op epinefrine. Deze resultaten laten zien dat het epicard van groot belang is voor autonome regulatie van het vroeg embryonale hart.

TOEKOMST PERSPECTIEF

De verschillende *cell tracing* en *fate mapping* technieken die in dit proefschrift werden beschreven (zie **hoofdstuk 3, 4, 7** en **9**) hebben met elkaar gemeen dat zij een statische weergave geven van een dynamisch proces. Het combineren van *live-imaging*, hoge resolutie confocale laserfluorescentiemicroscopie en fysieke (met bijvoorbeeld een *vital dye*) of genetische markering geeft de mogelijkheid om "vierdimensionale" analyse uit te voeren van het lot van voorlopercellen. Wanneer bijvoorbeeld myocard van de sinus venosus van een fluorescente markering wordt voorzien, dan kan met de bovenbeschreven combinatie van technieken definitief worden bevestigd dat er een actieve incorporatie is van myocard van de sinus venosus in de regio van de toekomstige atrioventriculaire knoop (zoals beschreven in **hoofdstuk 4**).

We hebben aangetoond dat de RHOA-ROCK signalerings cascade een essentiële rol speelt tijdens de ontwikkeling van het cardiale geleidingssysteem. Toekomstig onderzoek moet aantonen via welke moleculaire mechanismes RHOA-ROCK signalering invloed uitoefent op de ontwikkeling van de sinoatriale en atrioventriculaire knoop. *Microarray analysis* van specifieke gebieden van het geleidingssysteem (geïsoleerd met behulp van de in dit proefschrift beschreven *laser capture microdissection* methode) van zowel controle als ROCK-geremd materiaal zou een eerste stap kunnen zijn. Het in kaart brengen van afwijkingen in genexpressie na remming van RHOA-ROCK signalering zal helpen bij het

vaststellen welke processen leiden tot sinus knoop dysfunctie en AV-blok.

Tot slot werd in dit proefschrift een nieuwe functie van het epicard beschreven. Het epicard blijkt een belangrijke rol te spelen tijdens autonome regulatie van het hart, nog voordat het cardiale autonome zenuwstelsel is aangelegd. Eerder onderzoek heeft reeds aangetoond dat het epicard in staat is om verschillende factoren uit te scheiden en om gereactiveerd te worden na schade aan het hart. Hoe precies het epicard als autonome regulator fungeert moet nog worden uitgezocht. Toekomstige experimenten kunnen gericht zijn op het onderzoeken van het mogelijke *in vitro* neurogene potentieel van epicardcellen en epicard-afkomstige cellen. Tevens kan *single-cell microarray analysis* worden toegepast om genen te identificeren die betrokken zijn bij de door het epicard gereguleerde autonome respons. Tot slot is het interessant om de gevonden resultaten te verifiëren in zowel een zoogdiermodel als in volwassen stadia, bijvoorbeeld na schade aan het hart. *Microelectrode analysis* na epicard-specifieke *knockdown* van de β2 adrenerge receptor in muizenembryo's kan de belangrijke rol van het epicard en de epicardiale β2 adrenerge receptor tijdens autonome regulatie van het hart verder bevestigen.

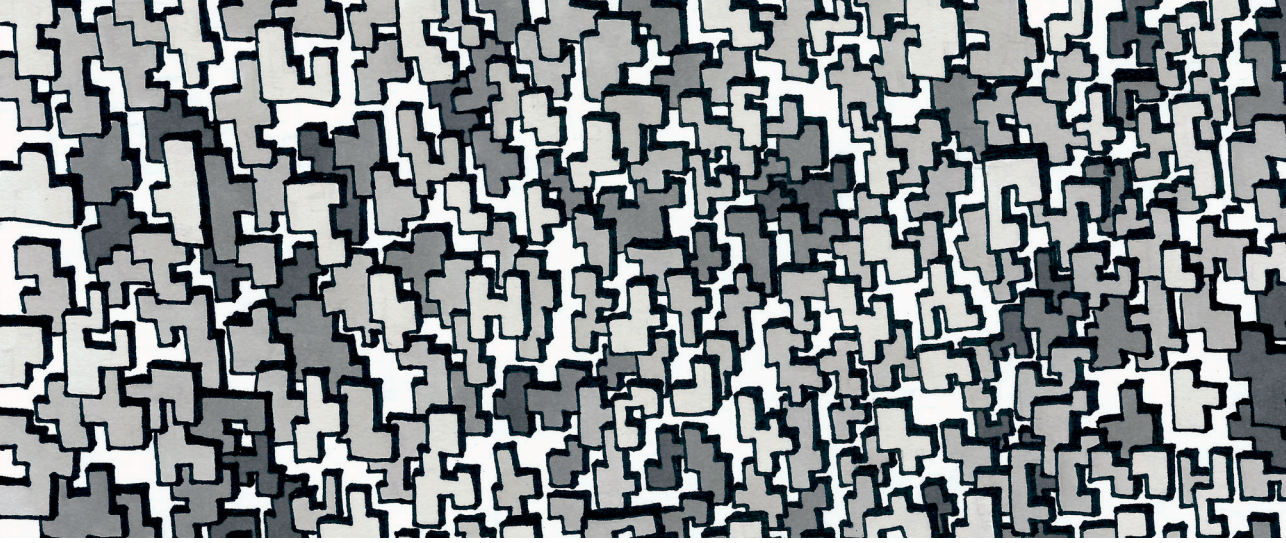

12

LIST OF PUBLICATIONS

DANKWOORD

CURRICULUM VITAE

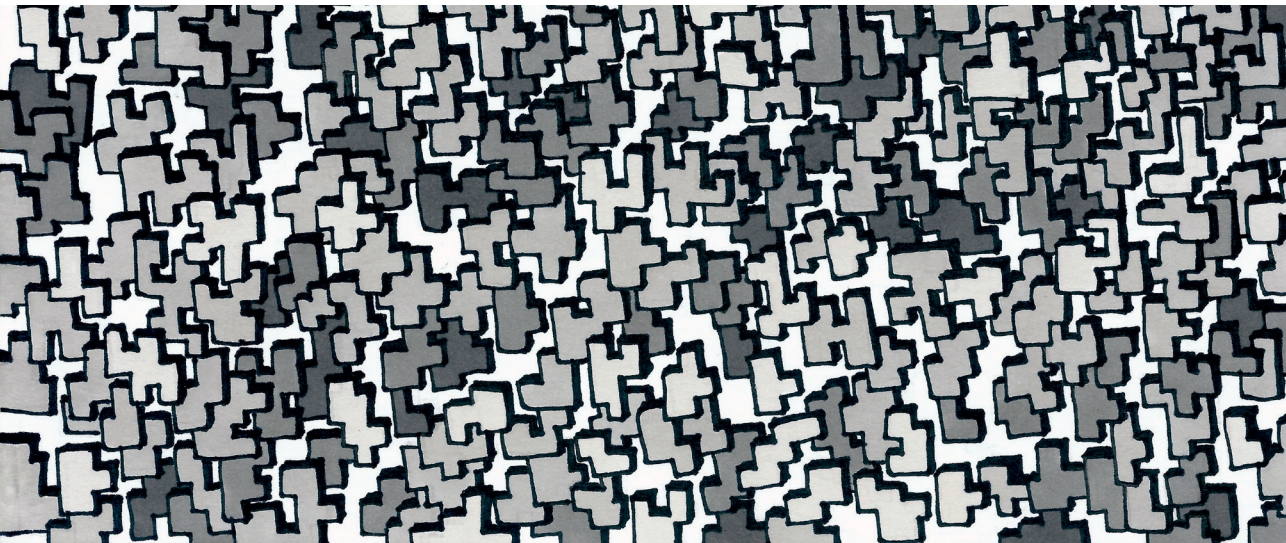

LIST OF PUBLICATIONS

Vicente-Steijn R, **Kelder TP**, Tertoolen LG, Wisse LJ, Pijnappels DA, Poelmann RE, Schalij MJ, DeRuiter MC, Gittenberger-de Groot AC, Jongbloed MRM. RHOA-ROCK signaling is necessary for lateralization and differentiation of the developing sinoatrial node. *Cardiovasc. Res*. 2017;113: 1186-1197.

Kelder TP, Vicente-Steijn R, Poelmann RE, Mummery CL, DeRuiter MC, Jongbloed MRM. The avian embryo to study development of the cardiac conduction system. *Differentiation*. 2016;91: 90-103.

Kelder TP, Duim SN, Vicente-Steijn R, Végh AM, Kruithof BP, Smits AM, van Bavel TC, Bax NA, Schalij MJ, Gittenberger-de Groot AC, DeRuiter MC, Goumans MJ, Jongbloed MRM. The epicardium as modulator of the cardiac autonomic response during early development. *J. Mol. Cell. Cardiol*. 2015; 89: 251-259

Kelder TP, Vicente-Steijn R, DeRuiter MC Gittenberger-de Groot AC, Jongbloed MRM. Does the dorsal mesenchymal protrusion act as a temporary pacemaker during heart development? *J. Biol. Chem*. 2015;290:8013-8014

Kelder TP, Vicente-Steijn R, Harryvan TJ, Kosmidis G, Gittenberger-de Groot AC, Poelmann RE, Schalij MJ, DeRuiter MC, Jongbloed MRM. The sinus venosus myocardium contributes to the atrioventricular canal: potential role during atrioventricular node development. *J. Cell. Mol. Med*. 2015; 19: 1375-1389

Veltman CE, Beeres SL, Kalkman DN, **Kelder TP**, Kies P, Vliegen HW, Hazekamp MG, Delgado V, Kroft LJ, Wall EE van der, Gittenberger-de Groot AC, Scholte AJ, Schalij MJ, Jongbloed MRM. Variation in coronary anatomy in adult patients late after arterial switch operation: A computed tomography coronary angiography study. *Ann. Thorac. Surg.* 2013;96:1390-1397

Jongbloed MRM, Vicente-Steijn R, Hahurij ND, **Kelder TP**, Schalij MJ, Gittenberger-de Groot AC, Blom NA. Normal and abnormal development of the cardiac conduction system; implications for conduction and rhythm disorders in the child and adult. *Differentiation.* 2012;84:131–148

Kelder TP, Penning ME, Uh HW, Cohen D, Bloemenkamp KW, Bruijn JA, Scherjon SA, Baelde HJ. Quantitative polymerase chain reaction-based analysis of podocyturia is a feasible diagnostic tool in preeclampsia. *Hypertension*. 2012;60:1538–1544

Jongbloed MRM, **Kelder TP**, Den Uijl DW, Bartelings MM, Molhoek SG, Tukkie R, Schalij MJ. Anatomical perspective on radiofrequency ablation of AV nodal reentry tachycardia after Mustard correction for transposition of the great arteries. *Pacing Clin. Electrophysiol*. 2012;35:e287–e290

Kelder TP, van Meurs AH, Rovekamp-Abels LW. A vomiting neonate. *Ned. Tijdschr. Geneeskd*. 2012;156:A3285

DANKWOORD

ZONDER JULLIE GEEN PROEFSCHRIFT!

Dr. Monique Jongbloed

-

Professor DeRuiter & Professor Goumans

-

Professor Gittenberger-de Groot, Professor Poelmann, Dr. Bartelings, Professor Schalij, Professor Mummery, Professor Passier, Dr. Tertoolen & Dr. Hierck

-

Leden van de promotiecommissie

-

Bert, Jan (†), Conny, Saskia, Simone, Liesbeth, Dorien, Jantine, Daniël, Paul, Ron, Job & Atie

-

Sabine, Marcelo, George, Berend, Matthew & Harsha

-

Matthias, Ana, Maria & Joshua

-

Joop, Annelies & Boudewijn

-

Tom, Tom & Inez

-

Mijn collega's in het Sint Franciscus Gasthuis en Juliana Kinderziekenhuis

-

Mijn vrienden, met in het bijzonder Sjoerd, Rebecca, Annelot, Emmeline, Saïd & Niels

-

Mijn familie en schoonfamilie, met in het bijzonder Thijs, Laure, Nina, Jessica, papa (†) & mama

-

Mijn allerliefste Fentje

CURRICULUM VITAE

Tim Peter Kelder was born on the 7th of December 1986 in Leiden, where he graduated from secondary school in 2005 (Da Vinci College, Leiden). In the same year he started medical training at the Leiden University Medical Center (LUMC), during which he worked as student-researcher at the Departments of Cardiology, Pathology and Obstetrics of the LUMC. Furthermore, he worked as student-assistant during microscopy and anatomical training courses for (bio) medical students, and as a technical assistant at the MRI imaging facility of the LUMC. In the course of his medical training he became interested in pediatric cardiology and cardiac development and therefore did his master thesis on the role of the epicardium in electrical activation of the embryonic chicken heart at the Department of Anatomy & Embryology of the LUMC (supervised by Prof. Dr. A.C. Gittenberger-de Groot and Dr. M.R.M. Jongbloed).

After finishing the theoretical (2010, *cum laude*) and clinical (2012, *cum laude*) part of his medical training, he started as PhD-student at the Department of Anatomy & Embryology of the LUMC (promotores: Prof. Dr. M.C. DeRuiter and Prof. Dr. M.-J. Goumans; co-promotor: Dr. M.R.M. Jongbloed). He stayed active in the training of (bio)medical students during courses in cardiac development, anatomy and microscopy. The work described in this thesis is largely published in international, peer-reviewed journals and the work was presented at different national and international conferences. In 2015, he completed the experiments described in the current thesis and started working as a pediatric resident (ANIOS) at the Sint Franciscus Gasthuis in Rotterdam. In February 2017, he started working as pediatric resident (ANIOS) at the Juliana Children's Hospital in The Hague. He aspires to become a pediatrician and remain active in medical research.